Investigating retinal pathology in patients carrying m.3243A>G mutation using human induced pluripotent stem cells

Valeria Chichagova

Doctor of Philosophy

Institute of Genetic Medicine

Faculty of Medical Sciences

Newcastle University

February 2017

Abstract

The heteroplasmic mutation in the mitochondrial gene *MT-TL1* encoding tRNALeucine (UUR) at nucleotide position 3243 resulting in the arginine to guanine transition (m.3243A>G) is the most common pathogenic mutation in the mitochondrial genome. Originally associated with mitochondrial encephalomyopathy, lactic acidosis, and stroke-like episodes syndrome, it has also been linked to a number of other clinical phenotypes. It is common for patients harbouring the mutation to develop a range of ocular abnormalities, including those affecting retinal pigment epithelium (RPE) cells. The underlying mechanisms of RPE degeneration remain unclear. Using fibroblasts derived from patients with retinal changes with the m.3243A>G, I generated heteroplasmic human induced pluripotent stem cell (hiPSC) clones harbouring the m.3243A>G mutation. RPE cells differentiated from patient hiPSCs displayed typical cobblestone morphology and expressed mature RPE-associated markers. The RPE cells retained their ability to form blood-retinal barrier as assessed by measuring transepithelial resistance. However, cells with high levels of the m.3243A>G showed reduced propensity for pigment formation. Additionally, the RPE cells contained abnormal mitochondria and melanosomes, which is likely to manifest as a reduced ability to absorb stray light. These findings have remarkable similarities to the ones seen in RPE cells described in post mortem tissues of patients with the m.3243A>G mutation. In addition, patient cells showed defects in phagocytosis of photoreceptor outer segments, a functional defect associated with other retinal diseases. Overall, the results provide an indication that RPE cells with the m.3243A>G have reduced ability to perform at least two of their main functions: absorption of stray light and phagocytosis, suggesting possible pathological processes associated with ocular symptoms seen in patients. The ability to mimic these manifestations *in vitro* would allow investigating pathological mechanisms further and allow testing novel therapeutic agents aimed at alleviating or treating the symptoms.

Acknowledgements

Table of contents

List of figures

List of tables

List of abbreviations

$\Delta\Psi_m$	mitochondrial membrane potential
AdRPMI	advanced RPMI 1640 Medium
AKT2	RAC-beta serine/threonine-protein kinase
AMD	age-related macular degeneration
ANOVA	analysis of variance
ARMS2	age-related maculopathy susceptibility 2
ATP	adenosine triphosphate
BIO	biotinylated
BMP	bone morphogenetic protein
bp	base pair
BrdU	5-bromo-2'-deoxyuridine
BSA	bovine serum albumin
bFGF	basic fibroblast growth factor
c-MYC	v-myc avian myelocytomatosis viral oncogene homolog
C	hiPSC clone derived on MEFs
cDNA	complementary DNA
CDX2	caudal type homeobox 2
CHX10	visual system homeobox 2
CNS	central nervous system
CNV	copy number variation
CoQ	coenzyme Q, ubiquinone
COX	cytochrome c oxidase
CPEO	chronic progressive external ophthalmoplegia
CRISPR	clustered regularly interspaced short palindromic repeats
CRX	cone-rod homeobox
CXR	carboxy-X-rhodamine

Cyt	cytochrome
D-loop	displacement loop
DAPI	4',6-diamidino-2-phenylindole
DHE	dehydroethidium
DHR	dihydrorhodamine123
DKK1	Dickkopf-related protein 1
DMEM	Dulbecco's Modified Eagle Medium
EB	embryoid body
ECAR	extracellular acidification rate
ECM	extracellular matrix
EMT	epithelial-to-mesenchymal transition
ESC	embryonic stem cell
FAD	flavin adenine dinucleotide
FBS	Fetal Bovine Serum
FCCP	cyanide-ptrifluoromethoxyphenylhydrazone
FITC	fluorescein isothiocyanate
FGF	fibroblast growth factor
FOXA2	forkhead box A2
G1	gap 1
G2	gap 2
GAPDH	glyceraldehyde-3-phosphate dehydrogenase
GFP	green fluorescent protein
H^+	proton
H-strand	heavy strand
HBSS	Hanks' balanced salt solution
HDFs	human dermal fibroblasts
hESC	human embryonic stem cell

hPSC	human pluripotent stem cell
hiPSC	human induced pluripotent stem cell
ICE	interleukin-1β (IL-1β)-converting enzyme
IGF1	insulin-like growth factor 1
IL-1β	interleukin-1β
JC-1 iodide	5,5',6,6'-tetrachloro-1,1',3,3'-tetraethylbenzimidazolylcarbocyanine
JNK	c-Jun N-terminal kinase
kDa	kilodalton
KLF4	Kruppel-like factor 4
KOS	hKlf4-hOct3/4-hSox2
KOSR	Knock-Out Serum Replacement
L-strand	light strand
LAMP1	lysosomal-associated membrane protein 1
LEFTY-A	left-right determination factor A
LHON	Leber's Hereditary Optic Neuropathy
LHX2	LIM homeobox 2
M	hiPSC clone derived on matrigel
MEFs	mouse embryonic fibroblasts
MELAS episodes	mitochondrial encephalomyopathy, lactic acidosis, and stroke-like
MERTK	MER proto-oncogene tyrosine kinase
MET	mesenchymal-to-epithelial
MFI	median fluorescence intensity
mg	milligram
MIDD	maternally inherited diabetes and deafness
miRNA	microRNA
MITF	microphthalmia-associated transcription factor

mitoSOX	mitochondrial-targeted DHE
mitoTALEN	mitochondria-targeted transcription activator-like effector nuclease
MIXL	mix paired-like homeobox
MOI	multiplicity of infection
mRNA	messenger RNA
mTOR	mammalian target of rapamycin
NAD	nicotinamide adenine dinucleotide
NAO	10-n-nonyl-acridine orange
mtDNA	mitochondrial DNA
ND	no difference
nm	nanometre
NMR	non-mitochondrial respiration
OC	optic cup
OCR	oxygen consumption rate
OCT4	octamer binding factor 4
OV	optic vesicle
OXPHOS	oxidative phosphorylation
PARP	poly(ADP-ribose) polymerase
PAX6	Paired Box 6
PBS	phosphate-buffered saline
PCR	polymerase chain reaction
PEDF	pigment epithelium-derived factor
PFA	paraformaldehyde
Pmol	picomole
POS	photoreceptor outer segment
PS	Pearson marrow-pancreas syndrome
qPCR	quantitative polymerase chain reaction

RA	retinoic acid
RGC	retinal ganglion cells
RLU	relative light units
RPMI	RPMI 1640 Medium
rRNA	ribosomal RNA
ROS	reactive oxygen species
RPE	retinal pigment epithelium
RX	retinal homeobox protein
S	synthesis
SAPK	stress-activated protein kinase
SD	standard deviation
SDH	succinate dehydrogenase
SEM	standard error of the mean
SHH	sonic hedgehog
SILV	silver locus protein homolog
SIMH	stress-induced mitochondrial hyperfusion
SNP	single-nucleotide polymorphism
SOD2	superoxide dismutase 2
SOX1	SRY (sex determining region Y)-box 1
SOX2	SRY (sex determining region Y)-box 2
SSEA4	stage-specific embryonic antigen 4
T	T brachyury transcription factor
TCA	tricarboxylic acid
TEM	transmission electron microscopy
TER	transepithelial resistance
TFGβ	transforming growth factor beta
τm^{5}U	5-taurinomethyluridine

TMRM   tetramethyl rhodamine methyl ester

tRNA   transfer RNA

tRNA^{Leu(UUR)} transfer RNALeucine (UUR)

TYR   tyrosinase

VEGF   vascular endothelial growth factor

VSX2   visual system homeobox 2

Chapter 1. Introduction

The heteroplasmic mutation in the mitochondrial gene *MT-TL1* at nucleotide position 3243 resulting in the arginine to guanine transition is the most common pathogenic mutation in the mitochondrial genome. Visual impairment with atrophic maculopathy akin to dry age-related macular degeneration (AMD) is observed in a high proportion of patients with the mutation. To date, the pathological mechanism of retinal abnormalities seen in this patient group remains unclear.

1.1 Overview of mitochondrial biology

1.1.1 Origin and features

The mitochondrion is a unique organelle that carries numerous essential cellular functions. It is involved in a number of critical processes, including its role in adenosine triphosphate (ATP) production through oxidative phosphorylation (OXPHOS), iron metabolism, the citric acid cycle, apoptosis, fatty acid oxidation, and amino acid biosynthesis (Sproule and Kaufmann, 2008). Research has shown that mitochondria originated from a proteobacterial ancestor. One of the earliest articles to suggest the endosymbiotic origin of mitochondria came out almost 100 years ago (Wallin, 1926). It took over 70 years to experimentally illustrate protein sequence similarities of mitochondria and the closest living relative of the original proteobacterial species, confirming its origins (Andersson *et al.*, 1998). Although, still retaining certain features of its ancestors, such as a double membrane, a circular genome and the ability to form dynamic networks, mitochondria have adapted to their eukaryotic cellular host by transferring most of their genes to the nuclear genome (Vafai and Mootha, 2012).

Mitochondria are highly heterogeneous organelles and they form dynamic networks by undergoing fusion and fission which results in the exchange of matrix proteins and mitochondrial DNA (mtDNA) (Nunnari *et al.*, 1997; Legros *et al.*, 2002). One of the fascinating features of mitochondria is the plasticity of the morphology and content. They can appear in different shapes from elongated tubules to spheres or rods depending on the cell type and the environmental cues (Figure 1.1). Additionally, mitochondria have defined subcellular distribution as they are continuously transported along the cytoskeletal tracks depending on the cells bioenergetic requirements (Hollenbeck and Saxton, 2005).
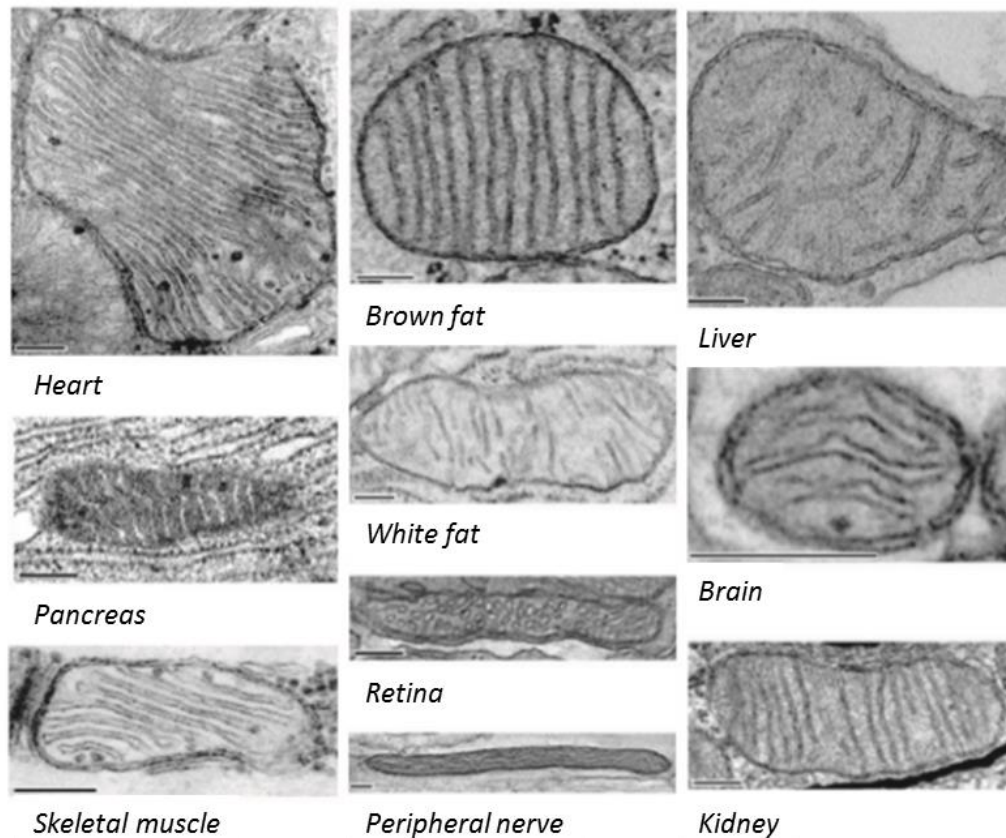
Figure 1.1. Heterogeneity of mitochondrial morphology in different tissues [adapted from Vafai and Mootha (2012)].

Structurally mitochondria are unusual since they have a double membrane. The inner membrane contains numerous invaginations that form the cristae protruding into the matrix, and the outer membrane separates the mitochondrion from the cytosol. The inner membrane contains the enzyme complexes of the OXPHOS system (McBride *et al.*, 2006).

1.1.2 Oxidative phosphorylation

The respiratory chain complexes are composed of 92 protein components that are encoded by both nuclear DNA and mtDNA (Figure 1.2).

	Complex I	Complex II	Complex III	Complex IV	Complex V
nuclear DNA	~38	4	10	10	14
mtDNA	7	0	1	3	2
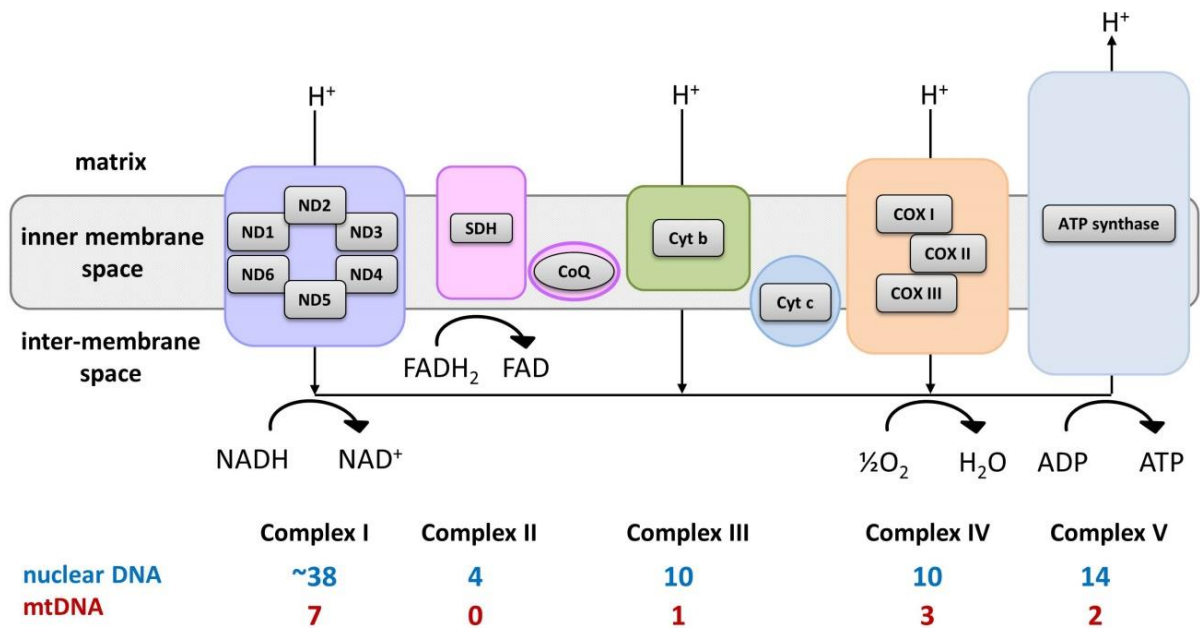
Figure 1.2. Schematic representation of the mitochondrial respiratory chain and the main components of OXPHOS, including the number of proteins in different complexes of the respiratory chain encoded by nuclear and mtDNA. Complexes I, II and III are involved in proton (H^+) transport from the matrix to the inter-membrane space generating electrochemical gradient resulting in driving H^+ back into the matrix by Complex V producing ATP [adapted from Sproule and Kaufmann (2008)]. NAD - nicotinamide adenine dinucleotide; FAD - flavin adenine dinucleotide; SDH - succinate dehydrogenase; CoQ – coenzyme Q, ubiquinone; Cyt - cytochrome; COX - cytochrome c oxidase.

The respiratory chain drives OXPHOS through a number of redox reactions. Donation of electrons to the respiratory chain drives protons through Complex I, Complex III and Complex IV, generating a proton motive force. Complex I and Complex II are involved in transferring electrons from NADH and $FADH_2$ to a mobile electron carrier coenzyme Q. Complex III passes on the electrons to cytochrome c. Complex IV accepts the electrons and reduces oxygen to water. The resulting pH gradient facilitates the production of ATP by Complex V (F1F0-ATPase) through the movement of protons back to the mitochondrial matrix. Almost all of the redox reactions within the cell are linked to the respiratory chain including the tricarboxylic acid (TCA) cycle. One of the by-products of the metabolic reactions in the respiratory chain, especially at Complex I and Complex III, are reactive oxygen species (ROS) which are potentially toxic to the cell. There is a dedicated control system which involves superoxide dismutase and catalase, which regulate ROS levels (Vafai and Mootha, 2012).

1.1.3 Mitochondrial genetics

Mitochondria are regulated by both the nuclear and mitochondrial genomes. mtDNA in humans is a circular, double-stranded molecule approximately 16 569 base pairs long (Anderson *et al.*, 1981). Each strand is different in nucleotide composition. H-strand (heavy strand) is guanine rich and L-strand (light strand) is cytosine-rich (Chinnery and Hudson, 2013). mtDNA is different from nuclear DNA in a number of respects. Firstly, it is exceptional in its economic organisation. Its genes do not contain intronic regions and the coding region represents ~93% of the genome with the only non-coding region located in the D-loop (displacement loop) which contains the site of mtDNA replication initiation and transcription (Chinnery and Hudson, 2013). Additionally, the mitochondrial genetic code deviates from the standard code. It contains only two stop codons comparing to three stop codons in the nuclear DNA (Temperley *et al.*, 2010). Despite the differences, mtDNA and nuclear DNA exist in synergy.

mtDNA contains 37 genes, 13 of which encode for polypeptide components of the OXPHOS system (components of Complex I, Complex III, Complex IV and Complex V) and 24 encoding for RNA products, including 22 mitochondrial transfer RNAs (tRNAs), a 16s ribosomal RNA (rRNA) and a 12s rRNA (Anderson *et al.*, 1981). A schematic of the human mtDNA is shown in Figure 1.3.
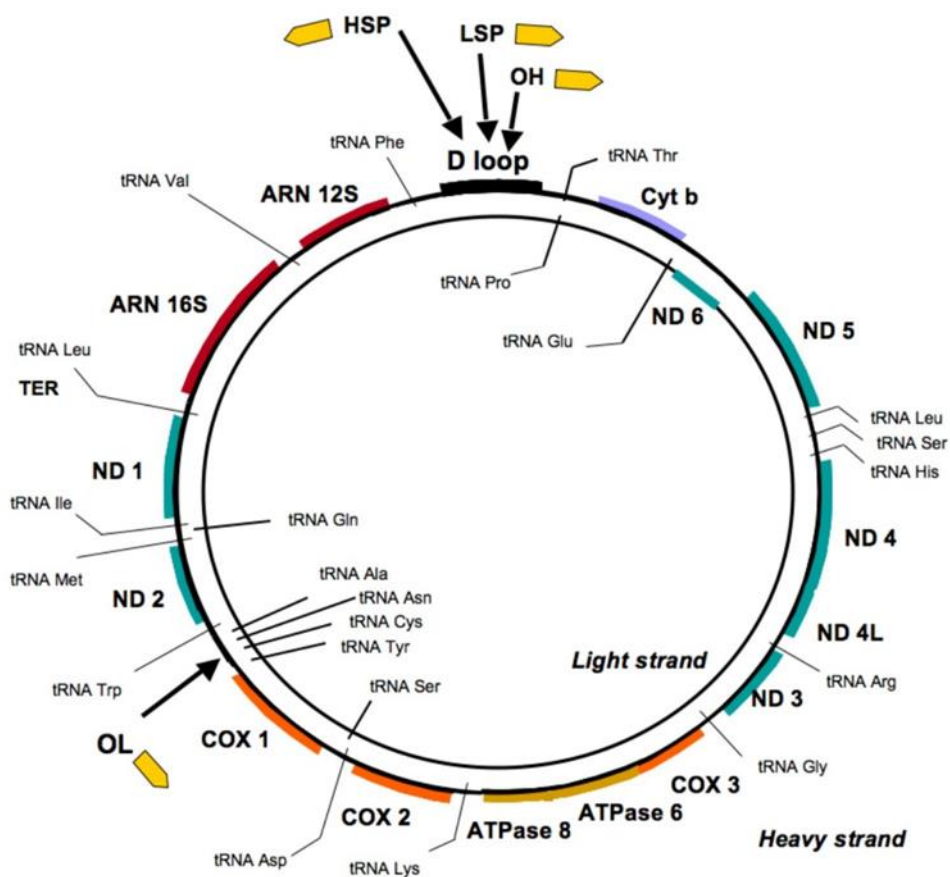
Figure 1.3. Schematic representation of the human mtDNA [adapted from Ding *et al.* (2013)].

One of the key features of mitochondrial genetics is the mode of inheritance of mtDNA. It has been widely accepted that mtDNA nucleoids are inherited exclusively through maternal lineage (Giles *et al.*, 1980). One of the proposed theories suggests that this is due to the ubiquitination of sperm mitochondria inside the male reproductive tract or upon entering the oocyte. This leads to targeted proteolysis resulting in the expression of only maternal mtDNA in the zygote (Sutovsky *et al.*, 1999). Thus far, only one case of paternal inheritance has been recorded (Schwartz and Vissing, 2002). mtDNA in mature mammalian oocytes is estimated to have approximately 100 000 copies containing between 1 and 2 copies per organelle. During early embryogenesis, various combinations of mitochondria are segregated between individual primordial cells and their number is reduced drastically to around 0.1% of the original population. This process characterises developmental bottleneck, when only a small proportion of the original population of mitochondria contributes to the offspring (Shoubridge and Wai, 2007).

1.1.4 mtDNA mutations

mtDNA does not have an efficient repair system and lacks protective histones. Furthermore, it has a high rate of replication independent of the cell cycle and it exists in the environment enriched with ROS. This therefore results in a high rate of mutations in mtDNA, especially when compared to nuclear DNA. Due to the polyploid nature of the mitochondrial genome, this leads to co-existence of mutant and wild-type mtDNA within a single organelle resulting in heterogeneous mutation levels in different cells and tissues. The mixture of different mtDNA genotypes in the same cell is referred to as heteroplasmy. When all of the copies of mtDNA are identical it is referred to as homoplasmy (McFarland *et al.*, 2002; Chinnery and Hudson, 2013). Heteroplasmy is one the most clinically important features of segregation of mitochondrial genome, as it is believed that pathogenic phenotypes arise as a result of the heteroplasmy reaching a pathogenic threshold level (Prigione *et al.*, 2011). Due to the fact that the developmental bottleneck is a stochastic process, it is difficult to predict how much mutant mtDNA will be passed on to the next generation. It should be noted that mtDNA haplogroups arose from the accumulation of benign mutations which became homoplasmic polymorphisms (McFarland *et al.*, 2002).

More than 200 mtDNA disease-causing mutations have been reported since the initial description of the first mtDNA mutations (Holt *et al.*, 1988; Wallace *et al.*, 1988; Hamalainen *et al.*, 2013). For the vast majority of cases, the diseases have variable penetrance depending on the proportion of mutated mtDNA and their stochastic segregation during development (Shoubridge and Wai, 2007). Epidemiological studies estimate that ~1:8000 of general population has clinically manifesting mtDNA disease and ~1:200 of healthy individuals harbours a potentially pathogenic mtDNA mutation (Chinnery *et al.*, 2000; Darin *et al.*, 2001; Elliott *et al.*, 2008; Schaefer *et al.*, 2008). The conditions resulting from the mutations manifest in various forms including myopathies, neurodegeneration, multi-organ failure, cardiomyopathies and retinopathies, with the age of onset varying between infancy and adulthood and presenting with high clinical variability (Ylikallio and Suomalainen, 2012) (Figure 1.4).
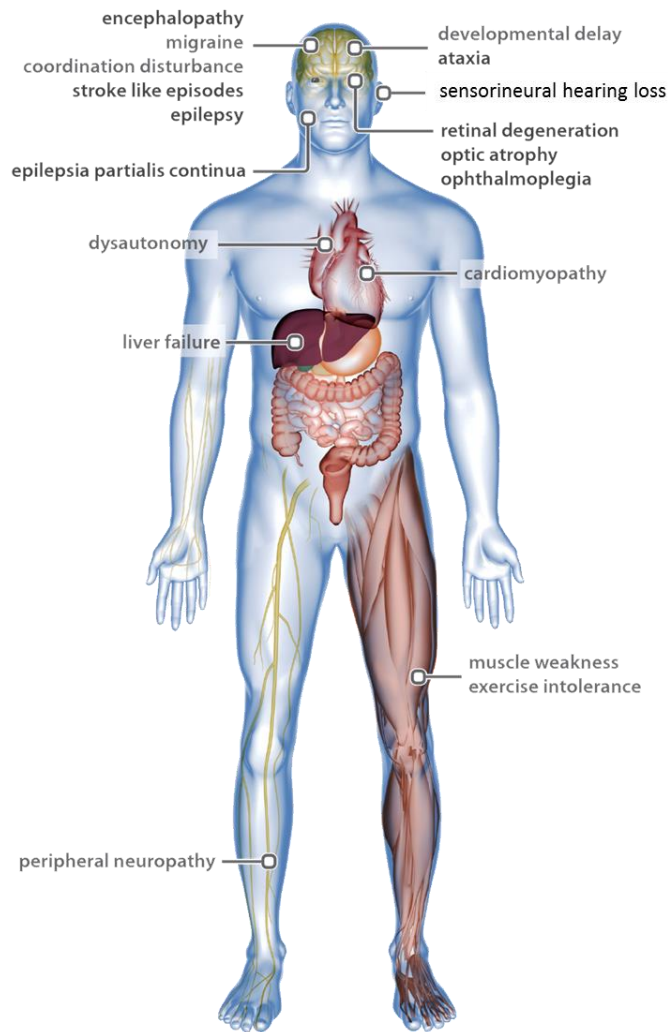
Figure 1.4. Schematic representation of the clinical spectrum of mitochondrial disorders [adapted from Khondrion (2014)].

Most pathogenic mtDNA mutations are heteroplasmic and mitochondrial respiratory chain activity becomes compromised when the level of the mutant species exceeds a critical threshold, which is both mutation and tissue specific. A recent study found that heteroplasmy level of 50% in any tissue was associated with the development of various clinical abnormalities (Dvorakova *et al.*, 2016).

1.1.5 Mitochondrial pathogenesis associated with m.3243A>G mutation

The heteroplasmic mutation in the mitochondrial gene *MT-TL1* encoding tRNALeucine (UUR) (tRNA$^{Leu(UUR)}$) at nucleotide position 3243 resulting in the arginine (A) to guanine (G) transition (m.3243A>G) has been identified as the most common pathogenic mutation in the mitochondrial genome (Moraes *et al.*, 1993; Majamaa *et al.*, 1998). Originally associated with mitochondrial encephalomyopathy, lactic acidosis, and stroke-like episodes (MELAS), it has also been linked to a

number of other clinical phenotypes including diabetes mellitus and chronic progressive external ophthalmoplegia (CPEO) (Moraes *et al.*, 1993; Kadowaki *et al.*, 1994; van den Ouweland *et al.*, 1994). Although, over 30 mitochondrial mutations have been found to be associated with MELAS, in over 80% of cases, it is caused by the m.3243A>G point mutation (Hirano *et al.*, 1992).

The molecular mechanisms underlying the pathogenesis of the m.3243A>G are complex and not completely understood, although the prevailing theory suggests that translation defects are a possible explanation. There are 22 species of mitochondrial tRNA which are able to recognise 60 codons. The reduced number of tRNAs required to decipher all the codons is achieved by post-transcriptional modification of the anticodons (Suzuki, 2014). tRNAs are able to recognise codons by having a modified first letter of the anticodon in the uridine position which leads to recognition of all four bases and reduction in the total number of tRNAs that are required (Barrell *et al.*, 1980; Bonitz *et al.*, 1980). Healthy mitochondrial tRNA[Leu(UUR)] has a 5-taurinomethyluridine ($\tau m^5 U$) post-transcriptional modification which is found at the anticodon wobble position and results in stabilisation of wobble pairing, specifically for decoding UUG (Suzuki and Nagao, 2011). Studies using cybrid cell lines containing mutant mtDNA derived from patients harbouring the m.3243A>G showed defects in mitochondrial protein synthesis attributed to wobble modification deficiency leading to reduced translational ability of tRNA[Leu(UUR)] (Kirino *et al.*, 2004). Wobble modification deficiency is thought to be due to the inability of a tRNA-modifying enzyme responsible for taurine modification to recognise the tRNA due to tertiary structure changes resulting from the mutation (Kirino and Suzuki, 2005). The effect of the m.3243A>G on tRNA[Leu(UUR)] is outlined in Figure 1.5. It has also been suggested that there are possible additional mechanisms that also attribute to the negative effect of the mutation, including defects in transcription termination and decreased aminoacylation (Suzuki and Nagao, 2011).
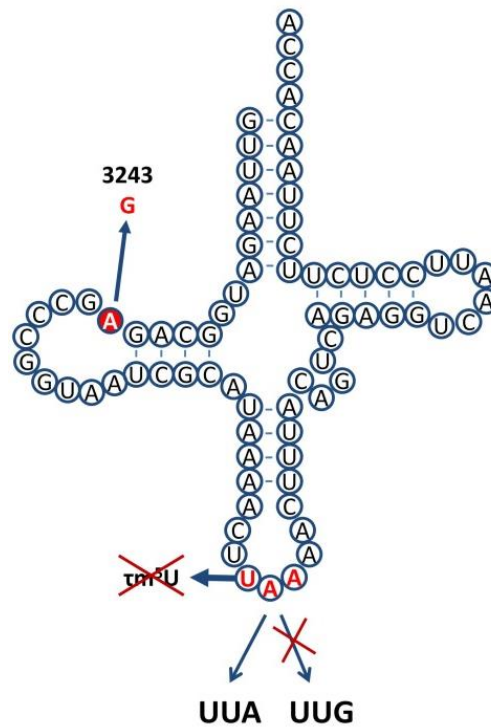
Figure 1.5. Deficiency in tRNA^{Leu(UUR)} wobble modification in m.3243A>G resulting from defects in taurine modification which in turn leads to altered UUG-rich gene translation.

Autopsy studies in MELAS patients have shown that patients most commonly have Complex I deficiency, however some studies show that combined deficiencies of respiratory chain complexes are observed (Hamalainen *et al.*, 2013). Complex I deficiency could be linked to the deficiency in mitochondrial translation and wobble modification deficiency in tRNA^{Leu}. Complex I contains 42.1% of the total leucine codons encoded by ND6 genes, which are rich in UUG, and defects in tRNA^{Leu} could potentially lead to a reduction in Complex I activity (Kirino *et al.*, 2004).

1.2 Clinical features of MELAS

Early clinical reports isolated a number of key features of MELAS. They included normal early development with later presentation of encephalopathy with seizures, stroke-like episodes, and evidence of mitochondrial dysfunction in the form of lactic acidosis and / or ragged red fibres. Patients can also present with additional features such as motor deficits, cortical blindness, dementia, exercise intolerance, migraine-like headaches, hearing loss and a short statue (Pavlakis *et al.*, 1984; Hirano *et al.*, 1992). According to one of the early case reports, patients can develop prominent neurological features before 40 years of age and although the signs and symptoms

may appear at various ages, most commonly patients present with the early symptoms between the ages of 2 and 20 years (Hirano *et al.*, 1992; Lin *et al.*, 2014). According to a recent study of 50 patients, 58% have four or more symptoms associated with MELAS and 12% are monosymptomatic (Dvorakova *et al.*, 2016). Sensorineural hearing loss and myopathy were the most common findings followed by CPEO.

One of the most debilitating features of MELAS is the clinical manifestation of stroke-like episodes. They are associated with transient neurological deficits and progress over a longer period of time unlike an ischaemic stroke (Fryer *et al.*, 2016). They are believed to be caused by an impaired binding of cytochrome c to mitochondrial respiratory chain proteins. In addition, excess extracellular potassium and glutamate within the synaptic cleft may lead to neuronal cytotoxicity causing epileptic seizures (Bhuvaneswar *et al.*, 2008). One study suggested that being a male was a risk factor for developing stroke-like episodes in patients with the m.3243A>G (64.7% or 33 out of 51 patients) (Mancuso *et al.*, 2014).

It is presumed that pathogenesis of MELAS is largely driven by a chronic state of energy failure where the cell is unable to generate sufficient amount of ATP due to the presence of dysfunctional mitochondria (Sproule and Kaufmann, 2008). Histopathological studies of patient muscle biopsies show appearance of ragged red fibres. This indicates that there is increased mitochondrial proliferation; a compensatory mechanism in response to deficient protein synthesis resulting in the increased overall cytochrome c oxidase activity. This could potentially be the driving force of the pathogenesis of MELAS. Picard *et al.* (2014) recently investigated the connection between the heteroplasmy levels of the m.3243A>G and the effect it has on nuclear gene expression, with the view of providing explanation for variable clinical phenotypes seen in patients that harbour the mutation. They created a series of cell cybrids with various levels of mutated mtDNA. There were a number of important findings that were described in this study. It was shown that there was a direct correlation between the levels of the m.3243A>G and the amount of mtDNA encoded proteins of the electron transport chain. In addition, presence of mutated mtDNA resulted in alterations in the mitochondrial morphology resulting in their elongated shape and ultra-structural changes affecting cristae. Interestingly, even when the mutation level was as low as 20-30%, the ability of the cells to generate enough energy was markedly reduced. The most important finding was that cells with

50-90% m.3243A>G had similar transcriptional profile comparable to that seen in some neurodegenerative diseases and was a result of altered retrograde signalling between the mitochondria and the nucleus.

To date all the treatment for MELAS is symptomatic with no curative options. Patients are often offered treatment in the form of coenzyme Q, vitamins C and E, riboflavin and creatine (Sproule and Kaufmann, 2008).

1.2.1 Ophthalmological findings in mitochondrial diseases

There are several primary mtDNA mutations and nuclear mutations that affect mitochondria that lead to ocular diseases, some of which are described below.

Optic neuropathies are a common manifestation in mitochondrial diseases. Leber's Hereditary Optic Neuropathy (LHON) is characterised by the degeneration of retinal ganglion cells (RGC) which leads to central vision loss by the age of 50 in the majority of patients. Prevalence of LHON has been estimated to be ~1:31,000 and over 90% of patients harbour one of the three mutations in mtDNA affecting Complex I: m.11778G>A, m.14484T>C, and m.3460G>A (Wallace *et al.*, 1988; Huoponen *et al.*, 1991; Johns *et al.*, 1992; Yu-Wai-Man *et al.*, 2003). Most of the affected individuals are males. The gender bias of LHON has been suggested to arise as a result of nuclear genetic factors, such as visual loss susceptibility gene located on the X-chromosome, which renders males to be more exposed to the mtDNA mutation acting in synergy with the nuclear gene (Bu and Rotter, 1991). More studies are required in order to identify the nuclear modifier genes that are specific to LHON (Yu-Wai-Man *et al.*, 2011a). Hormonal factors have also been shown to be associated with male prevalence in LHON. One study used cell cybrids harbouring the three mtDNA point mutations m.11778G>A, m.14484T>C, and m.3460G>A to investigate metabolic basis for gender bias in LHON (Giordano *et al.*, 2011). The authors showed that the addition of 17β-oestradiol to the cells reduced overproduction of ROS, thereby increasing cell viability and mitochondrial function in the cells, which supported the hypothesis of the protective effect of hormones in females.

Autosomal-dominant optic atrophy is another disorder that results in the loss of RGCs and their axons. It has a prevalence of 1:35,000 in the North of England and has a mean age of onset between 6 and 10 years of age (Yu-Wai-Man *et al.*, 2010). It has a less severe phenotype comparing to LHON, however most of patients have worsening symptoms with age (Cohn *et al.*, 2008; Yu-Wai-Man *et al.*, 2011b). The

majority of cases are caused by the mutation in the *OPA1* gene, which results in the reduced levels of OPA1 protein (Yu-Wai-Man *et al.*, 2011b). OPA1 is located in the inner domain of the mitochondrial membrane and is involved in mitochondrial fusion. The mutation in the gene leads to the impairment in mitochondrial fusion and a coupling defect of OXPHOS (Chevrollier *et al.*, 2008; Zanna *et al.*, 2008).

CPEO is a mitochondrial myopathy which manifests as bilateral ptosis and reduced eye movement (Richardson *et al.*, 2005). Patients harbour large-scale mtDNA deletions or multiple mtDNA point mutations secondary to nuclear DNA defect resulting in cytochrome *c* oxidase (COX) deficiency in extraocular muscles (Greaves *et al.*, 2010). Kearns-Sayre syndrome is a systemic disorder associated with single large-scale heteroplasmic deletions in mtDNA (Zeviani *et al.*, 1988). Patients are normally young at diagnosis and develop CPEO within a few years. In addition, this disorder is characterised by other symptoms, including retinopathy, central nervous system (CNS) deficits, ataxia and cardiac conduction abnormalities (Yamashita *et al.*, 2008).

Maternally inherited diabetes and deafness (MIDD) results from the m.3243A>G mutation and patients present with diabetes and sensorineural hearing loss with a maternal family history of the condition (van den Ouweland *et al.*, 1992). Macular pattern dystrophy has been shown to be present in 86% of MIDD patients with 8% of patients presenting with diabetic retinopathy (Guillausseau *et al.*, 2001). Both retinal pigment epithelium (RPE) and choroid atrophy have been reported, with RPE atrophy localising to the posterior pole (Murphy *et al.*, 2008).

Examples of retinal changes in a patient with m.3243A>G, and a patient with the same mutation and diagnosed with MELAS are shown in Figure 1.6 and Figure 1.7.
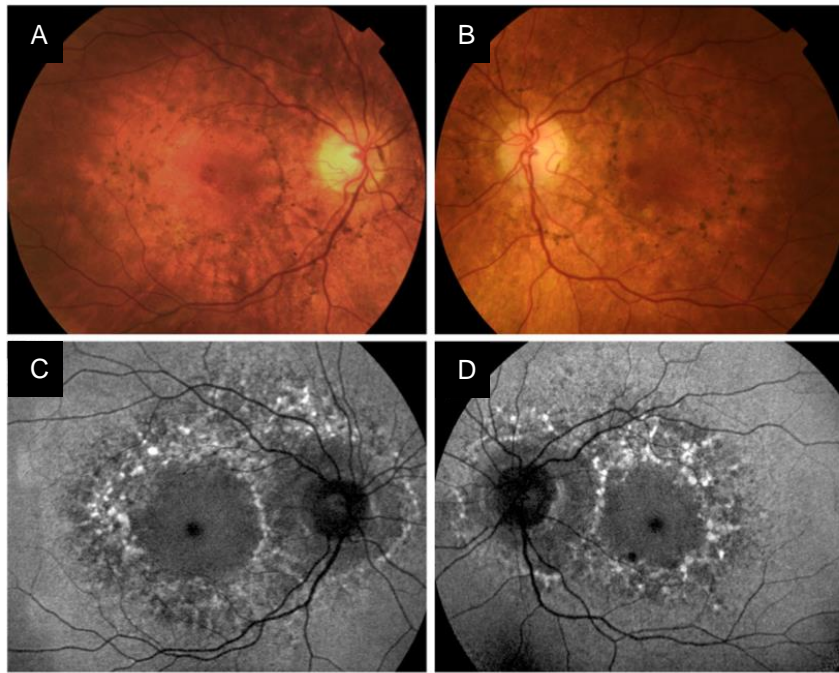
Figure 1.6. Images of the eyes of the patient with m.3243A>G. (A, B) Colour fundus photograph shows hyper-pigmented lesions in the area surrounding the macula and the optic disc, suggesting depigmentation of the RPE; (C, D) Fundus autofluorescence shows speckled appearance of the macula. [Adapted from Daruich *et al.* (2014)].
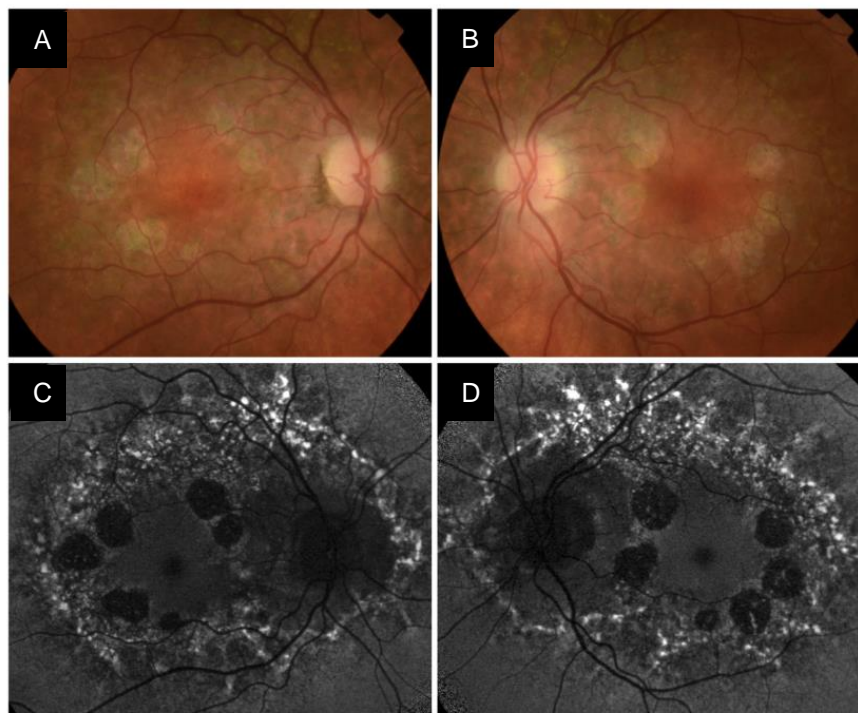
Figure 1.7. Images of the eyes of the patient with m.3243A>G diagnosed with MELAS. (A, B) Fundus photographs show perifoveal atrophy and pale deposits; (C, D) Atrophic areas show decreased autofluorescence, areas with deposits have increased autofluorescence. There is speckled autofluorescence around atrophic areas. [Adapted from Daruich *et al.* (2014)].

AMD is a neurodegenerative disease of the elderly which affects the macula of the eye. Its characteristic features include early presence of drusen with areas of depigmentation and hyperpigmentation, followed by geographic atrophy or choroidal neovascularisation as disease progresses (Barot *et al.*, 2011). There is a theory that suggests that AMD disease progression is related to oxidative stress which has damaging effects on lipids, proteins, and DNA. One study investigated oxidative stress response using donor eyes from AMD patients (Decanini *et al.*, 2007). Relative content of some antioxidant enzymes (cytosolic copper-zinc superoxide dismutase, mitochondrial manganese superoxide dismutase, and catalase) and total proteasome content were increased with disease progression, suggesting a compensatory mechanism against oxidative damage. Another study used donor eyes from AMD patients to show that compared to controls, patients diagnosed with AMD had significantly decreased number of mitochondria, with loss of cristae and matrix density (Feher *et al.*, 2006b). Together with changes in the mitochondrial membrane and mtDNA damage, reduced mitochondrial redox function has been reported in RPE cells exposed to H_2O_2, further suggesting potential mitochondrial involvement and oxidative damage in aetiology of AMD (Ballinger *et al.*, 1999; Liang and Godley, 2003). Increased mtDNA damage was also seen in aged rodent RPE and choroid (Wang *et al.*, 2008a). DNA polymerase gamma is involved in mtDNA replication and is a possible target of ROS and H_2O_2, potentially leading to reduced mtDNA replication (Graziewicz *et al.*, 2002). In order to evaluate the effect of antioxidants on AMD progression, a large 11-centre clinical trial was undertaken (AREDS, Age-Related Eye Disease Study), where patients were given an antioxidant cocktail with vitamins C and E, β-carotene, and zinc (Age-Related Eye Disease Study Research, 2001). It was found that in those over 55 years of age with non-central geographic atrophy, and intermediate and at least one large druse, there was a reduction in the risk of developing advanced AMD with antioxidants and zinc supplementation. A recent study suggested that there was a positive correlation between the effect of antioxidant and zinc supplementation and genotype, specifically amongst age-related maculopathy susceptibility 2 (*ARMS2*) gene carriers, highlighting the importance of further research on genetic variants, supplementation, and AMD progression (Seddon *et al.*, 2016). Lifestyle factors, such as cigarette smoking are also associated with an increased risk of developing AMD (Christen *et al.*, 1996; Khan *et al.*, 2006).

Ocular abnormalities are a common finding in mitochondrial diseases, however there is no consensus as to what the prevalence of these findings is. According to Gronlund *et al.* (2010), 80.7% (study based on 59 patients) of mitochondrial patients have one or more findings that affect ocular health, including reduced eye motility, optic atrophy, pigmentary retinopathy, retinal dystrophy, external ophthalmoplegia, ptosis and low visual acuity. Zhu *et al.* (2016) found that 35% of patients (from a cohort of 74 patients) had at least one ophthalmological abnormality, with 16% presenting with retinal pigmentary changes making it the most common finding.

Retinal pigmentary abnormalities similar to those found in AMD are one of the most common ophthalmological findings in MELAS patients with the m.3243A>G (Phillips and Newman, 1997; Sue *et al.*, 1997). Other histopathological changes that appear as a result of the mutation include degeneration of the choroid and photoreceptors (Rummelt *et al.*, 1993). RPE abnormalities are normally present in conjunction with other features associated with the mutation. A study of two patients reported observations of depigmentation of RPE surrounding the macula and formation of pigmented or pale deposits (Daruich *et al.*, 2014). Another study looked at twelve patients and common findings included perifoveal atrophy and RPE deposits (Rath *et al.*, 2008). de Laat *et al.* (2013) reported that 86% of the mutation carriers (out of 29 patients) had retinal abnormalities and visual acuity deterioration. Pigmentary abnormalities ranged from very mild changes seen in central fundus to the formation of sub-retinal deposits, changes in the macula and around the optic disc. More severe observations were made in some patients that presented with geographic atrophy often sparing central fovea, although in 7% of patients with the advanced stage of the disease it was not the case. This and the study by Sue *et al.* (1997) did not observe formation of sub-retinal deposits associated with typical drusen. Daruich *et al.* (2014) suggested that the drusen seen in m.3243A>G are different to the ones seen in AMD patients with the ones in AMD located more centrally. de Laat *et al.* (2013) reported observing accumulations of lipofuscin in atrophic areas of RPE. Latkany *et al.* (1999) reported a patient with progressive bilateral RPE atrophy. Another study investigated a group of patients with the m.3243A>G (diagnosed with MIDD) (Smith *et al.*, 1999). 77% of their cohort (10 out of 13 patients) had evidence of retinal pigment disease, including RPE and choroidal atrophy, areas of pigmentation and depigmentation, photophobia and reduced night vision pointing to photoreceptor involvement. One patient had appearance of drusen. The study suggested that the RPE cell layer was predominantly affected leading to

defects in photoreceptors. Dvorakova *et al.* (2016) reported that 67% of their patients (50 patient cohort) had ocular abnormalities, including optic nerve atrophy, pigmentary retinal degeneration and reduced visual acuity.

It has been suggested that there is a correlation between the degree of mutant heteroplasmy in the muscle and the risk of developing RPE abnormalities. Patients harbouring >68% of mutant load have a 2-3 fold higher risk (Latvala *et al.*, 2002). de Laat *et al.* (2013) found that in their patient cohort the mean level of the m.3243A>G in urinary epithelial cells was 55% ± 22 and 21% ± 13 in leukocytes; however, there was no correlation between heteroplasmy levels and disease severity.

Both RPE and photoreceptors are vulnerable even at low levels of heteroplasmy due to their localisation in a highly oxidative environment, however there is no evidence to clearly suggest whether it is RPE or photoreceptors that are affected first in MELAS (de Laat *et al.*, 2013). MELAS patients have striking overlapping features with the geographic retinal atrophy observed in AMD, the commonest cause of blindness in the United Kingdom (Sue *et al.*, 1997; Owen *et al.*, 2003; Bunce *et al.*, 2010). It is thought that AMD is a disease of the RPE which leads to secondary photoreceptor degeneration (Bhutto and Lutty, 2012). There is mounting evidence pointing towards oxidative stress and mitochondrial dysfunction as central pathological factors in the aetiology of AMD (Liang and Godley, 2003; Feher *et al.*, 2006a). Even though, m.3243A>G is a very rare cause of AMD, this suggests that there is a common pathogenic pathway in MELAS and AMD (Jones *et al.*, 2004). Investigating the pathophysiology of the outer retinal changes and specifically RPE in patients with the m.3243A>G mtDNA mutations may thus provide insight into the nature and role of the mitochondrial abnormalities seen in patients with AMD.

To date, there are no *in vivo* models for human mitochondrial tRNA mutations and the mechanism of retinal pathogenesis remains unknown. Generation of human induced pluripotent stem cells (hiPSCs) from patient-derived cells with the m.3243A>G mutation provides a potential tool to study the impact of mitochondrial dysfunction on RPE and photoreceptors. A recent publication demonstrated the ability to create hiPSCs from MELAS patients harbouring m.3243A>G mutation (Fujikura *et al.*, 2012). Another study investigating a different MELAS causing mtDNA mutation (m.13513G>A) has furthermore shown that the hiPSC clones produced can have varying levels of mtDNA heteroplasmy as in the donor cells (Folmes *et al.*,

2013). Significantly this means that the effect of varying degrees of heteroplasmy on the production and function of retinal cells can potentially be assessed.

1.3 Human pluripotent stem cells

The discovery of human pluripotent stem cells (hPSCs) has opened up extraordinary opportunities in various areas of biomedical research, including disease modelling, drug discovery and basic science. Animal models have contributed tremendously to our understanding of disease mechanisms; however, they do not always provide a solid platform for accurate recapitulation of human system. A number of key differences exist between animal models and humans including life span and physiology. In addition, for some developmental and pathological processes no animal models currently exist. It is especially significant for the disorders affecting the retina. Rodent models have been used extensively in eye research and they offer several advantages, such as quick disease progression and the possibility of genetic manipulation. However, the most important limitation of mouse and rat models is the absence of a macula. Non-human primates provide a close recapitulation of the anatomy of the human eye and bypass the limitations of rodent models. However, there are some ethical concerns related to their use, the disease progression is slow, their maintenance is costly, and there are difficulties in genetic manipulation (Pennesi *et al.*, 2012). In human studies, post mortem tissues are limited and represent the end stage of the disease without offering insight into disease pathogenesis. hPSCs provide an opportunity for establishment of model systems that would enhance our understanding of the disease mechanisms.

Embryonic and induced pluripotent cells are the two main types of stem cells that are used in disease modelling research. Pre-implantation blastocysts are used for the derivation of mammalian embryonic stem cells (ESCs) (Evans and Kaufman, 1981; Martin, 1981; Thomson *et al.*, 1998) [Figure 1.8 (A)]. They are characterised by their capability of indefinite *in vitro* undifferentiated proliferation and the potential to be differentiated into cell types representative of three embryonic germ layers and extraembryonic tissues that support development (Thomson and Marshall, 1998). There are thousands of research manuscripts that have been published exploring human ESCs (hESCs) as a tool for disease modelling, studying development, drug screening and therapeutics. However, there are numerous ethical issues and controversies that are associated with their derivation and use. It has also been

suggested that they might generate immunological and oncological barriers if used therapeutically (Preynat-Seauve *et al.*, 2009).
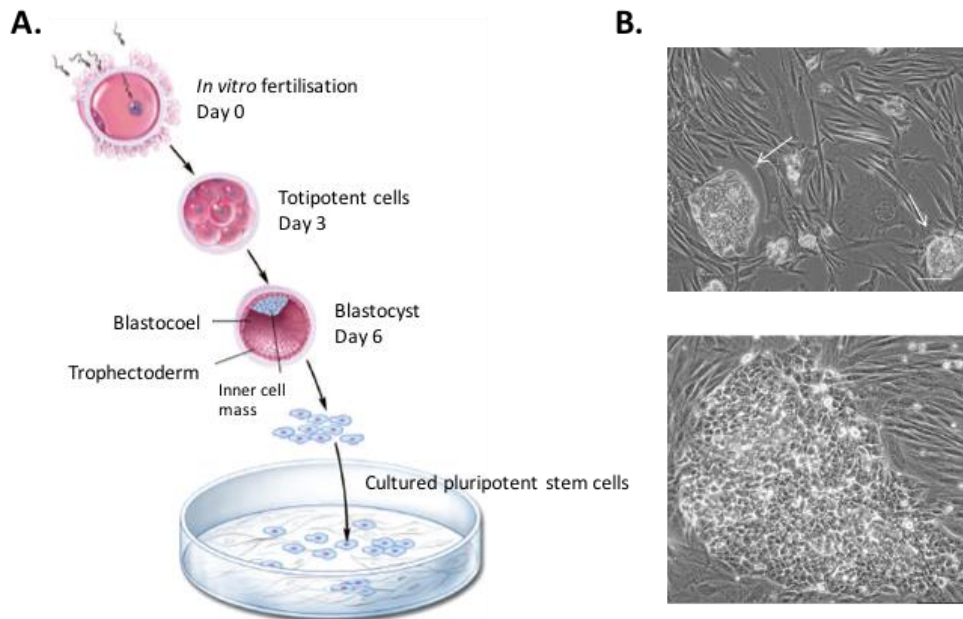
Figure 1.8. Derivation of hESCs. (A) Schematic representation of hESC derivation [adapted from Yu and Thomson (2006)]. (B) Example of hPSC colonies (white arrows). In culture, hPSCs form tightly packed colonies with clearly defined borders, and contain small round cells with large nuclei and notable nucleoli.

In 2007, a major breakthrough resulted in the discovery of an alternative to hESCs in the form of hiPSCs. Yu *et al.* (2007) and Takahashi *et al.* (2007) reported generation of hiPSCs by reprogramming terminally differentiated somatic cells by ectopically expressing four transcription factors required for resetting them to pluripotent state. These cells were similar to hESCs in pluripotency potential, morphology [Figure 1.8 (B)], proliferation and epigenetic status. The discovery of hiPSCs lead to their extensive use as a tool for disease modelling and investigating patient-specific mutations, studying human development and drug screening. They have also started being investigated as a potential therapeutic tool and are currently part of a clinical trial for wet AMD undertaken in Rikagaku Kenkyūsho Institute in Japan, albeit the trial is currently on hold (Kimbrel and Lanza, 2015).

Initial studies using hiPSCs identified a number of issues which have now been resolved, including development of chemically defined cell culture conditions in the absence of serum, reprogramming of human somatic cells with non-integrating vector systems and recent advances in site-specific genome editing in hPSCs (Hockemeyer *et al.*, 2009; Yu *et al.*, 2009; Chen *et al.*, 2011a; Hockemeyer *et al.*, 2011; Okita *et al.*, 2011; Okita *et al.*, 2013). However, there are still issues including

clonal and cell line variations in the propensity of hiPSCs to differentiate into specific lineages due to stochastic processes during reprogramming (Ghosh *et al.*, 2010; Kajiwara *et al.*, 2012).

Recently, an area of research emerged focussing on studying PSCs in alternative pluripotent states ranging between naïve and primed states which exist in murine PSCs. Epiblast cells constitute an extraembryonic set of cells which is uncommitted and provides cues to the blastocyst for embryonic development. Mouse ESCs derived from the pre-implantation epiblast have been suggested to be the only true totipotent (able to differentiate into any cell type) type of cells which constitutes naïve ground state (Nichols and Smith, 2009). Mouse post-implantation epiblast stem cells constitute a primed state. The main difference between the naïve and primed pluripotent states is that cells in the ground state are able to effectively form blastocyst chimeras, have no differentiation bias and have a high clonogenicity. Primate ESCs, including hESCs, have been associated with primed state and a lot of efforts have been invested in order to recapitulate mouse naïve state in human cells. Xiao *et al.* (2016) reviewed a number of publications that aimed at reprogramming human somatic and embryonic stem cells into naïve stem cells. Many of the studies only partially recapitulate ground state and the cells they describe vary in their morphology and chromosome status. Efficient generation of human naïve PSCs would allow better directed differentiation outcome.

1.3.1 Reprogramming human somatic cells

The process of cellular reprogramming is inefficient and Yamanaka (2009) proposed an explanation in the form of two mechanistic models. Firstly, the elite model of reprogramming suggests a deterministic approach where some but not all cells are capable of reprogramming. This has later been confirmed experimentally by Smith *et al.* (2010). The second model describes the idea that most somatic cells have potential to be reprogrammed due to the stochastic nature of the process. There has been a report which showed that reprogramming combines both of these models and consists of initial stochastic alterations in gene expression followed by a more deterministic phase (Buganim *et al.*, 2012). Polo *et al.* (2012) used genome-wide analyses to show that there are early and late deterministic phases with a probabilistic phase in-between.

1.3.2 Factors affecting reprogramming efficiency

Chromatin organisation and stochastic epigenetic events are some of the factors that could have an effect on reactivation of pluripotency circuitry. It has been shown that DNA hypermethylation at pluripotency-related genes may lead to the failure to achieve a stable reprogrammed state (Polo *et al.*, 2012). Treating partially reprogrammed cells with DNA methyltransferase inhibitor 5-aza-cytidine has been shown to induce full reprogramming (Mikkelsen *et al.*, 2008).

Similar to DNA methylation state, remodelling of histone modification is also implicated in the success of somatic cell reprogramming. Histone methylation was shown to be one of the epigenetic changes during the acquisition of the pluripotent state (Polo *et al.*, 2012). Addition of ascorbic acid improves reprogramming efficiency (0.1% to >10%) by reducing histone H3 lysine 36 methylation, reducing p53 levels and alleviating cell senescence by having an opposing effect on bone morphogenetic protein (BMP) (Esteban *et al.*, 2010; Chen *et al.*, 2013). Furthermore, ascorbic acid was shown to induce the activity of H3K36 demethylases Jhdm1a/1b (Wang *et al.*, 2011). Additionally, it was further shown that chromatin remodelling is a rate-limiting step in reprogramming and histone deacetylase inhibitor valproic acid induces 81% reprogramming efficiency (Huangfu *et al.*, 2008a; Huangfu *et al.*, 2008b).

A number of studies reported the existence of microRNAs (miRNAs) that are specific to ESCs and play a role in their phenotype by interfering with the different phases of the cell cycle (Wang *et al.*, 2007; Wang *et al.*, 2008b). miRNAs are non-coding RNA molecules that are involved in post-transcriptional gene regulation by binding to target messenger RNA (Bartel, 2004). A recent report has shown that miRNAs specific to ESCs can promote the shift to pluripotency and mimic reprogramming kinetics when combined with *Oct4, Sox2* and *Klf4* reprogramming factors thereby substituting *c-Myc* (Judson *et al.*, 2009). miRNA302 cluster has been shown to be abundantly expressed in hESCs and embryonal carcinoma cells and to be under transcriptional control of *Oct4* and *Sox2* which in turn might be involved in the regulation of the cell cycle by increasing the S-phase in pluripotent cells (Card *et al.*, 2008). hiPSC generation can also be affected by epigenetic signature of donor cells including miRNA expression and histone modification pattern (Li *et al.*, 2013). Recently our group demonstrated that overexpression of miR-1305 resulted in hPSC differentiation by having an effect on cell cycle and survival (Jin *et al.*, 2016).

During development, cell differentiation is accompanied by epithelial-to-mesenchymal transition (EMT) which is crucial for body plan formation (Thiery *et al.*, 2009). A study that used mouse embryonic fibroblasts demonstrated that mesenchymal-to-epithelial (MET) transition is required for cell reprogramming through upregulation of E-cadherin, a protein involved in cell adhesion by forming adherens junctions (Li *et al.*, 2010). Additionally, it has been shown that reprogramming is associated with three transitional phases including initiation, maturation and stabilisation and MET marks the initiation stage of the process accompanied by downregulation of EMT mediators including BMP and transforming growth factor beta (TGFβ) (Samavarchi-Tehrani *et al.*, 2010). H3K79 methyltransferase has been shown to be implicated in MET signalling indicating the importance of chromatin modification on MET completion (Onder *et al.*, 2012). Recently, our group showed that stress-activated kinases c-Jun N-terminal kinase (JNK) / stress-activated protein kinase (SAPK) are important for the induction of MET (Neganova *et al.*, 2016).

1.3.3 Reprogramming methods

In 1938, a first attempt of a nuclear transfer experiment was performed by Hans Spemann who suggested that a differentiated nucleus can express pluripotency. It took almost 15 years to confirm it experimentally by transplanting nuclei from frog blastula into enucleated eggs showing the possibility of subsequent normal embryonic development (Briggs and King, 1952). 10 years later, Sir John Gurdon used *Xenopus* cells to extend the previous studies to show that it was possible to transfer nuclei from fully differentiated epithelial cells into enucleated eggs which lead to development of normal tadpoles (Gurdon, 1962). This work was the basis of his award of a Nobel Prize. Later studies focused on the attempts to derive cloned mammals. Robl *et al.* (1986) and Tsunoda *et al.* (1987) showed that transferring nuclei of eight-cell mouse embryos to two-cell embryo resulted in some of them developing to 12 days of gestation and in some cases to full term. Subsequent studies showed successful transfer of adult nuclei to enucleated oocytes of a sheep producing viable offspring (Campbell *et al.*, 1996; Wilmut *et al.*, 1997). First attempts to generate ESC lines were performed using mouse and primate cells. Although those studies showed potential benefit in clinical applications, the induction efficiency of the technique was low (Hochedlinger and Jaenisch, 2002; Rideout *et al.*, 2002; Byrne *et al.*, 2007). Another study obtained hESCs by somatic cell nuclear transfer

with high efficiency, however the complexity of the process makes its wide application challenging (Tachibana *et al.*, 2013). Somatic cell nuclear transfer technique has been recently shown to be promising in studying mutations in mtDNA using patient cells (Ma *et al.*, 2015).

First reports of generating hiPSCs came in 2006, when two groups independently reprogrammed human somatic cells into hiPSCs by inducing pluripotent genes and chromatin modification with a set of transcription factors (Takahashi *et al.*, 2007; Yu *et al.*, 2007). Both of the groups used retroviral vectors to deliver the transcription factors. They identified *SOX2* (SRY (sex determining region Y)-box 2) and *OCT4* (octamer binding factor 4, also known as *POU5F1*) as transcription factors required for successful reprogramming. In addition, *KLF4* (Kruppel-like factor 4) and *c-MYC* (v-myc avian myelocytomatosis viral oncogene homolog) were introduced by Takahashi *et al.* (2007) and *NANOG* and *LIN28* by Yu *et al.* (2007).

Since these two reports came out, a number of novel delivery methods for target genes have been developed, including the use of integrating and non-integrating methods. Despite their efficiency, using integrating viral vectors, including retroviruses and lentiviruses, has its own disadvantages. They carry a risk of insertional mutagenesis potentially promoting tumorigenicity (Park *et al.*, 2013). A number of alternatives have been developed to avoid the issues described above, including using non-integrating viruses and non-viral delivery of the required factors.

1.3.4 Non-viral delivery
A number of groups used episomal vectors in order to avoid viral delivery, however the efficiency of the process remains low. Reprogramming human fibroblasts with *OCT4*, *SOX2*, *NANOG*, *LIN28*, *c-MYC*, *KLF4*, and *SV40LT* resulted in 0.0003– 0.0006 % efficiency; using new-born cord blood and introducing *OCT4*, *SOX2*, *KLF4*, *c-MYC*, and *LIN28* resulted in 0.0007% efficiency; another study used human dermal skin fibroblasts and dental pulp with *OCT4*, *SOX2*, *KLF4*, *LIN28*, *MYCL1*, and *TP53* resulting in ~0.003% reprogramming efficiency (Yu *et al.*, 2009; Chou *et al.*, 2011; Okita *et al.*, 2011).

Minicircle DNA, free of bacterial DNA, results in low reprogramming efficiency (~0.005%) and is labour-intensive requiring multiple transfections (Jia *et al.*, 2010; Narsinh *et al.*, 2011).

DNA-free reprogramming methods use recombinant cell-penetrating proteins. Studies using murine fibroblast cells showed successful reprogramming using Oct4, Sox2, Klf4 and c-Myc (Zhou *et al.*, 2009; Cho *et al.*, 2010). This technique may also require multiple transfections with the addition of valproic acid. In addition, it has been shown to be stochastic and inefficient (~0.001%). Similar experiments with human somatic cells showed similar results (0.001% efficiency) and required repeated protein treatment cycles (Kim *et al.*, 2009).

A more efficient way of delivering reprogramming factors is by using mRNA. This results in intracellular post-translational modification of the proteins. This technique is relatively efficient (2-4.4%) however it also requires numerous daily transfections (Warren *et al.*, 2010; Yakubov *et al.*, 2010).

1.3.5 Non-integrating viral vectors

In order to eliminate the risks of the insertion of foreign DNA into a host genome, a number of non-integrating viral vectors have been proposed as an alternative. Adenovirus transiently expresses reprogramming factors and allows transfecting of non-dividing cells (i.e. hepatocytes) without integrating into the genome. However the efficiency of this method is low (0.0002%) and it requires repeated transfections (Zhou and Freed, 2009).

A more efficient and less labour-intensive alternative exists that avoids the use of integrating viral vectors which is the Sendai virus. It was first isolated in Japan in 1950s from a mouse and was identified as a parainfluenza virus from the *Paramyxoviridae* family (Kuroya and Ishida, 1953; Li *et al.*, 2000). The viral particle is 150-200 nm in diameter and consists of 15 384 nucleotides. It replicates as a negative-strand RNA and was shown to be able to self-replicate in its inactive form (Li *et al.*, 2000). The virus replicates in the cytoplasm and does not enter the nucleus thereby avoiding the possibility of integrating into the host genome. It is cleared by clonal propagation of primary colonies resulting in the generation of Sendai-free sub-clones. An alternative way of clearing the virus involves using temperature-sensitive vectors which enables clearing of the virus with passaging (Ban *et al.*, 2011). A number of studies successfully used Sendai virus for the reprogramming of different types of somatic cells including T cells and fibroblasts with 0.1-0.2% efficiencies (Fusaki *et al.*, 2009; Seki *et al.*, 2010). Another group also successfully reprogrammed CD34+ cord blood cells (Nishishita *et al.*, 2012). Life Technologies

(now Thermo Fisher Scientific Inc.) developed the CytoTune® Sendai-based reprogramming kit, which contains either four individual vectors with *hKLF4*, *hc-MYC*, *hOCT3/4* and *hSOX2* or a polycistronic vector *hKLF4-hOCT3/4-hSOX2* (*KOS*) with two additional vectors with *hKLF4* and *hc-MYC*. This reprogramming system was chosen for the PhD project because it is relatively efficient, the vectors do not integrate into the host genome and it does not require multiple transfections.

Reprogramming methods and their efficiencies are summarised in Table 1.1.

Reprogramming method	Efficiency (%)	Source
Episomal vectors	0.003–0.0007	(Yu *et al.*, 2009; Chou *et al.*, 2011; Okita *et al.*, 2011)
Minicircle DNA	~0.005	(Jia *et al.*, 2010; Narsinh *et al.*, 2011)
Recombinant cell-penetrating proteins	0.001	(Kim *et al.*, 2009; Zhou *et al.*, 2009; Cho *et al.*, 2010)
mRNA	2-4.4	(Warren *et al.*, 2010; Yakubov *et al.*, 2010)
Adenovirus	0.0002	(Zhou and Freed, 2009)
Sendai virus	0.1-0.2	(Fusaki *et al.*, 2009; Seki *et al.*, 2010)

Table 1.1. Somatic cell reprogramming methods and their efficiencies.

1.4 Using hiPSCs for modelling mitochondrial diseases

Mitochondria play an important role in somatic cell reprogramming and differentiation and their dynamics and biogenesis change according to the state of the cell. Although this phenomenon is still poorly understood, it is believed that similar to hESCs, hiPSCs contain mitochondria that are spherical, underdeveloped and with perinuclear distribution as opposed to elongated and cristae-rich organelles found in somatic cells (Bukowiecki *et al.*, 2014). Additionally, the cells undergo a metabolic switch from OXPHOS to mainly glycolysis during reprogramming (Folmes *et al.*, 2011). Upon hiPSCs differentiation, the properties of mitochondria start to resemble those of somatic cells.

Since 2012, a number of studies have demonstrated the derivation of hiPSCs carrying various mtDNA mutations (Fujikura *et al.*, 2012; Cherry *et al.*, 2013; Folmes *et al.*, 2013; Hamalainen *et al.*, 2013; Kodaira *et al.*, 2015; Ma *et al.*, 2015; Yokota *et al.*, 2015). Most of these reports described derivation of cells with the m.3243A>G. The details of these papers are to be discussed in further chapters; however, the possibility of having fully established hiPSCs with mtDNA mutations seen in patients, able to give rise to cells of various lineages, provides a great platform for the

investigation carried out as part of this PhD project. In addition, they hold great promise in providing wild-type isogenic hiPSC clones that can be studied along with the cells harbouring various heteroplasmy levels without the requirement for gene editing.

1.5 Retinal development and in vitro differentiation

1.5.1 Structure of the eye and retinal development

The eye is a complex specialised organ, as shown in Figure 1.9. Sclera and cornea form part of the external layer of the eye. Iris, ciliary body, and choroid form the intermediate layer of the eye, and retina is located at the posterior layer. Cornea and iris are separated by the anterior chamber, iris and the lens are separated by the posterior chamber, and vitreous gel is located between the lens and the retina. Macula can be found in central retina 3 mm lateral to the optic disc; fovea can be found in its centre, where there is a high concentration of cone photoreceptors. Retina is positioned as an innermost layer of the eye and is involved in phototransduction by converting biochemical information into neural impulses to the brain. The two main components of the retina are neural retina and RPE (Kolb, 2012).
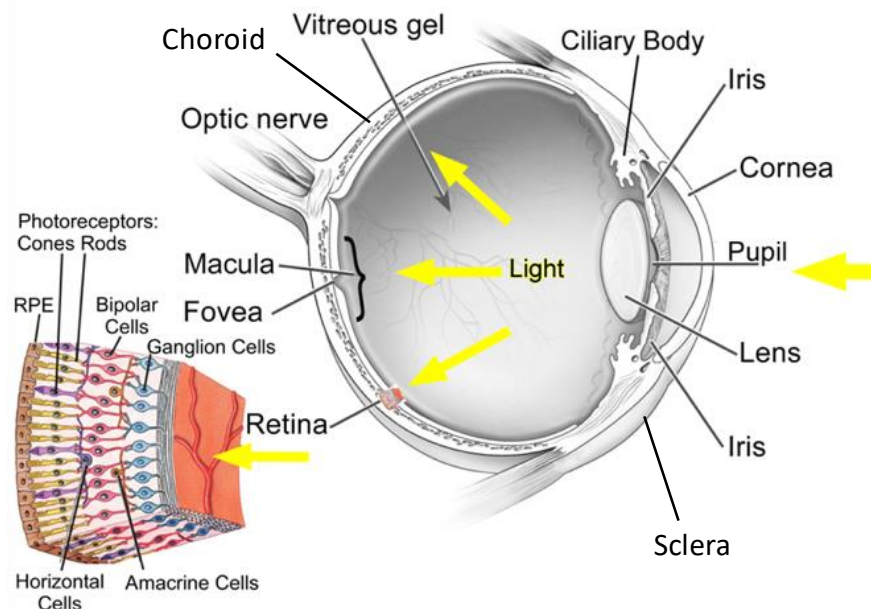
Figure 1.9. Gross anatomy of the eye [adapted from Vera-Díaz and Doble (2012)].

Neural retina is responsible for converting light energy to neural impulses that are passed on through the ganglion cells to the optic nerve and to the brain. The main

neural cell types in the retina are photoreceptors, bipolar cells and RGCs; the activity of these cells is regulated by horizontal and amacrine cells. The main types of photoreceptors are rods and cones, which are involved in dim light vision and fine resolution colour vision, respectively. Cones are mostly found in the macula and fovea, whereas rods are found predominantly in the peripheral retina. Bipolar cells form synapses primarily with photoreceptors, RGCs, and amacrine cells. Axons of RGCs form an optic nerve and eventually form synapses in the lateral geniculate nucleus of the thalamus connecting retinal impulses to the brain (Forrester *et al.*, 2008).

The RPE forms one of the blood-brain barriers of the eye. It faces Bruch's membrane with its basolateral membrane and photoreceptor outer segments with the apical membrane (Strauss, 2005). It is involved in light absorption and is essential for supporting a number of physiological processes including growth factor secretion in the form of pigment epithelium-derived growth factor (PEDF) and vascular endothelial growth factor (VEGF), phagocytosis of photoreceptor outer segments, retinol cycling and production of pigment (Ramsden *et al.*, 2013) (RPE functions are pictured in Figure 1.10).
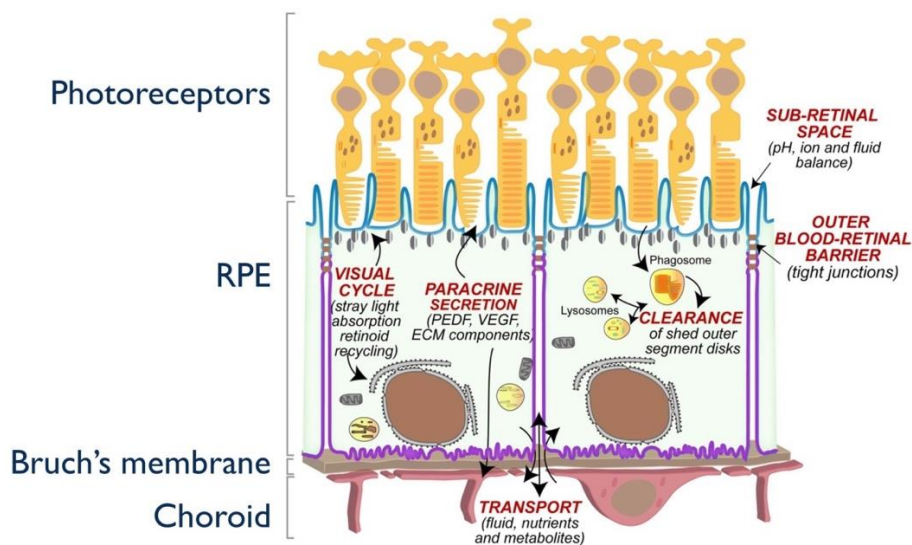
Figure 1.10. Summary of RPE functions [adapted from Toops *et al.* (2014)]. Basal layer of RPE cells lies adjacent to Bruch's membrane and apical layer is next to photoreceptors, where it forms a protective barrier.

In vivo, embryonic eye development commences in the fourth week as a result of complex interactions between embryological tissues. Prior to neural tube folding, optic sulci appear in the inner region of the neural plate which eventually will give rise to rostral diencephalon. Protrusion of the optic sulci leads to the formation of the optic

vesicles. Each optic vesicle extends until it contacts the surface ectoderm and as a consequence, it undergoes invagination to form the optic cup. The end of week eight is identified by the formation of the thin outer layer which will form RPE and a thick inner layer marking neural retina. First appearance of melanin within the embryonic RPE could be observed from day 28 of gestation. RPE cells show distinct hexagonal morphology and are homogenous in size. Mitotic activity is observed in early development and terminates at birth which leads to RPE growth by either enlargement or hypertrophy of the existing cells. At the optic cup stage, basal lamina of the RPE is recognisable and by 10 weeks, collagen fibrils are laid down beneath it (Forrester *et al.*, 2008) (Summarised in Figure 1.11).
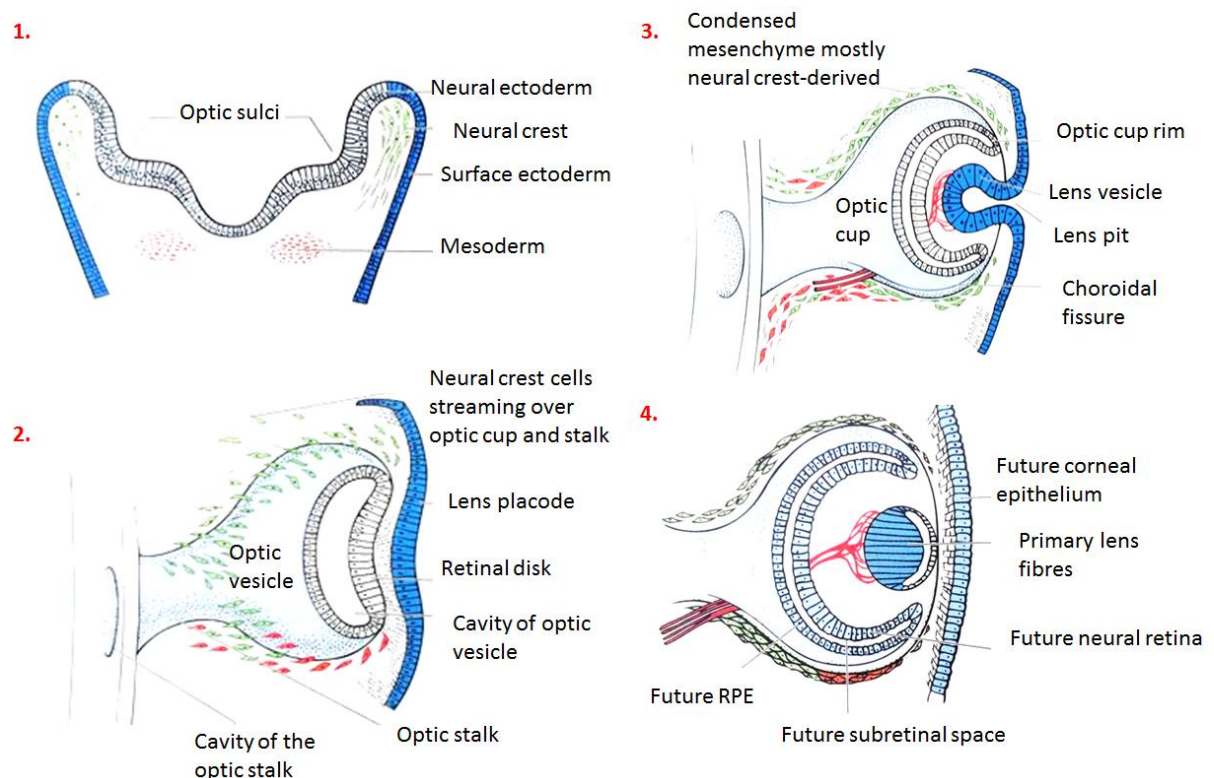
Figure 1.11. Schematic illustration of human retinal development *in vivo*. (1) Start of week 4 (day 22); (2) End of week 4 (day 27); (3) Start of week 5 (day 29); (4) Start of week 6 (day 37). [Adapted from Forrester *et al.* (2008)].

A number of molecular studies have shown that there are complex interactions between different retinal tissues and their formation could be interdependent. For example, formation of an optic vesicle and well-defined layers of neuroretina and RPE is dependent on fibroblast growth factors (FGFs) signalling from surface ectoderm, which drives the progenitor cells towards neural retina formation (Hyer *et al.*, 1998). Additionally, exposing RPE to bFGF has been shown to induce it to transdifferentiate into neural retina (Pittack *et al.*, 1991; Zhao *et al.*, 1995). Other

studies have shown that ablation of the surface ectoderm leads to optic vesicle formation with inverted localisations of retinal areas which could be a result of a lack of local signalling coming from the neuroepithelium of the brain, the mesenchyme or the RPE itself (Nguyen and Arnheiter, 2000).

Numerous studies have focused on identifying critical genes and transcription factors in ocular development. Retinal progenitor cell proliferation and optic vesicle formation is dependent on retinal homeobox protein *(RX)* (Mathers *et al.*, 1997). *PAX6* is expressed in anterior neural plate and together with LIM homeobox 2 (*LHX2)* is required for optic cup formation (Hill *et al.*, 1991; Porter *et al.*, 1997). Microphthalmia-associated transcription factor (*MITF)* has been shown to be critical in separation of an optic vesicle into RPE and neural retina (under the regulation of FGFs) becoming specifically restricted to RPE, whereas *CHX10* [same as visual system homeobox 2 (VSX2)] is characteristic of neural retina (Burmeister *et al.*, 1996; Nguyen and Arnheiter, 2000). Markers of different stages of retinal development are summarised in Figure 1.12.
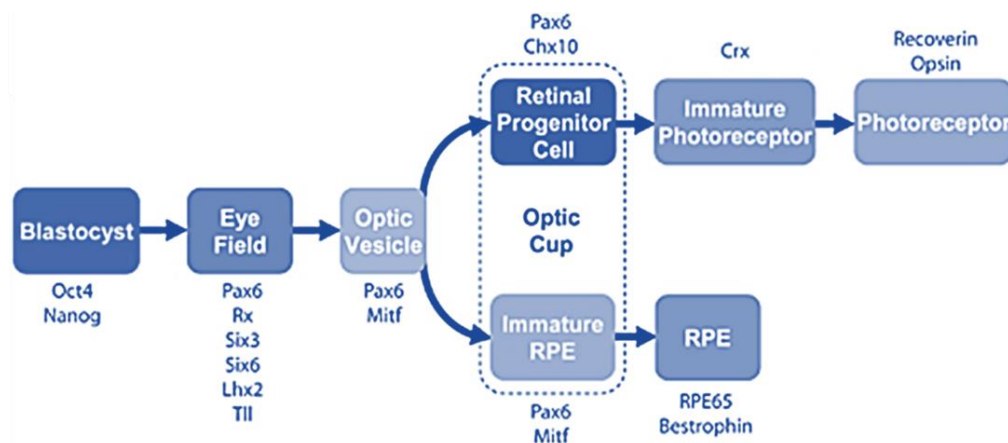
Figure 1.12. Markers identifying different stages of retinogenesis [adapted from Meyer *et al.* (2009)].

Borrowing the basic principles gained from developmental neurobiology, the field has identified a number of ways in which to direct pluripotent stem cells towards retinal fate. *In vitro* differentiation protocols have been developed for differentiation of hESCs and hiPSCs using two main principles: default differentiation in the absence of extrinsic factors, and differentiation with the addition of transcription factors, proteins and small molecules (Borooah *et al.*, 2013).

1.5.2 Default differentiation

In vivo, vertebrate neural development is a conserved process that generates distinct classes of progenitors that will make up the forebrain, midbrain, hindbrain and spinal cord (Stern *et al.*, 2006). Forebrain morphogenesis is more complex than in other parts of the CNS and results in the formation of ventrally positioned hypothalamus and caudally positioned diencephalon, dorsal telencephalon and ocular structures (Wilson and Houart, 2004). The default model of cell differentiation suggests that neural induction occurs in the absence of extrinsic factors, resulting in the differentiation to neural and retinal cell lineages (Munoz-Sanjuan and Brivanlou, 2002). hESCs and hiPSCs have been shown to recapitulate key events and follow the same principles of developent by differentiating into rostral telencephalic neuroectoderm in the absence of exogenous signalling molecules and presence of minimal media (Pankratz *et al.*, 2007; Hu *et al.*, 2010; Ozair *et al.*, 2013).

Differentiation to neuroectoderm occurs as a result of suppression of other cell lineages including mesoderm and endoderm. In the default model of differentiation it is believed to be a result of the inhibitory mechanisms on the BMP pathway (Tropepe *et al.*, 2001; Munoz-Sanjuan and Brivanlou, 2002). Extracellular antagonists such as Chordin and Noggin inhibit the BMP pathway which leads to induction of neuroectoderm with anterior positional identity (Wilson and Houart, 2004).

Early work on retinal differentiation showed that ESCs follow embryologic differentiation pathways and "spontaneously" differentiate. A pioneering study published by Yoshiki Sasai's group first showed that mouse ESCs are capable of spontaneously differentiating into retinal progenitors and form optic cup-like structures (Eiraku *et al.*, 2011). This study was followed by a study using hESCs demonstrating optic cup self-organisation (Nakano *et al.*, 2012). Studies using both hESCs and hiPSCs showed that differentiating cells go through different stages showing attributes of retinal progenitors and subsequently express more mature RPE and neuroretina markers (Klimanskaya *et al.*, 2004; Vugler *et al.*, 2008; Buchholz *et al.*, 2009). RPE cells are identified by the appearance of melanin pigment within four weeks and the display of typical cobblestone morphology similar to what is seen in primary cell cultures (Carr *et al.*, 2009). Spontaneous differentiation allows derivation of layers of RPE however the process is time consuming, relatively inefficient and could result in heterogeneous cell populations (Borooah *et al.*, 2013; Buchholz *et al.*, 2013). It has been suggested that hESCs display innate heterogeneity of the original stem cell populations and present differential propensity for differentiation based on

their histone modifications (Stewart *et al.*, 2006; Hong *et al.*, 2011). Additionally, some cells show bias toward certain retinal cell fates due to intrinsic difference in endogenous signalling molecules (Meyer *et al.*, 2009; Meyer *et al.*, 2011; Mellough *et al.*, 2012).

1.5.3 Directed differentiation

Retinal differentiation is controlled by a diverse set of signalling pathways which affect the regional identity of the resulting cell population. A number of studies used exogenous factors in order to direct differentiation towards the desirable retinal cell type more efficiently.

TGFβ and BMP pathways are involved in stem cell self-renewal and differentiation (Schmierer and Hill, 2007; Moustakas and Heldin, 2009). It has been shown that full neural conversion can be achieved using SB431542 and Noggin respectively as inhibitors generating neuroepithelium with rostral telencephalic identity (Chambers *et al.*, 2009; Chambers *et al.*, 2012). Mimicking development in a stepwise differentiation process using small molecules has been shown to produce retinal progenitors, RPE and photoreceptors with recombinant proteins Dickkopf-related protein 1 (DKK1) and left-right determination factor A (LEFTY-A), a Wnt and Nodal antagonists (Osakada *et al.*, 2008). A later study showed that similar efficiency could be achieved with small molecule CKI-7 which is known to act on casein kinase I and block Wnt, and an Activin receptor-like kinase-4 inhibitor SB431542 (Osakada *et al.*, 2009). Thus, these studies highlighted the importance of TGFβ, BMP, Wnt and Nodal signalling pathways in retinal fate commitment. Recently, it has been shown that *VSX2*, a transcription factor involved in proliferation of neural retinal progenitors, directly targets Wnt pathway thereby creating a fine balance between neural retina and RPE development (Capowski *et al.*, 2016). IGF1 signalling pathway has also been shown to be implicated in efficient differentiation of hESCs towards retinal progenitors, RPE, photoreceptors as well as 3D laminated retina (Lamba *et al.*, 2006; Mellough *et al.*, 2015). A recent study suggested that RPE differentiation is also regulated by non-coding regulatory RNA molecules, miRNAs, and in particular miR-184 (Jiang *et al.*, 2016). It was found that it targets and suppresses RAC-beta serine/threonine-protein kinase (*AKT2*) / mammalian target of rapamycin (mTOR) pathway thereby inhibiting cell proliferation and migration. Interestingly, patients with AMD show downregulation of miR-184 and upregulation of *AKT2* leading to reduction in lysosomal-associated membrane protein 1 (LAMP1) and as a result defects in

phagocytosis, suggesting one possible pathophysiological pathways of the disease. Miyagishima *et al.* (2016) showed that miRNA expression is unrelated to starting donor tissue or epigenetic status.

Some groups have tested variations in media composition by adding extra supplementation (Borooah *et al.*, 2013). B27 and N2 are known to promote retinal differentiation and are used widely in the field (Lu *et al.*, 2009; Meyer *et al.*, 2009; Meyer *et al.*, 2011; Mellough *et al.*, 2012; Buchholz *et al.*, 2013; Rowland *et al.*, 2013; Zhang *et al.*, 2013; Zhu *et al.*, 2013). Other conditions such as oxygen levels have been investigated as a possible modulator in cell differentiation. It has been previously suggested that in adult CNS oxygen levels are approximately 3% as opposed to the atmospheric 20% (Stacpoole *et al.*, 2011). There is growing evidence that oxygen levels during stem cell culture could have an implication on cell survival and differentiation at neuroectodermal stage (Stacpoole *et al.*, 2011). hESC and hiPSC studies showed that hypoxia was beneficial for derivation of retinal progenitor cells, whereas mESCs have been shown to have an improved efficiency in differentiating towards photoreceptors (Bae *et al.*, 2012; Garita-Hernandez *et al.*, 2013).

1.5.4 Differentiation to RPE

Molecular signature of differentiating RPE cells

A number of markers exist to identify different retinal cells types. The homeobox gene *OTX2* is expressed at pluripotent stem cell stage and is also required for the formation of the anterior neuroectoderm (Frantz *et al.*, 1994; Acampora *et al.*, 2013). *PAX6* and *RX* are expressed at the early eye field stage. At optic vesicle stage, neuroepithelial cells are able to become both RPE and neural retina. Expression of *PAX6* pre-determines RPE fate by targeting *MITF* promoter (Baumer *et al.*, 2003). Therefore, *PAX6* and *MITF* are upregulated and when the cells differentiate into RPE, *MITF* expression is increased whereas cells that are destined to differentiate towards neural retina suppress *MITF* and upregulate *CHX10* expression (Meyer *et al.*, 2009; Borooah *et al.*, 2013) (Figure 1.13).
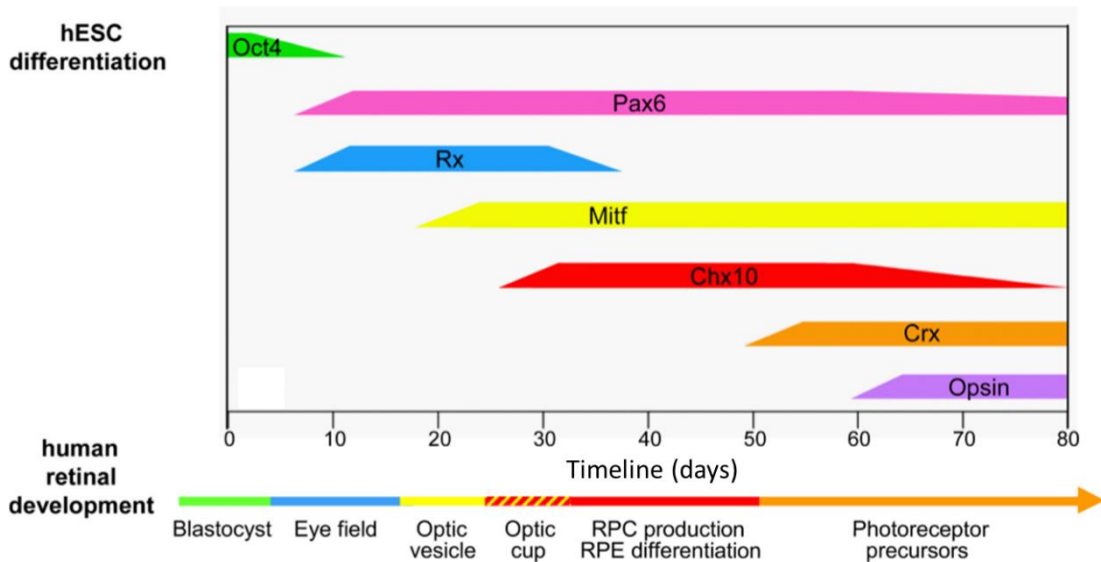
Figure 1.13. Retinal markers at different stages of hESCs differentiation [adapted from Meyer *et al.* (2009)].

Existing protocols for RPE differentiation from hPSCs

Differentiation protocols have been developed for derivation of RPE cells from both hESCs and hiPSCs (Klimanskaya *et al.*, 2004; Meyer *et al.*, 2009). Initial studies showed that RPE derived from hESCs express a similar genetic profile to primary human RPE cells and the resulting cell population initially goes through neuronal specification before attaining RPE features (Klimanskaya *et al.*, 2004). Further studies showed that it was possible to derive functional RPE cells capable of surviving sub-retinal transportation in rats with a functional defect of RPE (Lu *et al.*, 2009). Another study showed that hiPSCs-derived RPE cells were similar in function to foetal RPE and hESCs-derived RPE (Buchholz *et al.*, 2009). In this study, RPE were obtained by first removing bFGF from culture and later adding it for propagation of the resulting RPE sheets. However, the efficiency of differentiation was low and the first appearance of well-defined pigmented clusters ready for isolation was not observed until 40-90 days of differentiation. This issue was first addressed in 2009, when Idelson *et al.* (2009) showed that the addition of nicotinamide (Vitamin B3) together with Activin A substantially improved production of functional RPE cells with pigmented foci appearing after 4 weeks of differentiation. It was later suggested that at the early stages of neutralisation there is an increased mitochondrial respiration leading to oxidative stress and ROS leakage leading to apoptosis and the addition of nicotinamide has protective properties in the developing neuroectoderm (Cimadamore *et al.*, 2009). Subsequent studies showed that the addition of Activin A

augments generation of RPE and *MITF* expression from optic vesicle-like structures and results in the majority of cells in culture acquiring RPE morphology (Meyer *et al.*, 2011; Zhu *et al.*, 2013). Addition of sonic hedgehog (SHH) and retinoic acid (RA) together with Activin A did not show an improved yield or maturation of RPE (Zhang *et al.*, 2013). However, serial addition of SHH, RA, Noggin and bFGF generated 60% of *MITF* positive cells after 60 days of differentiation (Zahabi *et al.*, 2012). Other factors, such as NOGGIN, DKK1 and IGF1 were shown to be favourable for generation of retinal progenitor cells with over 80% expressing *Pax6* and *Chx10* (Lamba *et al.*, 2006). Based on the studies described above, Buchholz *et al.* (2013) showed efficient production of pigmented RPE sheets as early as 14 days after the start of differentiation with an efficiency of 80% by combined use of IGF1, NOGGIN, DKK1, bFGF, nicotinamide and Activin A resulting in expandable population of cells. Another group aimed at replacing growth factors and complex differentiation protocols with the use of small molecules. They screened a library of 300 compounds and identified chetomin as a potent promoter of RPE identity when used in combination with nicotinamide (Maruotti *et al.*, 2015).

Together with the addition of various factors, different groups have also looked at the effect of culture conditions on differentiation. Some groups have tested the initial differentiation steps in adherent cultures by allowing cells to overgrow and subsequently removing mitogens from culture and allowing the cells to differentiate (Klimanskaya *et al.*, 2004; Vugler *et al.*, 2008; Buchholz *et al.*, 2009; Liao *et al.*, 2010; Zhang *et al.*, 2012; Buchholz *et al.*, 2013; Rowland *et al.*, 2013). Patches of pigmented cells are normally seen from 14 to 90 days and when they reach the size of ~1mm, they are mechanically dissected, re-plated and propagated. Some groups expand cells in the same media as differentiation media, whereas others add bFGF or FBS (Buchholz *et al.*, 2009; Liao *et al.*, 2010; Zhang *et al.*, 2012). Groups also vary substrate that they use for cell culture including mouse embryonic fibroblasts, human embryonic fibroblasts and feeder-free matrices.

Substrates and culture conditions used for differentiation and growth of RPE cells

The use of animal-derived feeder layers could potentially introduce the risk of transmitting animal pathogens to human cells (Martin *et al.*, 2005). Human feeder cells have also been successfully utilised in RPE differentiation protocols with hESCs however they have not been extensively studied in their applications to hiPSCs

differentiation (Zhang *et al.*, 2012; Sorkio *et al.*, 2014). Some studies have reported that feeder-free cultures produced pigment faster (Klimanskaya *et al.*, 2004). Some studies have also looked at the effect of different extracellular matrix (ECM) proteins on hPSCs differentiation. *In vivo*, the RPE cell layer is supported by Bruch's membrane which contains several ECM proteins important to RPE including laminin-111, -332, -511 and -521, collagen I and IV, fibronectin and vitronectin (Rowland *et al.*, 2013). Rowland *et al.* (2013) showed that laminin-111 and matrigel are ideal substrates for generating high yields of RPE. This study provided a useful insight into the importance of the choice of ECM however the cells were cultured for a relatively short period of time (4-5 weeks until pigmentation and further 80 days to allow for enrichment) with a limited number of functional assays. A more recent study used laminin-521 and showed that hESC-RPE cells were similar to native RPE and showed integration and survival after sub-retinal transplantation into rabbits (Plaza Reyes *et al.*, 2016). A study by a different group did a more extensive analysis using several human ECM proteins including collagen I and IV, laminin, fibronectin, vitronectin and commercial substrates CELLstart and matrigel (Sorkio *et al.*, 2014). The cells were cultured for an extended period of time for a total of 140 days and specific RPE proteins were investigated as well as epithelial polarisation, phagocytic activity and transepithelial resistance as a measure of the integrity of the RPE layer. Although, different ECMs have shown to be heterogeneous in their performance in different tests, it was concluded that overall collagen IV was the most favourable for enrichment and maturation of functional RPE cells (personal communication; Dr Tanja Ilmarinen, University of Tampere). It is possible to propagate hPSC-derived RPE cells for several passages however after they reach senescence they lose some of the key features (Singh *et al.*, 2013). Additionally, cells express DNA damage and telomere shortening (Kokkinaki *et al.*, 2011).

Another popular method for inducing RPE fate is through neurosphere formation at the initial stages of neuroectoderm induction and subsequently plating the aggregates into adherent culture (Klimanskaya *et al.*, 2004; Meyer *et al.*, 2009; Meyer *et al.*, 2011; Gong *et al.*, 2015). A classical way of generating pigment is through gradual reduction of knock-out serum replacement in culture, however xeno-free defined culture conditions have also been shown to be able to produce functional RPE cells (Vaajasaari *et al.*, 2011; Plaza Reyes *et al.*, 2016).

Although few studies have compared two of the culture methods directly, some of the groups reported that differentiation in adherent cultures is more

favourable when compared to differentiation in suspension (Vugler *et al.*, 2008; Rowland *et al.*, 2013). Combining two of the culture conditions is possible by first culturing cells as neurospheres in matrigel and subsequently plating them down for further expansion (Zhu *et al.*, 2013).

A summary of previously published RPE differentiation protocols has been provided in Table 1.2.

hPSCs to retinal cells	Differentiation method	Substrate	Length of differentiation / first appearance of pigment	References
hESCs / hiPSCs to RPE	Monolayer spontaneous differentiation by removal of bFGF.	ECMs identified as the most favourable: mouse laminin-111, matrigel	21-33 days	(Rowland *et al.*, 2013)
hESCs / hiPSCs to RPE	Monolayer differentiation with the addition of Noggin, IGF1 and DKK1.	Matrigel	14 days	(Buchholz *et al.*, 2013)
hESCs / hiPSCs to RPE	3D culture in the presence of matrigel, KOSR, Activin A, N2 and B27.	hESC-qualified matrigel	18-30 days	(Zhu *et al.*, 2013)
hESCs to RPE	Monolayer differentiation in the presence of KOSR with RA and SHH, or Activin A. With the additional supplementation with N2 and B27.	hESC-qualified matrigel	3 weeks after Activin A treatment; 35 days with RA and SHH	(Zhang *et al.*, 2013)

hESCs / hiPSCs to RPE	Monolayer spontaneous differentiation by removal of bFGF in the presence of KOSR and FBS.	Gelatin	20-35 days	(Buchholz *et al.*, 2009)
hESCs to RPE	Monolayer spontaneous differentiation without bFGF.	Matrigel	3-4 weeks	(Zhang *et al.*, 2012)
hESCs / hiPSCs to retinal cells	Spontaneous differentiation in 3D culture with N2 and heparin or B27. In some experiments cells were then plated as monolayer.	Laminin for monolayer differentiation	30-50 days	(Meyer *et al.*, 2009)
hESCs to RPE	Spontaneous differentiation in the presence of KOSR and FBS.	Gelatin	6-8 weeks	(Klimanskaya *et al.*, 2004)
hESCs / hiPSCs to RPE	3D culture with subsequent plating in the presence of KOSR, Wnt and Nodal inhibitors CKI-7 and SB431542.	Poly-D-lysine-laminin fibronectin	35-140 days	(Osakada *et al.*, 2009)
hESCs to RPE	Spontaneous differentiation in floating cultures in the presence of N2 and heparin. Then B27 (-RA).	Laminin	40 days	(Capowski *et al.*, 2014)
hESCs to RPE	Monolayer spontaneous differentiation.	Growth factor reduced matrigel	4-5 weeks	(Lane *et al.*, 2014)

hiPSCs to RPE	Cells were allowed to overgrow for 8-14 days, until changing the medium to X-VIVO 10.	Matrigel	4-6 weeks	(Croze *et al.*, 2014)
hESCs / hiPSCs to RPE and neural retina	On day 4, differentiation was initiated with: DMEM/F12, 0.1 mM NEAA, 2 mM L-glutamine, 1% N2. By day 7, aggregates were transferred to adherent culture. On day 14 medium changed to: Neurobasal, 14% KOSR, 0.1 mM NEAA, 2 mM L-glutamine, 10 mM Nicotinamide. Days 18–22, Activin A (20 ng/ml).	Mouse embryonic fibroblasts	44 days	(Wang *et al.*, 2015)
hESCs to RPE	Adapted from (Buchholz *et al.*, 2013). Included 3 µM CHIR99021 from day 8 to 14. On day 14, RPE cells were manually enriched to passage 0 and maintained in X-VIVO 10 supplemented with 10 µM Y-27632 for 4 to 7 days.	Matrigel	97.77% PMEL17 positive cells at day 14	(Leach *et al.*, 2015)
hiPSCs to RPE	EB differentiation with GMEM, 0.1 mM NEAA, 1 mM pyruvate, 0.1 mM 2-mercaptoethanol. 20% KOSR for three days, then 15% KOSR for 9 days, and finally 10% KOSR. 5 µM CKI-7 and 5 µM SB431542 were added for 21 days during suspension culture, then plated down.	Matrigel	10 weeks	(Li *et al.*, 2016)

hiPSCs to RPE	hiPSC colonies were lifted and grown as uniform EBs in AggreWell™ plates (STEMCELL Technologies) for 4 days in EB formation medium (STEMCELL Technologies). At day 5, medium changed to DMEM/F12, 1% N2, MEM NEAA and 2 µg/mL heparin. At day 7, aggregates were plated onto laminin-coated culture plates for an additional 10 days. At day 16, medium replaced with: DMEM/F12 (3:1), 2% B27 (- RA), MEM NEAA and penicillin/streptomycin. After re-plating pigmented patches, cells cultured with 10% FBS, then 2% FBS until confluent. Thereafter, FBS was removed.	Laminin	60-90 days	(Gong *et al.*, 2015)
hiPSCs to RPE	Monolayer differentiation. Day 1: DMEM/F12, 15% KOSR, 2mM Glutamine, 0.1 mM NEAA, 1% Anti-Anti, 0.1 mM β-Mercaptoethanol. Day 2 – Day 16: addition of 10 mM nicotinamide, 25-100 nM chetomin. Day 17: DMEM (70% vol/vol), F12 (30% vol/vol), B27, Anti-Anti.	Synthetic vitronectin peptide-acrylate surfaces	1 month	(Maruotti *et al.*, 2015)
hESCs to RPE	3D method with xeno-free NutriStem hESC XF medium without bFGF and TGFβ.	Recombinant human laminin-521	3 weeks	(Plaza Reyes *et al.*, 2016)

Table 1.2. Summary of some published RPE differentiation protocols.

The field has identified a number of ways by which to characterise hPSC-derived RPE cells. These are summarised in Table 1.3.

Characteristic	Verification method / Marker
Morphology	Polygonal monolayer of pigmented cells ("cobblestone" morphology) verified with light microscopy Electron micrograph to show ultra-structural compartments
Early eye field transcription factor network	*OTX2, LHX2, RX, SIX, SIX6, Tll*
Optic vesicle markers	*PAX6, MITF*
RPE-specific markers	<u>Terminally differentiated RPE</u> MITF, CRALBP, RPE65, BEST1, MERTK, COLLAGEN IV <u>Tight junction proteins</u> Claudin, ZO1 <u>Pigment synthesis</u> Tyrosinase, Silver (Pmel17) <u>Polarity / growth factor secretion</u> PEDF (secreted apically) VEGF (secreted basally) Na^+/K^+ATPase staining (apical) BEST1 (basal) <u>Vectorial fluid flow</u> Aquaporin expression
Functional characterisation	Rod outer segment phagocytosis assay Sub-retinal injection of cells in animal models of RPE deficiency
RPE layer integrity	Transepithelial resistance Electrical impedance spectrum

Table 1.3. Examples of assays for verification of RPE cells derived from hPSCs (Rowland *et al.*, 2012; Borooah *et al.*, 2013; Juuti-Uusitalo *et al.*, 2013; Wright *et al.*, 2014; Miyagishima *et al.*, 2016).

There is no minimum requirement for the specific tests needed to be performed for classifying cells as RPE cells. However, some of the methods described in Table 1.3 are used more often than others, for example, confirming the morphology of the cells to appear "cobblestone", looking for the expression of RPE markers, such as MITF, RPE65, and CRALBP, and most importantly, confirming their functional maturity by performing the phagocytosis of photoreceptor outer segments assay. Therefore, these tests should comprise the minimum for confirming RPE status of the cells.

1.6 Aims and objectives

The aim of this research project was to investigate the pathological links between retinal degeneration, specifically RPE cells, and mitochondrial dysfunction seen in patients with the m.3243A>G mutation using hiPSCs as a tractable disease model. Specifically, during this project, it was aimed to:

- Create an hiPSC disease model for the m.3243A>G mutation
- Optimise RPE differentiation protocol using hESCs
- Assess the impact of the m.3243A>G mutation on RPE cells derived from hiPSCs with this mutation

1.7 Hypothesis

The main hypothesis was that reprogramming of fibroblasts from patients with the m.3243A>G mutation would result in the generation of hiPSC clones with varying heteroplasmy levels. It was expected for hiPSC-derived RPE cells to show deficiencies similar to those found in patient tissues and provide a novel model for retinal pathogenesis in patients with the m.3243A>G.

Chapter 2. Methods

2.1 Patients and healthy controls information

Adult human dermal fibroblasts (HDFs) used for the generation of control hiPSC lines were either obtained from Lonza (Control 1 (SB-Ad5), 57 year-old female), or obtained from a healthy control patient (Control 2 (SUN007), 74 year-old male) by Mr David Steel, Consultant Ophthalmologist, Sunderland Eye Infirmary. hiPSCs Ad2 (referred to as Control hiPSCs) were reprogrammed and characterised by Mrs Adriana Buskin using adult HDFs (Lonza) obtained from a 51 year-old male with no known clinical abnormalities. Skin biopsies from patients harbouring the m.3243A>G mutation were taken by Mr Patrick Yu Wai Man, Consultant Ophthalmologist, Royal Victoria Infirmary (Newcastle-upon-Tyne).

Patient 1 cells (F216) came from a 73 year-old female presenting with bilateral pigmentary macular degeneration (sparing left fovea), and significant visual acuity deterioration over the past ten years (visual acuities: right eye 6/60, left eye 6/9), insulin-treated type 2 diabetes mellitus and bilateral sensorineural hearing loss. The patient does not have any significant neurological deficits. Patient 2 cells (F350) came from a 62 year-old male with insulin-treated type 2 diabetes mellitus, bilateral sensorineural hearing loss and extensive macular geographic atrophy (visual acuities: right eye 6/36, left eye 6/36). Patient 3 cells (F217) came from a 61 year-old male who is the brother of Patient 1. Patient 3 has no pigmentary retinopathy or maculopathy and has normal vision in both eyes (visual acuities: right eye 6/6, left eye 6/6). He has insulin-treated type 2 diabetes mellitus and significant neurological deficits including bilateral sensorineural hearing loss, ataxia, peripheral neuropathy and epilepsy. Patients' ocular phenotype and proportion of m.3243A>G in different tissues is summarised in Table 2.1. All samples were obtained as part of a NHS research ethics committee approved biobank for fibroblasts from patients with retinal disease and based at the Institute of Genetic Medicine (ethics number 11/NE/0294), Newcastle University.

Patient, Age / Gender	Fundus images	Ocular phenotype	% m.3243A>G		
			Blood	Urine	Skeletal muscle
Patient 1, 73/F		• bilateral pigmentary macular degeneration (sparing left fovea) • significant visual acuity deterioration over the past ten years • visual acuities: right eye 6/60, left eye 6/9	10%	49%	*No data*
Patient 2, 62/M		• extensive macular geographic atrophy • visual acuities: right eye 6/36, left eye 6/36	*No data*	*No data*	*No data*
Patient 3, 61/M		• no pigmentary retinopathy or maculopathy • normal vision in both eyes • visual acuities: right eye 6/6, left eye 6/6	*No data*	66%	67%
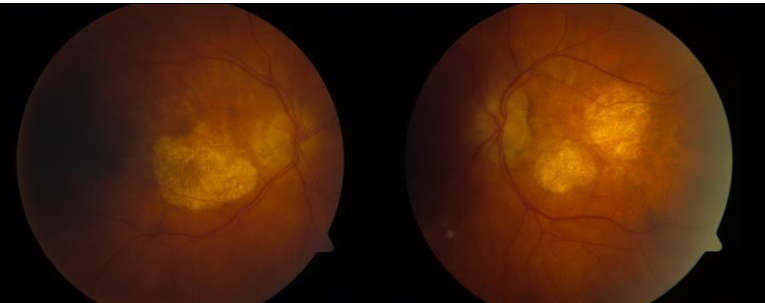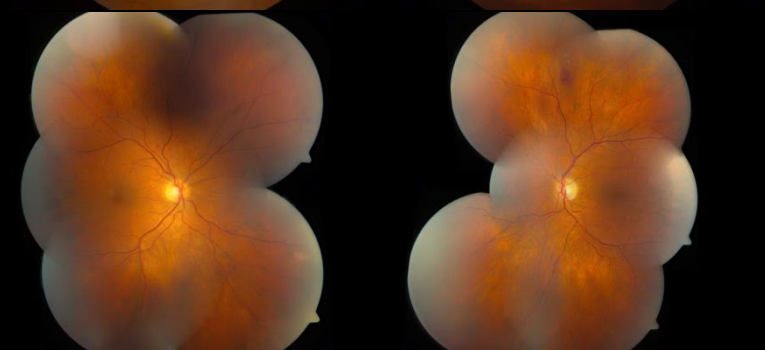
Table 2.1. Patient information.

2.2 Cell culture

2.2.1 Human fibroblast culture

Cells were maintained in fibroblast medium containing Advanced DMEM (Dulbecco's Modified Eagle Medium), high glucose (Life Technologies), supplemented with 10% Fetal Bovine Serum (FBS) (Life Technologies), 1% 100X GlutaMAX (Life Technologies), 1% Penicillin-Streptomycin (Life Technologies). When confluent, fibroblast cells were passaged with 0.05% Trypsin-EDTA (1X) solution (Life Technologies). For all cell culture experiments, cells were maintained in a humidified tissue culture incubator (37°C, 5% CO_2, 20% O_2). Additionally, for all cell culture experiments with MELAS cells 0.05 mg/ml uridine (Sigma) was added to the medium.

2.2.2 Preparation of mouse embryonic fibroblasts feeder layer

Mouse embryonic fibroblasts (MEFs) were derived and prepared by Dr Georgios Anyfantis from 12.5 – 13.5 day old embryos from Swiss MF1 mice. Fibroblasts were isolated via dissection and cultured in T75 flasks at a density of $13 – 15 \times 10^4$ cells per flask in fibroblast medium. Once confluent, the MEFs were mitotically inactivated by being subjected to irradiation using a Faxitron CP-160 radiation machine at a dose of 120 kV, 4.0 mA for 7 minutes and let to recover in an incubator for 1 hour. The irradiated MEFs were then harvested with 0.05% Trypsin-EDTA (1X) solution and plated on tissue culture plates pre-coated with 0.2% gelatin at a density of 1.5×10^4 cells/cm^2 and incubated for 24 hours prior to use.

2.2.3 Preparation of MEF conditioned medium

Proliferating MEFs were let to achieve 80 – 90% confluence and were subsequently irradiated using a Faxitron CP-160 radiation machine at a dose of 120 kV, 4.0 mA for 7 minutes and let to recover in an incubator for 1 hour. The cells were then harvested using 0.05% Trypsin-EDTA (1X) solution and plated in tissue culture flasks at a density of 5.6×10^4 cells/cm^2 in fibroblast medium. On the following day, the medium was changed to Knock-Out DMEM (Life Technologies) with 20% Knock-Out Serum Replacement (Life Technologies) (KOSR), 1% 100X MEM Non-Essential Amino Acids Solution (Life Technologies), 1% GlutaMAX (Life Technologies) and 1% Penicillin-Streptomycin Solution (Life Technologies). For the next 9 days, the medium was collected each day replacing it with fresh medium. Prior to use the medium was supplemented with 1% Insulin–Transferrin–Selenium (Life Technologies), 8 ng/ml

basic fibroblast growth factor (bFGF) (Life Technologies) and filtered through a 2 μm filter.

2.2.4 Induced pluripotent stem cell generation

Control and patient fibroblasts were seeded onto a 12-well plate at a density of 1×10^5 cells per well and cultured in fibroblast medium. 24 hours later the cells were transfected with the CytoTune®-iPS Sendai Reprogramming Kit (CytoTune 1) containing four reprogramming vectors expressing Yamanka factors: *hOCT3/4*, *hSOX2*, *hKLF4*, *hc-MYC* at multiplicity of infection (MOI) = 3 or CytoTune®-iPS 2.0 Sendai Reprogramming Kit (CytoTune 2) containing three reprogramming vector preparations: polycistronic *KOS*, *hKLF4*, and *hc-MYC* at MOI = 5-5-3 (Thermo Scientific). The medium was changed every other day for the next 7 days. On day 7 post transduction, cells were passaged on a 6-well plate either on irradiated MEF feeder layer or in feeder-free experiments on plates pre-coated with 0.08 mg/ml Matrigel® Basement Membrane Matrix (matrigel) (Corning). Cells on MEFs were plated at a density of 8×10^3 cells per well initially in hPSC medium with Knock-Out DMEM (Life Technologies), 20% KOSR (Life Technologies), 1% 100X MEM Non-Essential Amino Acids Solution (Life Technologies), 1% GlutaMAX (Life Technologies), 1% Penicillin-Streptomycin Solution (Life Technologies), and 8 ng/ml bFGF (Life Technologies). The medium was changed to conditioned medium seven days later. Cells cultured on matrigel were plated at a density of 50×10^3 cells per well and maintained in mTeSR™1 medium (STEMCELL Technologies) supplemented with 1% Penicillin-Streptomycin Solution (Life Technologies). The medium was changed every day thereafter. When visible hiPSC colonies with hESC-like morphology had developed and established (4 – 5 weeks), they were manually dissected out with a 10 μl pipette tip and re-plated on a 4-well plate either on MEFs or pre-coated with matrigel one colony per well and further expanded first on a 12-well and then on a 6-well plate.

2.2.5 Human pluripotent stem cell culture

hESC line H9 obtained from WiCell (Madison, WI) and the derived MELAS and control hiPSCs were maintained on either irradiated MEF feeder layer or on matrigel in hPSC medium or mTeSR™1 medium (STEMCELL technologies) respectively. The medium was changed daily. The areas of differentiation were mechanically removed

daily under a stereomicroscope using a 10 µl micropipette tip. The cells cultured on MEFs were passaged 1:3 either mechanically or by treating them with 1 µg/ml Collagenase type IV in hPSC medium solution (Life Technologies) for 5 – 10 minutes. The cells that were cultured on matrigel were passaged 1:6 with Versene® (EDTA) 0.02% solution (Lonza). Cells derived on MEFs were adapted to feeder-free culture conditions by re-plating them on plates pre-coated with matrigel in mTeSR1 medium prior to using in downstream analyses and experiments.

2.2.6 Retinal pigment epithelium differentiation and expansion

For the RPE differentiation experiments, hPSCs on matrigel were grown to different densities: normal density and overgrown density, where the cells were let to grow until no distinct borders between the colonies could be observed. On day 1 of differentiation, the medium was changed to RPE differentiation medium (different medium combinations are summarised in Table 2.2) and replaced every day for the first 3 weeks and twice a week thereafter. Differentiation continued for 3 – 4 months. When pigmented areas reached 3 – 5 mm in size, they were mechanically dissected out under a stereomicroscope using a 10 µl pipette tip, dissociated with TrypLE™ Select Enzyme (1X) or (10X) (Life Technologies), filtered through a 40 µm cell strainer (Fisher Scientific) and re-plated for enrichment and maturation at a density of 4.5×10^5 cells per cm^2 on plates or 0.33 cm^2 PET hanging cell culture inserts (Merck Millipore) pre-coated with laminin from human placenta (5 mg/ml), collagen IV or fibronectin (both 5 µg/cm^2) (all Sigma-Aldrich), or growth factor reduced matrigel.

Base medium	Additional supplementation for differentiation optimisation experiments
mTeSR™1 with 1% Penicillin-Streptomycin	None
Dulbecco's Modified Eagle Medium: Nutrient Mixture F-12, GlutaMAX™ (DMEM/F12) (Life Technologies) with 1% 100X MEM Non-Essential Amino Acids Solution and 1% Penicillin-Streptomycin Solution	None
	B-27® Supplement (50X) (B27) (Life Technologies)
	B27 and N-2 Supplement (100X) (N2) (Life Technologies)
	B27 and 5 ng/ml human Insulin-like Growth Factor-I (IGF1) (Sigma-Aldrich)
	B27, N2 and IGF1
RPMI 1640 Medium (RPMI) (Life Technologies) with 1% 100X MEM Non-Essential Amino Acids Solution and 1% Penicillin-Streptomycin Solution	None
	B27
	B27 and N2
	B27 and IGF1
	B27, N2 and IGF1
Advanced RPMI 1640 Medium (AdRPMI) (Life Technologies) with 1% 100X GlutaMAX, 1% Penicillin-Streptomycin	None
	B27
	B27 and N2
	B27 and IGF1
	B27, N2 and IGF1

Table 2.2. RPE differentiation medium composition.

2.2.7 In vitro differentiation into three germ layers

In order to assess the ability of hiPSCs to spontaneously differentiate into cell types representative of the three embryonic germ layers, two different experiments were performed: spontaneous differentiation in suspension culture with embryoid body (EB) formation, or differentiation of cells as a monolayer. For the EB formation experiment, cells from two 6-well plates were incubated with 1 ml of 1:1 solution of Collagenase type IV (Life Technologies) powder dissolved in hPSC medium to a concentration of 1 mg/ml and Dispase II (Life Technologies) powder dissolved in Knock-Out DMEM (Life Technologies) to a concentration of 0.5 mg/ml. The solution was then filtered through a 0.2 μm filter. Cells were incubated for 40 minutes at 37 °C

checking for colony detachment. Cells were then collected into a 50 ml conical tube, let to settle and re-suspended in EB formation medium containing DMEM/F-12 (Life Technologies), 20% FBS (Life Technologies), 1% Penicillin-Streptomycin Solution (Life Technologies) and 1% MEM Non-essential Amino Acids Solution (Life Technologies). Cells were then transferred to a 10 cm Petri dish and cultured for 7 days replacing medium every day. On day 8, the EBs were transferred to a 24-well plate pre-coated with 0.1% gelatin replacing the medium daily. For spontaneous monolayer differentiation experiments, cells were let to grow to a normal density and the medium was changed to EB formation medium and replaced daily for 14 days. Cells were then collected with the cell scraper, washed and stored as pellets at -80°C until further use.

2.3 Teratoma formation

Teratoma induction from the hiPSCs was undertaken by Prof L. Armstrong & Prof M. Lako, Newcastle University. Cells were injected subcutaneously into 8 weeks old male ICRF-Foxn1[nu] mice (Harlan Laboratories) at a concentration of 5×10^5 cells per 100 µl of PBS + 2% FBS pre-mixed with 100 µl of matrigel. Two mice were used per cell line. From three weeks after the injection onwards, mice were monitored weekly for the appearance of tumours for up to 12 weeks.

2.4 DNA extraction

DNA was isolated using the QIAamp DNA Mini Kit (Qiagen), following the instructions of the manufacturer. The purity of the DNA was checked with NanoDrop 2000 spectrophotometer expecting the A_{260}/A_{280} ratio to be ~1.8. Isolated DNA was stored at -20°C.

2.5 RNA extraction

Cells were harvested using a cell scraper (Sarstedt) or normal passaging treatment, washed with phosphate-buffered saline (PBS) (Life Technologies), pelleted and stored at -80°C until further analysis. RNA was isolated using ReliaPrep™ RNA Cell Miniprep System (Promega) following the instructions of the manufacturer. The purity of RNA was confirmed using NanoDrop 2000 spectrophotometer expecting the A_{260}/A_{280} ratio to be ~2.0.

2.6 cDNA synthesis

Complementary DNA (cDNA) was synthesised subsequently to RNA extraction from 1 mg of total RNA in 40 µl volume using GoScript™ Reverse Transcription System (Promega) according to the manufacturer's instructions. The resulting product was stored at -20°C.

2.7 Polymerase chain reaction

2.7.1 Sendai clearance experiments

The primary polymerase chain reaction (PCR) was a 20 µl GoTaq® DNA polymerase (Promega) reaction with 5X GoTaq® Reaction Buffer (1.5 mM $MgCl_2$, 0.2 mM dNTP), 1 µM forward and reverse primers, 0.025 U/µl GoTaq® DNA Polymerase and dH_2O. PCR program: denaturation 95°C 30 seconds, annealing 30 seconds, elongation 72°C 30 seconds for 35 cycles (primer sequences and specific annealing temperatures are shown in Table 2.3). The products were analysed by standard 2% agarose gel (Lonza) electrophoresis using GelRed™ (Biotium) at a concentration of 1:10 000 as a nucleic acid dye. The appearance of bands was visualised with a UV transilluminator (Gel Doc-II Imaging system).

Target	Primer sequence	Product size (bp)	Annealing temperature (°C)
SeV	**Forward:** GGATCACTAGGTGATATCGAGC **Reverse:** ACCAGACAAGAGTTTAAGAGATATGTATC	181	61
KOS	**Forward:** ATGCACCGCTACGACGTGAGCGC **Reverse:** ACCTTGACAATCCTGATGTGG	528	64
hKLF4	**Forward:** TTCCTGCATGCCAGAGGAGCCC **Reverse:** AATGTATCGAAGGTGCTCAA	410	63
hc-MYC	**Forward:** TAACTGACTAGCAGGCTTGTCG **Reverse:** TCCACATACAGTCCTGGATGATGATG	532	58
GAPDH	**Forward:** TGCACCACCAACTGCTTAGC **Reverse:** GGCATGGACTGTGGTCATGAG	87	60

Table 2.3. Primer sequences and annealing temperatures for Sendai clearance experiments.

2.7.2 Pyrosequencing experiments

Primers for PCR and pyrosequencing were designed using PyroMark® Assay Design SW 2.0 (QIAGEN) prior to the start of the PhD project.

PCR was set up with 50 ng DNA template. The primary PCR was a 25 µl MyTaq™ HS DNA Polymerase reaction (Bioline) with 5x MyTaq Reaction Buffer (3 mM MgCl$_2$, 1 mM dNTP), 0.4 µM forward and reverse primers, 5 U/µl MyTaq HS DNA Polymerase and dH$_2$O. PCR program: denaturation 95°C 15 seconds, annealing 65°C 30 seconds, elongation 72°C 10 seconds for 30 cycles (primer sequences are shown in Table 2.4). The products were analysed by standard 2.5% agarose gel electrophoresis using GelRed™ at a concentration of 1:10 000 as a nucleic acid dye. The appearance of bands was visualised with a UV transilluminator (Gel Doc-II Imaging system).

Target	Primer sequence	Position of primer
m.3243A>G	**Forward:** *BIO-TAAGGCCTACTTCACAAAGCG	3142-3353
	Reverse: GCGATTAGAATGGGTACAATGAG	3258-3244
	Sequencing: ATGCGATTACCGGGC	

Table 2.4. Primer sequences for pyrosequencing experiments. BIO – biotinylated.

Assay set up was created using PyroMark® Q24 Software (QIAGEN). Pyrosequencing was completed on PyroMark Q24 (QIAGEN) according to the manufacturer instructions. Briefly, 10 µl of the PCR product was added to 40 µl of binding buffer, 2 µl streptavidin-coated Sepharose® beads and 28 µl of high purity H$_2$O. The samples were agitated at 1400 rpm for 10 minutes to bind the DNA to the beads. The PyroMark vacuum workstation was used to wash the DNA with 70% ethanol, denaturation solution and wash buffer. The product was eluted in 25 µl annealing buffer containing 0.3 µM sequencing primer. The results were analysed using PyroMark® Q24 Software.

2.8 Quantitative PCR

2.8.1 Quantification of mtDNA copy number and mitochondrial common deletion levels

mtDNA was quantified using CFX96 Touch™ Real-Time PCR Detection System (Bio-Rad). Reaction volume was 20 µl containing iTaq™ Universal Probes Supermix (Bio-Rad), 0.3 µM forward and reverse primers and sample DNA.

Standard curves were used in order to ensure reaction efficiency and accurate quantification. Standard PCR reactions were run for each primer set to generate templates covering the amplification region of the quantitative PCR (qPCR). PCR

reaction conditions were as follows: initial denaturation at 95°C for 15 seconds, denaturation at 95°C for 15 seconds, annealing and extension at 61°C for 15 seconds, elongation at 72°C for 10 seconds for 30 cycles. The products were run on 1% agarose gel using GelRed™ at a concentration of 1:10 000 as a nucleic acid dye. The bands were dissected out under the UV transilluminator (Gel Doc-II Imaging system) and the product extracted and purified using QIAquick Gel Extraction Kit (Qiagen) according to the manufacturer's instructions. The amount of total DNA was quantified with NanoDrop 2000 spectrophotometer and mtDNA copy number was calculated using the following equation:

mtDNA copy number = [C ÷ (L x 2 x 330)] x A

C – total DNA concentration (10^{-9} nL)

L – amplicon length (bp)

A – Avogadro's number

Once copy number was calculated, the templates were serially diluted with dH_2O to generate standard curves with 1×10^9 to 1×10^1 copies. qPCR was performed in triplicate reactions using iTaq™ Universal Probes Supermix system (Bio-Rad). The data were analysed using the Bio-Rad CFX Manager software (Bio-Rad). mtDNA was quantified using the $2^{-\Delta\Delta Ct}$ method, where copy number equals $2 \times (2^{-\Delta\Delta Ct})$. *B2M* was used as a nuclear reference gene. For the quantification of the common deletion levels, the ratio of *MTND1* and *MTND4* was used. The method for mtDNA copy number quantification was modified from a previous publication (Pyle *et al.*, 2007). Probe and primer details can be found in Table 2.5, Table 2.6 and Table 2.7.

Target	Primer sequence	Product size (bp)	Annealing temperature (°C)
B2M	**Forward:** CGCAATCTCCAGTGACAGAA **Reverse:** GCAGAATAGGCTGCTGTTCC	1092	61
MTND1	**Forward:** CAGCCGCTATTAAAGGTTCG **Reverse:** AGAGTGCGTCATATGTTGTTC	1040	61
MTND4	**Forward:** ATCGCTCACACCTCATATCC **Reverse:** TAGGTCTGTTTGTCGTAGGC	1072	61

Table 2.5. Primer sequences for PCR reactions for generation of standards.

Target	Primer sequence	Product size (bp)
B2M	**Forward:** CACTGAAAAAGATGAGTATGCC **Reverse:** AACATTCCCTGACAATCCC	231
MTND1	**Forward:** ACGCCATAAAACTCTTCACCAAAG **Reverse:** GGGTTCATAGTAGAAGAGCGATGG	111
MTND4	**Forward:** ACCTTGGCTATCATCACCCGAT **Reverse:** AGTGCGATGAGTAGGGGAAGG	107

Table 2.6. pPCR primer sequences.

Target	Sequence	Fluorophore	Quencher
B2M	CCGTGTGAACCATGTGACTTTGTC	FAM	BHQ_1
MTND1	ACCCGCCACATCTACCATCACCCTC	HEX	BHQ_1
MTND4	CAACCAGCCAGAACGCCTGAACGCA	Cy5	BHQ_2

Table 2.7. Sequences for iTaq probes.

2.8.2 qPCR for the analysis of gene expression

qPCR was performed in triplicate reactions using GoTaq® qPCR Master Mix reagent system (Promega) which uses carboxy-X-rhodamine (CXR) as a reference dye. The reaction was run on the Applied Biosystems® QuantStudio™ 7 Flex Real-Time PCR System (Life Technologies). The data was analysed using the QuantStudio™ software (Life Technologies) and relative gene expression was determined using the $2^{-\Delta\Delta Ct}$ method using *GAPDH* as a housekeeping gene. List of primers can be found in Table 2.8.

Gene	Forward primer (5'→3')	Reverse primer (5'→3')
APC2	CTGGACATCGCTTGCTGGAT	TGCCTCTCCACTTTGACACC
CDX2	CTCGGCAGCCAAGTGAAAAC	CTCCTTTGCTCTGCGGTTCT
CRALBP	ACCTTTGATGAGATCTTGCAG	GAAGCCATTGATTTGAGTTTCC
CTSB	GACGGCTGTAATGGTGGCTA	GTACGGTCTGCACCCTACAT
CTSD	TGGACATCGCTTGCTGGAT	CCTGCCTCTCCACTTTGACA
FGF5	ATTTGCTGTGTCTCAGGGGAT	CTGTGAACTTGGCACTTGCAT
FOXA2	GCATTCCCAATCTTGACACGGTGA	GCCCTTGCAGCCAGAATACACATT
GAPDH	TGCACCACCAACTGCTTAGC	GGCATGGACTGTGGTCATGAG
MERTK	AGCCTGAGAGCATGAATGTCACCA	TGTTGATCTGCACTCCCTTGGACA
MFN2	ATGCATCCCCACTTAAGCAC	ACCTCACTGATGCCTCTCAC
MITF	GCCTCCAAGCCTCCGATAAG	CATCTGCTCACGCATGAGTTG
MIXL	GAGACTTGGCACGCCTGT	GGTACCCCGACATCCACTT
N-CADHERIN	ACAGTGGCCACCTACAAAGG	CCGAGATGGGGGTTGATAATG
NANOG	AGAAGGCCTCAGCACCTAC	GGCCTGATTGTTCCAGGATT
NESTIN	GAGAGGGAGGACAAAGTCCC	GAGAGGGAGGACAAAGTCCC
OPA1	CGGACCCAAGAACAGTGTGT	GGTTCTTCCGGACTGTGGTT
OTX2	CAAAGTGAGACCTGCCAAAAAGA	TGGACAAGGGATCTGACAGTG
PAX6	GCCTATGCAACCCCCAGT	TCACTTCCGGGAACTTGAAC
PEDF	AGATCTCAGCTGCAAGATTGCCCA	ATGAATGAACTCGGAGGTGAGGCT
RPE65	GCCCAGGAGCAGGACAAAG	GCGCATCTGCAAGTTAAAACCA
SILV	GGGCCCCCTGCTGGATGGTA	CCCGCCTTGGCAGGACACAG
SOD2	GGAACAACAGGCCTTATTCCAC	TGACTAAGCAACATCAAGAAATGC
SOX1	GGAATGGGAGGACAGGATTT	ACTTTTATTTCTCGGCCCGT
T	CAGTGGCAGTCTCAGGTTAAGAAGGA	CAGTGGCAGTCTCAGGTTAAGAAGGA
TYR	TAGCGGATGCCTCTCAAAGC	CAATGGGTGCATTGGCTTCT

Table 2.8. List of primers used in the qPCR experiments.

2.9 Flow cytometric analysis

2.9.1 Quantification of the expression of pluripotency markers

Single cell suspension was made with Versene® (EDTA) 0.02% solution and cells were fixed with 2% paraformaldehyde (PFA) for 10 minutes at 37°C. Cells were then washed with PBS and re-suspended in ice cold methanol. They were then stored at -20°C for at least 30 minutes and for up to 1 month. For the quantification of the expression of pluripotency markers cells were washed with PBS, 1×10^6 cells/ml were re-suspended in 100 µl of 2% FBS in PBS with the appropriate concentrations of antibodies, Anti-TRA-1-60, FITC conjugate (Merck Millipore; dilution 1:5) and Nanog XP® Rabbit mAb Alexa Fluor® 647 Conjugate (New England Biolabs; dilution 1:50). Cells were then incubated for 40 minutes on a shaker at room temperature. Cells were washed using BD FACS™ Lyse Wash Assistant (BD Biosciences) and analysed on BD FACSCanto™ II system (BD Biosciences). Data was analysed on BD FACSDiva software (BD Biosciences). A minimum of 10 000 events were recorded for each sample.

2.9.2 Apoptosis, DNA damage and cell proliferation

The assay was set up using the Apoptosis, DNA damage and Cell Proliferation Kit (BD Biosciences) according to the manufacturer's instructions. Briefly, 10 µl of 1 mM 5-bromo-2'-deoxyuridine (BrdU) solution per 1 ml of growth medium was added directly to the cells for 45 minutes. After that, single cell suspension was made with Versene® (EDTA) 0.02% solution and cells were fixed and permeabilised with BD Cytofix/Cytoperm Fixation/Permeabilisation Solution for 15 minutes. Cells were then permeabilised with BD Cytofix/Cytoperm Plus Permeabilization Buffer and incubated for 10 minutes on ice. Cells were then re-fixated with BD Cytofix/Cytoperm Fixation/Permeabilization Solution for 5 minutes on ice. In order to expose incorporated BrdU, cells were treated with 300 µg/ml DNase and incubated for 1 hour at 37°C. Cells were then re-suspended in BD Perm/Wash Buffer with PerCP-Cy™5.5 Anti-BrdU, Alexa Fluor® 647 Mouse Anti-H2AX (pS139), PE Anti-Cleaved PARP (Asp214) antibodies. Cells were incubated for 20 minutes at room temperature. Total DNA was labelled with 1 µg/ml 4',6-diamidino-2-phenylindole (DAPI). Cells were analysed straight away on BD FACSCanto™ II system (BD Biosciences) and the data was analysed on BD FACSDiva software (BD Biosciences). A minimum of 10

000 events were recorded for each sample. Population of cells was gated using appropriate single-stained (for each antibody) and unstained controls.

2.9.3 Measurement of intracellular peroxides

The following experimental procedure was performed by Dr Gabriele Saretzki (ICaMB, CAV, Newcastle University). Cellular peroxide levels were measured by using DHR (dihydrorhodamine123) fluorescent probe and DCF (2',7'-dichlorofluorescin) (both from Molecular Probes). 2×10^5 cells were re-suspended in serum free DMEM with 30 µM DHR or 80 µM DCF. Cells were incubated for 30 minutes at 37°C in the absence of light, then centrifuged at $800 \times g$ for 5 minutes and re-suspended in serum free DMEM. Before the analysis, flow cytometer was calibrated using 3 µM calibration beads (Polysciences Inc.). The gain for FL-1 (green) was set to 100 and FL-3 (red) to 180. Cells were analysed immediately by flow cytometry (Partec PAS, Muenster, Germany) using FL-1 and FL-3 channels. The median FL-1 and FL-3 fluorescence peak was used to estimate the concentration of intracellular peroxides. Background fluorescence was removed by subtracting values for unstained cells in the FL-3 channel. All analyses were repeated three times.

2.9.4 Measurement of mitochondrial reactive oxygen species

The following experimental procedure was performed by Dr Gabriele Saretzki (ICaMB, CAV, Newcastle University). Mitochondrial ROS levels were assessed by using DHE (dehydroethidium) (Molecular Probes) and MitoSOX™ Red (Molecular Probes) staining. To measure mitochondrial superoxide levels with DHE, around 2×10^5 cells were stained with 10 µM DHE for 30 minutes at 37°C protecting the samples from light. After incubation, cells were centrifuged and re-suspended in 3 ml DMEM without serum. FL-3 (red) median fluorescence was measured by flow cytometry (Partec PAS, Muenster, Germany). For the MitoSOX™ Red staining experiments, cells were stained with 5 µM of the solution for 15 minutes at 37 °C in the dark. Cells were centrifuged and re-suspended in 3 ml of DMEM without serum. Samples were analysed by flow cytometry as described in 2.9.3. Unstained cells were always analysed alongside in FL-3 and the values subtracted from FL-3 of the stained samples.

2.9.5 Measurement of mitochondrial mass

The following experimental procedure was performed by Dr Gabriele Saretzki (ICaMB, CAV, Newcastle University). Mitochondrial mass was measured with NAO (10-n-nonyl-acridine orange) fluorescent probe (Molecular Probes). Cells were prepared as a single cell suspension, centrifuged and re-suspended in 1 ml of DMEM without serum with 10 µM NAO and incubated for 10 minutes at 37°C in the dark. Cells were then centrifuged and re-suspended in 3 ml DMEM with no serum and analysed by flow cytometry recording fluorescence in green channel FL-1 by setting the FL-1 value to 200 (Partec PAS, Muenster, Germany).

2.9.6 Measurement of mitochondrial membrane potential

The following experimental procedure was performed by Dr Gabriele Saretzki (ICaMB, CAV, Newcastle University). Mitochondrial membrane potential was measured with the JC-1 (5,5',6,6'-tetrachloro-1,1',3,3'-tetraethylbenzimidazolylcarbocyanine iodide) (Molecular Probes) fluorescent probe. Single cells were re-suspended in RPMI 1640 medium without phenol red (Life Technologies) with 1 µg/ml JC-1. The cells were incubated for 30 minutes at 37°C in the dark. Cells were centrifuged at 300 × g at 4°C for 5 minutes, washed with cold PBS and re-suspended in 3 ml of PBS at room temperature. Mitochondrial permeability transition was quantified by flow cytometry (Partec PAS, Muenster, Germany) by measuring fluorescence in FL-1 and FL-3 and then determining the ratio of fluorescence in FL-3 (red) and FL-1 (green) corresponding to signals from JC-1 monomer and aggregate.

2.9.7 Phagocytosis of photoreceptor outer segments

Bovine photoreceptor outer segments (POSs) were obtained from InVision BioResources. Prior to performing the assay, POSs were fluorescein isothiocyanate (FITC) labelled using the following procedure. The POSs were centrifuged at 4500 × g for 4 minutes. They were then re-suspended in AdRPMI, 10% FBS with 0.4 mg/ml FITC (Sigma) and incubated for 1 hour at room temperature protected from light. This was followed by another centrifugation for 4 minutes at 4500 × g. POSs were washed three times with PBS and then re-suspended in 2.5% (73 mM) sucrose (Sigma) in PBS and stored in -80°C until further use. For phagocytosis experiments, normal RPE cell medium was changed to the POS medium (AdRPMI, B27, 10% FBS). Once

thawed, POSs were re-suspended in POS medium. 1×10^6 FITC-labelled POSs were added per cell culture insert for 4 hours at 37°C. In parallel to that, a negative control experiment was set up when cells were kept for the same time duration but at 4°C. The incubations were followed by two cell washes with PBS. Cells were then dissociated with TrypLE™ Select Enzyme (10X) and washed. They were then re-suspended in 2% FBS solution in PBS with the addition of DRAQ5™ (1:400, BioStatus) for 5 minutes. Extracellular fluorescence was quenched with 0.2% Trypan Blue Stain (Life Technologies) for 10 minutes. Cells were then washed at least three times with PBS and re-suspended in 2% FBS solution in PBS. Cells were analysed on BD™ LSR II flow cytometer (BD Biosciences) collecting 10 000 events per sample. The data was analysed on BD FACSDiva software (BD Biosciences).

2.10 Immunofluorescence microscopy

2.10.1 Pluripotency assessment

Cells were washed with PBS and then fixed with 4% PFA for 15 minutes at room temperature. Cells were then washed three times with PBS and permeabilised with 0.25% Triton-X-100 (Sigma) for 40 minutes at room temperature. Cells were then washed with PBS following by a blocking step with 10% FBS + 1% bovine serum albumin (BSA) in PBS for 45 minutes at room temperature. Cells were then stained with Alexa Fluor® 555 Mouse anti-SSEA-4 antibody (BD Biosciences) and goat anti-human Oct-3/4 Affinity Purified Polyclonal primary antibody (R&D Systems) both at a concentration of 1:100 in blocking solution at 4°C overnight, followed by incubation with a secondary antibody anti-goat IgG—FITC secondary antibody (Sigma) at a concentration of 1:200 for 1 hour at room temperature. All the antibodies were diluted in blocking solution. Nuclei were counterstained with DAPI (CyStain® DNA, PARTEC). Images were taken with Zeiss Axiovert 200M – Inverted Widefield microscope with Zeiss AxioCam HRm camera (all Carl Zeiss Microscopy GmbH).

2.10.2 Assessment of retinal differentiation

Cells or retinal structures were washed with PBS and then fixed with 4% PFA for 15 minutes at room temperature. Cells were then washed three times with PBS and permeabilised with 0.25% Triton-X-100 (Sigma) for 40 minutes at room temperature. Cells were then washed with PBS following by a blocking step with 10% normal goat serum (Invitrogen) and 1% BSA in PBS for 45 minutes at room temperature. Cells

were then stained with primary antibodies at 4°C overnight, followed by incubation with secondary antibodies for 1 hour at room temperature. All the antibodies were diluted in blocking solution. Nuclei were counterstained with DAPI (CyStain® DNA, PARTEC) or Hoechst 33342. The list of antibodies can be found in Table 2.9.

Antibody	Company	Dilution
Anti-RPE65 antibody, mouse	Abcam, ab13826	1:200
Anti-ZO1, rabbit	Invitrogen, 61-7300	1:200
Anti-CRX monoclonal antibody, mouse	Abnova, H00001406-M02	1:100
Cy™3 AffiniPure Goat Anti-Rabbit IgG	Jackson ImmunoResearch, 111-165-003	1:800
Anti-mouse IgG–FITC antibody	Sigma, F2012	1:800

Table 2.9. List of antibodies.

2.11 Single-nucleotide polymorphism array

hiPSCs and fibroblasts that they were derived from were tested for DNA mutations and chromosomal abnormalities. The assay and data analysis were performed in collaboration with Dr Hussein Sheekh (King Abdulaziz University. Jeddah, Saudi Arabia) using Infinium HD Assay Ultra (Illumina). The basic principle of the method is as follows; DNA isolation is performed in-house as described previously (Section 2.4) and 50 ng of DNA is sent away for the analysis. The assay consists of DNA amplification and fragmentation, DNA fragment hybridisation to a probe on the array when the probe binds to a complementary sequence on the DNA and stops at the site of the variant, the probe is then extended with labelled nucleotides matching the target DNA sequence, the nucleotide label is excited by a laser which causes the signal to emit detected by the scanner which results in the identification of the allelic ratio for a specific locus, the data is then analysed using GenomeStudio® software (Illumina).

2.12 Analysis of RPE pigmentation

Method of quantification of the pigmentation yield by RPE cells was modified from (Lane *et al.*, 2014). Area covered by the emerging pigmented RPE foci was measured by taking the images of the 6-well plates with differentiating RPE cells using the Epson Perfection V500 Photo scanner (Seiko Epson Corporation). Images were acquired at a resolution of at least 300 dots per inch at multiple points during

differentiation. The images were analysed with ImageJ (NIH, Bethesda, MD). Images were first converted to greyscale and then using threshold tool only isolated pigmented foci were made visible. Total pigmented area was quantified by measuring grey areas using the software obtaining the total area covered by pigment on a 6-well plate.

2.13 Transmission electron microscopy

Cells were fixed with 2% glutaraldehyde and kept at 4°C. Transmission electron microscopy (TEM) including all the cell processing was performed by Ms Tracey Davey at Newcastle University Electron Microscopy Research Services.

2.14 Transepithelial resistance

Transepithelial resistance (TER) was measured in order to assess barrier properties and integrity of the hPSC-RPE cells cultured on hanging cell culture inserts. Measurements were carried out with Millicell ERS-2 Voltohmmeter (Millipore). TER of the blank insert with PBS was measured first followed by the resistance measurements of the cells of interest. An average of two recordings for each sample and a blank was taken. In order to calculate the TER values, the recordings for the blank were subtracted from the recordings of the samples. The result was multiplied by the surface area of the insert and data presented as Ωcm^2.

2.15 Oxygen consumption

Oxygen consumption rate in control and patient fibroblasts and hiPSCs was measured using Seahorse Bioscience XF^{e}96 Extracellular Flux Analyser (Seahorse Bioscience). The experiments were performed in a Seahorse 96-well XF Cell Culture Microplate. hiPSCs were seeded in the presence of 10 μM Y-27632 (Chemdea) on the microplates pre-coated with matrigel at a density of 4×10^4 cells per well in 200 μl of growth medium 48 hours prior to the experiment. Medium was changed 5 hours after seeding the cells and then 24 hours later. Fibroblasts were seeded at a density of 2.5×10^4 cells per well in 200 μl of growth medium 24 hours prior to the experiment. On the day of the experiment, medium was changed to 175 μl bicarbonate-free DMEM with the appropriate concentrations of glucose (Sigma), L-glutamine (Life Technologies) and sodium pyruvate (Sigma) to maintain the same concentration as in the usual growth medium, pH was adjusted to 7.0 - 7.4. Cells

were incubated at 37°C for 1 hour prior to starting the assay. First the baseline oxygen consumption rate (OCR) was measured. Proton leak was measured by the addition of 1.5 µM and 1 µM of oligomycin (inhibits ATP synthase) to hiPSCs and fibroblasts respectively. Maximal capacity respiration was determined by the sequential injection of carbonyl cyanide-ptrifluoromethoxyphenylhydrazone (FCCP) (uncouples the electron transport chain and OXPHOS by dissipating the proton gradient) (first injection 0.3 µM and 0.5 µM for hiPSCs and fibroblasts, second injection 0.5 µM and 1 µM for hiPSCs and fibroblasts respectively). Non-mitochondrial respiration (NMR) was measured by the addition of 1 µM and 2 µM of rotenone (Complex I inhibitor, prevents electron transfer to CoQ) / antimycin (Complex III inhibitor, disrupts proton gradient) to the hiPSCs and 1 µM to fibroblasts respectively. Data was corrected by the NMR and normalised to the total protein concentration measured by Bradford method. Data is presented as pmol of oxygen / minute / mg of protein.

2.16 Protein concentration quantification by Bradford method

In order to determine protein concentration, cells were lysed with 50 mM Tris-HCl (pH 7.4), 150 mM NaCl, 1 mM EDTA and 0.1% (vol/vol) Triton-X-100 overnight at 4°C. A range of standards was made up with BSA (Sigma) and dH_2O to the concentrations of 0.05, 0.1, 0.2, 0.3, 0.4, and 0.5 mg/ml. 10 µl of each standard and the appropriate volume of sample cell lysis were added in duplicates to a 96-well plate. BioRad Protein Assay Solution (Bio-Rad) was diluted 1:5 with dH_2O and 190 µl added to each well. The plate was incubated in the dark at room temperature for 10 – 30 minutes. Absorbance was detected at 595 nm using a UV spectrophotometer. In order to determine protein concentration of the samples, standard curve plot of absorbance vs. known varying amount of protein of the standards was used. The average absorbance taken from the duplicate measurements was used to plot the graph.

2.17 ATP assay

ATP measurements were performed with the CellTiter-Glo® Luminescence Assay (Promega). Cells were seeded on 96-well white microplates (Thermo Scientific) pre-coated with matrigel at a density of 3×10^4 cells per well in 200 µl of cell culture medium. Cells were expanded for 2 weeks. On the day of the assay, cells were

incubated for 1 hour 30 minutes at 37°C in 200 µl of the ATP buffer with either 5 mM glucose (Sigma) or 5 mM 2-Deoxy-D-glucose (Sigma) or 5 mM glucose with 2.5 µg/ml oligomycin (Sigma) or 5 mM 2-Deoxy-D-glucose and 2.5 µg/ml oligomycin. Following incubation, 90 µl of the buffer was removed and 110 µl of the CellTiter-Glo® Reagent Buffer was added. The plate was shaken in the dark for 10 minutes to induce cell lysis and then left in the dark for further 15 minutes. Luminescence was measured with 1000 ms integration time on a Luminoskan Ascent (Thermo Scientific). The signal was normalised to mg of protein as determined by Bradford assay.

2.18 Cytosolic calcium measurement

Cells were seeded on 96-well optical bottom microplates pre-coated with matrigel at a density of 3×10^4 cells per well in 200 µl of cell culture medium and let to expand for 2 weeks. On the day of the assay cells were washed two times with PBS. Subsequently, cells were loaded with 5 µM Fura-2 Calcium Indicator (Life Technologies) for 1 hour at 37°C in 100 µl of Hanks' Balanced Salt Solution (HBSS) (Life Technologies). Cells were washed with PBS and re-suspended in cell culture medium and further incubated for 30 minutes at 37°C. Detection of fluorescence was achieved with Thermo Scientific™ Varioskan™ LUX Multimode Microplate reader (Thermo Scientific) (excitation at 340 nm and 380 nm, emission 510 nm). Fluorescence was measured at 340 nm and 380 nm. R_{min} 340/380 ratio (under Ca^{2+} free conditions used to calibrate the probe) was measured after loading cells with 2 µM ionomycin (ThermoFisher) and 10 mM EGTA (Sigma) in HBSS. R_{max} 340/380 ratio was measured after loading cells with 2 µM Ionomycin and 10 mM $CaCl_2$ (Sigma). The following equation was used for calculating cytosolic Ca^{2+}:

[Ca2+] = Kd x Q x [(R-Rmin)/Rmax-R]

R – 340/380 ratio

R_{min} – 340/380 ratio under Ca^{2+} free conditions

R_{max} – 340/380 ratio under Ca^{2+} saturating conditions

Q – ratio of emission intensity at 380 nm for Ca^{2+} free and Ca^{2+} saturated

Fura-2 and Kd was assumed to be 225 nM. The recordings were performed in triplicates at 37°C.

2.19 Statistical analysis

All data was expressed as mean ± standard error of the mean (SEM) unless otherwise stated. One-way analysis of variance (ANOVA) was used to assess variation across multiple samples. The test was followed by Tukey's multiple comparisons test. Representation of significance of p value was as follows: $p \leq 0.05$ *, $p \leq 0.01$ **, $p \leq 0.001$ ***, $P \leq 0.0001$ ****. All statistical analyses were done using GraphPad Prism Software Inc. (San Diego, CA, USA) or IBM SPSS Statistics 22 (IBM Corporation).

Chapter 3. Generation and characterisation of patient-derived hiPSCs

3.1 Overview

Fibroblasts derived from patients and healthy controls were reprogrammed in feeder-dependent and feeder-free culture conditions using Sendai-based reprogramming systems from Life Technologies. After transfection with the virus, cells were cultured for 7 days until they were transferred to plates with matrigel or MEFs for further expansion. Emergence of colonies was monitored daily expecting to see the appearance of first hESC-like colonies after 21-30 days post transduction. Schematic representation of the experimental timeline is shown in Figure 3.1.
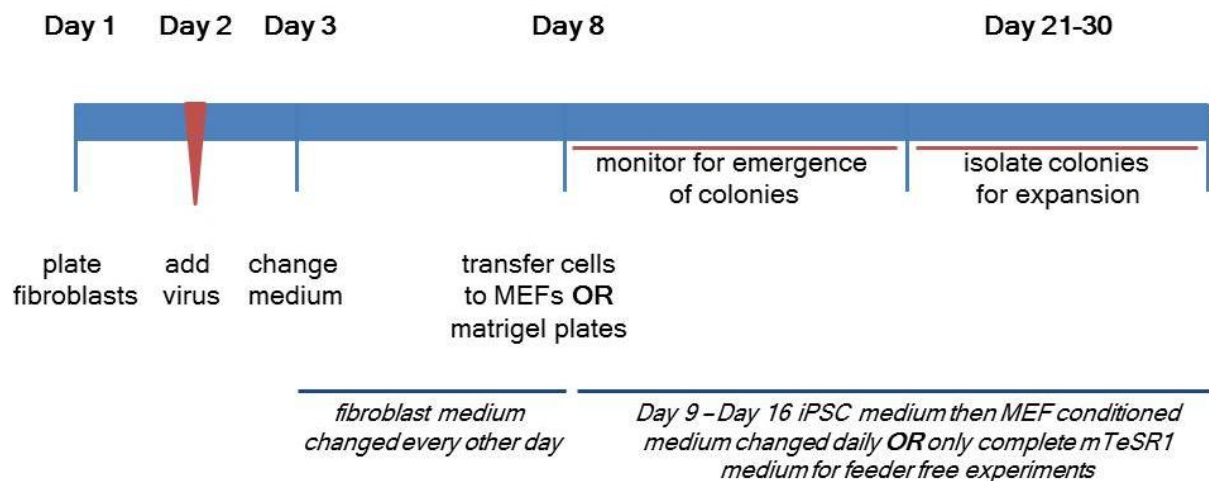
Figure 3.1. Experimental timeline for feeder-dependent and feeder-free reprogramming of patient fibroblasts [adapted from Chichagova *et al.* (2015)].

Once the hiPSCs are expanded it is important to confirm their pluripotency status in order to ensure that the cells are fully as opposed to partially reprogrammed. During somatic cells reprogramming it is possible that some cells become partially reprogrammed meaning that they can have features of both *bona fide* hiPSCs and differentiated cells. This phenomenon can be associated with cells inducing anti-proliferative genes, but failing to downregulate lineage-specific transcription genes, failing to undergo necessary epigenetic remodelling such as DNA hypomethylation and repression or failure to activate the reprogramming factors (Mikkelsen *et al.*, 2008). For that reason, the field has identified a number of rigorous molecular and functional tests in order to validate iPSC status.

Firstly, it is confirmed that cells have a typical hESC-like morphology, packed in tight colonies with defined borders with cells containing high nuclear to cytoplasm ratio. Subsequently, they are tested for the expression of a number of pluripotency-associated markers including those involved in pluripotency gene regulation network. A number of cell-surface antigens and developmentally regulated genes have been shown to be associated with the undifferentiated state in hESCs and therefore these markers were chosen for pluripotency validation of hiPSCs derived in this study (Adewumi *et al.*, 2007). Stage-specific embryonic antigen (SSEA4) has been shown to be unique to human embryonic teratocarcinoma cells, which are malignant counterparts to hESCs (Kannagi *et al.*, 1983). Keratin sulphate antigen Tra-1-60 has been shown to be associated with undifferentiated embryonal carcinoma cells and hESCs with cells reducing expression levels upon differentiation (Badcock *et al.*, 1999; Draper *et al.*, 2002). Another study showed that cells that are to become hiPSCs upregulate both SSEA4 and Tra-1-60 (Chan *et al.*, 2009). Transcription factor *OCT4* was used as it has been previously shown to be important for maintenance of undifferentiated state / pluripotency in hESCs (Okamoto *et al.*, 1990; Hay *et al.*, 2004; Matin *et al.*, 2004). It is associated with the founder population of cells during early embryogenesis and has been shown to be a robust identification marker of hESCs (Nichols *et al.*, 1998; Adewumi *et al.*, 2007). Homeodomain protein NANOG is associated with undifferentiated state by repressing differentiation into primitive endoderm and supporting self-renewal in mouse ESCs (Chambers *et al.*, 2003; Mitsui *et al.*, 2003). It has been shown that some of these markers expression is correlated with each other such as NANOG and TRA-1-60. Additionally, lack of SSEA4 expression in TRA-1-60 positive cells and lack of detection of nuclear NANOG staining has been shown to be associated with partially reprogrammed cells. Therefore it is important to check the expression of a combination of markers (Chan *et al.*, 2009). All of the above provides evidence that these markers are robust against identification of pluripotent stem cells and they form part of the panel identified as being characteristic of hPSCs (Adewumi *et al.*, 2007).

There are a number of assays that are used to demonstrate the potential of pluripotent cells to differentiate into other cell types. One of these assays is induction of teratoma in mice which over the years has become a 'gold standard' experiment. Teratoma induction in mice and other mammals has been carried out for decades with earlier studies describing the ability of embryonal cells to form tumours containing specialised tissues (Jackson and Brues, 1941; Stevens and Little, 1954).

Early studies used teratoma formation assay for investigating the potential of mouse and human ESCs and iPSCs to form derivatives of three embryonic germ layers (endoderm, ectoderm, mesoderm) after injecting the cells into immunocompromised mice (Evans and Kaufman, 1981; Thomson *et al.*, 1998; Gertow *et al.*, 2007; Takahashi *et al.*, 2007).

Alternative methods exist that provide proof of differentiation ability of cells by studying differential potential *in vitro*. The ability of cells to spontaneously differentiate *in vitro* after allowing cells to grow to confluence has been used as a test for many years (Evans and Kaufman, 1981; Thomson *et al.*, 1998). For the purpose of this project, both the *in vitro* and *in vivo* methods were used.

As a final quality control, the hiPSCs derived for the project together with their parental fibroblasts were tested for cytogenetic abnormalities using a single-nucleotide polymorphism (SNP) array technique (testing against ~300 000 SNPs). Various contributors to genomic instability in hPSCs have been described in both hESC and hiPSC studies. Variations within the iPSC genome could arise from the reprogramming process itself, prolonged cell culture and heterogeneity in the parental fibroblast cells (Liang and Zhang, 2013).

3.2 Results

3.2.1 Reprogramming patients' and control fibroblasts with CytoTune 1 kit

The first round of the reprogramming was performed using CytoTune 1 reprogramming kit containing four reprogramming vectors each expressing one of the four Yamanaka factors *hOct3/4*, *hSox2*, *hKlf4*, and *hc-Myc*. Three cell lines were used in this set of experiments, Patient 1 and Patient 3 cells and Control 1 cells. Cells were cultured on MEFs and matrigel with the view of deriving both feeder-dependent and feeder-free hiPSC clones. Representative images of the appearance of cells throughout the experiment are shown in Figure 3.2. The results of the experiment showed that as expected 7 days post transfection, all of the cells showed some sign of cytotoxicity with some cells rounding up and detaching. However, 28 days from the start of the reprogramming, cells changed morphology but there was no appearance of hESC-like colonies in any of the cells.
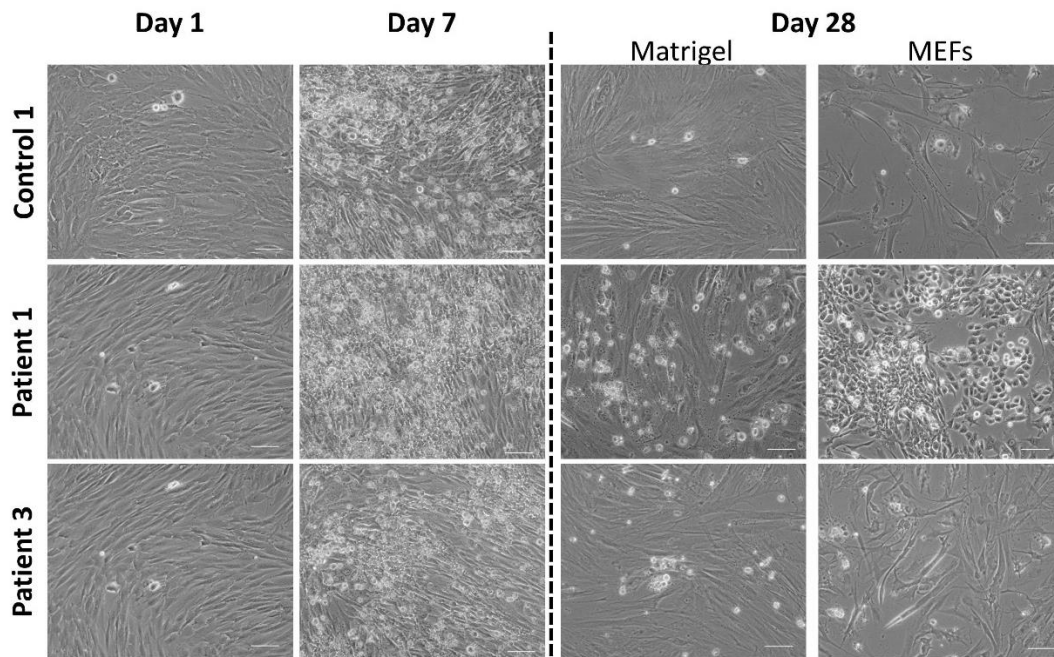
Figure 3.2. Reprogramming patients' and control fibroblasts using CytoTune 1 kit using both matrigel and MEFs as substrates. Some cytotoxicity was observed by day 7 in all cells; however, no hESC-like colonies were noted 28 days after the start of the reprogramming. Scale bar, 100 μm.

3.2.2 Reprogramming patients' and control fibroblasts with CytoTune 2 kit

In order to facilitate cell reprogramming, CytoTune 2 – an improved Sendai virus reprogramming kit was used. The kit contains three vector preparations: polycistronic *hKlf4-hOct3/4-hSox2* (*KOS*), *hKlf4*, and *hc-Myc*. This method has been previously used in the lab and showed an increased reprogramming efficiency (Dr Tomas Barta, personal communication). Introducing reprogramming factors via a polycistronic vector increases the likelihood of successful transfection by only requiring one viral particle entering the cell in order to deliver multiple transgenes. Once again Control 1, Patient 1 and Patient 3 cells were transfected. In addition, Control 2 cells and Patient 2 cells were obtained and also transfected. Cells were reprogrammed using matrigel and /or MEFs as substrates. Representative images from the experiment are shown in Figure 3.3. Control 1 cells failed to produce any colonies. Patient 1 cells gave rise to hESC-like colonies both on matrigel and MEFs. Patient 2 cells produced colonies on MEFs. Patient 3 cells failed to generate any colonies. Control 2 gave rise to some colonies however they failed to successfully expand (data not shown).
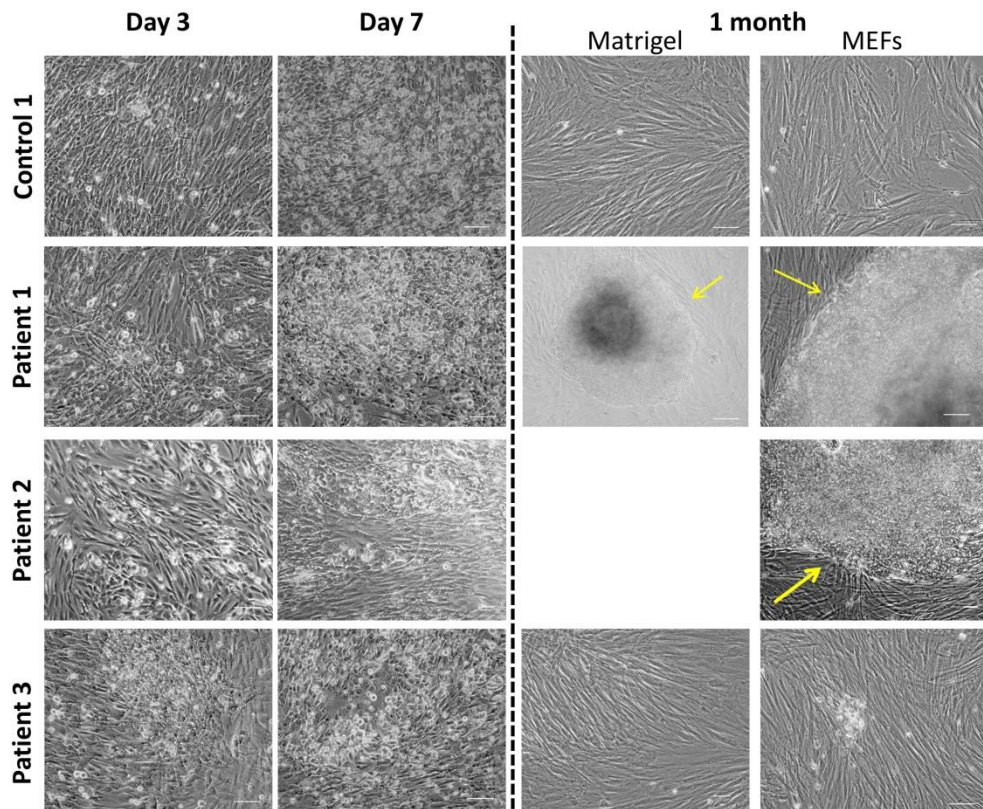
Figure 3.3. Reprogramming patients' fibroblasts using CytoTune 2 kit using matrigel, MEFs or both as substrates. Some cytotoxicity was observed by day 7 in all cells; however, no hESC-like colonies were noted 1 month after the start of the reprogramming in Control 1 and Patient 3 cells. Patient 1 cells produced colonies both on MEFs and matrigel. Patient 2 cells produced colonies on MEFs. hESC-like colonies are shown with yellow arrows. Scale bar, 100 µm.

Patient 3 cells were originally chosen for the project as they came from the sibling of Patient 1. Both of the patients have the same mitochondrial mutation however they present with different ocular phenotypes: Patient 1 has a bilateral pigmentary retinopathy whilst Patient 3 has normal vision and ocular fundi, making an interesting contrast. However, as a result of the reprogramming attempts described above, Control 1, Control 2 and Patient 3 cells were excluded from the project. Since the attempts to derive hiPSCs from healthy controls failed, already established Control hiPSCs reprogrammed and characterised prior to the start of the PhD project by Mrs Adriana Buskin (Prof Majlinda Lako's lab) were used. The results from the reprogramming experiments are summarised in Table 3.1.

Fibroblast source	Mitochondrial mutation	Age / Gender	Ocular phenotype	Reprogramming Kit	Efficiency (%)
Patient 1	m.3243A>G	73/F	• bilateral pigmentary macular degeneration (sparing left fovea) • significant visual acuity deterioration over the past ten years • visual acuities: right eye 6/60, left eye 6/9	CytoTune 1	0
				CytoTune 2	0.08 (MEFs) 0.02 (matrigel)
Patient 2	m.3243A>G	62/M	• extensive macular geographic atrophy • visual acuities: right eye 6/36, left eye 6/36	CytoTune 2	0.03 (MEFs)
Patient 3 (sibling of Patient 1)	m.3243A>G	61/M	• no pigmentary retinopathy or maculopathy • normal vision in both eyes • visual acuities: right eye 6/6, left eye 6/6	CytoTune 1	0
				CytoTune 2	0
Control 1	N/A	57/F	Healthy control	CytoTune 1	0
				CytoTune 2	0
Control 2	N/A	74/M	Healthy control	CytoTune 2	0.002 (MEFs)
Control hiPSCs **	N/A	51/M	Healthy control	CytoTune 2	0.29 (MEFs)

Table 3.1. Summary of the reprogramming experiments outlining patient details, reprogramming kit and efficiency. Blue shading represents successful reprogramming and red shading represents failed attempts to obtain hiPSC clones. ** Cells reprogrammed and characterised by Mrs Adriana Buskin prior to the start of the PhD project.

In the initial stages of cell culture, some of the clones failed to proliferate. As a result, those clones were only partially characterised as described below.

3.3 Characterisation of the resulting hiPSC population

Once the hiPSCs were generated and expanded, they were tested for the presence of the Sendai virus genome and transgenes. Subsequently, pluripotency potential of the hiPSCs was validated using a number of different molecular and functional assays. Prior to all the validation experiments, cells that were cultured on MEFs were adapted to matrigel to ensure less batch-to-batch variation and avoid contamination with undefined components potentially secreted by MEFs thereby providing more reproducibility.

3.3.1 Sendai clearance

Although, Sendai virus does not integrate into the host genome, it can take a number of passages for it to clear from the cytoplasm. Therefore, prior to carrying out any downstream analyses, it is necessary to test whether the transgene and the viral genome have cleared from the cells in order to avoid the possibility of its continuous expression and mutagenesis. Verification of Sendai clearance is achieved by RT-PCR once the hiPSC clones are expanded. The absence of transgene and viral genome amplicon confirms the absence of Sendai. The results of the experiment showed that all clones were clear of the virus by passage 12 (Figure 3.4).
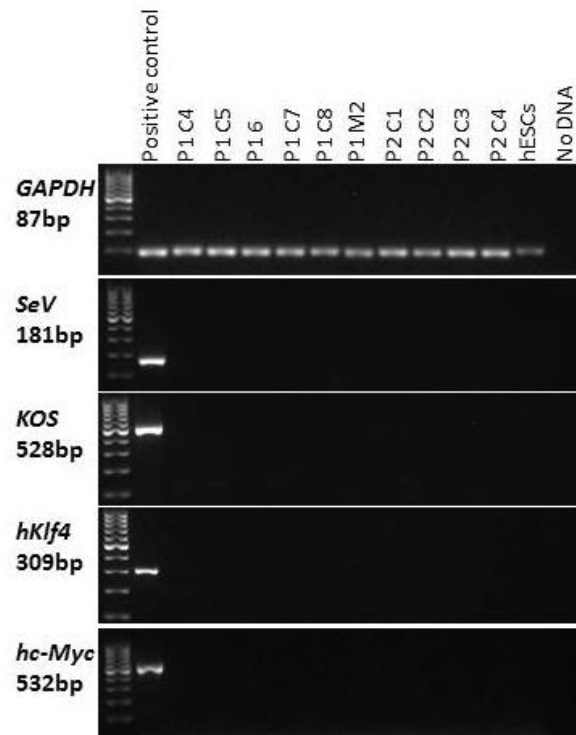
Figure 3.4. Verification of Sendai virus genome and transgenes clearance in patient hiPSC lines using RT-PCR. No reprogramming factor genes (*KOS*, *hKLF4*, *hc-Myc*) or viral vector genome (*SeV*) was detected in patient clones. hESCs were used as a negative control. Glyceraldehyde 3-phosphate dehydrogenase *(GAPDH)* was used as a housekeeping gene. The expected size of the product is shown next to each gene. P – patient, C – clones derived on MEFs, M – clone derived on matrigel.

Once the absence of the transfection virus was confirmed, cells were ready to be used in downstream analyses.

3.3.2 Pluripotency markers expression

Patient hiPSCs were assessed for the expression of pluripotency-associated markers; surface antigen SSEA4 and nuclear localised transcription factor OCT4 by immunocytochemistry. All the clones tested were positive for these markers showing their correct localisation. hESCs were used as positive control (Figure 3.5).
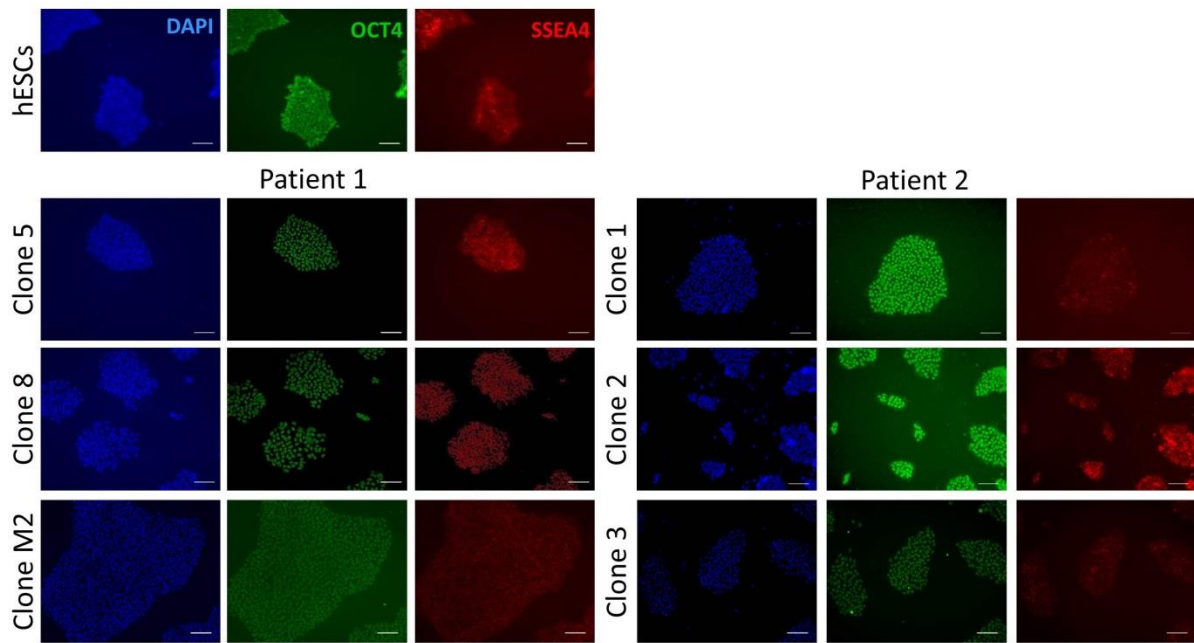
Figure 3.5. Immunocytochemistry results showing pluripotency markers expression in patient hiPSCs. Patient-derived hiPSC clones expressed OCT4 and SSEA4. hESCs were used as a positive control. Secondary only antibody was used as a negative control and showed no signal (data not shown due to the absence of the image). Scale bar, 100 μm.

Flow cytometry analysis for TRA-1-60 and NANOG showed that the majority of the cells were positive for both of the markers. hESCs were used as a positive control.
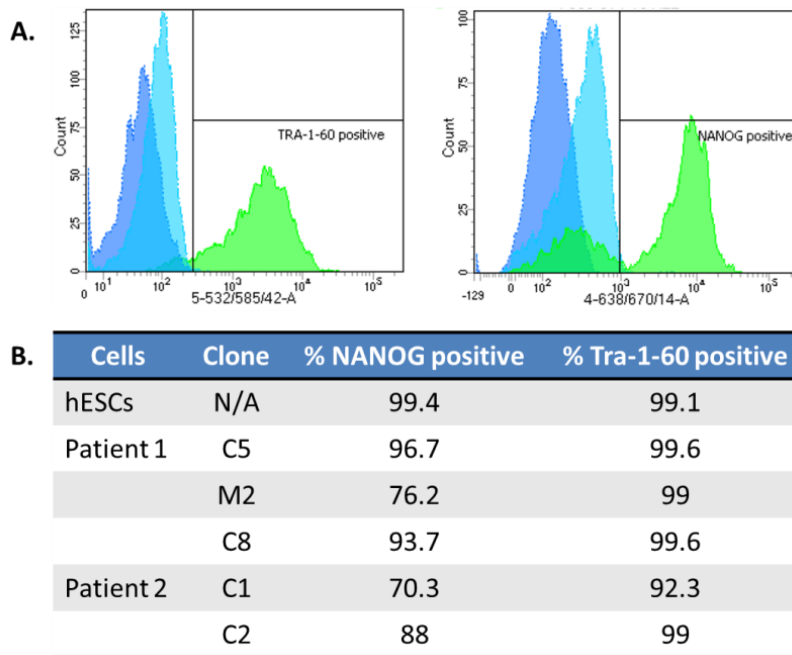
Figure 3.6. Quantification of the percentage of cell population expressing pluripotency-associated markers Tra-1-60 and NANOG by flow cytometry. (A) Representative image of the gating strategy for the experiment, including negative cell population (dark blue) and isotype control (light blue). Cells are shown in green. (B) Patient cells showed similar expression of pluripotency markers when compared to hESCs. The majority of cells were positive for both of the makers.

3.3.3 Assessing the developmental potential of hiPSCs

There are a number of assays that exist that test the potential of PSCs to generate differentiated cell types. Initially, one hiPSC clone from each patient was used to test whether the cells are capable of generating germ cell tumours in immunocompromised mice. Both of the clones failed to form teratomas after 12 weeks (data not shown). Subsequently, it was decided to test differentiation potential of the cells by inducing spontaneous differentiation *in vitro*. Cells failed to form EBs however they were able to differentiate in monolayer cultures after allowing them to proliferate in bFGF-free media for 2 weeks. RT-qPCR showed that at the end of the experiment the cells expressed differentiation markers associated with three germ layers and extraembryonic tissues (Figure 3.7). The results are shown for Patient 1 clones.
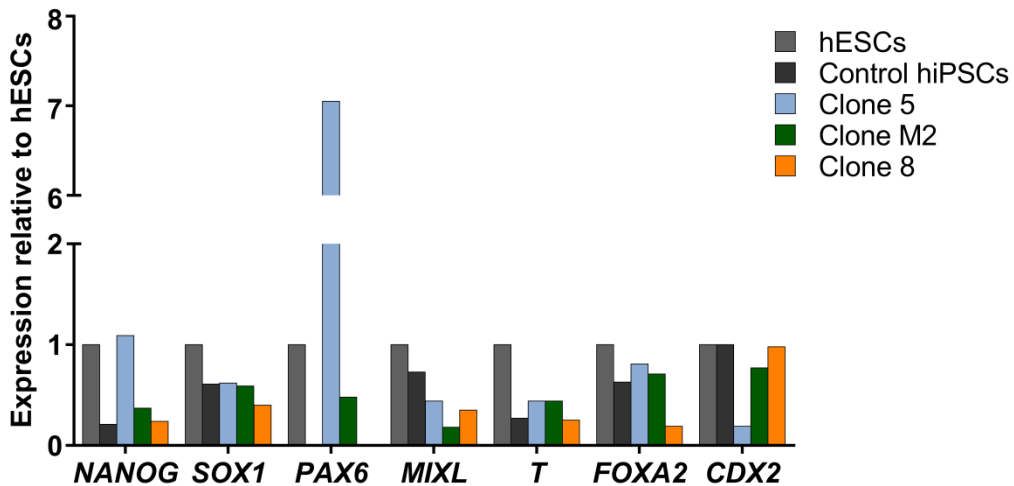
Figure 3.7. Differentiation potential of patient hiPSCs *in vitro* (day 14 of the differentiation). Patient cells showed similar levels of downregulation of pluripotency-associated marker *NANOG* when compared to hESCs. Patient cells expressed neuroectoderm markers SRY (sex determining region Y)-box 1 (*SOX1)* and paired box 6 (*PAX6)*, with Clone 8 having the least and Clone 5 the most potency for neural differentiation taken from the expression of *PAX6*. All cells expressed mesodermal markers mix paired-like homeobox (*MIXL*) and T brachyury transcription factor *(T)* with less potency comparing to hESCs. Cells also showed propensity for endodermal differentiation as assessed by the expression of forkhead box A2 (*FOXA2*). Cells also expressed caudal type homeobox 2 *(CDX2)*, a trophectoderm marker. Results are shown as relative expression when compared to hESCs. *GAPDH* was used as a housekeeping gene.

3.3.4 Cytogenetic analysis

Reprogramming somatic cells can result in accumulation of genetic mutations which necessitates tests to eliminate the possibility of *de novo* changes in the DNA. Genomic SNP array was performed on hiPSC clones from both patients as well as on parental fibroblasts. Patient 1 fibroblasts had no clinically significant imbalance. Clone 4, 5, 7 and 8 had no major changes. Clone M2 had changes on chromosome 20 resulting in large-scale deletion on 20p and duplication on 20q. Fibroblasts from Patient 2 cells showed no major abnormalities. Patient 2 Clone 1 and Clone 2 showed major changes on chromosome 20 similar to the ones seen in Clone M2. Clone 2 did not have changes of known significance. Representative images of the results are shown in Figure 3.8.
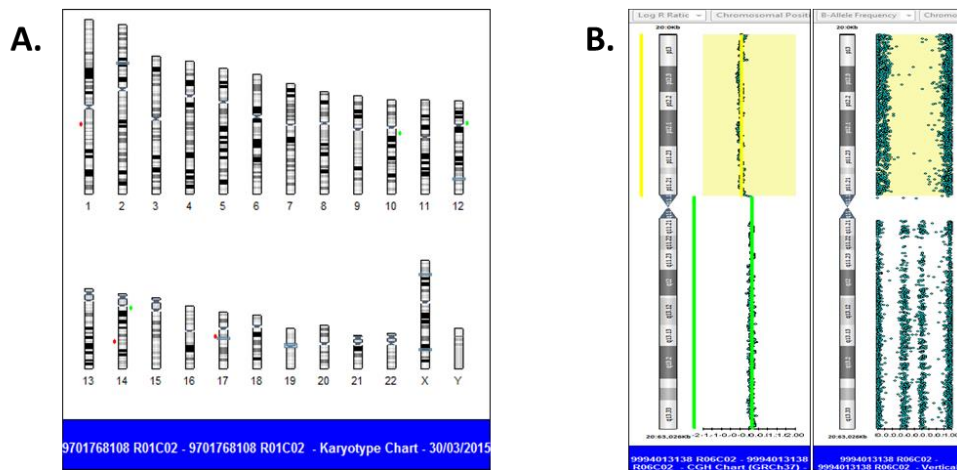
Figure 3.8. Representative images of SNP array results. (A) Karyotype chart showing no major DNA abnormalities. (B) Major changes found on chromosome 20 showing deleted region on the left-hand side and duplicated region on the right.

Summary of the hiPSC characterisation is outlined in Table 3.2. Not all cells survived in the initial stages of cell culture and therefore only the cells that were viable and able to proliferate were investigated.

	Sendai clearance	Flow cytometry (TRA-1-60, NANOG)	IHC (SSEA4, OCT4)	*In vitro* spontaneous differentiation	SNP array
Patient 1					
Clone 4	✓				✓
Clone 5	✓	✓	✓	✓	✓
Clone 6	✓				
Clone 7	✓				✓
Clone 8	✓	✓	✓	✓	✓
Clone M2	✓	✓	✓	✓	✓
Patient 2					
Clone 1	✓	✓	✓		✓
Clone 2	✓	✓	✓		✓
Clone 3	✓		✓		✓
Clone 4	✓				

Table 3.2. Summary of the hiPSCs characterisation.

3.4 Discussion

In the last few years, the use of hiPSCs to model mitochondrial disorders has increased and a number of studies reported generation of hiPSCs from patients with

the m.3243A>G and other mutations associated with MELAS. The results in this chapter described successful derivation and characterisation of hiPSCs from patients' fibroblasts harbouring the m.3243A>G mutation. However, not all patient and control cells successfully gave rise to hiPSC clones. There are a number of potential reasons that would explain such results and these are discussed below.

Firstly, reduced reprogramming efficiency could be to do with the reprogramming kit itself in the case of the experiments that involved using CytoTune 1 kit. The same kit was used for the first round of the reprogramming experiments which were unsuccessful in both control and patient cells (Figure 3.2). It has been previously shown that CytoTune 1 kit shows severe cytotoxicity and lowers reprogramming efficiency compared to CytoTune 2 kit. Additionally, CytoTune 1 kit could require batch testing in order to ensure its safety, so it is possible that the batch used produced cytotoxic effects incompatible with cell survival (Beers *et al.*, 2015).

In subsequent experiments where CytoTune 2 kit was used, in the case of patients' cells it can be speculated that the presence of the mitochondrial mutation could have an effect on their reprogramming efficiency. However, not all cells failed to reprogram and in addition, there are a few publications that also described successful reprogramming of cells with mtDNA mutations. In 2012, the derivation of hiPSC lines from two diabetic patients harbouring the m.3243A>G mutation was shown (Fujikura *et al.*, 2012). A year later, another study generated hiPSCs from fibroblasts of MELAS patients with the m.13513G>A mutation (Folmes *et al.*, 2013). One study showed the potential of hiPSCs obtained from MELAS patients to differentiate into neurones (Hamalainen *et al.*, 2013). On the other hand, Yokota *et al.* (2015) demonstrated that high levels of the m.3243A>G over the pathogenic threshold ($\geq 90\%$) represent a reprogramming roadblock. Another study looked further into the mechanisms of reduced reprogramming efficiency using MEFs from mutator mice and showed that mtDNA mutagenesis leads to increased mitochondrial H_2O_2 leading to reprogramming defects (Hamalainen *et al.*, 2015). A recent study looked at the effect of homoplasmic mtDNA mutations affecting Complex I and causing LHON (m.11778G>C, m.14484T>C, m.4160T>C) and showed a mild but not statistically significant reprogramming impairment (Hung *et al.*, 2016). Overall this shows that more studies are needed in order to elucidate the effect and the mechanism of mtDNA mutations in cellular reprogramming. Some further investigations on this matter will be discussed in the next chapter.

In addition to the patients' cells, two of the control cells failed to give rise to hiPSCs, cells from a 57 year-old female and a 74 year-old male. It is more difficult to speculate what caused the reprogramming failure of these cells without any additional experiments. Firstly, reprogramming is a stochastic process which could be affected by a number of factors. Chromatin organisation and stochastic epigenetic events are some of the factors that could have an effect on reactivation of pluripotency circuitry. It has been shown that DNA hypermethylation at pluripotency-related genes may lead to the failure to achieve a stable reprogrammed state (Polo *et al.*, 2012). Treating partially reprogrammed cells with DNA methyltransferase inhibitor 5-aza-cytidine has been shown to induce full reprogramming (Mikkelsen *et al.*, 2008). Similar to DNA methylation state, remodelling of histone modification is also implicated in the success of somatic cell reprogramming. Histone methylation was shown to be one of the epigenetic changes during the acquisition of pluripotent state (Polo *et al.*, 2012). hiPSC generation can also be affected by epigenetic signature of donor cells including miRNA expression and histone modification pattern (Li *et al.*, 2013). Other studies suggested that reprogramming could be affected by low proliferative capacity of cells (Chan *et al.*, 2009). In the case of the cells that came from a 74 year-old donor, it could be speculated that a potential reason for poor reprogramming results is the age of the individual the cells came from, which could be attributed to upregulation of the cell cycle inhibitory protein p21 (Trokovic *et al.*, 2015). Although, other studies claim that the age of donor cells has little effect on reprogramming efficiency (reviewed by Mahmoudi and Brunet, 2012).

According to Cahan and Daley (2013), pluripotency can either be defined as a state or as a function. All patient hiPSC clones tested expressed markers that have been previously described to be specific to undifferentiated cells, which could be attributed to pluripotency as a state. On the other hand, pluripotency as a function is related to the ability of cells to differentiate. Patients' hiPSC clones were all pluripotent when it came to pluripotency as a state. Cells were also assessed for their functionality using a number of tests. hiPSCs derived from the patients with m.3243A>G failed to form teratomas in immunocompromised mice. Previous studies showed that even uniform expression of pluripotency genes can lead to variations in cells' propensity to differentiate (Cahan and Daley, 2013). Stewart *et al.* (2010) used clonal tracking with lentiviruses expressing enhanced green fluorescent protein (GFP) to show that hESC clones had varying developmental potential when subjected to *in vitro* and *in vivo* differentiation assays. There was not a single hESC

clone that contributed to both assays suggesting that some cells might be self-renewing but not clonogenic. This type of cells is more likely to differentiate *in vitro* but not *in vivo*. Therefore, it can be concluded that *in vitro* and *in vivo* differentiation assays might not be comparable with each other. Studies using mESCs showed that low mitochondrial membrane potential results in failed teratoma formation (Schieke *et al.*, 2008). Considering that the cells used in the study have a mitochondrial mutation it is possible that they might have alterations in the membrane potential leading to failed *in vivo* differentiation.

In the context of this discussion, it is also important to consider the validity of the assays used for assessing differentiation potential of hPSCs. Even though teratoma formation assays have been part of stem cell characterisation for many years, there are still no standardised procedures or consistency in the way the assay is performed, also little is known about host factors guiding cells to differentiate (Muller *et al.*, 2010; Buta *et al.*, 2013). Despite the 'gold standard' status of the teratoma assay, it can be argued that it is a good assay to assess *in vivo* tumorigenic potential of cells which is of paramount importance in clinical safety studies but might have little interest for *in vitro* disease modelling studies as it provides little information on the *in vitro* potential of cells to differentiate or on their potential for normal development. Additionally, it has been previously shown that some partially reprogrammed cells are able to form teratomas which makes the validity of the assay uncertain (Chan *et al.*, 2009). There are a number of alternatives to the teratoma formation assays which have been recognised and accepted by the field. EB formation or monolayer cultures based on spontaneous or directed differentiation of cells with subsequent immunostaining and gene expression analyses is an *in vitro* alternative to teratoma formation. It lacks the physiological cues and oxygen and blood supply that are present in teratoma formation assay nevertheless it is an acceptable model for assessing the ability of cells to differentiate (Itskovitz-Eldor *et al.*, 2010; Buta *et al.*, 2013). Buta *et al.* (2013) also suggested that the EB formation method has several advantages over the teratoma assay by allowing the monitoring of differentiation progression over time. Additionally, analysing large numbers of EBs gives more powerful statistical measures which is normally not always possible when using mice. In the case of the teratoma formation experiments performed with patient-derived hiPSCs only one round of injections was performed and it was not possible to retest the cells again. However, the cells were able to form derivatives of

the three embryonic germ layers demonstrated by the levels of gene expression when differentiated as monolayers *in vitro*.

As a final quality control component for the hiPSCs, the cells were tested for the presence of genomic abnormalities. The results showed that some clones had major changes on chromosome 20. Having genomic aberrations in hPSCs is not uncommon with cells being prone to acquire small scale mutations as well as major abnormalities such as chromosome aneuploidy. Genome defects that are directly associated with the reprogramming process are most commonly deletions of tumour-suppressor genes, whereas at later passages cells tend to duplicate tumour-promoting genes (Laurent *et al.*, 2011).

Large duplications of chromosome 20 have been found to be common in hiPSCs and it has been suggested to be a mutation hot spot in hESCs (Spits *et al.*, 2008). Changes on chromosome 20 are common during both early and late passaging and 25% of otherwise karyotypically normal cells have gain of 20q. This region has a highly repetitive sequence which predisposes it to structural rearrangement (Amps *et al.*, 2011). Interestingly, hESCs with amplification of 20q11.21 acquired during long-term culture have no noticeable difference between these and normal cells with regards to morphology, pluripotency marker expression and growth (Lefort *et al.*, 2008). It has been reported that several genes involved in cell survival and cell growth are contained on the amplified region, including *BCL2L1*, *PDRG1*, *ID1*, *TPX2, HM13* and *KIF3B*. Additionally, *DNMT3B* gene is located on the chromosome and codes for *de novo* DNA methyltransferase. However, it does not always mean that those genes are getting overexpressed (Lefort *et al.*, 2008; Amps *et al.*, 2011). Recurrent abnormalities in hiPSCs on chromosomes 12 and 20 are independent of the reprogramming method chosen for stem cell generation (Taapken *et al.*, 2011). In addition to chromosome 20 abnormalities, hPSCs have a number of other hot spots associated with the increased risk of genomic aberrations. Early reports showed that prolonged culture of hESCs may lead to karyotypic changes, such as trisomy of chromosomes 12 and 17 giving the cells a proliferative advantage, reduced doubling time and inhibiting apoptosis (Cowan *et al.*, 2004; Draper *et al.*, 2004). In some cases, despite this adaptation, cells still retained their ability to differentiate, however they sometimes also showed increased expression of pluripotency genes and expression of early differentiation genes (Enver *et al.*, 2005; Mitalipova *et al.*, 2005). Interestingly, *NANOG* is located on the 12p region which is

often duplicated. Similarly, SNP array copy number analysis of multiple hiPSC lines showed that some cell lines acquire chromosome 12 abnormalities early on. In some cases changes only start to occur at later passages when the cell population becomes mosaic with both normal and adapted cells present (Mayshar *et al.*, 2010). MELAS hiPSC clone with changes on chromosome 20 (Clone M2) did not show a difference in its ability to silence *NANOG* or upregulate genes associated with three embryonic germ layers when subjected to spontaneous differentiation.

The mechanisms that are involved in genomic instability in hPSCs have been investigated by a number of research groups. The process of reprogramming is associated with downregulation of the p53 pathway which could affect DNA integrity leading to an increase in copy number variation (CNV) in hiPSCs. CNVs result in mosaicism with the increase in cell numbers with abnormal copy number state with increased passaging (Hussein *et al.*, 2011). Overall, 20% of all hiPSCs are abnormal. However, the method by which the cells are analysed may affect the results and it has also been shown that SNP array is more sensitive than other types of analysis such as karyotyping (Mayshar *et al.*, 2010).

In conclusion, hiPSCs derived from patients' fibroblast cells harbouring m.3243A>G mutation were successfully generated and characterised to be further used in the project.

Chapter 4. Derivation of patient hiPSCs with m.3243A>G mutation

4.1 Overview

Somatic cells obtained from patients with mutations in the mtDNA give rise to hiPSC clones with varying levels of heteroplasmy (Prigione *et al.*, 2011) (Figure 4.1). Multiple studies that reprogrammed patient cells obtained homoplasmic, heteroplasmic (mutation level range in different studies: 51-87%; ~7-85%; 3.6-99.4%; 33-100%; ~5-100%) and mutation free clones, which could be used as isogenic controls (Fujikura *et al.*, 2012; Hamalainen *et al.*, 2013; Kodaira *et al.*, 2015; Ma *et al.*, 2015; Yokota *et al.*, 2015).
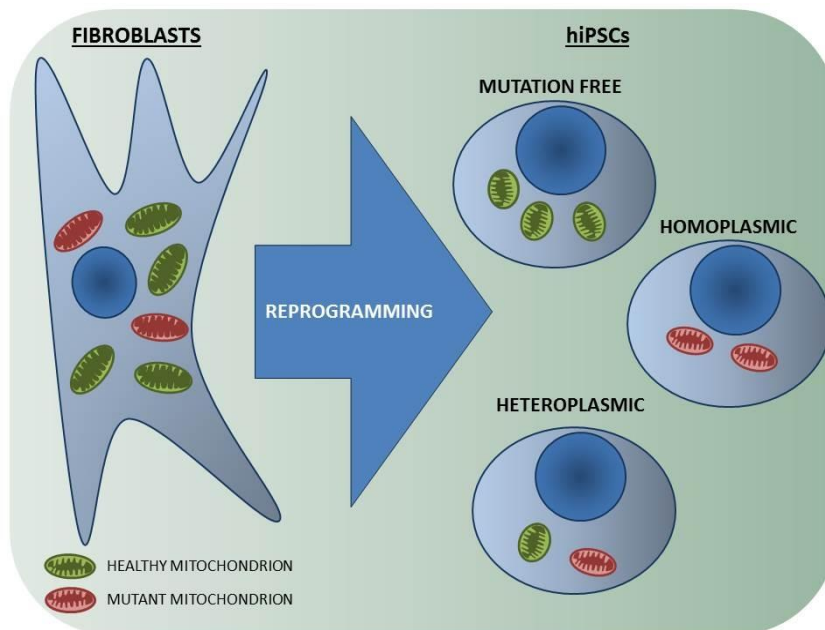
Figure 4.1. Schematic representation of healthy and mutant mitochondria segregation during the process of reprogramming.

The mechanism of mitochondrial segregation is not completely understood. Some suggest that it could be a result of a mitochondrial genetic bottleneck where mtDNA copy number is reduced during the process of reprogramming followed by selective amplification of mtDNA (Hamalainen *et al.*, 2013). Another hypothesis is that the hiPSC clones retain similar heteroplasmy levels to the individual fibroblast cells each clone was derived from suggesting that there is no change in the m.3243A>G proportions during the reprogramming potentially allowing the selection of hiPSC clones with desired levels of the mutation (Yokota *et al.*, 2015). Ma *et al.* (2015) saw mosaic distribution of the mutation in fibroblasts.

The effects of the m.3243A>G on the efficiency of somatic cell reprogramming are not fully understood. The results from Chapter 3 showed that cells from Patient 3 failed to give rise to hiPSC clones. This could be due to the initial levels of mutated mtDNA being over the pathogenic threshold or the general inability of the cells to support the process of the reprogramming.

The aim of this chapter was to investigate the levels of mutant mtDNA in patient hiPSC clones and to explore the reasons for the failed reprogramming attempts of Patient 3 fibroblasts.

4.2 Results

4.2.1 Level of m.3243A>G in patient-derived hiPSCs

Once the hiPSC clones from both patients were derived, the levels of the m.3243A>G mutation were checked. The results are summarised in Figure 4.2.
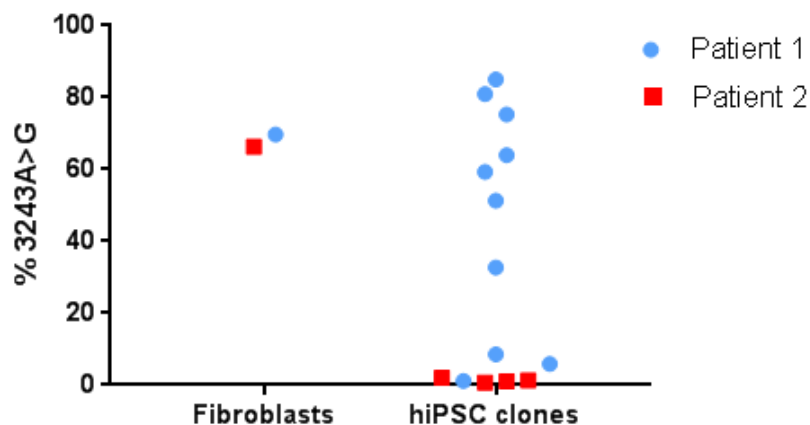
Figure 4.2. Mutant mtDNA amount in patient fibroblasts and hiPSC clones. The parental fibroblast cells had similar levels of the m.3243A>G mutation. Upon cellular reprogramming hiPSC clones with various levels of mutated mtDNA were derived from Patient 1 cells. Patient 2 hiPSC clones all had low levels of the mutation.

The parental population of fibroblast cells had similar levels of the mutation in both patients (69.67% ± 0.48 in Patient 1; 66.3% ± 0.57 in Patient 2). Patient 3 fibroblasts had 82% ± 0.00 heteroplasmy and they failed to give rise to hiPSCs. Once the hiPSC clones were isolated and sequenced, a wide range of heteroplasmy levels was found in Patient 1 hiPSCs with the lowest level being 1.11% ± 1.09 and the highest level 85.05% ± 0.98. Patient 2 hiPSC clones however had low mutation levels (ranging between 0.67% ± 1.15 and 2% ± 1). Patient 2 hiPSC clones were again tested for mutant mtDNA at later passages (passage 13, 16 and 24, data not shown) confirming that they were all wild-type.

4.2.2 Derivation of Patient 2 hiPSCs with high level of m.3243A>G

In order to isolate Patient 2 hiPSCs with mutant mtDNA, fibroblast cells were serially diluted and clones with high (>90%, ~4-30 cells per clone) or mid-level m.3243A>G (55-65%, ~125 cells per clone), were isolated. Figure 4.3 (A) shows the clonal dilution experiment set up and Figure 4.3 (B) shows the sequencing results for the parental fibroblast population and the isolated clones. Patient 1 clones were also isolated in the same way in order to assess the range of the mutation levels across different fibroblast clones to see whether the level of mosaicism in parental cells corresponds to the hiPSCs' sequencing results.
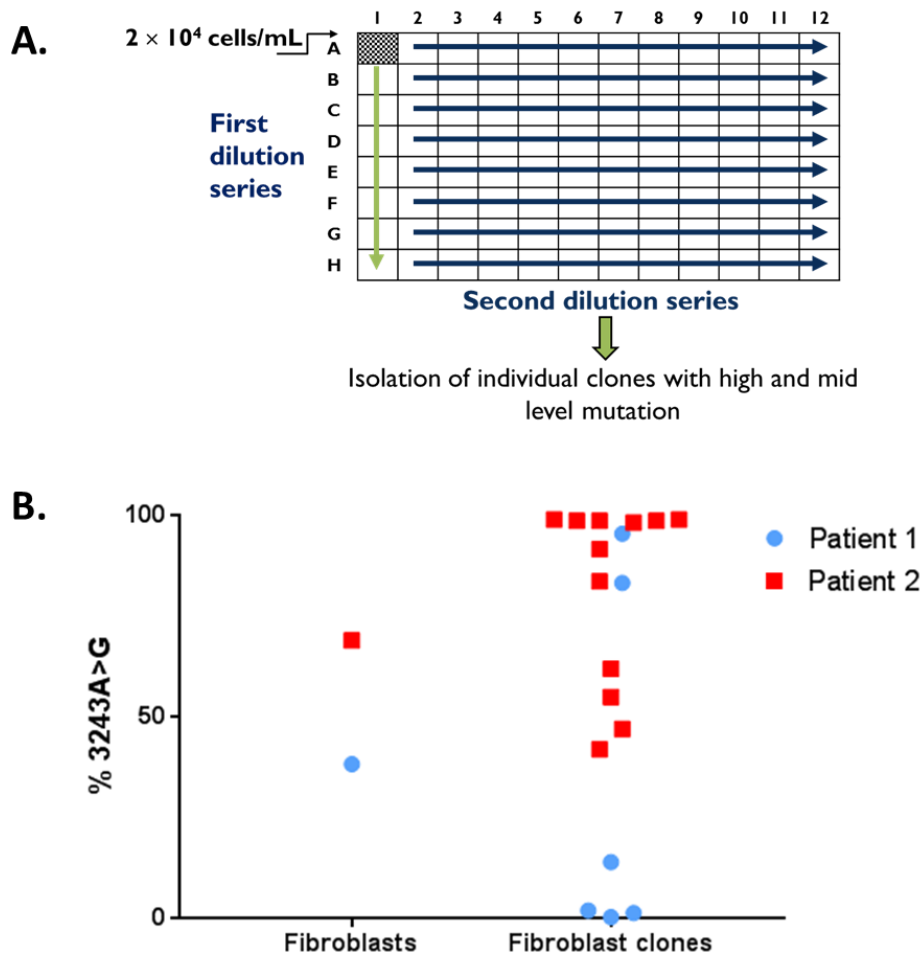
Figure 4.3. Isolation of fibroblast clones with various levels of m.3243A>G. (A) Experimental set up of clonal dilution on a 96 well plate. (B) Pyrosequencing results for the levels of mutant mtDNA in individual fibroblast clones from both patients.

Fibroblast clones from Patient 1 cells that were tested had a range of m.3243A>G heteroplasmy complementing the results obtained for hiPSC clones. This potentially shows that each individual hiPSC clone had the levels of the mutation of the parental fibroblast cell. Interestingly, the original fibroblast population had lower level of

mutated mtDNA 38.3% ± 1.5 comparing to the parental fibroblast cell population in the first reprogramming experiment (Figure 4.2). This finding demonstrates the heterogeneous nature of heteroplasmy levels across populations of cells.

Parental fibroblast cells from Patient 2 had 69.0% ± 1.0 of mutant mtDNA. For the reprogramming experiments, 2 clones with high level mutant mtDNA and 2 clones with mid-level of the mutation were chosen. Cells were reprogrammed with the same reprogramming kit as in the previous experiments (CytoTune 2, Life Technologies). Representative images of the reprogramming results are shown in Figure 4.4.
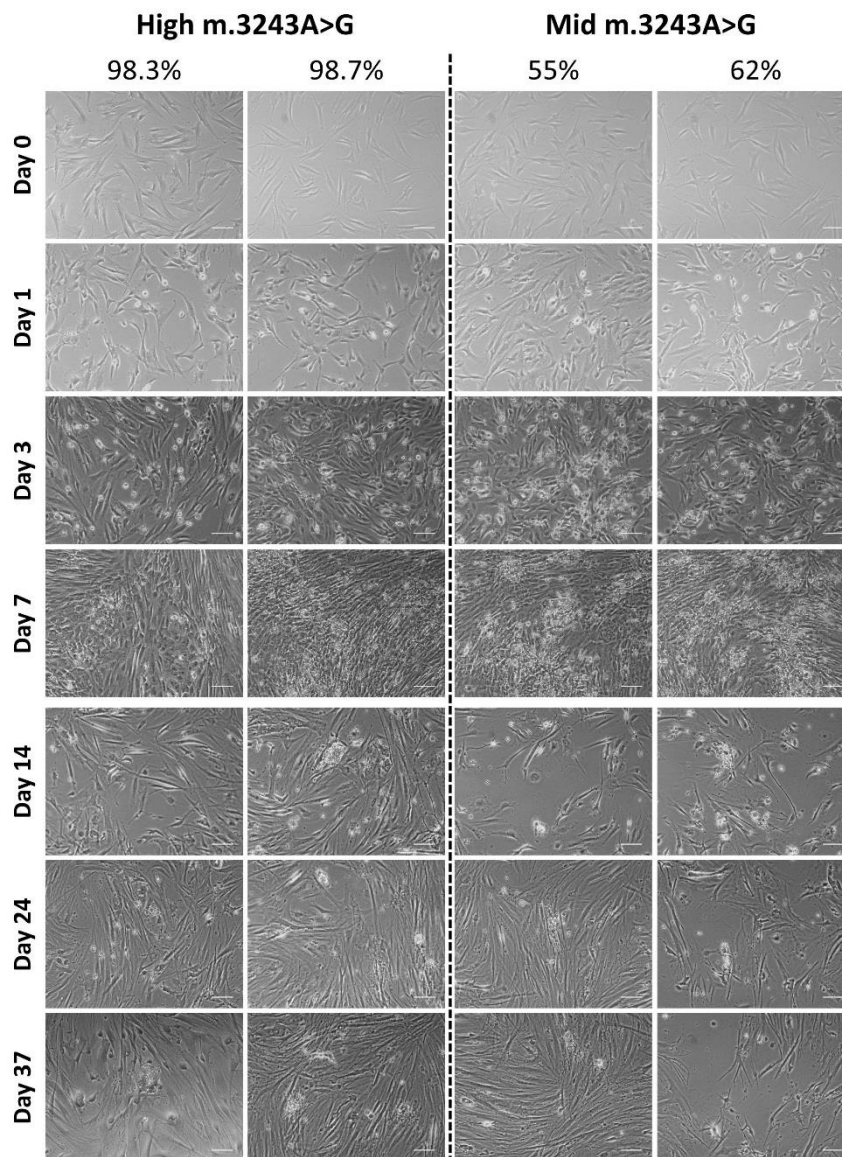
Figure 4.4. Reprogramming Patient 2 fibroblast clones with different levels of m.3243A>G. Neither of the clones with high or mid-level mutated mtDNA gave rise to hiPSCs after 37 days in culture. Scale bar, 100 μm.

Patient 2 cells failed to give rise to hiPSCs when only fibroblasts with high or mid-level of the m.3243A>G were used as a starting cell population. As can be seen from the images in Figure 4.4, cells started to change morphology by day 7, however by day 37 no hiPSC colonies were found.

In order to explain these results, fibroblast cells were tested for a number of parameters in order to elucidate the differences between them.

4.2.3 Investigating patients' fibroblasts

Patient 2 cells failed to give rise to hiPSC clones with mutant mtDNA and Patient 3 cells failed to reprogram altogether. For this reason, these cells were further investigated with the attempt to uncover potential explanation.

Heteroplasmy levels across different passages varied depending on which patient the cells came from. The level of heteroplasmy slightly reduced with passaging for Patient 1 and 3 cells. Interestingly, Patient 2 cells had increased levels of the mutation reaching 95% ± 1.7 by passage 24 [Figure 4.5 (A)]. Next, total mtDNA amount and mtDNA common deletion levels were checked in all cells. Patient 1 cells had significantly higher levels of mtDNA copy number comparing to other patients and control, which could potentially indicate that there is a mechanism attempting to compensate pathogenic m.3243A>G mtDNA mutation. No mtDNA common deletions were found in any of the cells [Figure 4.5 (B, C)].
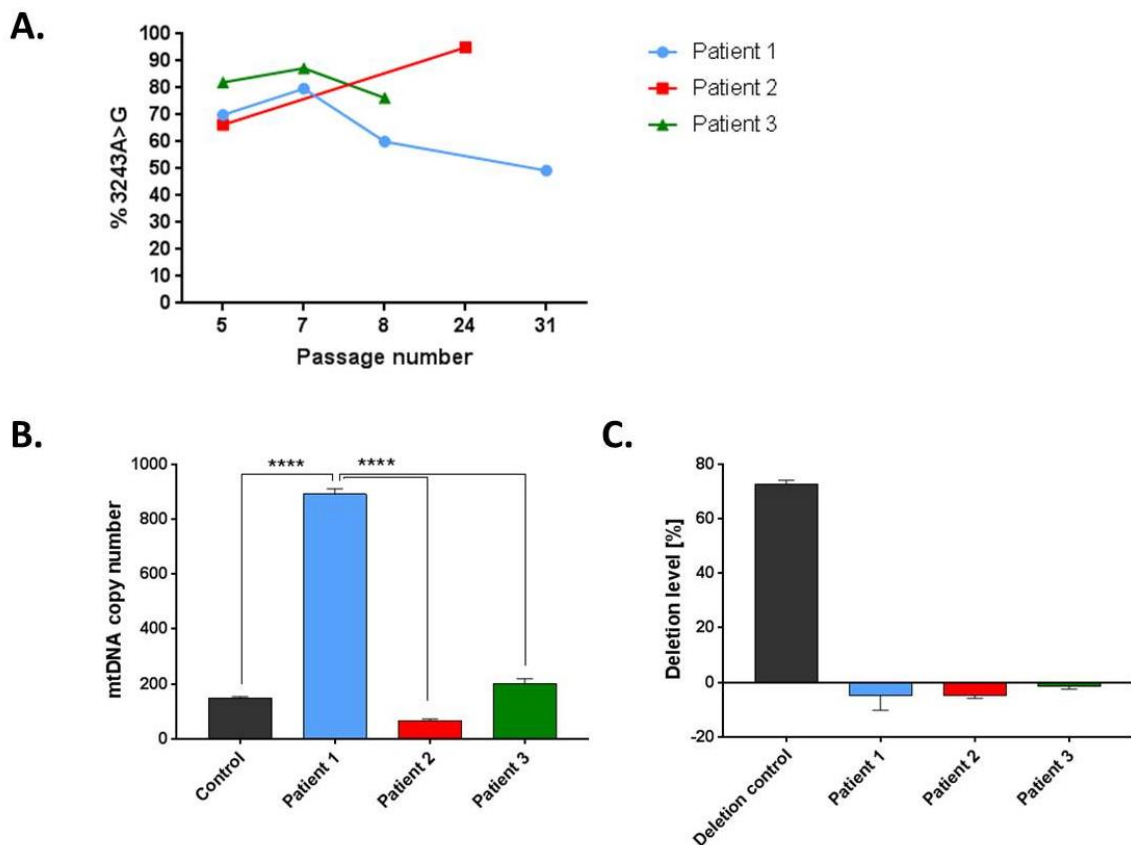
Figure 4.5. Mutational profiling of patients' fibroblasts. (A) Pyrosequencing results for heteroplasmy level change in patient fibroblast cells over passaging. (B) qPCR results for total mtDNA copy number. (C) qPCR results for mtDNA common deletion levels. N=3. Data presented as Mean ± SEM. Significance was established with one-way ANOVA followed by Tukey's post hoc test.

Oxygen consumption experiments for Patient 1 and Patient 2 cells showed that Patient 2 cells had significantly lower levels of basal and maximal respiration. These results are consistent with the reduced mtDNA copy number and potentially lower protein levels when compared to Patient 1 and control [Figure 4.6 (A, B)]. Patient 3 cells were not included in the experiments due to timing issues.
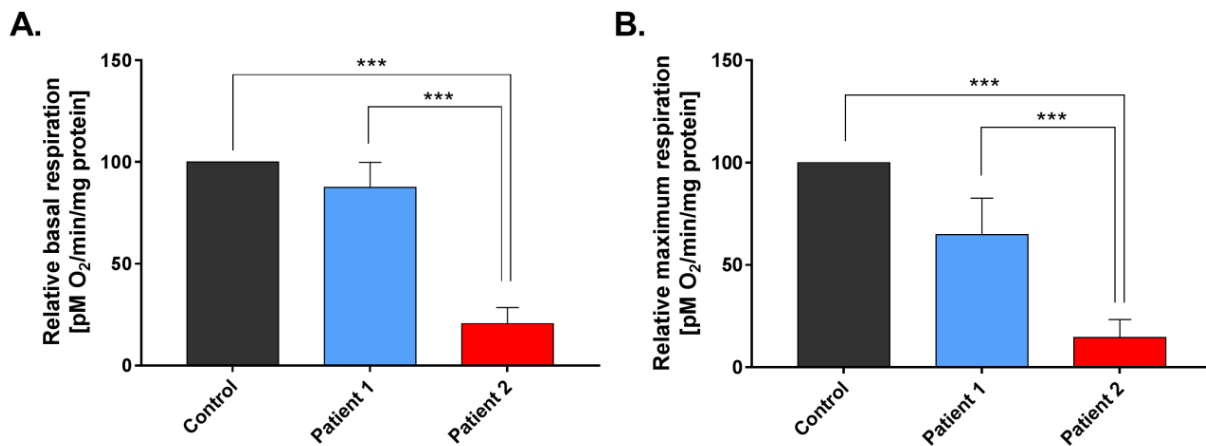
Figure 4.6. Mitochondrial respiration in patients' fibroblasts. (A) Seahorse results for basal respiration. (B) Seahorse results for maximal respiration. N=3. Data presented as Mean ± SEM. Significance was established with one-way ANOVA followed by Tukey's post hoc test.

4.3 Discussion

Reprogramming experiments resulted in the derivation of hiPSC clones with varying levels of the m.3243A>G from Patient 1 cells, Patient 2 cells only gave rise to wild-type hiPSCs and Patient 3 cells failed to give rise to hiPSCs. Clonal isolation of Patient 2 fibroblasts with high and mid-level of heteroplasmy and subsequent transfection with the reprogramming factors failed to give rise to any hiPSC clones.

Somatic cell reprogramming is accompanied by a number of changes within the cells, many of which involve remodelling of mitochondria. Firstly, ATP production shifts from OXPHOS to glycolysis to allow rapid proliferation and reduced production of ROS. In addition, mitochondria undergo a number of morphological changes including formation of more globular-shaped immature mitochondria with perinuclear localisation [reviewed by Lopes and Rego (2016)]. Furthermore, mtDNA goes through a number of changes. Using mouse cells, it has been previously demonstrated that mtDNA copy number is tightly controlled during the process of reprogramming and differentiation (Kelly *et al.*, 2013). The effects of the m.3243A>G on the process of cellular reprogramming have not been fully elucidated. It has been

previously shown that initial high level of heteroplasmy in the starting population of fibroblasts creates a reprogramming block preventing generation of hiPSCs (Yokota *et al.*, 2015). Indeed, Patient 2 high mutation level fibroblast clones and Patient 3 fibroblasts which had >80% of m.3243A>G failed to give rise to hiPSCs. However, it is still not clear why Patient 2 fibroblast clones with 55 – 62% of m.3243A>G did not give rise to hiPSCs and why in general only wild-type clones were derived from cells from this patient. For this reason, further investigations were conducted on fibroblast cells to provide additional insight into the reprogramming process.

The potential variations in mutated mtDNA levels were tested over a number of passages in fibroblast cells of all patients. Interestingly, unlike the other two patients, Patient 2 cells had an increase in the levels of m.3243A>G over passaging reaching ~95% by passage 24. These same cells failed to give rise to hiPSC clones with mutated mtDNA. It could be speculated, that due to high proliferative capacity of mutated mtDNA in these cells, over time they selected out the low mutation level clones. Consequently, high level clones failed to give rise to hiPSCs as a result of the reprogramming block discussed earlier (Yokota *et al.*, 2015). Proliferative advantage of mutant mtDNA with m.3243A>G has been previously observed by Yoneda *et al.* (1992). The same group suggested that the cells might still be able to survive when the proportion of wild-type mtDNA is below 10% by adapting to glycolytic energy production or alternatively there might be enough wild-type mtDNA in individual mitochondrion that compensates for the presence of mutated mtDNA. Small amount of wild-type mtDNA is able to support respiratory activity of the cells or alternatively, residual activity of the mutant mtDNA is sufficient to provide this support (Bentlage and Attardi, 1996). Dunbar *et al.* (1995) showed that some cells shift mtDNA ratios towards wild-type and some show proliferative advantage of mutant mtDNA depending on the cells' nuclear background. Therefore, in this study, we can postulate the differences in heteroplasmy levels change over time by the difference in the nuclear background of the cells.

The level of the mutated mtDNA in cells is important, however, it is also necessary to consider the total amount of mtDNA in the cells. One study that looked at tissues derived from MELAS patients with the m.3243A>G found that mtDNA amount was increased in patient samples when compared to controls (Kaufmann *et al.*, 1996). It has also been suggested that cells with lower mtDNA copy number reach the pathogenic threshold of the mutation earlier than cells with higher mtDNA

copy number. Therefore, increased mtDNA copy number could have a compensatory effect on high proportion of mutant mtDNA as the amount of mitochondrial DNA could be indicative of the cells ability to produce ATP via OXPHOS (Bentlage and Attardi, 1996). In this study, Patient 2 and Patient 3 cells had similar levels of mtDNA copy number to the controls, however, Patient 1 cells had significantly increased levels. It could be speculated that Patient 1 cells were compensating for the defects in translation by increasing the amount of mtDNA and thereby allowing successful cellular reprogramming. On the other hand, Patient 2 and Patient 3 cells did not have this compensatory effect which potentially resulted in failed reprogramming attempts and failed attempts to derive clones with m.3243A>G. It is also plausible that Patient 2 cells were unable to undergo a switch between OXPHOS and glycolysis to reach successful reprogramming.

Increased mtDNA copy number might not necessarily predict mitochondrial protein synthesis and function. In order to test mitochondrial function, oxygen consumption was assayed using Seahorse XF analyser. The results showed that Patient 2 cells had significantly lower levels of basal and maximal respiration which could possibly account for the results of the reprogramming experiments.

Chin *et al.* (2014) previously reported that ~12% of patients with m.3243A>G also have mtDNA deletions which lead to additional clinical features, including retinitis pigmentosa and migraine. After testing patients' fibroblasts for mtDNA common deletions, none of the MELAS patients in this study were found to have the deletions. Therefore, this is not the feature that can be associated with failed reprogramming.

One study showed that the bioenergetic profile of parent cells affects their ability to generate hiPSCs and cells with higher propensity for glycolytic metabolism reprogram with higher efficiency (Panopoulos *et al.*, 2012). Therefore, extracellular acidification rate (ECAR) could be used as a pre-screen to estimate the likelihood of successful reprogramming. ECAR is a powerful tool for measuring the levels of glycolysis in the medium surrounding the cells from excretion of lactic acid per time unit. It is performed by supplying the cells with glucose and inhibiting ATP synthase with oligomycin stimulating glycolysis (TeSlaa and Teitell, 2014). Mitochondrial membrane potential, assessed by the tetramethyl rhodamine methyl ester (TMRM) dye, has also been shown to be elevated in hPSCs compared to fibroblasts which again could mean that Patient 2 fibroblasts with high m.3243A>G were unable to

undergo this change resulting in failed reprogramming attempts (Schieke *et al.*, 2008). These parameters could be used in future studies as a pre-screen of cells to be reprogrammed.

Based on the findings in this and the previous chapter, three Patient 1 hiPSC clones were chosen to be used in further experiments.

Chapter 5. Functional characterisation of patient hiPSCs

5.1 Overview

The main aim of this chapter was to elucidate potential differences that hiPSCs with different levels of the m.3243A>G might have. Not all patient clones were able to survive at the initial stages of cell culture and some of them had decreased expansion rate when compared to controls. A large number of factors can affect cell cycle kinetics and survival and some of those were investigated in the experiments discussed below.

Eukaryotic cells undergoing division go through a number of stages during proliferation. Typical cell cycle includes G1 (gap 1), S (synthesis), G2 (gap 2) and M (mitosis) phases under control of a series of cyclin-dependent kinases. G1 and G2 phases allow cell growth and include multiple checkpoints ensuring the cell is ready for replication and ensuring DNA integrity, whilst DNA synthesis occurs during the S-phase (Pardee, 1974; Sanchez *et al.*, 1997). hESCs have an average cell cycle of ~16 hours (as opposed to ~24-32 hours in somatic cells). On average 52-65% of the total population of hESCs reside in the S-phase, 20-24% in G1 and 10-20% in G2 phases. The shortening of the division time in hESCs is attributed to truncated G1 phase and has been shown to be linked to the maintenance of an undifferentiated state (Becker *et al.*, 2006; Filipczyk *et al.*, 2007; Neganova *et al.*, 2009). Ghule *et al.* (2011) used hiPSCs to show that they have similar distribution of the proportions of cells at different stages of the cell cycle when compared to hESCs. They found that >50% of cells were in S-phase and that cells had a reduced G1 phase. One of the most common methods to study cells synthesising DNA is by BrdU, which is a synthetic analogue of thymidine and is actively incorporated into newly synthesised DNA during the S-phase (Gratzner, 1982). DAPI can be used to quantify the number of cells in G1 and G2 phases. Cells in G2 will have double the amount of DNA compared to G1 which can be quantified by flow cytometry using appropriate gating technique outlined by Pozarowski and Darzynkiewicz (2004).

In order to ensure genomic integrity, cells employ a number of check points to allow transmission of only healthy DNA during proliferation. Abnormalities in DNA can cause cell cycle arrest (in G1, S and G2), DNA repair or apoptosis (Bartek and Lukas, 2007). Therefore, in the context of cell cycle kinetics it is of value to also test

for the presence of apoptosis and DNA damage markers. DNA damage might be induced internally (e.g. ROS) or externally (e.g. UV radiation). It has been suggested that in most cases, DNA damage is caused by endogenous factors (Momcilovic *et al.*, 2011). A range of proteins is deployed to chromatin regions that are damaged, which in turn initiates a cascade of events including propagation of damage signals. A key cellular response to DNA double strand breaks and apoptosis is the histone H2A variant H2AX which is phosphorylated at serine 139 as a result of DNA damage (forming γH2AX) (Rogakou *et al.*, 1998). Such modification leads to chromatin modification providing recruiting sites for repair protein complexes (Rogakou *et al.*, 1999). Mouse ESCs deficient in H2AX display elevated levels of genomic instability as a result of ionising radiation (Bassing *et al.*, 2002). Additionally, MEFs derived from H2AX$^{-/-}$ embryos have been shown to have growth abnormalities, premature senescence and impaired DNA repair (Celeste *et al.*, 2002). Therefore, assessing levels of γH2AX was chosen as a way to test for possible DNA damage in patient-derived hiPSCs.

The process of cell death can be classified into two main types. Programmed cell death occurs as part of development and morphogenesis and is genetically pre-determined. The second type is apoptosis, the principal form of cell death. Initially, it was associated with the changes in the morphology of cells undergoing cell death, including disintegration of plasma membrane, condensation of nuclear chromatin and cytoplasmic organelles and loss of mitochondrial membrane potential. The process is accompanied by the activation of caspases which leads to protein degradation and death [reviewed by Chipuk and Green (2005)]. In this chapter, cell death was studied in the context of apoptosis. The field of apoptosis research has been greatly advanced by studies using *Caenorhabditis elegans*. Early studies identified a gene called *ced-3* as the key regulator of cell death (Ellis and Horvitz, 1986). Later on it was shown that CED-3 bears similarities with the human analogue interleukin-1β (IL-1β)-converting enzyme (ICE) which is a cysteine-aspartate protease (Yuan *et al.*, 1993). Altogether, there are nine ICE-like proteases and as a group they have been denoted as caspases ('c' – cysteine protease, 'aspase' – cleaving of aspartic residue) (Cohen, 1997). Caspase-3 is one of the key executioners of apoptosis. It proteolytically cleaves a number of key proteins including poly(ADP-ribose) polymerase (PARP) which is a nuclear protein largely involved in DNA repair as has been demonstrated in an early study by Benjamin and Gill (1980). Cleavage of PARP results in formation of 89 kDa (catalytic) and 24 kDa (DNA binding domain) fragments

and is recognised to be a hallmark of apoptosis (Lazebnik *et al.*, 1994; Chaitanya *et al.*, 2010). The 89 kDa domain is translocated to the cytosol whereas 24 kDa domain binds to DNA preventing DNA repair enzymes binding to the sites of damage (Chaitanya *et al.*, 2010). The 89 kDa-cleaved domain is therefore an acceptable indicator of apoptosis and it was used in the current study.

Mitochondria generate ROS primarily as part of OXPHOS resulting in redox signalling. ROS are highly reactive oxygen metabolites that are able to react with cellular macromolecules. If ROS homeostasis is unbalanced and the cells are not able to cope with it, it can lead to oxidative stress resulting in damage to nucleic acids, lipids and proteins which might influence cell survival and proliferation [reviewed by Ray *et al.* (2012)]. Superoxide radical is the primary ROS species and it is formed when molecular oxygen is reduced [$O_2 + e^- \rightarrow O_2^{-}$], a process which can be affected by the mitochondrial membrane potential ($\Delta\Psi_m$). Oxygen can be reduced further to produce hydrogen peroxide [$2O_2^{-} + 2H \rightarrow H_2O_2 + O_2$] (Hancock *et al.*, 2001). There are a number of markers that are used for the direct and indirect detection of ROS. DHE and mitochondrial-targeted DHE (mitoSOX) are small molecule fluorescent probes which specifically target superoxide (Wang *et al.*, 2013). When they react with superoxide they generate 2-hydroxyethidium (2-OH-E$^+$), which emits fluorescence (Zhao *et al.*, 2005). Dihydrorhodamine123 (DHR) is another probe used for ROS detection. It is converted to fluorescent rhodamine when it reacts with H_2O_2 by-product OH· (Wang *et al.*, 2013). Mitochondrial mass was measured by looking at the levels of NAO, a probe for mitochondrial membrane. It binds to cardiolipin, a phospholipid found in the inner mitochondrial membrane (Petit *et al.*, 1992). Cardiolipin binds respiratory chain complexes and it has been suggested that without it, Complex I and III are inactive (Fry and Green, 1981). It is involved in mitophagy by redistribution to the outer mitochondrial membrane (Chu *et al.*, 2014) Additionally, some studies suggested that cytochrome *c* binds cardiolipin as part of a pro-apoptotic signalling cascade [reviewed by Jacobson *et al.* (2002)]. Another dye which is widely used is JC-1, which provides assessment of mitochondrial $\Delta\Psi_m$ and serves as a marker of apoptosis. JC-1 exists as a monomer (green fluorescent peak representative of cytoplasmic JC-1) and as an aggregate (red fluorescent peak representative of mitochondrial aggregates); mitochondria uptake the monomer into the matrix and when it reaches a certain level in energised mitochondria, it is converted into aggregates and the ratio of the two provides information about $\Delta\Psi_m$ (Reers *et al.*, 1991). Measurement of $\Delta\Psi_m$ is important because it reflects the ability

of mitochondria to force proton flow into mitochondrial cytoplasm and JC-1 has been suggested to be an ideal probe for this kind of assessment (Perry *et al.*, 2011).

A range of other assessments were based on previous work undertaken using hiPSCs derived from patients with mitochondrial diseases. As part of this chapter, patient-derived hiPSCs were studied for mtDNA copy number, oxygen consumption and heteroplasmy levels.

5.2 Results

As discussed in the previous chapter, three Patient 1 hiPSC clones were selected for further work. Clone 5 had ~50% m.3243A>G, Clone M2 ~70% m.3243A>G, and Clone 8 was an isogenic control. These values correspond to average levels of mutated mtDNA at the time when the experiments were conducted (Figure 5.1).
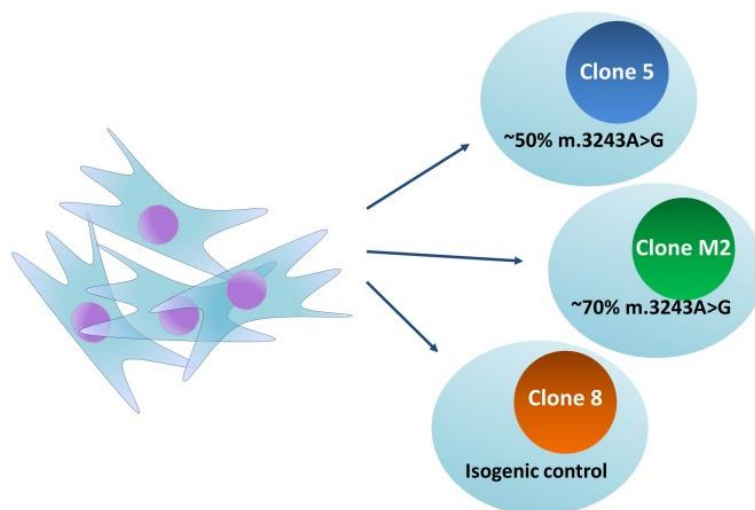
Figure 5.1. Patient 1 hiPSC clones selected for further work, including clone designations and the percentage of mutated mtDNA.

5.2.1 Cell cycle, apoptosis and DNA damage assessment

Initially, ten hiPSC clones were derived from Patient 1 fibroblasts. In the early stages of cell culture, most of the clones failed to propagate. Additionally, there were marked differences in the ability of these cells to expand. Cells with higher levels of the mutation grew more slowly with minimal requirements for passaging. In the initial stages, it was noted that Clone 5 (~50% m.3243A>G) in particular did not expand well. The differential levels of expansion observed could be explained by either reduced cell proliferation or increased levels of cell death. Cell cycle, apoptosis and DNA damage assays were carried out in order to investigate whether there were differences in these parameters across different clones. Results in Figure 5.2 show

that there was no significant difference between control hiPSCs and patient-derived hiPSCs in terms of the percentage of cells residing in different stages of the cell cycle [Figure 5.2 (A)]. On average, there were ~50% of cells in the S-phase, ~38% in G1 phase and 13% in G2 phase. The percentage of cells in G1 phase was higher than what is expected for this cell type. There was no difference between hiPSCs with regards to the levels of the apoptosis marker 89 kDa-cleaved fragment of PARP or DNA damage marker γH2AX [Figure 5.2 (B)]. Overall, there was no clear indication that patient-derived hiPSCs differed across any of these parameters.
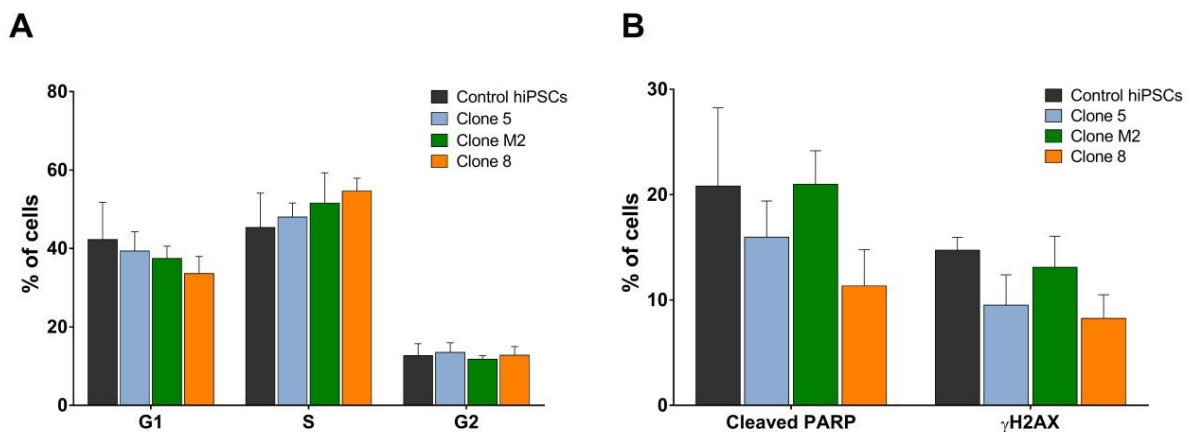
Figure 5.2. Measurement of cell proliferation, apoptosis and DNA damage in hiPSCs by flow cytometry. (A) Cells showed similar proliferation capacity as determined by incorporated BrdU (S-phase) and DAPI (G1, G2 phases). (B) Cells showed similar levels of apoptosis (cleaved PARP) and response to DNA double strand breaks (analysis for phosphorylated γH2AX). N=3. Data presented as Mean ± SEM. Significance was established with one-way ANOVA followed by Tukey's post hoc test.

5.2.2 mtDNA levels and cellular respiration in hiPSCs

Previous study has showed that hiPSCs with a high mutation load have increased levels of mtDNA copy number (Hamalainen *et al.*, 2013). Similarly, in this study patient hiPSC clone with the highest level of mutated mtDNA (Clone M2) had significantly increased levels of mtDNA copy number compared to the other two clones and hESCs. The mtDNA deletions in the major arc of the mtDNA, historically referred to as 'common deletion', were also checked and it was confirmed that, just like in the original fibroblasts, no common deletions were detected. The results are shown in Figure 5.3 (A, B). Interestingly, the overall mtDNA copy number significantly decreased in all hiPSC clones compared to their parental fibroblasts which could be explained by their low energy demands and reliance on OXPHOS compared to fibroblasts [Figure 5.3 (C)].
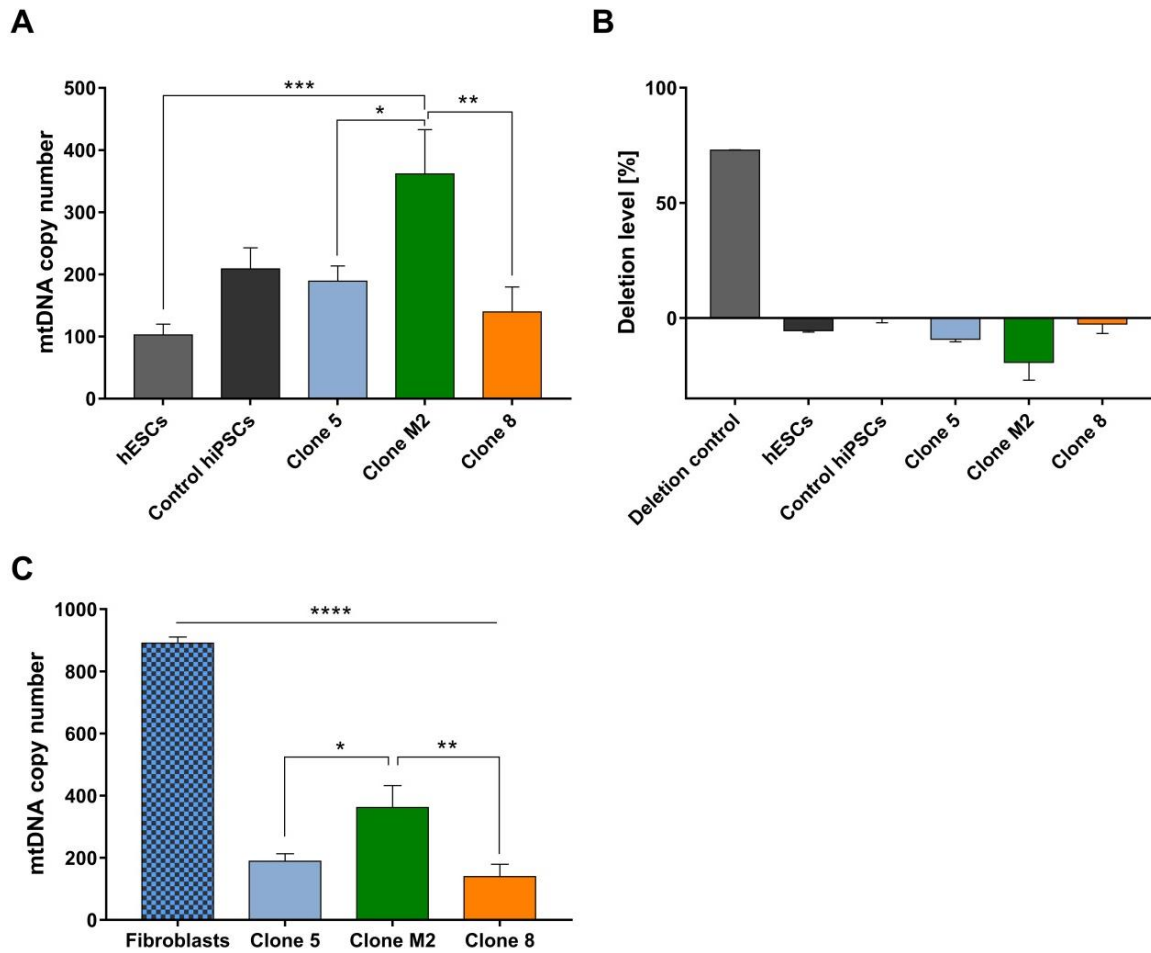
Figure 5.3. Analysis of mtDNA copy number and common deletion levels by qPCR. (A) Patient 1 Clone M2 (heteroplasmy ~70%) had significantly higher level of mtDNA compared to hESCs, Clone 5 (heteroplasmy ~50%) and Clone 8 (isogenic control). (B) None of the cells had mtDNA common deletions. (C) All hiPSC clones had significantly lower levels of mtDNA compared to parental fibroblasts. N=3. Data presented as Mean ± SEM. Significance was established with one-way ANOVA followed by Tukey's post hoc test.

In order to test whether cells had different levels of oxygen consumption, analysis using the Seahorse platform was performed. No significant difference was found between control and patient hiPSC clones in terms of basal and maximal capacity respiration (Figure 5.4).
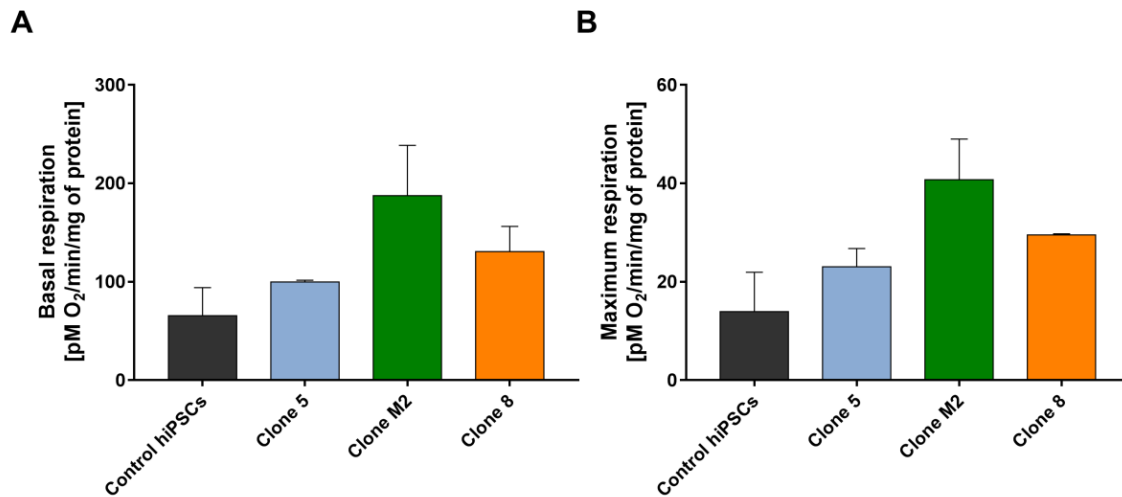
Figure 5.4. Analysis of oxygen consumption by Seahorse. Seahorse analysis showed no difference in basal respiration (A) or maximal capacity respiration (B) in different cells. N=3. Data presented as Mean ± SEM. Significance was established with one-way ANOVA followed by Tukey's post hoc test.

5.2.3 Assessment of ROS production, mitochondrial mass and mitochondrial membrane potential

In order to further investigate potential differences between hiPSCs, additional parameters of mitochondrial function were investigated. As determined by NAO stain, there was no trend towards cells having differences in mitochondrial mass, and no difference in $\Delta\Psi_m$ as determined by JC-1 [Figure 5.5 (A, B)]. Clone M2 (~70% m.3243A>G) seemed to have lowered levels of H_2O_2 and superoxide when compared to the other hiPSCs [Figure 5.5 (C, D)].
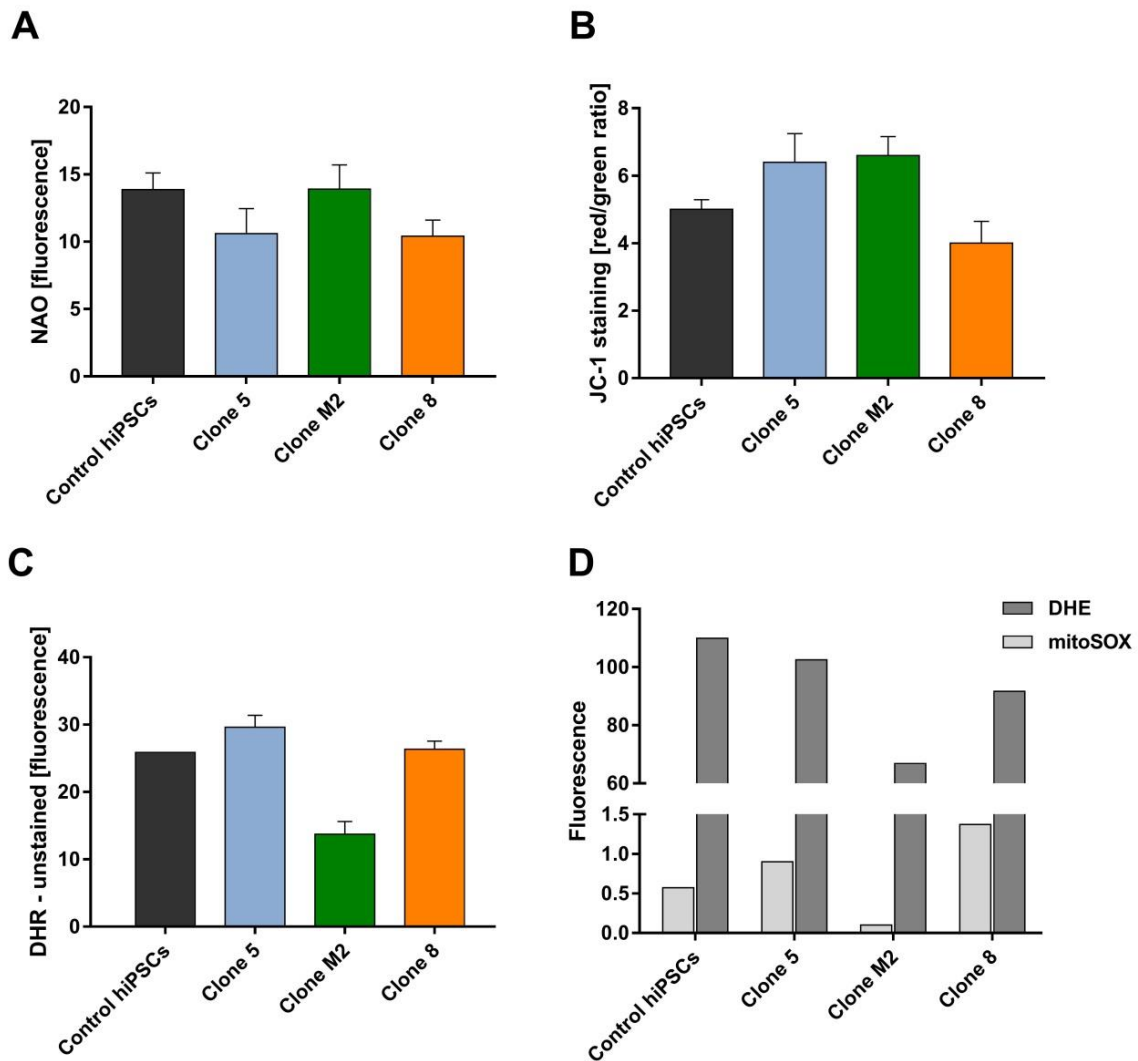
Figure 5.5. Measurement of mitochondrial mass, mitochondrial membrane potential, intracellular superoxide and peroxides by flow cytometry. (A) Cells showed comparable levels of mitochondrial mass, (B) the levels of ΔΨ$_m$, (C) peroxides, and (D) superoxide. Error bars represent Mean ± SD between 3 technical repeats. Where no error bars are shown, only one repeat was possible due to low cell numbers.

5.2.4 Heteroplasmy level change in patient hiPSC clones over passaging

Two of the hiPSC clones were monitored for changes in the levels of mutated mtDNA over passaging. As can be seen in Figure 5.6, in Clone 5, although initially having ~32% m.3243A>G, once the mutation load was established in the early passages, it remained around ~50% throughout the rest of the study. It should be noted that for all the experiments described here and later on, cells were used within the passages where the level of the mutation was around 50%. Clone M2 cells were derived with high level of mutated mtDNA of 75%. Over passaging the levels of the mutation remained at ~70%. Interestingly, by passage 20 the mutation level went down to 53%. Due to the fact that the cells were tested at passage 15 and 20 and not at

passages in-between, it is difficult to speculate at what point the mutation level went down. Passage 19 was the latest passage at which these cells were used in any of the analyses in the experiments described in this chapter or in any further work.
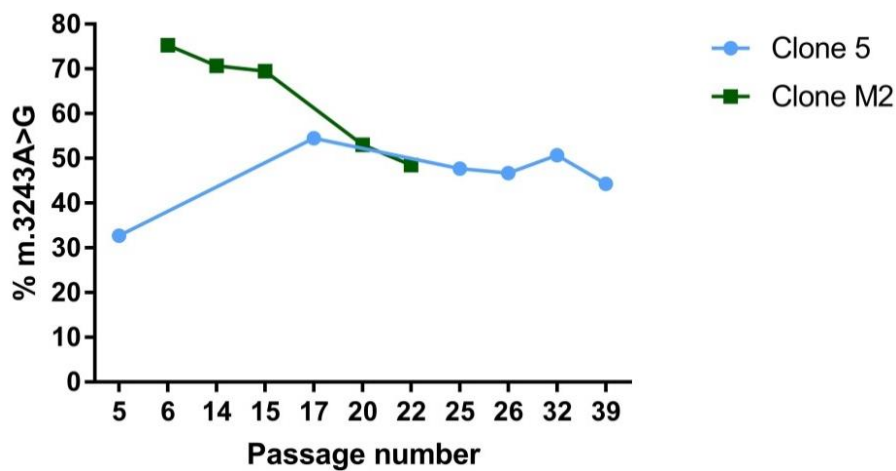
Figure 5.6. Heteroplasmy level change in patient hiPSCs over passaging. Clone 5 cells had similar levels of m.3243A>G over passaging. Clone M2 retained the levels of mutated mtDNA over the first 15 passages. Mutation level went down by passage 22 from ~70% to 53%.

5.3 Discussion

The main aim of this chapter was to investigate potential differences in patient-derived hiPSC clones with different levels of the m.3243A>G mutation.

One of the first observations made was that cells with mutated mtDNA displayed reduced expansion capacity. This finding was also presented by Cherry *et al.* (2013) and Wahlestedt *et al.* (2014), however, they investigated cells with other mutations; the Pearson marrow-pancreas syndrome (caused by single large-scale deletions in mtDNA leading to bone marrow failure) and the "mutator" mouse (which carry amino acid substitution of the nuclear-encoded *Polg* gene) respectively. Other studies did not comment on whether there was a difference in cell growth therefore it is difficult to draw conclusions whether it is a common trait in these cells.

In order to elucidate whether patient and control hiPSCs had differences in cell proliferation, apoptosis and DNA damage they were analysed using BrdU incorporation, DAPI, cleaved PARP and γH2AX. No difference was found in cell proliferation between control and patient hiPSCs. As discussed earlier in this chapter, hPSCs normally have 50-65% of cells residing in S-phase and the results in this chapter showed that on average there were ~50% of cells in this phase of the cell cycle (Neganova *et al.*, 2009; Ghule *et al.*, 2011). Additionally, it would be expected

to see 20-24% and 10-20% in G1 and G2 phases respectively. It was found that ~38% of cells were in G1 phase and ~13% in G2 phase. There could be a number of explanations as to why there is such discrepancy between results associated with G1 phase. There is some evidence that a shortened G1 phase is associated with the pluripotency state in hPSCs and is required for successful reprogramming (Ruiz *et al.*, 2011). It was shown that hESCs undergoing cell cycle arrest are subject to irreversible differentiation as assessed by expression of pluripotency-related markers Tra-1-60 and Tra-1-81. Cells used in this project were checked daily for morphological changes associated with differentiation and no such changes were observed. Although, it was not feasible to regularly test the cells for the expression of pluripotency markers, they were differentiated into RPE at a later stage strongly suggesting that the cells remained pluripotent.

Since no difference in cell proliferation was found between patient and control cells, it was next determined whether patient cells had higher levels of apoptosis and DNA damage. As shown in Figure 5.2 (B), there was no significant difference between patient and control cells. This experiment could be improved by testing the cells under stress conditions because it is possible that they have similar base levels of these markers, but under adverse conditions they might be more susceptible to DNA damage and cell death.

It is important to keep in mind that Clone M2 had changes on chromosome 20 which could mean that several genes involved in cell growth and survival were amplified masking the effect of the mutation in mtDNA. Moreover, it was Clone 5 that grew at a slower rate and this clone did not have DNA abnormalities. However, it is not guaranteed that having duplication on chromosome 20 means overexpression of the genes located on it as discussed in Chapter 1 (Amps *et al.*, 2011). More work would be required to verify whether chromosomal abnormalities had an effect on the behaviour of these cells and assessments such as RNA-seq or ChIP-sequencing could be performed.

A number of studies have emerged in the last four years where hiPSCs have been derived from patient cells with mitochondrial abnormalities. This provides an opportunity to draw some comparisons between the results from this study and published work particularly where there are divergent findings in the literature. A summary has been provided in Table 5.1.

Study	Mutation	hiPSCs growth rate	Total mtDNA	Heteroplasmy change over passaging	Basal respiration	Maximal respiration	$\Delta\Psi_m$ (*)	ROS (*)	Cell cycle	Apoptosis	DNA damage	Mitochondrial mass (*)
This chapter	**m.3243A>G**	↓ expansion	↑	Clonal variation	ND	ND	↓	↓	ND	ND	ND	↓
Fujikura _et al._ (2012)	**m.3243A>G**		ND	No change								
Hamalainen _et al._ (2013)	**m.3243A>G**		↑	No change								
Folmes _et al._ (2013)	G13513A				ND							
Cherry _et al._ (2013)	PS	↓ expansion		Clonal variation	↓		↓					
Wahlestedt _et al._ (2014)	_Polg_ (-/-) mouse	↓ expansion						↓				
Yokota _et al._ (2015)	**m.3243A>G**		↑	Clonal variation								
Kodaira _et al._ (2015)	**m.3243A>G**		ND	Clonal variation								
Ma _et al._ (2015)	**m.3243A>G**				↓							
Hatakeyama _et al._ (2015)	m.5541C>T (myoblasts)						↓	↑				

Table 5.1. Comparison of studies that use iPSCs to study mitochondrial mutations (compared to controls). ND – no difference; PS - Pearson marrow-pancreas syndrome; m.5541C>T, mutation in tRNA[trp] in _MT-TW_ gene. Green shading – similar findings to current study; red shading – opposing results; grey shading – no data. (*) more repeats needed for definitive conclusions.

In this chapter, hiPSC clone with the highest level of the mutation was found to have significantly higher total mtDNA copy number compared with hESCs and hiPSCs with lower levels of the m.3243A>G mutation. All clones had significantly lower mtDNA copy number compared with the parental fibroblasts. Two other studies that described derivation of hiPSCs with m.3243A>G had similar results (Hamalainen *et al.*, 2013; Yokota *et al.*, 2015). However, some studies saw no correlation between heteroplasmy level and mtDNA copy number (Fujikura *et al.*, 2012; Yokota *et al.*, 2015). As discussed in the previous chapter, patients with m.3243A>G have increased levels of mtDNA and inability to upregulate the copy number can lead to development of a pathological phenotype. Therefore, increase in mtDNA copy number was attributed to compensatory mechanisms to account for translational defects (Bentlage and Attardi, 1996; Kaufmann *et al.*, 1996). This compensatory effect was also observed in a patient with Kearns-Sayre syndrome, which is characterised by the diagnostic triad of pigmentary retinal degeneration and CPEO developing before the age of 20 years old. This particular patient harboured 3 kb mtDNA deletion at a level of 92% in their muscle, nevertheless they had a relatively mild clinical phenotype (Wong *et al.*, 2003). It is not clear why there are discrepancies in studies discussed in this chapter. Fujikura *et al.* (2012) suggested that low metabolic demand of hiPSCs means that there is no requirement for amplification of mtDNA, but this was not observed in this and another study that looked into it (Kodaira *et al.*, 2015). Given these inconsistencies, further work is required to elucidate the mechanism of mtDNA copy number regulation in hPSCs carrying pathogenic mitochondrial mutations. It is also possible that the failure to increase mtDNA copy number is the result of increased mitophagy, which allows the removal of damaged mtDNA in diseased cells [reviewed by Clay Montier *et al.* (2009)].

No difference in oxygen consumption was found between patient and control cells, similar to what has been reported by Folmes *et al.* (2013). This observation could be due to the fact that hiPSCs do not rely primarily on mitochondrial respiration or possibly because our patient cells had increased number of mtDNA copies. However, Cherry *et al.* (2013) and Ma *et al.* (2015) saw a decrease in basal respiration rate in their cells. Additionally, they saw a decrease in $\Delta\Psi_m$ which could mean that there were abnormalities in the electron transport chain function (Cherry *et al.*, 2013).

Cells were also tested for mitochondrial mass, $\Delta\Psi_m$ and the presence of ROS. Decrease in $\Delta\Psi_m$ has been previously described as an early marker of apoptosis leading to uncoupling of electron transport from ATP production. The same study showed that a drop in $\Delta\Psi_m$ is possibly followed by alternations of mitochondrial membrane structure as assessed by NAO fluorescence (Petit *et al.*, 1995). With the use of the NAO stain, we found no trend towards cells having differences in mitochondrial mass between the different clones tested [Figure 5.5 (A)]. There was a trend towards Clone M2 (~70% m.3243A>G) having lowered $\Delta\Psi_m$ as determined by JC-1 [Figure 5.5 (B)]. The same clone seemed to have lowered levels of H_2O_2 and superoxide when compared to other hiPSCs, which could imply that the electron transport chain is not active due to reduced $\Delta\Psi_m$ and therefore there is less ROS production [Figure 5.5 (C, D)]. Future work would require testing for these parameters using a pharmacologic control such as FCCP which acts by depolarising mitochondrial membrane potential [as first described by Heytler and Prichard (1962)]. Furthermore, adding a stress stimulus could give an idea of whether these cells differ in their ability to react to adverse conditions. Other studies that used hiPSCs derived from patients with mitochondrial diseases also showed a decrease in $\Delta\Psi_m$ in their cell models (Cherry *et al.*, 2013; Hatakeyama *et al.*, 2015).

Wahlestedt *et al.* (2014), Hatakeyama *et al.* (2015) and results described herein showed conflicting data with regards to ROS production. Only Hatakeyama *et al.* (2015) showed an increase in ROS in their cells and this discrepancy could be explained by the different mitochondrial mutations that were studied in all three projects; m.3243A>G, mouse model of *Polg*$^{/-}$ and m.5541C>T. Additionally, m.5541C>T was studied in myoblasts which probably have higher energy requirements than PSCs and therefore might utilise OXPHOS more resulting in higher ROS production. Since, it is not expected that hiPSCs heavily rely on OXPHOS, this biochemical feature could explain our observation of no difference in ROS production.

Most of the studies outlined in Table 5.1 also looked at the dynamics of heteroplasmy levels over passaging. Isogenic control derived from patient hiPSCs did not induce mutation over passaging (data not shown), and similar results were obtained in a study by Fujikura *et al.* (2012). Most previously published studies (including this chapter) were in agreement that there is clonal variation when it comes to the levels of mutated mtDNA. Some clones retained constant levels whereas

others eliminated the mutation or saw an increase (Cherry *et al.*, 2013; Wahlestedt *et al.*, 2014; Kodaira *et al.*, 2015). Folmes *et al.* (2013) observed that the mutation purged over passaging (by passage 44) and all the original clones had less than 50% m.3243A>G. Fujikura *et al.* (2012) and Hamalainen *et al.* (2013) on the other hand did not see variability in the levels of m.3243A>G over passaging. As discussed in the previous chapter, Dunbar *et al.* (1995) suggested that the dynamics of the mutated mtDNA levels depend on nuclear background. Although, this hypothesis might explain the difference between the results in different studies, it is still not clear why in this chapter it was shown that hiPSCs clones derived from the same MELAS patient showed either stable levels of the mutated mtDNA or reduced levels over passaging.

More work is required to elucidate the effect of m.3243A>G on hiPSCs. It is not clear what causes these cells to have lowered cellular proliferation. More efficient ways to derive hiPSCs from mitochondrial patients would provide more isogenic hiPSCs to draw more rigorous conclusions. At the moment, it is difficult to directly compare results between different studies because the hiPSCs used in them are derived from different patients with different nuclear backgrounds and disease severity, which is a characteristic feature of mitochondrial disease.

Chapter 6. Derivation and characterisation of hPSC-derived RPE cells

6.1 Overview

The main aim of this chapter was to optimise differentiation and propagation conditions of RPE cells and compare patient hiPSC-derived RPE cells to controls. At present, it is not yet known whether retinal defects seen in patients with the m.3243A>G mutation originate in neural retina or RPE cells. Even though the main aim of the chapter was to investigate RPE cells, some preliminary conclusions on neural retina development were also drawn.

6.2 Results

6.2.1 Optimising RPE differentiation protocol using hESCs

Prior to starting the differentiation experiments with patient hiPSCs, optimal conditions for obtaining RPE cells were first identified using hESCs. Initially, a total of 30 different differentiation conditions were tested, including variations in base medium, supplementation and initial seeding density (some of these were previously tested by Dr Joseph Collin, Prof Majlinda Lako's group). All cells were differentiated as a monolayer with two different starting plating densities:

- "Normal initial density", where medium was changed to differentiation medium when cells reached passaging density.
- "High initial density", where cells were left to overgrow forming a confluent monolayer with all cells being in contact with each other.

Three different base media were tested: DMEM/F12, RPMI and AdRPMI. DMEM/F12 is a widely used medium and RPMI has been successfully used for maintenance of primary RPE cells (Sonoda *et al.*, 2009). AdRPMI is a more defined version of RPMI. In addition, it was supplemented with varying combinations of B27, N2 and IGF1. After 3-4 months of differentiation, pigmented areas were manually isolated and re-plated on 24-well plate transwell inserts where they were left to mature for further ~ 3 months. Experimental set up with timeline, medium combinations and examples of cell seeding is summarised in Figure 6.1.

A.

Normal density   High density

d0   ~ 1 month   ~ 3-4 months   ~ 5-7 months

hPSCs medium   RPE differentiation medium

Characterisation

Transwell inserts
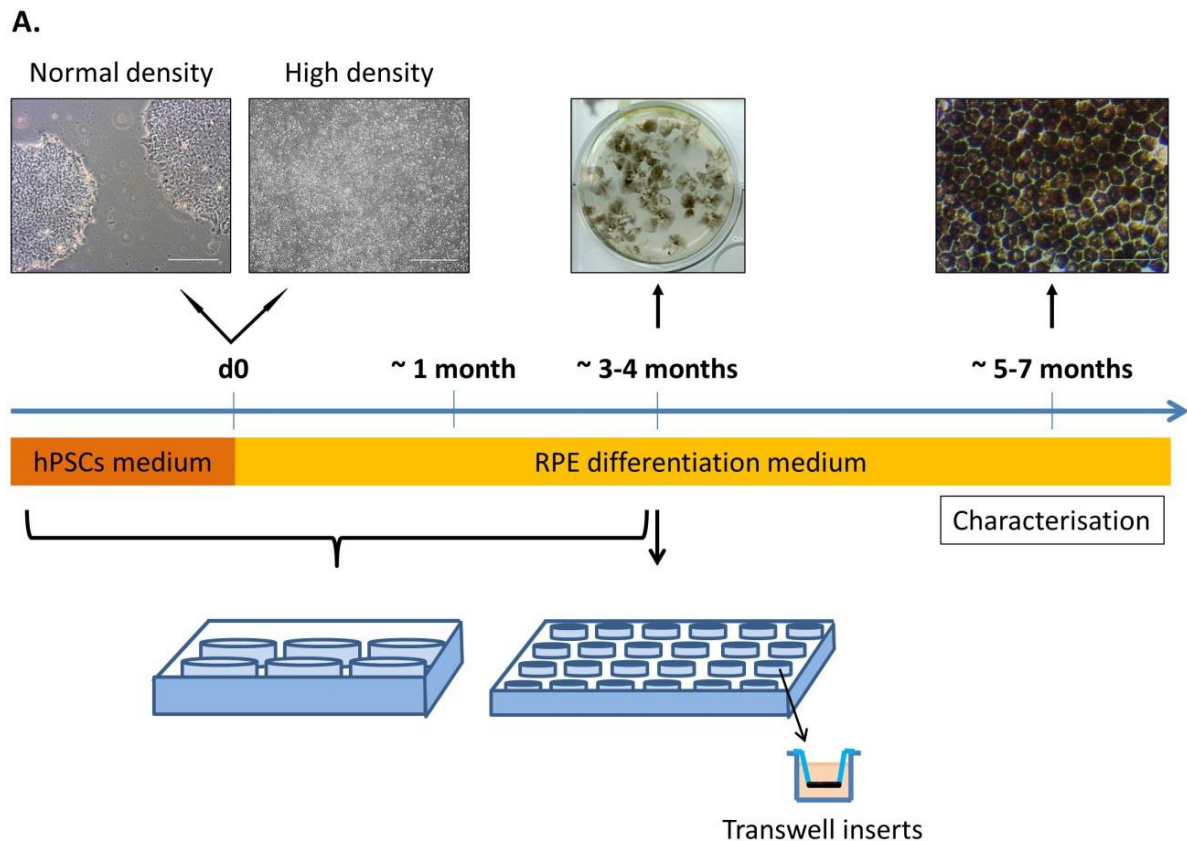
B.

DMEM/F12	RPMI	AdRPMI
DMEM/F12 + B27	RPMI + B27	AdRPMI + B27
DMEM/F12 + B27 +N2	RPMI + B27 + N2	AdRPMI + B27 + N2
DMEM/F12 + B27 +IGF1	RPMI + B27 + IGF1	AdRPMI + B27 + IGF1
DMEM/F12 + B27 + N2 + IGF1	RPMI + B27 + N2 + IGF1	AdRPMI + B27 + N2 + IGF1

Figure 6.1. Summary of the experimental set up for RPE differentiation experiments.
(A) Differentiation timeline, including representative images of cells at various time points; (B) Differentiation medium combinations. d – day.

Optimal RPE differentiation medium

In the first round of experiments, the time was noted when the first pigmented cells appeared. There was some variation between the conditions where pigment could be observed, however, in all but one condition pigment appeared by day 40 of differentiation (37.4 ± 2.4 days from the start of differentiation). Only one combination of supplementation of RPMI, where all B27, N2 and IGF1 were added, resulted in pigment production but not until after 83 days of differentiation (Figure 6.2). For this reason, RPMI base medium was not used in further experiments. Overall, it appeared that in most conditions, only normal initial cell density supported pigment production. In most of the conditions with AdRPMI as base medium, initial seeding

density did not seem important. These conclusions were drawn from the initial pilot experiment (N=1).
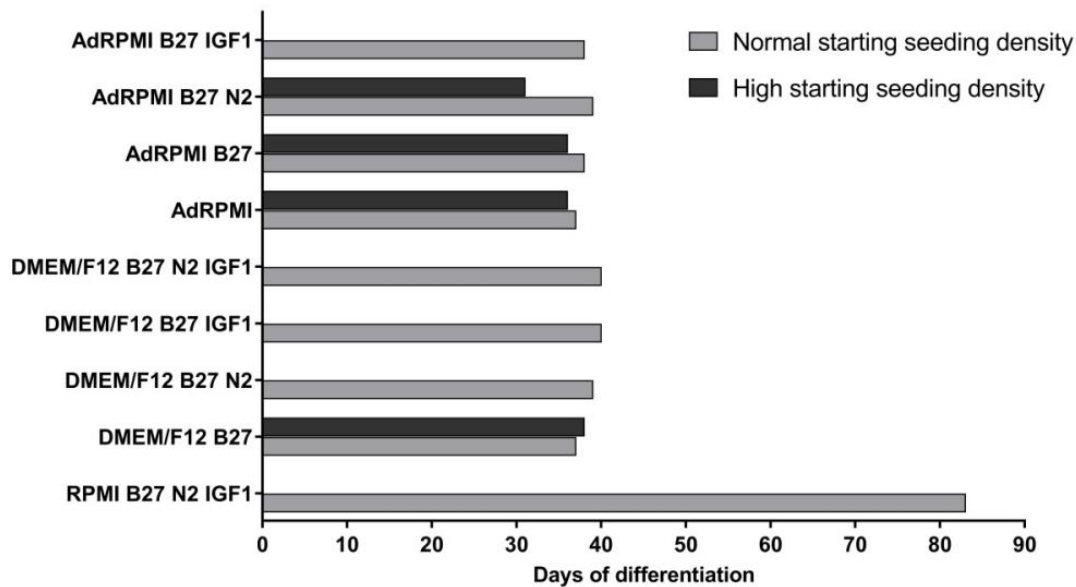
Figure 6.2. First pigment appearance in a pilot RPE differentiation experiment. In most conditions, pigment appeared within 40 days of differentiation, RPMI base medium was the least favourable for differentiation. N=1.

The next set of experiments aimed to further narrow down favourable differentiation conditions. DMEM/F12 and AdRPMI were further investigated as base media with all different supplementation combinations. In order to measure differentiation outcome, the number of isolated pigmented patches was quantified. After repeating the experiment three times, it became clear that there was a trend towards a better differentiation outcome with AdRPMI supplemented with B27 with high density starting population of cells. Additional supplementation with N2 and IGF1 did not appear to improve the results. DMEM/F12 media consistently produced less pigment. The results are presented in Figure 6.3.
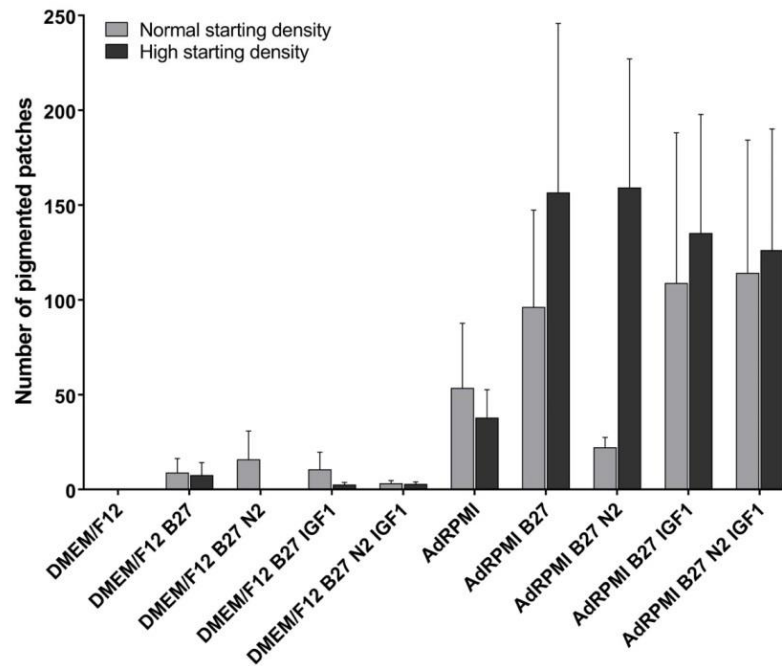
Figure 6.3. Assessing different media combinations for their support of pigment formation. In conditions with AdRPMI, there were consistently more pigmented patches formed. Although, there was no statistical significance, there was a trend towards a better differentiation outcome when using AdRPMI and B27 with high density starting cell population. The results represent the number of pigmented patches per well of a 6-well plate (9.5 cm^2) N=3. Data presented as Mean ± SEM. Significance was established with one-way ANOVA followed by Tukey's post hoc test.

RPE differentiation medium supported the formation of pigmented cells as well as 3D structures resembling optic vesicles and optic cups. Some examples of the structures formed are shown in Figure 6.4 (A). Monolayer outgrowths of pigmented cells were positive for the expression of RPE65 [Figure 6.4 (B)]. 3D structures were randomly isolated, cryosectioned and stained for RPE and early neural retina markers, RPE65 and cone-rod homeobox (CRX). They were also tested for the expression of a RPE tight junction marker ZO1 (Stevenson *et al.*, 1986). The 3D structures showed presence of RPE65, ZO1 and CRX positive cells [Figure 6.4 (C)]. In addition, the number of optic vesicle- and optic cup-like structures was quantified and the results are presented in Figure 6.4 (D-F). There was considerable variation in the differentiation experiments and it was not possible to conclude which media supported neural retinal structures formation; however, in general it seemed that AdRPMI was a more favourable base medium.
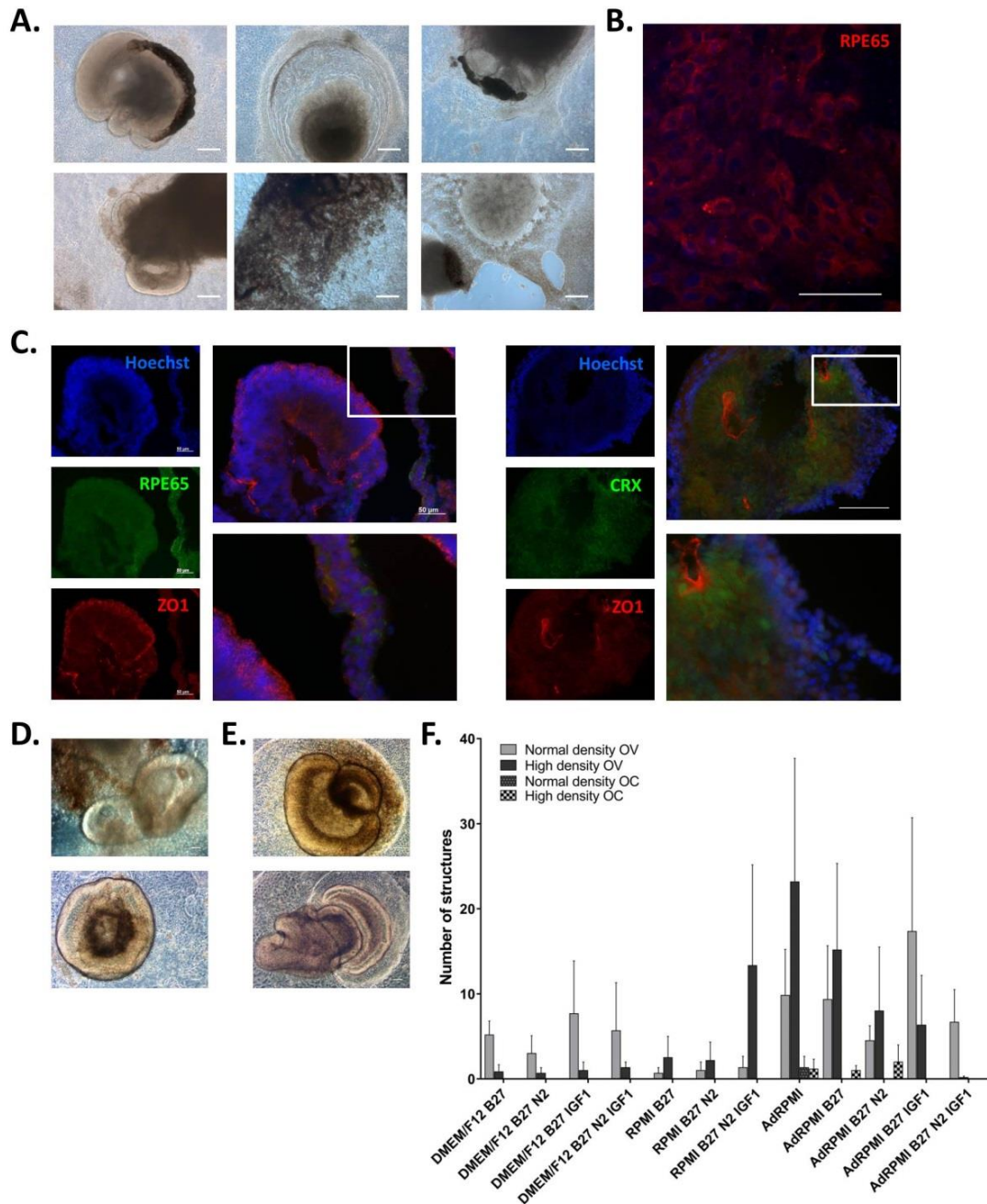
Figure 6.4. Retinal structures formation. (A) Examples of different neural retina-like structures and pigmented cells; (B) Immunofluorescence of RPE cells showing that they express RPE65; (C) Immunofluorescence of optic vesicles showing expression of RPE65, ZO1 and CRX; (D) Representative images of optic vesicle-like structures; (E) Representative images of optic cup-like structures; Scale bar, 100 μm. (F) Quantification of neural retina-like structures in cell cultures is presented as average number of structures per well. No statistically significant differences were found between the different conditions. N=3. Scale bar, 100 μm (unless otherwise stated). Data presented as Mean ± SEM. Significance was established with one-way ANOVA followed by Tukey's post hoc test. OV – optic vesicle, OC – optic cup.

Investigating RPE propagation methods

As well as testing differentiation media, a number of pilot experiments were performed to test various ECM substrates and expansion methods. Collagen IV,

laminin and fibronectin were compared as potential substrates for RPE propagation and maturation. Fibronectin did not allow the cells to form a monolayer resulting in the formation of areas of cell detachment [Figure 6.5 (A)]. Collagen IV and laminin appeared to be more supportive of RPE growth however neither of the substrates allowed increase of TER values over time or continuous growth of cells without detachment (data not shown). As a result, it was decided to use matrigel as a substrate as it contains a mix of ECM proteins, including both laminin and collagen. RPE enrichment was performed by either manual dissection of pigmented patches with their further re-plating or by subsequent dissociation of the cells into single cell suspension prior to re-plating. Direct re-plating resulted in a mixed population of cells in cultures however dissociation with a further use of cell strainer ($\varnothing$ 40 µm, Millipore) resulted in more homogenous populations of cells [Figure 6.5 (B)].
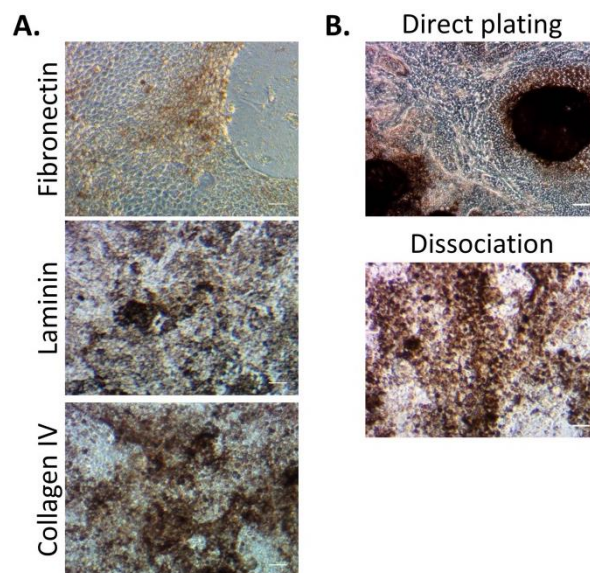
Figure 6.5. Testing different RPE propagation methods. (A) Testing different ECM substrates. Fibronectin did not promote good cell attachment 1 month after plating. (B) Testing expansion methods. Direct plating of pigmented patches resulted in a mixed cell population, whereas initial dissociation supported expansion of a more pure population of pigmented cells. Scale bar, 100 µm.

Summary

To conclude, as a result of the experiments described above, RPE differentiation conditions were selected to be used in further work with patient hiPSCs. Cells would be overgrown to a confluent monolayer with subsequent change of medium to AdRPMI supplemented with B27. Pigmented patches of cells would then be manually dissected out, dissociated, strained and re-plated on matrigel coated transwell inserts

for further maturation and characterisation. For RT-qPCR experiments cells were expanded on 24-well plates rather than on transwell inserts.

6.2.2 Derivation and investigation of RPE cells from hiPSCs with the m.3243A>G mutation

Patient 1 Clone 5, Clone M2 and Clone 8 hiPSCs were differentiated along with Control hiPSCs and hESCs. Based on published literature (described in Table 1.2), additional expeirments were performed with media supplementation with KOSR. Addition of 10% KOSR resulted in better cell survival; therefore, it was added to all subsequent hiPSC differentiation cultures.

Initial characterisation of RPE cells

hESCs, Control hiPSCs, Clone 5 and Clone M2 all formed pigmented cells with typical cobblestone RPE morphology. Interstingly, numerous attempts to differentiate Clone 8 hiPSCs to RPE cells failed (at least three attepmts were made). It formed cystic bodies and did not produce any neural or retinal-like cells after multiple differentiation attempts. Therefore, this clone was not used in subsequent differentiation experiments. Representative images are shown in Figure 6.6 (A). No notable difference was seen between Control hiPSCs, hESCs, Clone 5 and Clone M2 derived RPE cells in the amount of time it took them to produce fist pigment patches (30.3 ± 5.6 days, mean ± SD). All cells expressed genes associated with differentiating and mature RPE cells assessed by RT-qPCR using RPE cell line ARPE19 as a control [Figure 6.6 (B)]. (Note: in all RT-qPCR experiments, statistical analyses were performed including all samples and difference between ARPE19 and other cells is presented on the graphs. However, the significance of these findings will not be discussed as it does not form part of the main objective of this chapter). Immunofluorescence was performed for detecing mature RPE marker RPE65 and tight junction marker ZO1 in hiPSC-derived RPE cells [Figure 6.6 (C)].
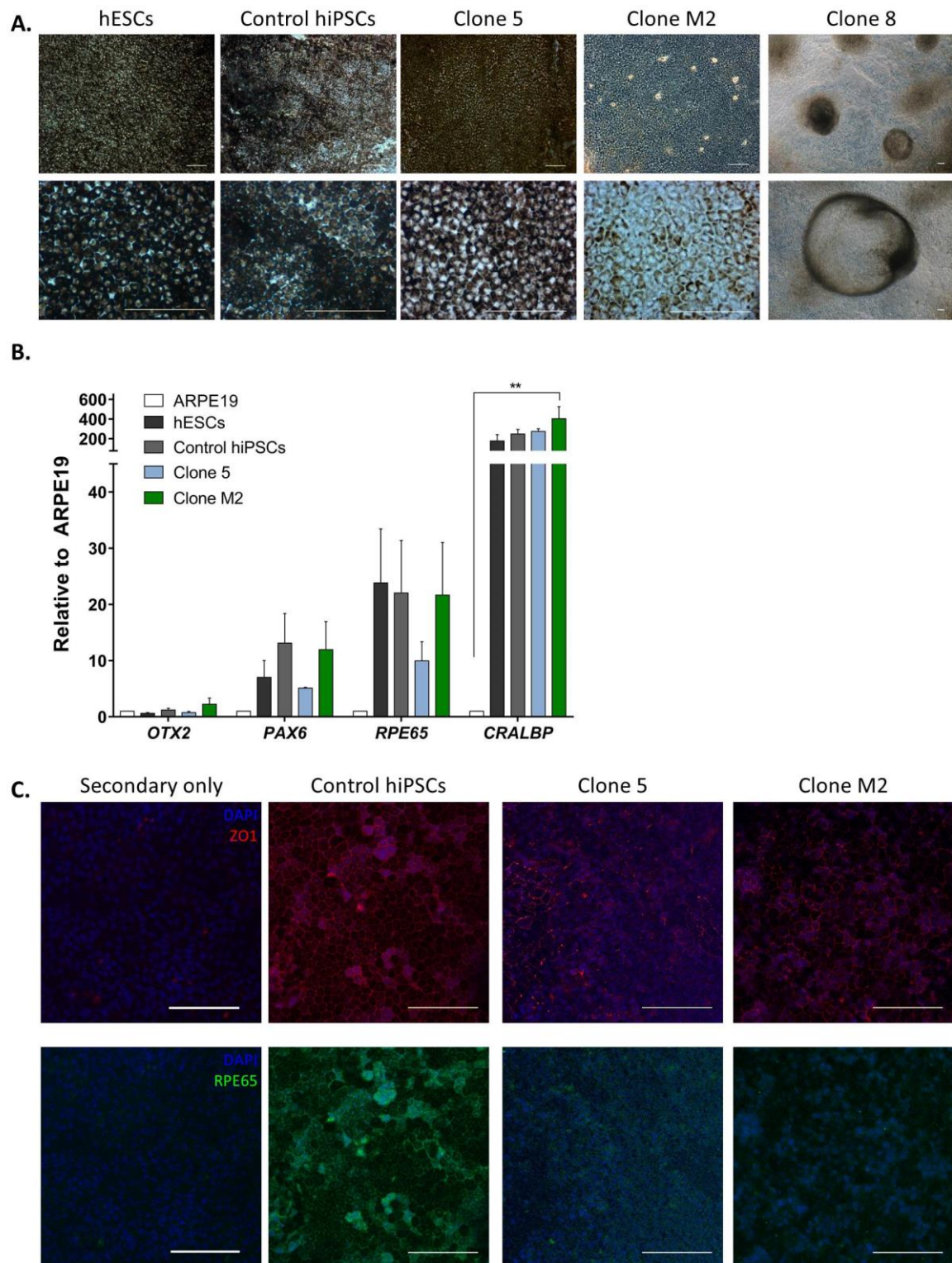
Figure 6.6. Initial characterisation of RPE cells. (A) Representative images of hPSC-derived RPE cells after 4 months of differentiation. Clone 8 failed to produce RPE cells. Scale bar, 100 μm. (B) RPE differentiation markers expression relative to ARPE19 cells assessed by RT-qPCR. N=3. Data presented as Mean ± SEM. Significance was established with one-way ANOVA followed by Tukey's post hoc test. (C) Immunofluorescence for RPE marker RPE65 (expected to be expressed either in the membranes or in the cytoplasm) and tight junction marker ZO1, nuclei counterstained with DAPI. Secondary only antibody was used as a control. Scale bar, 100 μm. The figure legend states the cell populations RPE cells were derived from herein and in subsequent figures.

Reduced differentiation propensity of cells harbouring the m.3243A>G mutation

There was an immediate observation that Clone M2 produced the least pigmented cells. To quantify differentiation outcome, plates with differentiating RPE cells were scanned and proccessed with ImageJ software. First the images were converted to grayscale and then the threshold was adjusted ensuring that only pigmented areas were visible. The software was then used to calculate the percentage of the total area occupied by pigment [image processing example is illustrated in Figure 6.7 (A)]. There was a continuous trend that, Clone M2 had the least percentage of surface area occupied by pigmented cells [Figure 6.7 (B)].
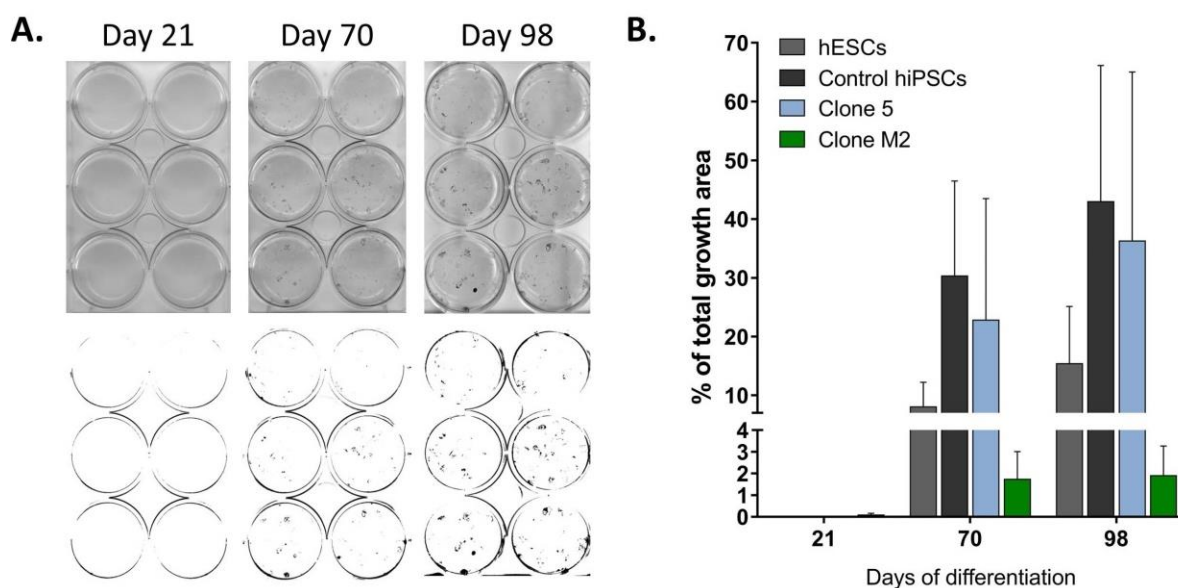
Figure 6.7. Pigment appearance over time in hPSC-derived RPE cells. (A) Representative example of image processing. Original plate scans were converted to grayscale and threshold was changed to make only pigmented areas visible. ImageJ software was used to calculate pigmented areas within the wells. (B) Percentage of total growth area covered by pigmented cells. There was a trend towards Clone M2-RPE cells repeatedly producing the least amount of pigment. N=3. Data presented as Mean ± SEM. Significance was established with one-way ANOVA followed by Tukey's post hoc test.

Along with RPE cells, neural retina-like structures were developing at the same time. In order to make an initial assessment of the ability of the cells to make optic vesicle- and optic cup-like structures, these were quantified within 6-8 weeks of the start of the differentiation. Interestingly, patient cells produced less optic vesicle-like strucutres and no optic cup-like strucutres. Results are presented in Figure 6.8.
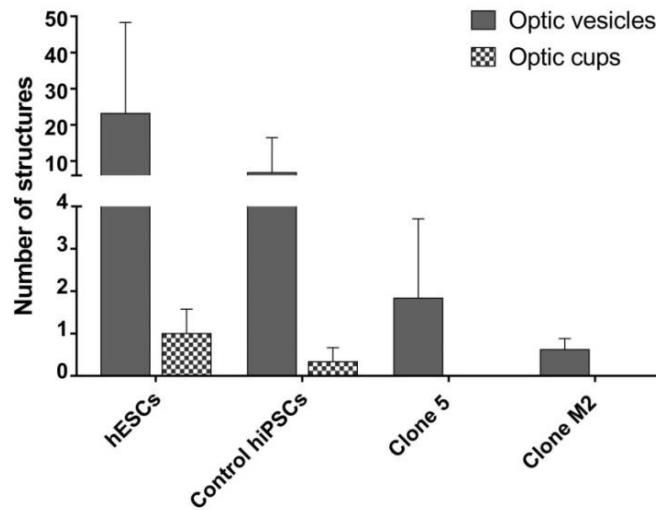
Figure 6.8. Neural retina formation from patient hiPSCs. Quantification of optic vesicle- and optic cup-like structures. Patient-derived RPE cells produced less optic vesicle- and no optic cup-like structures. N=3. Data presented as Mean ± SEM. Significance was established with one-way ANOVA followed by Tukey's post hoc test.

Subsequent experiments focused on investigating RPE cells.

Functional assays

Firstly, cells were assessed for their ability to perform functions that are known to be typical for RPE cells *in vivo*. TER measurements were used as an indirect measurement of the ability of the cells to form the outer blood-retinal barrier by detecting functional tight junctions. No significant difference was found between the cells (Figure 6.9).
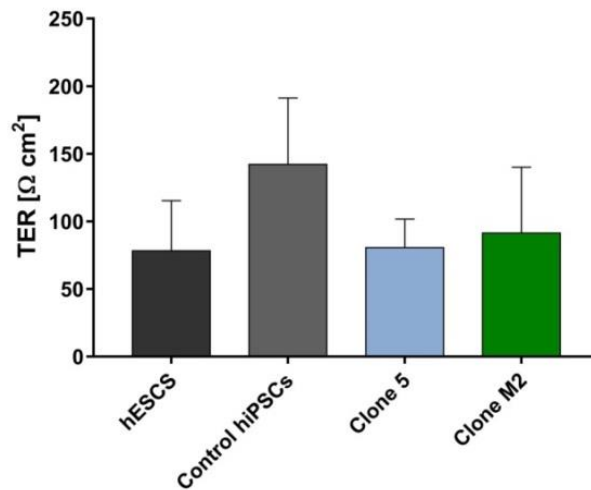
Figure 6.9. Transepithelial resistance measurement in patient hiPSCs-derived RPE cells expanded on transwell inserts. N=3. Data presented as Mean ± SEM. Significance was established with one-way ANOVA followed by Tukey's post hoc test.

Next, relative expression of genes related to phagocytosis pathway [MER proto-oncogene tyrosine kinase *(MERTK)*] and cytokine secretion (*PEDF*) was assessed by RT-qPCR. No difference was found between the cells. Results are shown in Figure 6.10.
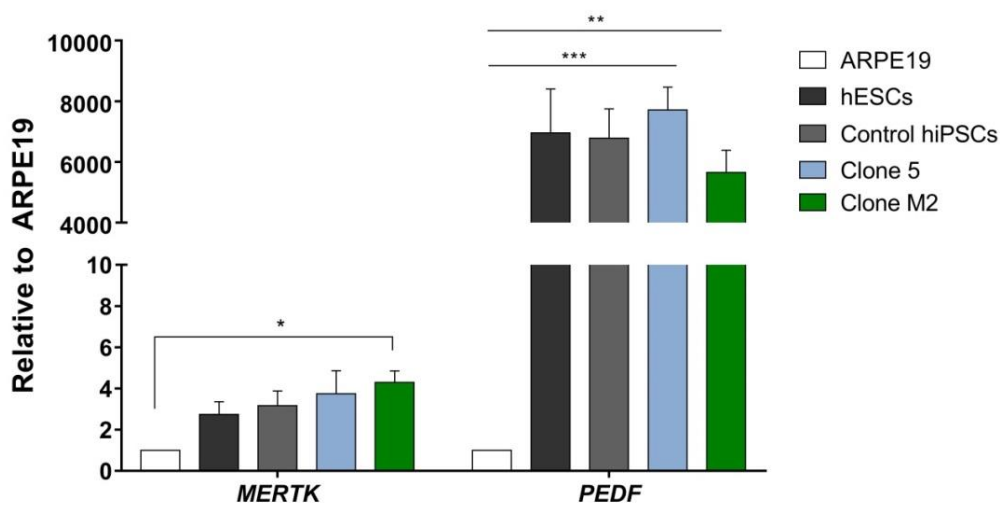
Figure 6.10. Relative expression of functional RPE markers assessed by RT-qPCR. N=3. Data presented as Mean ± SEM. Significance was established with one-way ANOVA followed by Tukey's post hoc test.

The ability to phagocytose POSs is one of the main functions of RPE cells and defects in this process could lead to various retinal diseases. Although, gene expression analysis is a good initial assessment of the differences between the cells, it does not confirm whether the cells perform a certain function or not. Therefore, an additional assessment of the ability of the cells to phagocytose was carried out by

feeding the RPE cells with FITC-labelled POSs and using flow cytometry to quantify the results. Prior to the start of the experiment, an attempt had been made to isolate POSs from bovine eyes however it was not possible to have a homogenous population of POSs (data not shown), therefore they were acquired commercially. POSs were FITC-labelled and the labelling was confirmed with immunofluorescence [Figure 6.11 (A)]. A number of control experiments were set up to ensure the robustness of the data. Firstly, cells were kept at 4°C in order to block their ability to phagocytose (Yan *et al.*, 1998). Trypan blue was used to quench any extracellular fluorescence produced by POSs bound to the extracellular membrane but not ingested, giving false positive results on the cytometer (Westenskow *et al.*, 2012). Cells were also fed with unlabelled POSs to assess background fluorescence. Representative images of the settings results are shown in Figure 6.11 (B-F). Two different types of conclusions were drawn from the results of the experiment. Percentage of FITC-positive cells indicates the number of cells within the population that ingested POSs. Median fluorescence intensity (MFI) represents the amount of POSs ingested by individual cells as an indirect indication of cell-surface receptor density involved in phagocytosis (Westenskow *et al.*, 2012). The MFI values were obtained by subtracting background fluorescence values in the FITC channel in the absence of labelled POSs. The results of the experiment showed that there were approximately 1/3 less cells within the population of patient-derived RPE cells that were able to phagocytose (hESCs 14.5%; Control hiPSCs 17.8%; Clone 5 9.4%; Clone M2 10.9%). On the other hand, patient cells that were able to ingest had higher numbers of POSs per cell as indicated by MFI values. Quantifications are shown in Figure 6.11 (G). The MFI data is suggestive of the potential of the cells to ingest POSs by giving a representation of the amount of POSs inside the cells. This parameter is important as it gives another valuable dimension to the data and provides information on the whole cell population level about the potential of the cells to internalise POSs as opposed to the number of cells that are able to phagocytose.
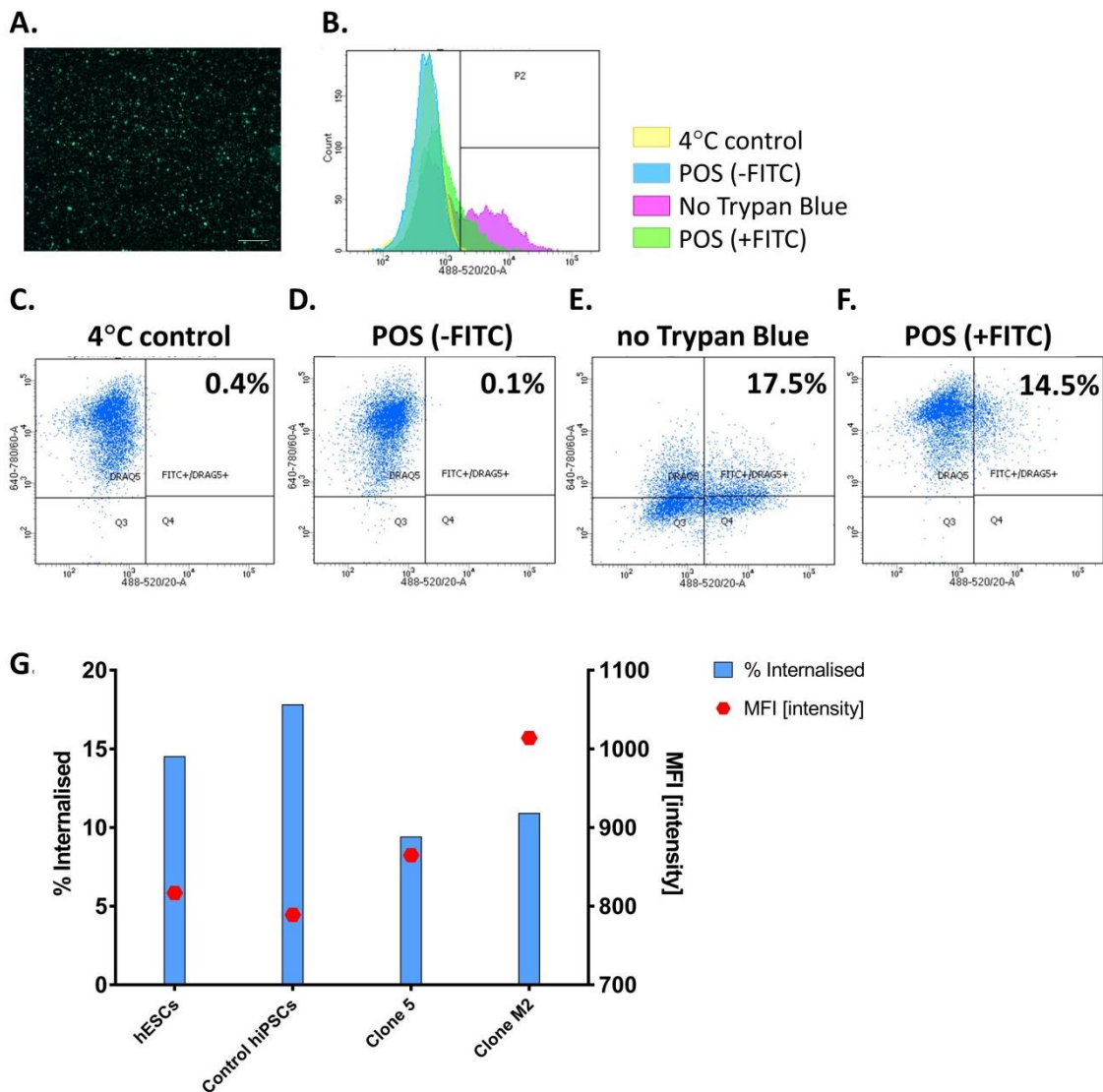
Figure 6.11. Photoreceptor outer segments phagocytosis by hPSC-RPE cells, including examples of experimental set up, assessed by flow cytometry. (A) FITC-labelled POSs. Scale bar, 100 µm; (B) Histogram representation of the control experiments; (C) Blocking phagocytosis by incubating the cells at 4°C; (D) Feeding cells with POSs without FITC-labelling; (E) Performing the experiment without quenching extracellular FITC-labelled POSs; (F) Example of the results with cells fed with FITC-labelled POSs and quenching extracellular POSs with Trypan blue, showing its effect; (G) The phagocytosis experiment results showed that hESCs and control hiPSCs had higher number of cells that were able to phagocytose. Patient cells that were able to phagocytose had the ability of ingesting more POSs per cell, as determined by MFI values. All cells were matched with regards to the length of differentiation time and were all ~6.5 months old. N=1.

Summary of the initial findings of patient-derived RPE cells

From the experiments described above it can be concluded that RPE cells derived from Clone M2 (highest level of m.3243A>G) behaved differently with regards to their propensity to differentiate producing cells with lowered pigmentation levels. Additionally, RPE cells derived from both of the patient hiPSC clones had reduced

ability to perform one of the main RPE functions – phagocytosis of POSs. Therefore, it was decided to study the cells further.

Ultra-structural and molecular assessment of RPE cells

Cells were imaged with TEM in order to investigate their morphology. There were striking differences in the morphology of RPE cells derived from patient Clone M2 hiPSCs, which had ~ 70% of the mutation. As can be observed in Figure 6.12 (A), cells did not display the baso-apical distribution of organelles normally seen in RPE cells where melanosomes are located apically. They also had underdeveloped microvilli. However, most importantly, they contained melanosomes which were hollow inside potentially indicating their state of degradation. Clone M2-RPE had similar numbers of mature melanosomes and melanosomes associated with lysosomes. However, there were significantly more hollow melanosomes with atypical morphology. This finding was important as it is in line with clinical observations that showed that MELAS patients have areas of RPE depigmentation. RT-qPCR results of genes related to pigment synthesis did not reveal differences between patient and control RPE cells [Figure 6.12 (C)].
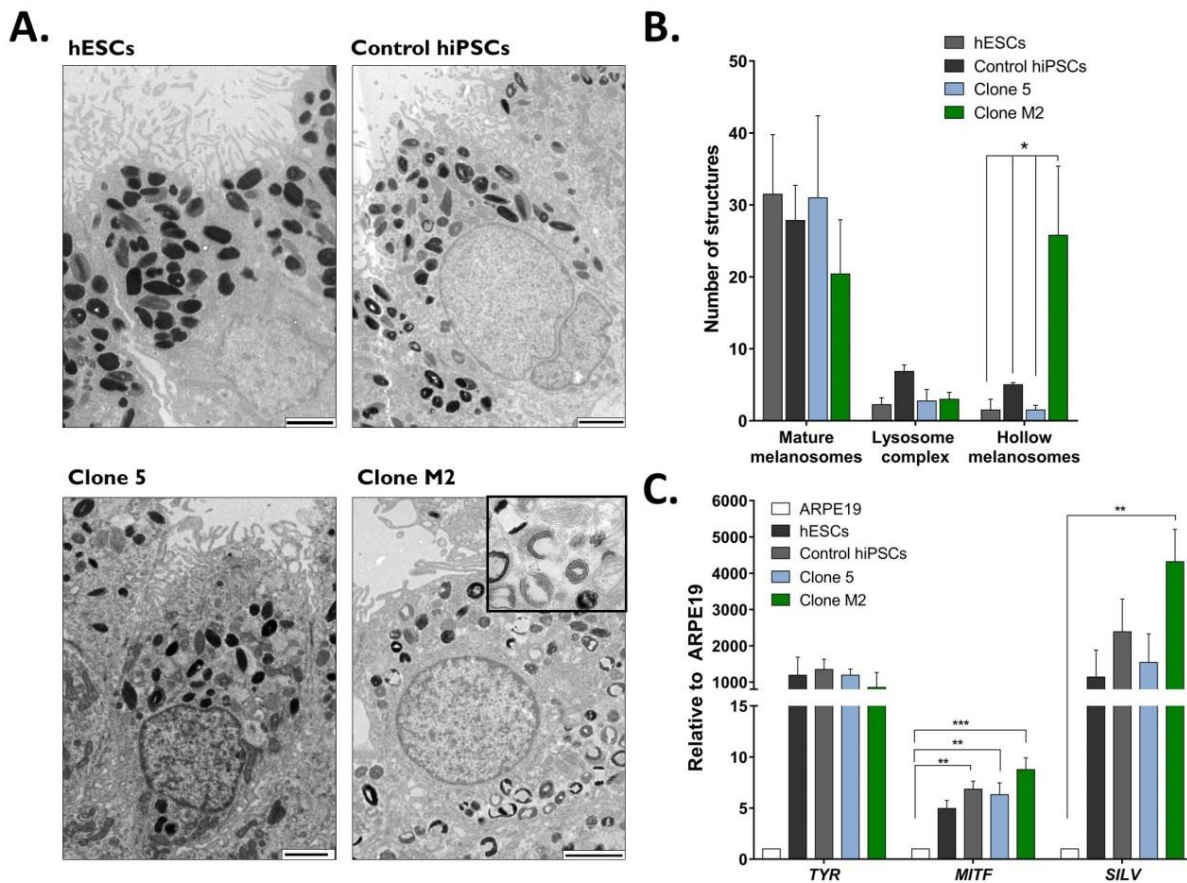
Figure 6.12. TEM of patient hiPSC-RPE cells with further quantifications. (A) Representative TEM images of RPE cells (Scale bar, 2 μm). Patient RPE cells with high level m.3243A>G have atypical melanosomes with hollow morphology. (B) Quantification of the numbers of melanosomes. Clone M2-RPE cells had significantly higher levels of hollow melanosomes. No difference was found in the numbers of mature melanosomes and melanosomes associated with lysosomes. Quantifications are based on cells from 3-7 random fields. (C) Relative expression of genes associated with pigment synthesis (RT-qPCR). No difference was found between patient-derived RPE cells, hESCs and control hiPSCs. N=3. Data presented as Mean ± SEM. Significance was established with one-way ANOVA followed by Tukey's post hoc test. *TYR* (tyrosinase); *MITF* (microphthalmia-associated transcription factor); *SILV* (silver locus protein homolog).

In addition to quantifying melanosomes with different morphologies, mitochondrial morphology was also considered. Although there was no statistical significance in the findings, there was a trend towards patient-derived RPE cells having less mature and more fragmented / damaged mitochondria, which could be a direct result of the m.3243A>G mutation. Ideally, more samples would need to be tested to confirm whether this trend could be significant. The results are presented in Figure 6.13.
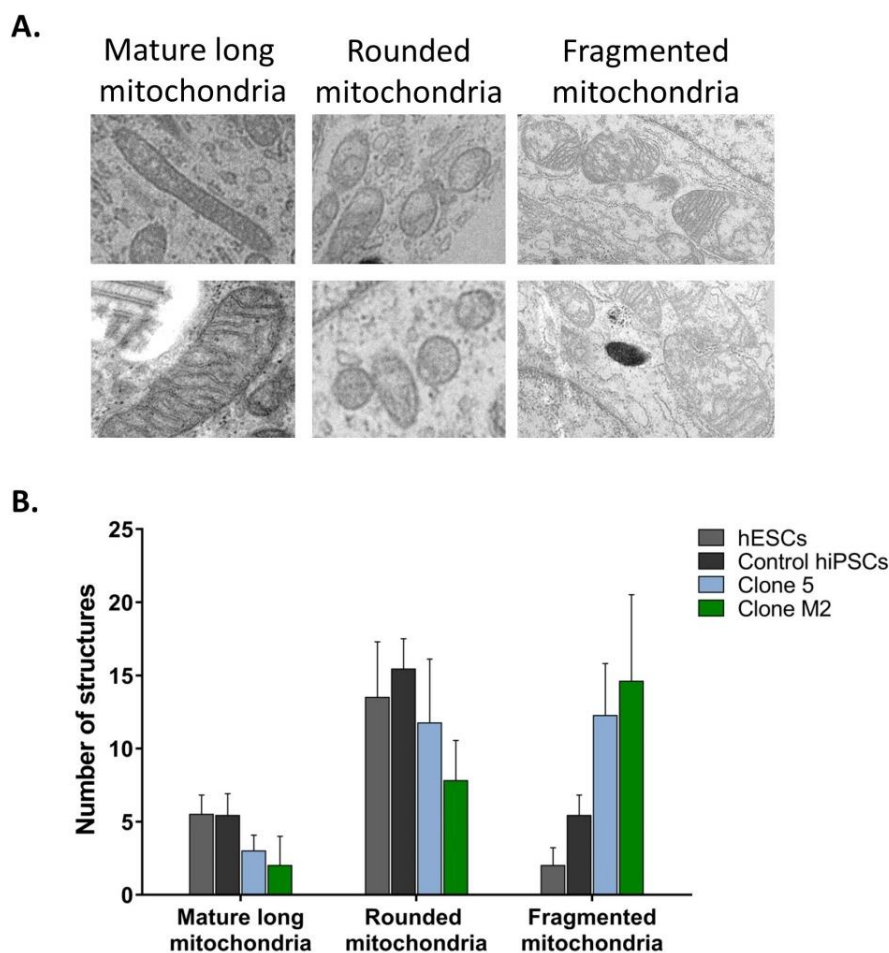
Figure 6.13. Quantification of mitochondria with varying morphology. (A) Examples of mitochondrial classification. (B) Quantifications of various types of mitochondria. No difference was found between cells. Quantifications are based on cells from 3-7 random fields. Data presented as Mean ± SEM. Significance was established with one-way ANOVA followed by Tukey's post hoc test.

The TEM results indicated that patient RPE cells had defects in mitochondrial dynamics and contained what looked like degrading melanosomes. In order to elucidate potential mechanism behind these findings, relative expression levels of genes that are involved in lysosomal degradation and mitochondrial dynamics were compared (Figure 6.14). Additionally, cells were tested for the expression of a marker related to oxidative stress. *CTSD*, *CTSB* and *ACP2* are markers associated with lysosomal degradation and *ACP2* is assumed to have a specific role in melanosome degradation (Hayasaka *et al.*, 1975). Looking at these genes was of particular interest as it has been previously suggested that melanosomes are specialised lysosomes and hollow melanosomes represent the process of autophagy when they start degrading their own melanin (Schraermeyer *et al.*, 1999). *OPA1* and *MFN2* are associated with mitochondrial fusion (Griparic *et al.*, 2004). Additionally, *MFN2* has been implicated in establishment of physical contacts between mitochondria and

melanosomes (Daniele *et al.*, 2014). There was no difference in the expression of these markers between hPSC-RPE cells apart from one. Clone M2-RPE had significantly higher levels of *OPA1* compared to hESCs. There was no difference between hPSC-RPE cells in the expression of *SOD2* (superoxide dismutase 2, an enzyme that clears mitochondrial ROS) (Flynn and Melov, 2013).
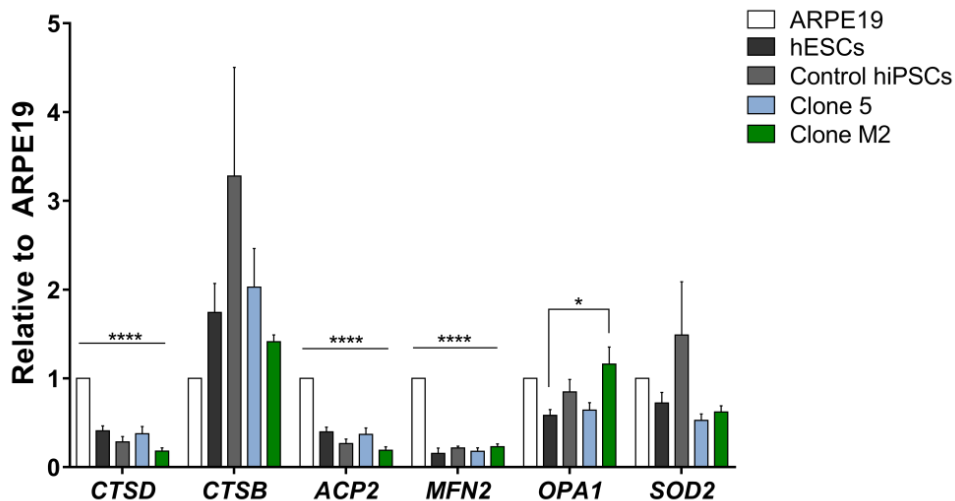
Figure 6.14. Relative expression levels of lysosomal and oxidative stress genes by RT-qPCR. No difference was found in the expression levels of lysosomal and melanosomal degradation genes *CTSD*, *CTSB* and *ACP2*. No difference was found in the fusion gene *MFN2*. *OPA1* was significantly upregulated in RPE cells derived from Clone M2 compared to hESC-RPE. No difference was found in the expression of *SOD2*. Data presented as Mean ± SEM. N=3. Significance was established with one-way ANOVA followed by Tukey's post hoc test.

Although, Figure 6.14 showed no difference in the expression of the selected lysosomal genes, in order to confirm that there is no difference between the RPE cells it would be necessary to perform lysosomal enzyme activity assay. This would be particularly interesting as previous studies have shown an association between lysosomal activity and disturbed homeostasis in RPE cells (Chen *et al.*, 2009).

Three months after the first TEM images were taken, another set of RPE cells that were grown in parallel to the first set of cells were imaged in order to confirm whether the cells retained their pathological morphology over time. As seen in Figure 6.15, hESC-RPE cells looked similar to the previous batch of cells in Figure 6.12 (A). Control hiPSC-RPE cells had baso-apical distribution of organelles with less signs of developing microvilli. Interestingly, Clone 5-RPE cells contained some swollen fragmented mitochondria and lipid droplets. Clone M2-RPE cells looked apoptotic across all images. Additionally, the cells had disturbed membranes, dysmorphic mitochondria, underdeveloped microvilli, vacuoles and a mix of melanosomes with

various morphologies. Due to the difficulty of distinguishing between organelles it was not possible to replicate the quantifications performed for the first set of TEM images. However, from the images in Figure 6.15 it can be seen that patient cells looked diseased indicating potential effect of the mutation on their ability to support survival.
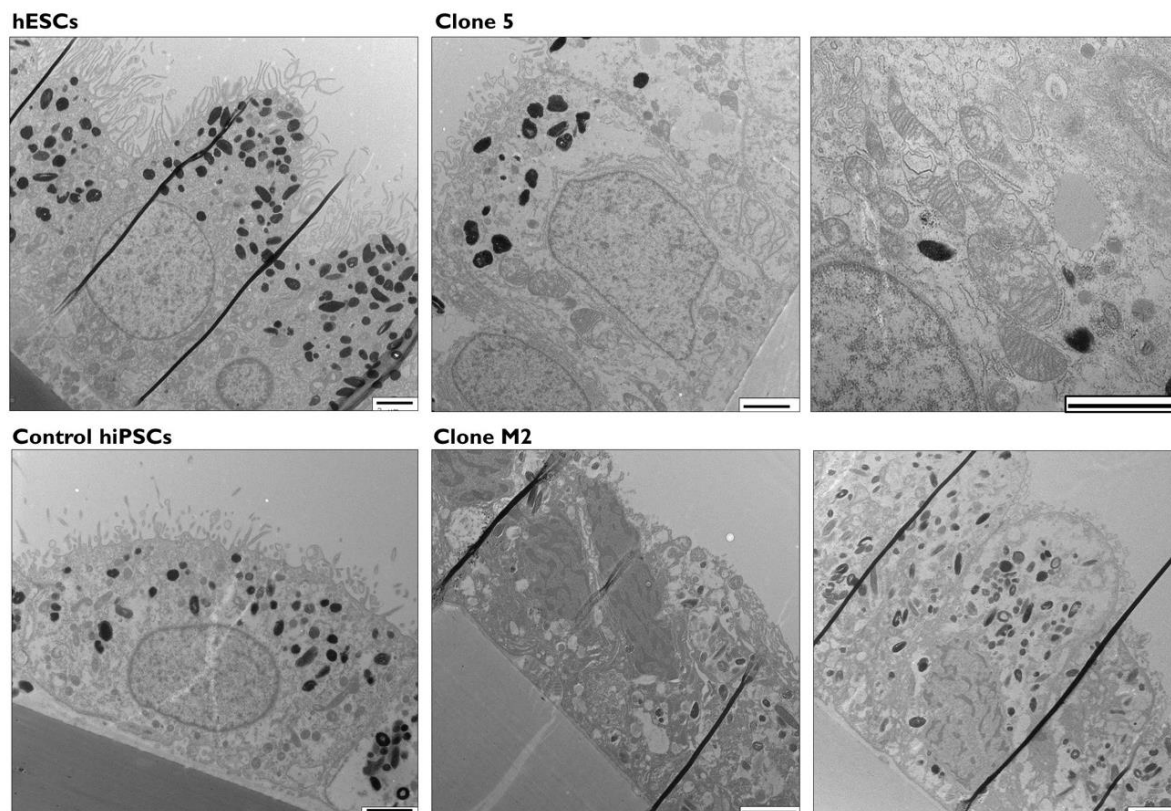
Figure 6.15. Representative TEM images of hPSC-RPE cells three months after the original images were taken [Figure 6.12 (A)]. hESC-RPE continued their development and showed more mature microvilli. Control hiPSC-RPE had apical melanosomal distribution and less developed microvilli. Clone 5-RPE had very large fragmented mitochondria and lipid droplets. Clone M2-RPE had apoptotic nuclei, disturbed membranes, disorganised cytoplasm and dysmorphic mitochondria. Scale bar, 2 μm. Note: black vertical lines seen in hESCs and Clone M2 are a processing artefact.

From the TEM images it could be seen that there were signs of a loss of membrane integrity in RPE cells harbouring the m.3243A>G mutation. One of the functions of melanosomes is to reduce oxidative stress produced by ROS and lipid peroxidation (Holliday *et al.*, 2013). Additionally, melanosomes sequester calcium thereby protecting the cells. Therefore, morphological changes in these organelles could affect the fate of the cells. A pilot experiment was performed to see whether there were differences in cytosolic calcium between different RPE cells. The results are shown in Figure 6.16. No difference was found between different RPE cells. This

experiment would need to be repeated with further optimisations and more biological repeats which was not possible to do due to low cell numbers.
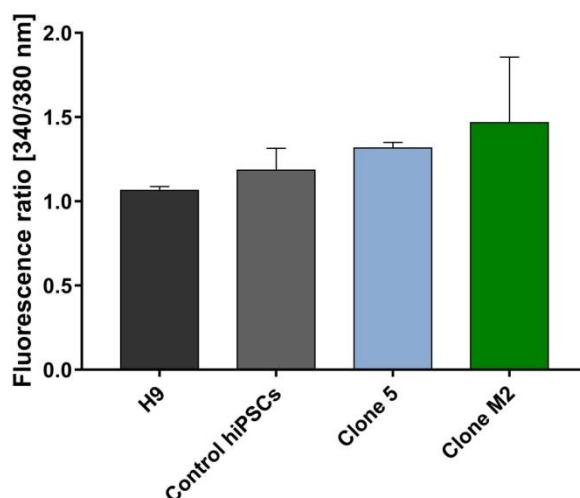
Figure 6.16. Cytosolic calcium levels in RPE cells. No significant difference was found between different cells. N=2. Data presented as Mean ± SD.

Mitochondrial assessment of RPE cells

In order to investigate how the dynamics of the mitochondrial mutation of the cells changed throughout the differentiation process, they were checked for heteroplasmy level, mtDNA copy number and ATP levels. Figure 6.17 (A) shows the levels of m.3243A>G in the RPE cells; on the X-axis, the approximate levels of the mutation of the parental hiPSCs they were derived from are indicated. Overall RPE cells derived from Clone 5 had slightly increased levels of heteroplasmy comparing to the original hiPSCs. Clone M2 had differing results from two different differentiation experiments. There did not appear to be a notable difference in heteroplasmy level of RPE cells comparing to the original hiPSCs in one differentiation experiment resulting in the derivation of RPE cells with ~ 70% of the mutation. Another experiment resulted in the derivation of cells with ~ 57% m.3243A>G. The trend in the levels of the mtDNA in patient hiPSC-RPE cells mimicked the results obtained for hiPSC clones.

Clone M2 had significantly higher number of mtDNA copies compared to RPE cells derived from Clone 5 and hESCs [Figure 6.17 (B)]. None of the cells had mtDNA common deletions (data not shown). There was no notable difference in the levels of ATP produced by OXPHOS and glycolysis [Figure 6.17 (C)]. However, it should be taken into account that there were only enough cells to perform this experiment once and further optimisation could potentially show a different result.

It should be pointed out that although Clone M2-RPE cells from different experiments had varying levels of the m.3243A>G mutation, cells performed similarly in different assays, potentially indicating that pathological phenotype in these cells stems from an early time point during development when they were derived from hiPSCs with a high level of heteroplasmy.
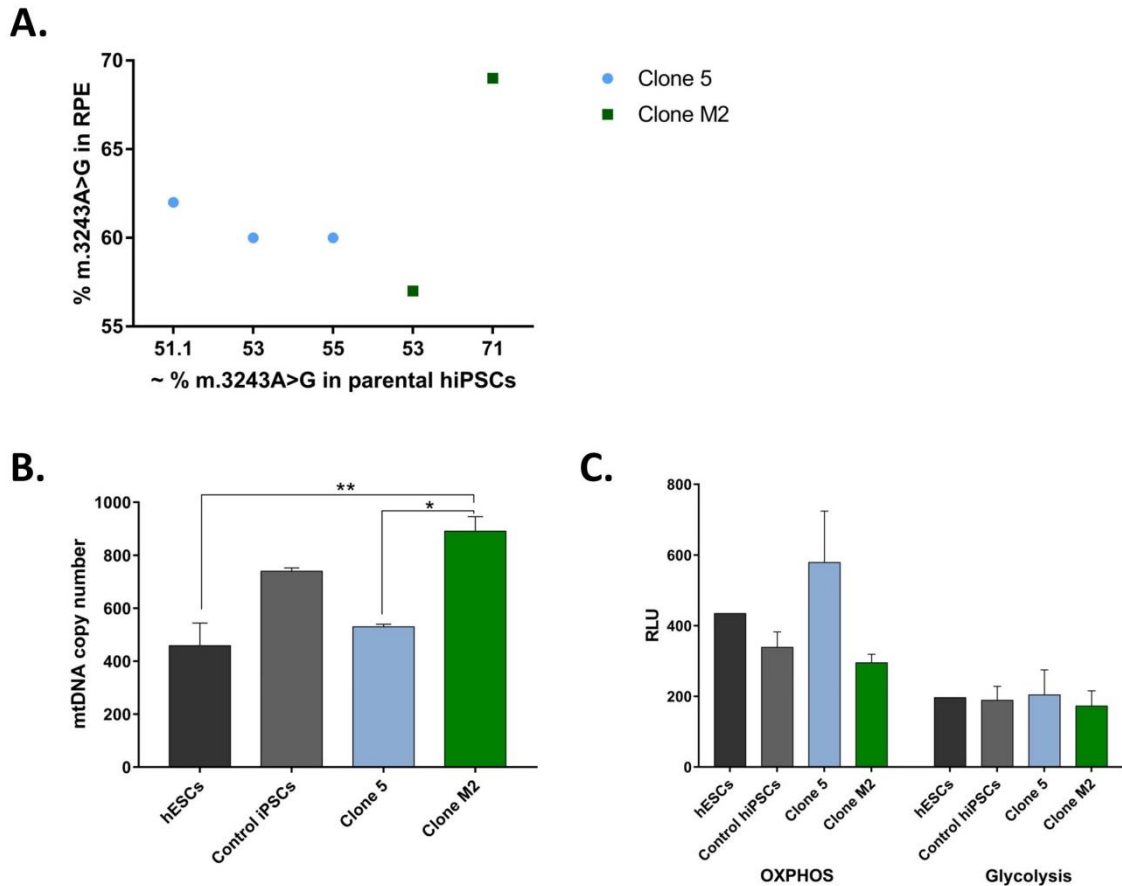
Figure 6.17. Heteroplasmy levels in patient hiPSC-RPE, mtDNA copy number and level of ATP produced by OXPHOS and glycolysis. (A) Percentage of m.3243A>G in patient hiPSC-RPE cells, including approximate heteroplasmy levels of the parental hiPSCs (X-axis); (B) mtDNA copy number of patient hiPSC-RPE. Clone M2-RPE cells had significantly higher levels of mtDNA copy number comparing to hESCs and Clone 5-RPE cells. N=2. (C) ATP produced by OXPHOS and glycolysis. No observable difference between the cells, additional experiments required. N=2. Data presented as Mean ± SD. RLU – relative light units.

6.3 Discussion

This chapter describes one of the key elements of this project aimed at investigating patient hiPSC-derived RPE cells with the view of elucidating potential differences between them. Prior to that, a number of experiments were undertaken in order to establish an optimal RPE differentiation protocol using hESCs.

6.3.1 Main findings

RPE differentiation optimisation experiments with hESCs

Initially, it was established that AdRPMI supplemented with B27 and 10% KOSR was the most favourable medium for RPE differentiation. In addition, growth factor reduced matrigel was chosen as substrate. This is not surprising as B27, KOSR and matrigel have all been successfully used in differentiation experiments by various research groups (summarised in Table 1.2). Up until now, there is no published evidence of AdRPMI being used for differentiating hPSCs to RPE. It is similar to DMEM/F12 however it is more defined, contains insulin, transferrin and trace elements which might be more supportive of cell growth. The final medium composition supported the development of both RPE and neural retina progenitors which was expected. These structures develop together as a result of complex interactions as discussed in the overview of this chapter and in the study by Nakano *et al.* (2012), where it was suggested that optic cup formation relies on the formation of neural retina and RPE in a balanced fashion.

Summary of the findings from the experiments with patient-derived RPE cells

A number of conclusions were drawn from the experiments performed with patient-derived cells.

- Patient hiPSCs were able to differentiate to RPE cells, apart from the isogenic control hiPSCs (Clone 8), which failed to give rise to RPE cells
- They were comparable to the controls in terms of the expression of early and mature RPE markers, barrier properties (as measured by TER), expression of some genes related to their function (*MERTK* and *PEDF*), genes associated with pigmentation (*TYR*, *MITF* and *SILV*) and in terms of their mitochondrial morphology in the initial TEM experiments albeit with a tendency for an increased number of fragmented mitochondria
- Clone M2-RPE had significantly increased levels of *OPA1*
- All RPE cells had comparable levels of *SOD2*
- Patient RPE cells derived from hiPSCs with high m.3243A>G (Clone M2-RPE) differed from controls and RPE cells derived from hiPSCs with lower levels of the mutation (Clone 5) across a number of parameters, including:
  - Their propensity to differentiate towards RPE and neural retina was reduced

- Pigmentation level when examined by light microscopy was lower
- mtDNA copy number was significantly increased compared with other cells
- Percentage of cells that were able to phagocytose POSs was lower (although had slightly higher values for MFI suggesting that phagocytosing cells were not compromised)
- Ultra-structurally cells looked abnormal, less developed with significantly increased levels of hollow / degrading melanosomes
- Ultra-structural examination at a later time point revealed further deterioration with apoptotic nuclei, fragmented mitochondria (in both patient cell clones), disturbed membranes and vacuoles. Clone 5-RPE cells also looked abnormal with large fragmented and dysmorphic mitochondria.

These particular findings are discussed below in more detail.

6.3.2 Reduced differentiation propensity of patient hiPSCs

It is not clear why Clone 8-hiPSCs failed to give rise to RPE cells. Previous work has shown that there is donor and hiPSC clone-specific variation in the expression of RPE-specific genes (Miyagishima *et al.*, 2016). Although, in this case it cannot be attributed to donor variation, it is possible that these cells had reduced intrinsic propensity to differentiate and probably required additional supplementation of the medium to achieve successful differentiation outcome. As discussed in the overview section of this chapter, early eye development is under the control of multiple transcription factors. Therefore, it is plausible that the inability of Clone 8 hiPSCs to produce neuronal and RPE cell types was a result of changes in regulation of crucial pathways required for default differentiation. From the spontaneous monolayer differentiation experiment described in (Figure 3.7) it can be seen that Clone 8 had reduced upregulation of *PAX6*, which is crucial for RPE differentiation. A recent study investigated reactivation of *OTX2* expression after reprogramming under the regulation of *SOX2* and *OCT4* (Li *et al.*, 2016). They showed that there is a formation of *OCT4-SOX2* regulatory axis which establishes the propensity of the cells to differentiate into retinal lineages. In turn, *PAX6* is a transcriptional target of *SOX2* and therefore it is plausible to speculate that due to the fact that Clone 8 hiPSCs expressed *SOX2* and not *PAX6* upon spontaneous differentiation this resulted in

defects in activation of *PAX6* which resulted in the inability of the cells to produce RPE cells without subjecting them to directed differentiation (Lee *et al.*, 2013).

The initial finding in patient RPE cells derived from hiPSCs with high initial m.3243A>G was their reduced pigmentation levels and reduced differentiation propensity as measured by percentage of pigmented cells that occupy growth surface area and by the number of neural retina-like structures formed. Defects in mitochondria did not seem to affect patient hiPSCs across multiple parameters (discussed in Chapter 5); therefore, it was interesting to see that there was an effect on their ability to undergo differentiation. There is conflicting evidence for whether mutations affecting mitochondria lead to defects in differentiation propensity of hiPSCs. Most papers that have been published on this topic claim that the cells differentiate in the same manner as controls. However, Wahlestedt *et al.* (2014) used mutator mouse iPSCs (mutation in *Polg* gene) to show pronounced defects in their ability to form EBs and teratomas and complete failure to produce chimeric mice. The same study showed that even though there was little difference between wild-type and mutator iPSCs, mutator iPSCs had differentiation defects due to impaired ability to switch from glycolysis to OXPHOS. Interestingly, characterisation of the mutator mouse model lead to the discovery that these animals have respiratory chain dysfunction and age prematurely (Trifunovic *et al.*, 2004). Similarly, another study showed that maternally transmitted mtDNA mutations lead to premature ageing and brain malformation in mice (Ross *et al.*, 2013). Another study showed that mouse ESCs with severe respiratory chain deficiencies show defects in neuronal differentiation (Kirby *et al.*, 2009). Therefore, it could be speculated that reduced RPE and neural retina differentiation was a result of a failed metabolic switch in these cells. These results are also in line with the findings that these cells had defects in the ability to form teratomas.

Due to their potential to be used in cell replacement therapies, it has become evident that robust methods for RPE characterisation need to be utilised. In the initial optimisation differentiation experiments with hESCs described in the first part of this chapter, manual counting was used as a method for identifying the efficiency of the protocol. In further experiments with patient hiPSC-RPE, a more reliable method was used based on the work by Lane *et al.* (2014), where scanned images of cell culture plates were used to calculate percentage surface area occupied by pigmented cells. The disadvantage of this method is that it might miss out on RPE cells with very low

level of pigmentation as could be the case with Clone M2-RPE cells. To overcome this, Kamao *et al.* (2014) used Photoshop's Info Palette (Adobe Systems) which gives the user the colour profile of the image based on single cells and produces objective quantification of the level of pigmentation of the cells. This method could be used to further assess the cells. Another group developed their own method to assess the extent of cuboidal cobblestone morphology of RPE cells based on computational analysis (Joshi *et al.*, 2016). Automation of evaluation of RPE cell maturation status is fast-developing and other parameters have been considered in other studies. Based on the notion that RPE cells display spontaneous transient increases of Ca^{2+} mediated by ATP, controlling differentiation and proliferation, another group showed that RPE organisation is also connected to Ca^{2+} and cells with uniform morphology have minor calcium waves (Abu Khamidakh *et al.*, 2016). In this study the authors developed a semi-automatic method for measuring intracellular Ca^{2+} to assess maturation of cells. For the first time they showed that hESC-RPE cells display spontaneous and mechanically induced transient increases in Ca^{2+}.

Combining multiple observer-independent measurement approaches would be a simple and effective assessment of differentiating RPE cells and provide quantifiable information for evaluation of differences between patient and healthy control cells. Future work would have to take this into account.

The differences found between patient RPE and control RPE cells are key to elucidating the pathogenesis of the retinal disease seen in patients with the m.3243A>G mutation. These differences form the basis of the rest of the discussion.

6.3.3 mtDNA dynamics in RPE cells

Clone M2-RPE cells had significantly higher mtDNA copy number comparing to other cells. The variation in mtDNA copy number has already been discussed in the previous two chapters and these results are consistent with the findings in Clone M2-hiPSCs suggesting the persistence of the phenotype across different cell types with high level of m.3243A>G. Interestingly, control RPE cells had five times more mtDNA comparing to fibroblasts (739.9 ± 17.4 compared to 147.1 ± 11.2; Mean ± SD). Whereas Clone M2 RPE cells had the same number of mtDNA copies (~ 890 copies). Furthermore, Clone 5 RPE cells had reduced number of mtDNA compared to fibroblasts (529.6 ± 14.7 compared to 891.0 ± 34.1; Mean ± SD). This is interesting and could potentially imply that the cells did not manage to increase their mtDNA

population in order to fulfil the energy demands of RPE cells which potentially resulted in them expressing deleterious functional defects. As suggested in the previous chapter, there is yet no clear explanation to the differences in the heteroplasmy dynamics in patient clones.

6.3.4 Patient hiPSC-derived RPE cells show functional defects

Photoreceptor outer segments are continually renewed in a balanced fashion being replaced by newly formed outer segment discs. The daily renewal of POSs is approximately 10% of their total length and RPE cells are responsible for the removal of POSs from 30-40 photoreceptors by the process of heterophagy (Kaarniranta *et al.*, 2013). Clearance of shed POSs is one of the most important functions of RPE cells and consists of multiple steps and pathways, summarised in Figure 6.18. Photoreceptors have high exposure to light and high oxygen concentration environment which subjects them to chronic oxidative stress. By eliminating them, RPE protects photoreceptors from oxidative damage and accumulation of lipid-protein aggregates called lipofuscin thereby maintaining healthy sub-retinal environment (Sparrow *et al.*, 2010). Clone M2-RPE cells had ~1/3 less cells that were able to phagocytose and MFI values suggested that the cells that were able to ingest POSs were potentially more efficient at it than controls and Clone 5-RPE cells. MFI data showed that Clone M2-RPE cells that were phagocytosing did not show deficit in the ability to recognise and engulf POSs and the values were comparable to findings by another research group that used the same technique (Westenskow *et al.*, 2012). From this finding, a possible conclusion is that there was a smaller number of functional RPE cells within the total population of Clone M2-RPE. The potential reasons for this observation are discussed in more detail below.
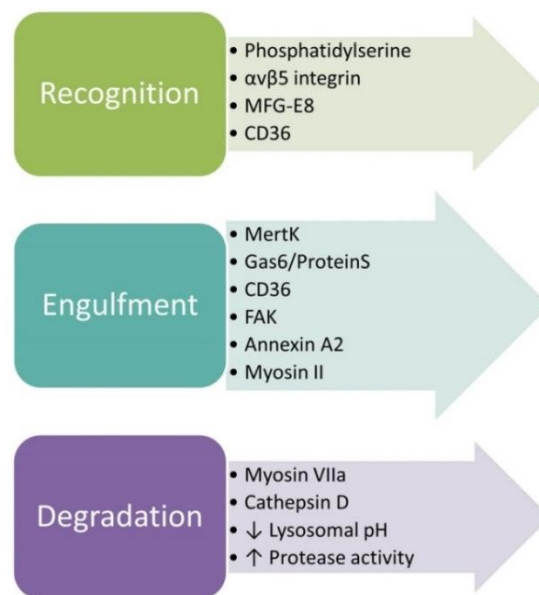
Figure 6.18. Components of phagocytosis of POSs [adapted from Kevany and Palczewski (2010)].

At a population level, there was no difference in the expression of *MERTK* (transmembrane receptor that triggers POSs ingestion) between the RPE cells (Figure 6.10). Although it is not the only component of the "engulfment" step and it does not give an indication of protein levels, it provides an indication that the cells might have been able to perform this step. Therefore, it could be speculated that the cells were not able to degrade the POSs in phago-lysosomes. When checked for the gene expression level of lysosomal proteases *CTSB* and *CTSD*, no difference was found between the samples (Figure 6.14). Although gene expression levels were comparable, defects in lysosomal function cannot be ruled out and ideally lysosomal activity would have to be tested additionally. This is especially important because lysosomal overload has been shown to be associated with lipofuscin accumulation, vacuolation and phagocytosis disruption in RPE cells (Sundelin *et al.*, 1998; Chen *et al.,* 2011b). Interestingly, the effect of lipofuscin accumulation on the ability of cells to perform phagocytosis is exacerbated by the presence of mtDNA mutations by not providing the cells with enough ATP energy to perform the function (Vives-Bauza *et al.,* 2008). It is possible that the cells were not metabolically active enough to perform the entire phagocytosis cascade, which could be explained by the TEM results that showed that there were a lot of apoptosing cells in those samples with what looked like disturbed membranes. Disturbances in the ability of RPE to phagocytose could have major impact on retinal health. Early studies using Royal College of Surgeons rat (a widely used animal model of retinal degeneration) showed that due to a genetic

defect (mutation in *MERTK* gene), their RPE cells were unable to phagocytose POSs resulting in the accumulation of a layer of debris and consequently photoreceptor death (Bok and Hall, 1971; Mullen and LaVail, 1976). In humans, defects in RPE phagocytosis lead to development of retinitis pigmentosa, Usher syndrome and AMD by a variety of different mechanisms (Gal *et al.*, 2000; Gibbs *et al.*, 2003; Kevany and Palczewski, 2010). Disturbances to phagocytosis in these diseases were described to be a result of mutations in the *MERTK* gene, myosin VIIa gene leading to perturbed transport of ingested discs, or by the accumulation of toxic by-products from RPE phagosomes in the form of lipofuscin. One study looked at the eyes of donors with AMD with the view of linking the disease-associated pathology to mitochondria (Terluk *et al.*, 2015). They mapped mtDNA into nine regions and showed that RPE cells had an increase in mtDNA damage. There were a number of hot spots where the mutations were most common and strikingly one of them was in the same mtDNA region as the m.3243A>G mutation. Interestingly, clinical observations showed that MELAS patients with m.3243A>G accumulate lipofuscin that are often localised in the areas surrounding the optic disc, and tend to spare the areas in the foveal region (de Laat *et al.*, 2013). The same study suggested that the phenomenon of foveal sparing could be explained by slower regeneration of cones and their lesser dependence on RPE comparing to rods. On the other hand, the macular area outside the fovea is densely packed with photoreceptors especially rods and therefore this area is primarily affected in mitochondrial retinopathies. Histopathological studies on post mortem eyes of MELAS patients have also indicated an increased presence of lipofuscin in RPE (Chang *et al.*, 1993; Rummelt *et al.*, 1993). Due to the fact that RPE atrophy is localised to only some areas, it could explain why patient hiPSC-RPE had comparable MFI values.

To conclude, disturbances in phagocytosis could be one of the possible mechanisms of retinal atrophy seen in patients with the m.3243A>G mutation.

6.3.5 Patient-derived RPE cells have abnormal melanosome and mitochondrial ultrastructure

Another set of major findings was derived from analysing TEM images of hiPSC-RPE cells. There were striking differences in the morphology of melanosomes in patient-derived RPE cells with the highest level of m.3243A>G compared to other RPE cells. The cells had comparable numbers of "normal" melanosomes, but they had significantly higher levels of hollow melanosomes resembling a process of

degradation. Additionally, there was a clear trend that patient RPE cells contained more fragmented mitochondria. Overall, cells looked unhealthy and lacked structures such as microvilli (also termed as photoreceptor sheaths) which are vital for RPE-photoreceptors crosstalk, apical transport and visual cycle [reviewed by Bonilha (2008)]. Furthermore, when samples were analysed again three months later, patient hiPSC-RPE cells looked so unhealthy with such little cytoplasmic organisation, that it was impossible to perform any sort of quantifications. Cells contained swollen mitochondria, loss of cristae morphology, vacuoles, very little membrane integrity and Clone M2-RPE had apoptotic nuclei. There were striking similarities between these cells and cells described in studies which looked at post mortem retinas of MELAS patients with m.3243A>G, where it was shown that RPE cells were depigmented and mitochondria had abnormal morphology (Chang *et al.*, 1993; Rummelt *et al.*, 1993). As can be seen from Figure 6.19 (A, B), similar to the RPE cells derived from hiPSCs from patients with the m.3243A>G, RPE cells found in post mortem eyes of patients with the same mutation show areas of hypopigmentation and vacuolation. There were also similarities in the morphology of mitochondria seen in cells described in the literature and the cells derived during this project [Figure 6.19 (C, D)]. Mitochondria were elongated and swollen, however some mitochondria described in the literature contains denser cristae, than what was seen in hiPSC-derived RPE cells (Figure 6.15).
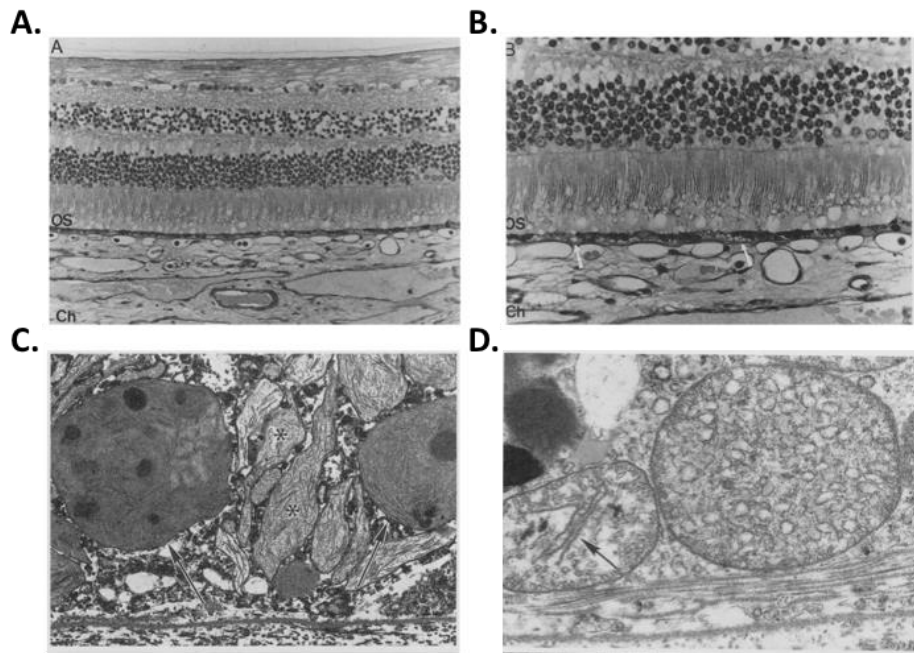
Figure 6.19. Histopathological findings in post mortem tissues from patients with m.3243A>G mutation. (A, B) RPE cell layer has areas of hypo and hyperpigmentation (seen underneath the photoreceptor outer segments [OS] layer) and some vacuoles can be seen (white arrows) [adapted from Rummelt *et al.* (1993)]; (C, D) RPE mitochondria are elongated (asterisks), swollen, and abnormal (arrow) [adapted from Chang *et al.* (1993)].

These findings complement findings on disturbances in phagocytosis. It appears that there is a back log of degrading and possibly undigested material inside the cells, possibly leading to cell death.

When melanosomes with defective morphology were first observed, it was not clear whether it was to do with them being immature and not forming properly or whether they were mature melanosomes undergoing degradation. The first hypothesis was ruled out after establishing that the cells had comparable levels of expression of genes involved in melanogenesis, such as *TYR*, *MITF* and *SILV* (Figure 6.12). *TYR* regulates synthesis of tyrosinase which is located in melanocytes and is involved in the first step of melanin production. Tyrosinase catalyses the conversion of tyrosine to dopaquinone which is a precursor to two types of melanin: eumelanin (dark coloured, photoprotective, antioxidant, located on the surface) and pheomelanin (yellow, reddish-brown, phototoxic, pro-oxidant, core location) (Ito and Wakamatsu, 2008). *SILV* encodes a protein involved in biogenesis and maturation of melanosomes and is a structural protein (Kobayashi *et al.*, 1994). *SILV* expression is regulated by *MITF* which is pivotal for RPE maturation as discussed earlier in this chapter. Melanogenesis is an energy demanding process. Daniele *et al.* (2014) showed that mitochondria contact melanosomes via the MFN2 protein thereby

facilitating the process of melanogenesis by supplying ATP to the organelles. At gene expression level, there was no difference found in *MFN2* levels between different RPE cells as shown in Figure 6.14 providing another indication that the process of melanosomal synthesis was not altered in the cells.

Melanin is mainly synthesised in postnatal RPE and there are studies that show that there is general decrease in the number of pigment granules per macular RPE with age which is accompanied with the association of melanosomes with lysosomes and formation of lipofuscin, as a result of the inability of RPE to cope with phagosomal load (Feeney-Burns *et al.*, 1984). Sarna *et al.* (2003) suggested photo-oxidation as a possible trigger to decreased melanin content. Also, there is a positive correlation between age and the number of RPE cells undergoing apoptosis at a rate of about 1.96% per year. They suggested that expression of BCL-2 (anti-apoptotic gene) inhibits apoptosis (Del Priore *et al.*, 2002). Some melanin biosynthetic gene variants have been shown to be a risk factor for AMD (Holliday *et al.*, 2013). It has been shown experimentally that damaged melanosomes could adversely affect cellular health. Repopulation of ARPE19 cells with melanosomes from aged donors results in decreased mitochondrial activity and increased cell death after exposure to blue light (Rozanowski *et al.*, 2008). This is unsurprising, considering their functional significance.

Melanosomes are located near the apical surface of RPE cells where they are in close contact with photoreceptors. Their transport inside the cytoplasm is facilitated by myosin VIIa along actin filaments – an ATP dependent process. [Interestingly, mutations in myosin VIIa leads to Usher syndrome (Sparrow *et al.*, 2010)]. The main function of melanosomes is to protect the cells from light damage. Indeed, it is known that short wavelengths of light are filtered by the cornea and the lens (<295 nm and 300-400 nm respectively), whereas vitreous filters the infrared light (>1400 nm). Visible light (400-760 nm), which is damaging to the retina, is absorbed by various pigments, including melanin, leading to generation of ROS. Interestingly, various mitochondrial proteins such as COX and flavins absorb 450-520 nm light inducing production of H_2O_2 and singlet oxygen (Lascaratos *et al.*, 2007; Osborne *et al.*, 2010). In general, melanosomes prevent light from being absorbed by other chromophores, they have an important antioxidant function as well as sequestering free radicals, metal ions and Ca^{2+} preventing apoptosis (Borovansky and Riley, 2011). A literature search showed that the melanosomes observed in

Clone M2-RPE had a striking resemblance to degrading melanosomes described by others (Insausti and Casas, 2009). It could be hypothesised that these changes lead to the inability of the melanosomes to perform one of their key functions namely absorption of stray light. It is possible that the changes seen in MELAS RPE cells could be an exacerbation of the processes seen in normal ageing. Indeed, RPE cells from aged donors have been shown to contain large disrupted mitochondria unable to cope with cellular energy demands increasing their susceptibility to oxidative stress and a similar trend is seen in AMD patients (He *et al.*, 2010). Melanosomes possess lysosomal activity in RPE cells (Schraermeyer *et al.*, 1999). Gouras *et al.* (2011) investigated RPE cells in rhesus monkeys (*Macaca mulatta*) and described hollow melanosomes found in those cells as a new class of organelles that degrade their own melanin via lysosomal and autophagic actions. As can be seen from Figure 6.20, melanosomes in rhesus monkeys described in this study have a remarkable resemblance to the melanosomes in the TEM images of RPE cells derived in this project (Figure 6.12). Gouras and colleagues suggested that such morphological changes were the result of vulnerability to stress and pointed out that melano-lysosomes accumulated in monkey RPE lead to early maculopathy. Another study showed that RPE in the macular area contain a greater content of melano-lysosomes due to the higher exposure to stress in that area, which follows the hypothesis of a loss of melanin due to an increased amount of stress (Feeney-Burns *et al.*, 1984). This is consistent with mitochondrial stress secondary to the m.3243A>G mutation. The exact mechanism of maculopathy as a result of accumulation of hollow melanosomes is not clear, however it is clear that retinal atrophy in MELAS patients might have common pathways with the pathological reduction of pigment seen in patients with AMD [reviewed by Bonilha (2008)]. It is also possible that loss of melanin in these organelles is an exacerbation of a normal ageing process as a result of the cells being under stress (Feeney-Burns *et al.*, 1984). It may be that as a result of the m.3243A>G mutation the melanosomes acquire their lysosomal characteristics which leads to self-degradation via autophagic actions.
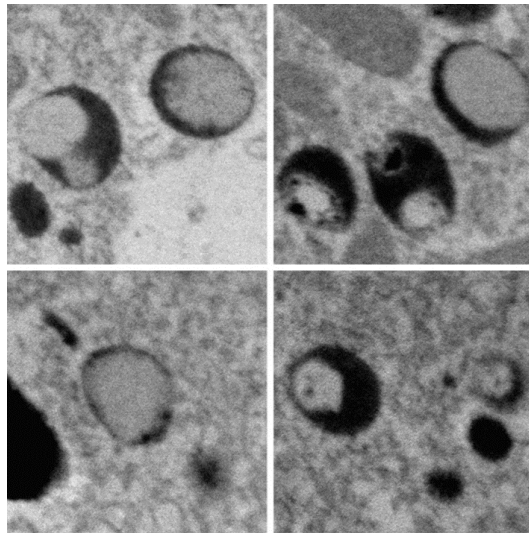
Figure 6.20. Examples of degrading melanosomes found in rhesus monkeys (*Macaca mulatta*). Melanosomes described by the authors show resemblance to hollow melanosomes seen in RPE cells derived from patients with m.3243A>G. [Adapted from Gouras *et al.* (2011)].

TEM images also showed that patient RPE cells had enlarged fragmented mitochondria and RT-qPCR results showed that Clone M2-RPE had increased levels of *OPA1* which is associated with mitochondrial fusion and formation of cristae junction. Tondera *et al.* (2009) introduced a concept of stress-induced mitochondrial hyperfusion (SIMH), when enlarged mitochondria accumulate in cells as a result of various stress stimuli, including UV irradiation and serum deprivation. Elevated mitochondrial fusion, and as a result mitochondrial size, is associated with resistance of cells to apoptotic stimuli and autophagy and has been observed in RPE of ageing rhesus monkeys (Gouras *et al.*, 2016). Indeed, increase in autophagy has been associated with clearance of mtDNA with pathogenic mutations. Dombi *et al.* (2016) showed an increase in autophagy in fibroblasts from patients with pathogenic m.13051G>A mutation. Studies looking at impaired autophagy, and specifically mitophagy, have gained a lot of popularity in recent years. There has been a report suggesting a link between disturbed mitophagy and neurodegeneration associated with a nuclear-encoded mutation in *OPA1* (Carelli *et al.*, 2015). Degradation of enlarged organelles is energy dependent and it is possible that the cells have a limit of the volume of the organelle they can process. Senescent mitochondria produce more ROS and the inability of the cells to perform autophagy and lysosomal degradation can be detrimental. Alternatively, it is possible that damaged mitochondria have less respiration and produces less ROS which means they are not tagged for removal. Accumulation of partially or non-degraded material leads to cells

being unable to perform their function. This is especially crucial in post-mitotic cells such as RPE, as there is no dilution of the material as a result of cell division. It is possible that if the cells contain too much non-degraded material in their lysosomes, the cells start directing lysosomal enzymes to these aggregates which in turn leads to not having enough enzymes for the newly formed autophagocytosed material (this hypothesis goes in line with the finding that patient RPE cells had comparable levels of gene expression for lysosomal enzymes). [Reviewed by Terman *et al.* (2010)].

As can be seen from TEM images in Figure 6.15, the membranes in the cells seem to have lost their integrity and there were numerous vacuoles observed inside the cells, which could be a sign of RPE stress (Justilien *et al.*, 2007). The consequences of damaged melanosomal membranes could be drastic. Firstly, melanosomes contain quinones which are involved in melanin synthesis. If they were to be released they could have a cytotoxic effect by inhibiting DNA polymerase or binding to DNA (interestingly, this is sometimes the reason for isolated RPE DNA being pigmented) (Borovansky and Riley, 2011). Cytotoxic effects of damaged melanosomes have been previously observed in malignant melanoma (Borovansky *et al.*, 1991). Additionally, lost integrity of lysosomes can lead to release of their material into the cytosol leading to cell death (Terman *et al.*, 2010).

In general, the degree of pigmentation of RPE cells is related to their function and cells with less pigment have reduced secretion of growth factors, including VEGF and PEDF (Kamao *et al.*, 2014). PEDF has a protective effect on mitochondria after exposure to ROS by improving mitochondrial function, therefore it could be speculated that in the cells, such as RPE harbouring m.3243A>G, where mitochondrial function is already compromised having fully functional RPE cells is evermore crucial (He *et al.*, 2014).

6.3.6 Conclusion

To conclude, two major findings have been made in this chapter. Firstly, patient-derived RPE cells had striking morphological similarities to cells seen in patients with m.3243A>G at post mortem. Interestingly, there were clear morphological abnormalities in melanosomes which could explain the areas of RPE hypopigmentation seen in patients. Secondly, there were less patient RPE cells that were able to perform the most crucial RPE function namely phagocytosis. Defects in phagocytosis are associated with a number of other retinal diseases. Accumulation of

undigested material in the cells, including melanosomes and enlarged mitochondria, could explain their inability to perform their function. These events are typically associated with normal ageing however in RPE cells with m.3243A>G they are potentially exacerbated and pathological.

Chapter 7. Conclusion and future perspectives

The main aim of my project was to investigate the molecular and cellular basis that underpin the characteristic retinal pathology seen in patients with the m.3243A>G mutation by making use of hiPSCs obtained from patient somatic cells. It was hypothesised that the resulting hiPSC clones would have varying levels of the mutated mtDNA, providing an ideal setting to make comparisons between isogenic clones. Based on previous clinical findings, it was expected that, when differentiated to RPE, the cells would have the phenotype similar to that seen in patients, providing a validated model system for current and future work.

7.1 Major findings

As shown in Figure 7.1 (A), attempts were made to reprogramme fibroblasts obtained from three patients with the m.3243A>G and two healthy control donors. As a result, it was possible to obtain hiPSCs from two patients' cells. Multiple attempts were made to isolate hiPSCs from other donors however they were unsuccessful. Control hiPSCs previously generated in the lab and hESCs were used for comparisons with patient cells.

Somatic cells from Patient 1 gave rise to 10 hiPSC clones with 3 clones being selected for further analyses. The fibroblasts from this patient had ~70% of the mutated mtDNA and elevated levels of mtDNA copy number. hiPSC clones that harboured the mutation had initial reduced propensity for proliferation (Clone 5 with ~50% mutation) or increased levels of mtDNA copy number (Clone M2 with ~70% mutation). hiPSC clones did not differ from the controls across a number of other parameters, including cell cycle kinetics, oxygen consumption, mitochondrial mass, mitochondrial membrane potential, intracellular superoxide or levels of peroxide. Fibroblasts from Patient 2 gave rise to 4 hiPSC clones that all purged the mutation. Subsequent attempts to isolate clones with high levels of the mutated mtDNA have failed. Fibroblasts from this patient had ~66% of the mutated mtDNA and had reduced basal and maximal respiration. There was no difference in mtDNA copy number between these cells and the control. Schematic summary is shown in Figure 7.1 (B).

Two Patient 1 hiPSC clones, both with mutant mtDNA, were able to differentiate to RPE cells. They were comparable to each other and to control hPSCs

across a number of parameters, including gene expression levels, protein expression and TER values. RPE cells derived from the hiPSC clone with ~50% m.3243A>G were deficient in phagocytosis and had ultra-structural changes associated with the disease state, including presence of enlarged and fragmented mitochondria. RPE cells from the hiPSC clone with ~70% m.3243A>G had reduced differentiation propensity, reduced pigmentation levels, defects in phagocytosis, degrading melanosomes, altered mitochondrial morphology, apoptotic nuclei and increased levels of *OPA1* gene encoding mitochondrial fusion protein, which could indicate that cells were under stress. A schematic representation is shown in Figure 7.1 (C).
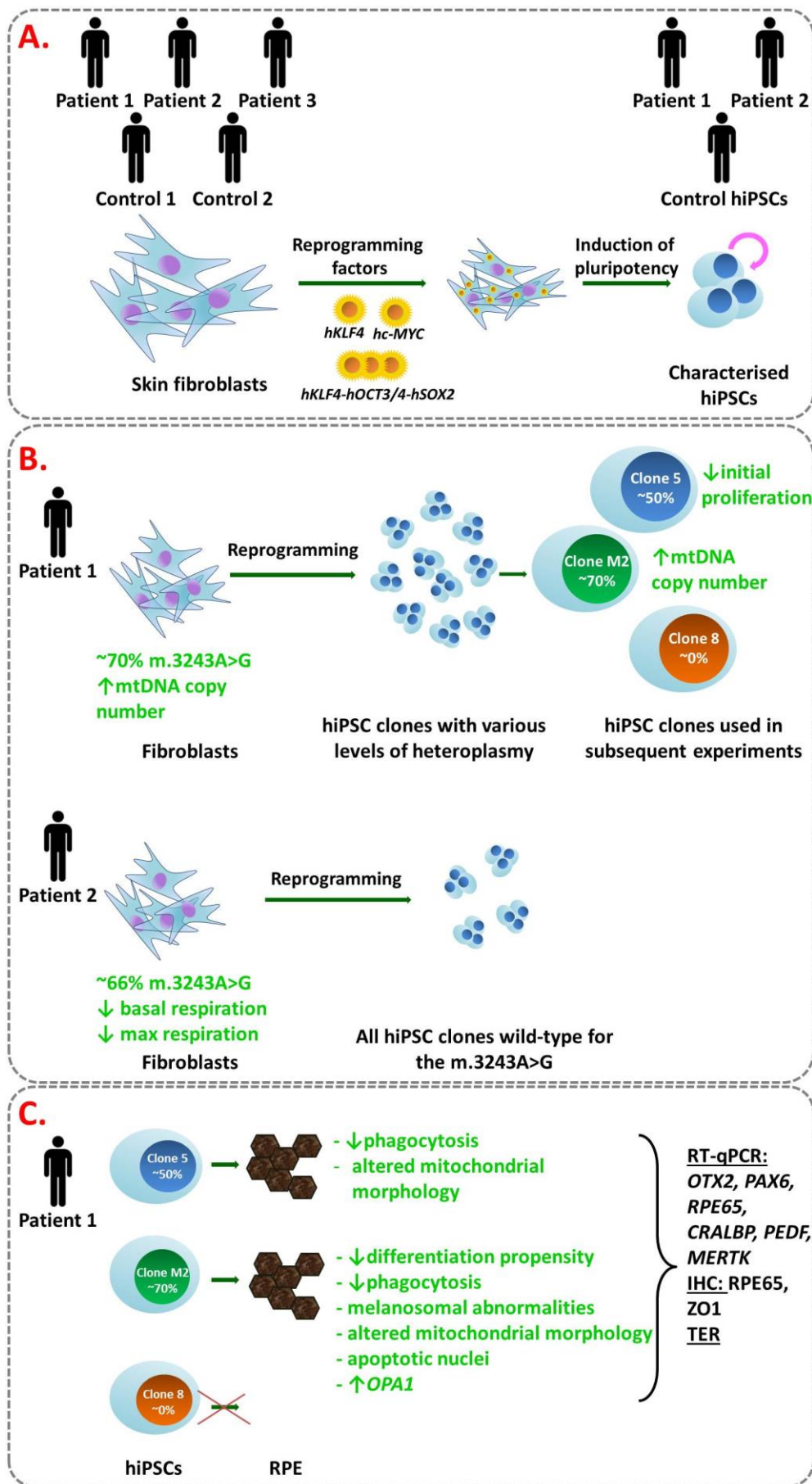
Figure 7.1. Schematic representation of the major findings of this PhD project.

7.2 Limitations of the study

Like any other study, the work described in this thesis has its limitations, some of which are described below.

7.2.1 Patient samples and controls

Two hiPSC clones from one 73 year-old patient were used to demonstrate retinal dysfunction seen in clinical observations. Cells from a 51 year-old donor were used as an hiPSC control. A better way to interpret the results would be to have more patient samples or more clones from the same patient to compare. In addition, an isogenic homoplasmic control or an age matched control would have given a better comparison.

An alternative could be to use the same control, but instead introduce the m.3243A>G mutation. A persistent pathological phenotype in the control would make a convincing argument for a proposed pathogenesis. Or alternatively, the mutation in Patient 1 cells could be corrected. Some preliminary reports have been published in recent years that explored the possibility of this approach. Bacman *et al.* (2013) used mitochondria-targeted transcription activator-like effector nucleases (mitoTALENs) in order to eliminate mtDNA with common deletion or m.14459G>A mutation in the *MT-ND6* gene, associated with LHON disease, from osteosarcoma cell cybrids. A later study also showed the application of mitoTALENs in eliminating mtDNA harbouring the same LHON mutation by generating mouse oocytes carrying human mutated mtDNA (Reddy *et al.*, 2015). Jo *et al.* (2015) used clustered regularly interspaced short palindromic repeats (CRISPR) / mitoCas9 system in HEK-293T cells to target Cox1 and Cox3. Although still in its infancy, a mtDNA manipulation approach holds many promises.

A primary sample of RPE cells from a donor of similar age would have been better as a RT-qPCR control rather than ARPE19 cell line.

7.2.2 Cytogenetic abnormalities

In an ideal setting, it would be better to compare hiPSCs without acquired nuclear DNA changes, such as those seen in Clone M2. One of the suggestions for future work would be to test the hiPSCs for cytogenetic abnormalities early in the project in order to avoid using cells with nuclear abnormalities in disease modelling studies.

7.2.3 Using hiPSCs as a disease model

Although, hiPSCs hold a great potential for elucidating mechanisms in many diseases, including the diseases associated with mitochondria, they have a number of limitations that could affect interpretation of the results. Firstly, there is significant variation between different hiPSC clones, even if they are derived from the same person. Such variation could be in the form of differentiation propensity and maturation, and as a result their ability to mimic patient phenotype. Additionally, robust differentiation protocols that work across multiple clones and cell lines are still lacking, which makes it difficult to assess the effect of the mutation on differentiation propensity. Ideally, more patient and control cells should be used to increase statistical power of the experiments. However, tissue availability, time and financial restrictions could impede on increasing sample size.

7.3 Suggestions for future work

Apart from some of the comments that were already made in individual chapter discussions, some additional experiments that could be done are outlined below.

I.   Whole-genome sequencing of patient and control cells would give an indication of whether there were any additional nuclear DNA and / or mtDNA abnormalities that could have influenced the results.

II. An experiment to confirm tRNA$^{Leu(UUR)}$ translational deficiency would be required to confirm the mechanism of the mitochondrial involvement in the pathology seen in RPE cells.

III. Lysosomal activity assay and assays assessing autophagy would confirm aberrant clearance of degraded melanosomes, abnormal mitochondria and photoreceptor outer segments in RPE cells.

IV. Analysis of mitochondrial network disturbances in RPE cells to elucidate its potential involvement in apoptosis and mitophagy.

V.   ROS levels and mitochondrial mass would be another way to assess RPE cellular health.

VI. The nuclei of some RPE cells were apoptotic as seen in the TEM images. Molecular analysis of apoptosis would be useful as an additional confirmation.

VII. Testing additional RPE functions, such as growth factor secretion, would show whether there are additional effects of the mutation on cellular health.

VIII. Differentiation of the hiPSCs towards neural retinal subtypes, especially photoreceptors and RGCs, would further elucidate the effect of the m.3243A<G on retina. Alternatively, having a fully laminated retina with an integrated RPE layer would allow a better model of the disease.

IX. Test more ECM proteins to enhance RPE propagation.

7.4 Significance of the findings

The RPE cells derived from patient hiPSCs had remarkable similarities to the cells found in post mortem retinal tissues of patients harbouring the same mutation. This is the first time retinal manifestations associated with m.3243A>G have been recapitulated *in vitro*. Up to 25% of patients with the mutation have ophthalmological complications, including pigmentary retinopathy (El-Hattab *et al.*, 2015). The ability to mimic these manifestations would allow elucidating potential pathological mechanisms of the disease and allow testing novel therapeutic agents aimed at alleviating or treating the symptoms. Crucially, what the results in this thesis have shown is that retinal pathology could be a result of the inability of RPE cells to perform at least two of their major functions: phagocytosis of photoreceptor outer segments, and stray light absorption due to dysfunctional melanosomes. Furthermore, understanding the mechanisms of RPE abnormalities associated with the m.3243A>G mutation could uncover pathological mechanisms in similar conditions, including AMD.

References

Abu Khamidakh, A.E., Dos Santos, F.C., Skottman, H., Juuti-Uusitalo, K. and Hyttinen, J. (2016) 'Semi-automatic Method for Ca2+ Imaging Data Analysis of Maturing Human Embryonic Stem Cells-Derived Retinal Pigment Epithelium', *Ann Biomed Eng*.

Acampora, D., Di Giovannantonio, L.G. and Simeone, A. (2013) 'Otx2 is an intrinsic determinant of the embryonic stem cell state and is required for transition to a stable epiblast stem cell condition', *Development*, 140(1), pp. 43-55.

Adewumi, O., Aflatoonian, B., Ahrlund-Richter, L., Amit, M., Andrews, P.W., Beighton, G., Bello, P.A., Benvenisty, N., Berry, L.S., Bevan, S., Blum, B., Brooking, J., Chen, K.G., Choo, A.B., Churchill, G.A., Corbel, M., Damjanov, I., Draper, J.S., Dvorak, P., Emanuelsson, K., Fleck, R.A., Ford, A., Gertow, K., Gertsenstein, M., Gokhale, P.J., Hamilton, R.S., Hampl, A., Healy, L.E., Hovatta, O., Hyllner, J., Imreh, M.P., Itskovitz-Eldor, J., Jackson, J., Johnson, J.L., Jones, M., Kee, K., King, B.L., Knowles, B.B., Lako, M., Lebrin, F., Mallon, B.S., Manning, D., Mayshar, Y., McKay, R.D., Michalska, A.E., Mikkola, M., Mileikovsky, M., Minger, S.L., Moore, H.D., Mummery, C.L., Nagy, A., Nakatsuji, N., O'Brien, C.M., Oh, S.K., Olsson, C., Otonkoski, T., Park, K.Y., Passier, R., Patel, H., Patel, M., Pedersen, R., Pera, M.F., Piekarczyk, M.S., Pera, R.A., Reubinoff, B.E., Robins, A.J., Rossant, J., Rugg-Gunn, P., Schulz, T.C., Semb, H., Sherrer, E.S., Siemen, H., Stacey, G.N., Stojkovic, M., Suemori, H., Szatkiewicz, J., Turetsky, T., Tuuri, T., van den Brink, S., Vintersten, K., Vuoristo, S., Ward, D., Weaver, T.A., Young, L.A. and Zhang, W. (2007) 'Characterization of human embryonic stem cell lines by the International Stem Cell Initiative', *Nat Biotechnol*, 25(7), pp. 803-16.

Age-Related Eye Disease Study Research, G. (2001) 'A randomized, placebo-controlled, clinical trial of high-dose supplementation with vitamins C and E, beta carotene, and zinc for age-related macular degeneration and vision loss: AREDS report no. 8', *Arch Ophthalmol*, 119(10), pp. 1417-36.

Amps, K., Andrews, P.W., Anyfantis, G., Armstrong, L., Avery, S., Baharvand, H., Baker, J., Baker, D., Munoz, M.B., Beil, S., Benvenisty, N., Ben-Yosef, D., Biancotti, J.C., Bosman, A., Brena, R.M., Brison, D., Caisander, G., Camarasa, M.V., Chen, J., Chiao, E., Choi, Y.M., Choo, A.B., Collins, D., Colman, A., Crook, J.M., Daley, G.Q., Dalton, A., De Sousa, P.A., Denning, C., Downie, J., Dvorak, P., Montgomery, K.D., Feki, A., Ford, A., Fox, V., Fraga, A.M., Frumkin, T., Ge, L., Gokhale, P.J., Golan-Lev, T., Gourabi, H., Gropp, M., Lu, G., Hampl, A., Harron, K., Healy, L., Herath, W., Holm, F., Hovatta, O., Hyllner, J., Inamdar, M.S., Irwanto, A.K., Ishii, T., Jaconi, M., Jin, Y., Kimber, S., Kiselev, S., Knowles, B.B., Kopper, O., Kukharenko, V., Kuliev, A., Lagarkova, M.A., Laird, P.W., Lako, M., Laslett, A.L., Lavon, N., Lee, D.R., Lee, J.E., Li, C., Lim, L.S., Ludwig, T.E., Ma, Y., Maltby, E., Mateizel, I., Mayshar, Y., Mileikovsky, M., Minger, S.L., Miyazaki, T., Moon, S.Y., Moore, H., Mummery, C., Nagy, A., Nakatsuji, N., Narwani, K., Oh, S.K., Olson, C., Otonkoski, T., Pan, F., Park, I.H., Pells, S., Pera, M.F., Pereira, L.V., Qi, O., Raj, G.S., Reubinoff, B., Robins, A., Robson, P., Rossant, J., Salekdeh, G.H., Schulz, T.C., et al. (2011) 'Screening ethnically diverse human embryonic stem cells identifies a chromosome 20 minimal amplicon conferring growth advantage', *Nat Biotechnol*, 29(12), pp. 1132-44.

Anderson, S., Bankier, A.T., Barrell, B.G., de Bruijn, M.H., Coulson, A.R., Drouin, J., Eperon, I.C., Nierlich, D.P., Roe, B.A., Sanger, F., Schreier, P.H., Smith, A.J., Staden, R. and Young, I.G. (1981) 'Sequence and organization of the human mitochondrial genome', *Nature*, 290(5806), pp. 457-65.

Andersson, S.G., Zomorodipour, A., Andersson, J.O., Sicheritz-Ponten, T., Alsmark, U.C., Podowski, R.M., Naslund, A.K., Eriksson, A.S., Winkler, H.H. and Kurland, C.G. (1998) 'The genome sequence of Rickettsia prowazekii and the origin of mitochondria', *Nature*, 396(6707), pp. 133-40.

Bacman, S.R., Williams, S.L., Pinto, M., Peralta, S. and Moraes, C.T. (2013) 'Specific elimination of mutant mitochondrial genomes in patient-derived cells by mitoTALENs', *Nat Med*, 19(9), pp. 1111-3.

Badcock, G., Pigott, C., Goepel, J. and Andrews, P.W. (1999) 'The human embryonal carcinoma marker antigen TRA-1-60 is a sialylated keratan sulfate proteoglycan', *Cancer Res*, 59(18), pp. 4715-9.

Bae, D., Mondragon-Teran, P., Hernandez, D., Ruban, L., Mason, C., Bhattacharya, S.S. and Veraitch, F.S. (2012) 'Hypoxia enhances the generation of retinal progenitor cells from human induced pluripotent and embryonic stem cells', *Stem Cells Dev*, 21(8), pp. 1344-55.

Ballinger, S.W., Van Houten, B., Jin, G.F., Conklin, C.A. and Godley, B.F. (1999) 'Hydrogen peroxide causes significant mitochondrial DNA damage in human RPE cells', *Exp Eye Res*, 68(6), pp. 765-72.

Ban, H., Nishishita, N., Fusaki, N., Tabata, T., Saeki, K., Shikamura, M., Takada, N., Inoue, M., Hasegawa, M., Kawamata, S. and Nishikawa, S. (2011) 'Efficient generation of transgene-free human induced pluripotent stem cells (iPSCs) by temperature-sensitive Sendai virus vectors', *Proc Natl Acad Sci U S A*, 108(34), pp. 14234-9.

Barot, M., Gokulgandhi, M.R. and Mitra, A.K. (2011) 'Mitochondrial dysfunction in retinal diseases', *Curr Eye Res*, 36(12), pp. 1069-77.

Barrell, B.G., Anderson, S., Bankier, A.T., de Bruijn, M.H., Chen, E., Coulson, A.R., Drouin, J., Eperon, I.C., Nierlich, D.P., Roe, B.A., Sanger, F., Schreier, P.H., Smith, A.J., Staden, R. and Young, I.G. (1980) 'Different pattern of codon recognition by mammalian mitochondrial tRNAs', *Proc Natl Acad Sci U S A*, 77(6), pp. 3164-6.

Bartek, J. and Lukas, J. (2007) 'DNA damage checkpoints: from initiation to recovery or adaptation', *Curr Opin Cell Biol*, 19(2), pp. 238-45.

Bartel, D.P. (2004) 'MicroRNAs: genomics, biogenesis, mechanism, and function', *Cell*, 116(2), pp. 281-97.

Bassing, C.H., Chua, K.F., Sekiguchi, J., Suh, H., Whitlow, S.R., Fleming, J.C., Monroe, B.C., Ciccone, D.N., Yan, C., Vlasakova, K., Livingston, D.M., Ferguson, D.O., Scully, R. and Alt, F.W. (2002) 'Increased ionizing radiation sensitivity and genomic instability in the absence of histone H2AX', *Proc Natl Acad Sci U S A*, 99(12), pp. 8173-8.

Baumer, N., Marquardt, T., Stoykova, A., Spieler, D., Treichel, D., Ashery-Padan, R. and Gruss, P. (2003) 'Retinal pigmented epithelium determination requires the redundant activities of Pax2 and Pax6', *Development*, 130(13), pp. 2903-15.

Becker, K.A., Ghule, P.N., Therrien, J.A., Lian, J.B., Stein, J.L., van Wijnen, A.J. and Stein, G.S. (2006) 'Self-renewal of human embryonic stem cells is supported by a shortened G1 cell cycle phase', *J Cell Physiol*, 209(3), pp. 883-93.

Beers, J., Linask, K.L., Chen, J.A., Siniscalchi, L.I., Lin, Y., Zheng, W., Rao, M. and Chen, G. (2015) 'A cost-effective and efficient reprogramming platform for large-scale production of integration-free human induced pluripotent stem cells in chemically defined culture', *Sci Rep*, 5, p. 11319.

Benjamin, R.C. and Gill, D.M. (1980) 'Poly(ADP-ribose) synthesis in vitro programmed by damaged DNA. A comparison of DNA molecules containing different types of strand breaks', *J Biol Chem*, 255(21), pp. 10502-8.

Bentlage, H.A. and Attardi, G. (1996) 'Relationship of genotype to phenotype in fibroblast-derived transmitochondrial cell lines carrying the 3243 mutation associated with the MELAS encephalomyopathy: shift towards mutant genotype and role of mtDNA copy number', *Hum Mol Genet*, 5(2), pp. 197-205.

Bhutto, I. and Lutty, G. (2012) 'Understanding age-related macular degeneration (AMD): relationships between the photoreceptor/retinal pigment epithelium/Bruch's membrane/choriocapillaris complex', *Molecular Aspects of Medicine*, 33(4), pp. 295-317.

Bhuvaneswar, C.G., Goetz, J.L. and Stern, T.A. (2008) 'Multiple neurologic, psychiatric, and endocrine complaints in a young woman: a case discussion and review of the clinical features and management of mitochondrial myopathy, encephalopathy, lactic acidosis, and stroke', *Primary Care Companion to The Journal of Clinical Psychiatry*, 10(3), pp. 237-44.

Bok, D. and Hall, M.O. (1971) 'The role of the pigment epithelium in the etiology of inherited retinal dystrophy in the rat', *J Cell Biol*, 49(3), pp. 664-82.

Bonilha, V.L. (2008) 'Age and disease-related structural changes in the retinal pigment epithelium', *Clin Ophthalmol*, 2(2), pp. 413-24.

Bonitz, S.G., Berlani, R., Coruzzi, G., Li, M., Macino, G., Nobrega, F.G., Nobrega, M.P., Thalenfeld, B.E. and Tzagoloff, A. (1980) 'Codon recognition rules in yeast mitochondria', *Proc Natl Acad Sci U S A*, 77(6), pp. 3167-70.

Borooah, S., Phillips, M.J., Bilican, B., Wright, A.F., Wilmut, I., Chandran, S., Gamm, D. and Dhillon, B. (2013) 'Using human induced pluripotent stem cells to treat retinal disease', *Prog Retin Eye Res*, 37, pp. 163-81.

Borovansky, J., Mirejovsky, P. and Riley, P.A. (1991) 'Possible relationship between abnormal melanosome structure and cytotoxic phenomena in malignant melanoma', *Neoplasma*, 38(4), pp. 393-400.

Borovansky, J. and Riley, P.A. (2011) *Melanins and Melanosomes: Biosynthesis, Structure, Physiological and Pathological Functions*. Weinheim, Germany: Wiley-Blackwell.

Briggs, R. and King, T.J. (1952) 'Transplantation of Living Nuclei From Blastula Cells into Enucleated Frogs' Eggs', *Proc Natl Acad Sci U S A*, 38(5), pp. 455-63.

Bu, X.D. and Rotter, J.I. (1991) 'X chromosome-linked and mitochondrial gene control of Leber hereditary optic neuropathy: evidence from segregation analysis for dependence on X chromosome inactivation', *Proc Natl Acad Sci U S A*, 88(18), pp. 8198-202.

Buchholz, D.E., Hikita, S.T., Rowland, T.J., Friedrich, A.M., Hinman, C.R., Johnson, L.V. and Clegg, D.O. (2009) 'Derivation of functional retinal pigmented epithelium from induced pluripotent stem cells', *Stem Cells*, 27(10), pp. 2427-34.

Buchholz, D.E., Pennington, B.O., Croze, R.H., Hinman, C.R., Coffey, P.J. and Clegg, D.O. (2013) 'Rapid and efficient directed differentiation of human pluripotent stem cells into retinal pigmented epithelium', *Stem Cells Transl Med*, 2(5), pp. 384-93.

Buganim, Y., Faddah, D.A., Cheng, A.W., Itskovich, E., Markoulaki, S., Ganz, K., Klemm, S.L., van Oudenaarden, A. and Jaenisch, R. (2012) 'Single-cell expression analyses during cellular reprogramming reveal an early stochastic and a late hierarchic phase', *Cell*, 150(6), pp. 1209-22.

Bukowiecki, R., Adjaye, J. and Prigione, A. (2014) 'Mitochondrial function in pluripotent stem cells and cellular reprogramming', *Gerontology*, 60(2), pp. 174-82.

Bunce, C., Xing, W. and Wormald, R. (2010) 'Causes of blind and partial sight certifications in England and Wales: April 2007-March 2008', *Eye*, 24(11), pp. 1692-9.

Burmeister, M., Novak, J., Liang, M.Y., Basu, S., Ploder, L., Hawes, N.L., Vidgen, D., Hoover, F., Goldman, D., Kalnins, V.I., Roderick, T.H., Taylor, B.A., Hankin, M.H. and McInnes, R.R. (1996) 'Ocular retardation mouse caused by Chx10 homeobox null allele: impaired retinal progenitor proliferation and bipolar cell differentiation', *Nat Genet*, 12(4), pp. 376-84.

Buta, C., David, R., Dressel, R., Emgard, M., Fuchs, C., Gross, U., Healy, L., Hescheler, J., Kolar, R., Martin, U., Mikkers, H., Muller, F.J., Schneider, R.K., Seiler, A.E., Spielmann, H. and Weitzer, G. (2013) 'Reconsidering pluripotency tests: do we still need teratoma assays?', *Stem Cell Res*, 11(1), pp. 552-62.

Byrne, J.A., Pedersen, D.A., Clepper, L.L., Nelson, M., Sanger, W.G., Gokhale, S., Wolf, D.P. and Mitalipov, S.M. (2007) 'Producing primate embryonic stem cells by somatic cell nuclear transfer', *Nature*, 450(7169), pp. 497-502.

Cahan, P. and Daley, G.Q. (2013) 'Origins and implications of pluripotent stem cell variability and heterogeneity', *Nat Rev Mol Cell Biol*, 14(6), pp. 357-68.

Campbell, K.H., McWhir, J., Ritchie, W.A. and Wilmut, I. (1996) 'Sheep cloned by nuclear transfer from a cultured cell line', *Nature*, 380(6569), pp. 64-6.

Capowski, E.E., Simonett, J.M., Clark, E.M., Wright, L.S., Howden, S.E., Wallace, K.A., Petelinsek, A.M., Pinilla, I., Phillips, M.J., Meyer, J.S., Schneider, B.L., Thomson, J.A. and Gamm, D.M. (2014) 'Loss of MITF expression during human embryonic stem cell differentiation disrupts retinal pigment epithelium development and optic vesicle cell proliferation', *Hum Mol Genet*.

Capowski, E.E., Wright, L.S., Liang, K., Phillips, M.J., Wallace, K., Petelinsek, A., Hagstrom, A., Pinilla, I., Borys, K., Lien, J., Min, J.H., Keles, S., Thomson, J.A. and Gamm, D.M. (2016) 'Regulation of WNT Signaling by VSX2 During Optic Vesicle Patterning in Human Induced Pluripotent Stem Cells', *Stem Cells*.

Card, D.A., Hebbar, P.B., Li, L., Trotter, K.W., Komatsu, Y., Mishina, Y. and Archer, T.K. (2008) 'Oct4/Sox2-regulated miR-302 targets cyclin D1 in human embryonic stem cells', *Mol Cell Biol*, 28(20), pp. 6426-38.

Carelli, V., Musumeci, O., Caporali, L., Zanna, C., La Morgia, C., Del Dotto, V., Porcelli, A.M., Rugolo, M., Valentino, M.L., Iommarini, L., Maresca, A., Barboni, P., Carbonelli, M., Trombetta, C., Valente, E.M., Patergnani, S., Giorgi, C., Pinton, P., Rizzo, G., Tonon, C., Lodi, R., Avoni, P., Liguori, R., Baruzzi, A., Toscano, A. and Zeviani, M. (2015) 'Syndromic parkinsonism and dementia associated with OPA1 missense mutations', *Ann Neurol*, 78(1), pp. 21-38.

Carr, A.J., Vugler, A.A., Hikita, S.T., Lawrence, J.M., Gias, C., Chen, L.L., Buchholz, D.E., Ahmado, A., Semo, M., Smart, M.J., Hasan, S., da Cruz, L., Johnson, L.V., Clegg, D.O. and Coffey, P.J. (2009) 'Protective effects of human iPS-derived retinal pigment epithelium cell transplantation in the retinal dystrophic rat', *PLoS One*, 4(12), p. e8152.

Celeste, A., Petersen, S., Romanienko, P.J., Fernandez-Capetillo, O., Chen, H.T., Sedelnikova, O.A., Reina-San-Martin, B., Coppola, V., Meffre, E., Difilippantonio, M.J., Redon, C., Pilch, D.R., Olaru, A., Eckhaus, M., Camerini-Otero, R.D., Tessarollo, L., Livak, F., Manova, K., Bonner, W.M., Nussenzweig, M.C. and Nussenzweig, A. (2002) 'Genomic instability in mice lacking histone H2AX', *Science*, 296(5569), pp. 922-7.

Chaitanya, G.V., Steven, A.J. and Babu, P.P. (2010) 'PARP-1 cleavage fragments: signatures of cell-death proteases in neurodegeneration', *Cell Commun Signal*, 8, p. 31.

Chambers, I., Colby, D., Robertson, M., Nichols, J., Lee, S., Tweedie, S. and Smith, A. (2003) 'Functional expression cloning of Nanog, a pluripotency sustaining factor in embryonic stem cells', *Cell*, 113(5), pp. 643-55.

Chambers, S.M., Fasano, C.A., Papapetrou, E.P., Tomishima, M., Sadelain, M. and Studer, L. (2009) 'Highly efficient neural conversion of human ES and iPS cells by dual inhibition of SMAD signaling', *Nat Biotechnol*, 27(3), pp. 275-80.

Chambers, S.M., Qi, Y., Mica, Y., Lee, G., Zhang, X.J., Niu, L., Bilsland, J., Cao, L., Stevens, E., Whiting, P., Shi, S.H. and Studer, L. (2012) 'Combined small-molecule inhibition accelerates developmental timing and converts human pluripotent stem cells into nociceptors', *Nat Biotechnol*, 30(7), pp. 715-20.

Chan, E.M., Ratanasirintrawoot, S., Park, I.H., Manos, P.D., Loh, Y.H., Huo, H., Miller, J.D., Hartung, O., Rho, J., Ince, T.A., Daley, G.Q. and Schlaeger, T.M. (2009) 'Live cell imaging distinguishes bona fide human iPS cells from partially reprogrammed cells', *Nat Biotechnol*, 27(11), pp. 1033-7.

Chang, T.S., Johns, D.R., Walker, D., de la Cruz, Z., Maumence, I.H. and Green, W.R. (1993) 'Ocular clinicopathologic study of the mitochondrial encephalomyopathy overlap syndromes', *Arch Ophthalmol*, 111(9), pp. 1254-62.

Chen, G., Gulbranson, D.R., Hou, Z., Bolin, J.M., Ruotti, V., Probasco, M.D., Smuga-Otto, K., Howden, S.E., Diol, N.R., Propson, N.E., Wagner, R., Lee, G.O., Antosiewicz-Bourget, J., Teng, J.M. and Thomson, J.A. (2011a) 'Chemically defined conditions for human iPSC derivation and culture', *Nat Methods*, 8(5), pp. 424-9.

Chen, H., Lukas, T.J., Du, N., Suyeoka, G. and Neufeld, A.H. (2009) 'Dysfunction of the retinal pigment epithelium with age: increased iron decreases phagocytosis and lysosomal activity', *Invest Ophthalmol Vis Sci*, 50(4), pp. 1895-902.

Chen, J., Liu, H., Liu, J., Qi, J., Wei, B., Yang, J., Liang, H., Chen, Y., Wu, Y., Guo, L., Zhu, J., Zhao, X., Peng, T., Zhang, Y., Chen, S., Li, X., Li, D., Wang, T. and Pei, D. (2013) 'H3K9 methylation is a barrier during somatic cell reprogramming into iPSCs', *Nat Genet*, 45(1), pp. 34-42.

Chen, P.M., Gombart, Z.J. and Chen, J.W. (2011b) 'Chloroquine treatment of ARPE-19 cells leads to lysosome dilation and intracellular lipid accumulation: possible implications of lysosomal dysfunction in macular degeneration', *Cell Biosci*, 1(1), p. 10.

Cherry, A.B., Gagne, K.E., McLoughlin, E.M., Baccei, A., Gorman, B., Hartung, O., Miller, J.D., Zhang, J., Zon, R.L., Ince, T.A., Neufeld, E.J., Lerou, P.H., Fleming, M.D., Daley, G.Q. and Agarwal, S. (2013) 'Induced pluripotent stem cells with a mitochondrial DNA deletion', *Stem Cells*, 31(7), pp. 1287-97.

Chevrollier, A., Guillet, V., Loiseau, D., Gueguen, N., de Crescenzo, M.A., Verny, C., Ferre, M., Dollfus, H., Odent, S., Milea, D., Goizet, C., Amati-Bonneau, P., Procaccio,

V., Bonneau, D. and Reynier, P. (2008) 'Hereditary optic neuropathies share a common mitochondrial coupling defect', *Ann Neurol*, 63(6), pp. 794-8.

Chichagova, V., Sanchez-Vera, I., Armstrong, L., Steel, D. and Lako, M. (2015) 'Generation of human induced pluripotent stem cells using RNA-based Sendai virus system and pluripotency validation of the resulting cell population', *Methods Mol Biol*.

Chin, J., Marotta, R., Chiotis, M., Allan, E.H. and Collins, S.J. (2014) 'Detection rates and phenotypic spectrum of m.3243A>G in the MT-TL1 gene: a molecular diagnostic laboratory perspective', *Mitochondrion*, 17, pp. 34-41.

Chinnery, P.F. and Hudson, G. (2013) 'Mitochondrial genetics', *Br Med Bull*, 106, pp. 135-59.

Chinnery, P.F., Johnson, M.A., Wardell, T.M., Singh-Kler, R., Hayes, C., Brown, D.T., Taylor, R.W., Bindoff, L.A. and Turnbull, D.M. (2000) 'The epidemiology of pathogenic mitochondrial DNA mutations', *Ann Neurol*, 48(2), pp. 188-93.

Chipuk, J.E. and Green, D.R. (2005) 'Do inducers of apoptosis trigger caspase-independent cell death?', *Nat Rev Mol Cell Biol*, 6(3), pp. 268-75.

Cho, H.J., Lee, C.S., Kwon, Y.W., Paek, J.S., Lee, S.H., Hur, J., Lee, E.J., Roh, T.Y., Chu, I.S., Leem, S.H., Kim, Y., Kang, H.J., Park, Y.B. and Kim, H.S. (2010) 'Induction of pluripotent stem cells from adult somatic cells by protein-based reprogramming without genetic manipulation', *Blood*, 116(3), pp. 386-95.

Chou, B.K., Mali, P., Huang, X., Ye, Z., Dowey, S.N., Resar, L.M., Zou, C., Zhang, Y.A., Tong, J. and Cheng, L. (2011) 'Efficient human iPS cell derivation by a non-integrating plasmid from blood cells with unique epigenetic and gene expression signatures', *Cell Res*, 21(3), pp. 518-29.

Christen, W.G., Glynn, R.J., Manson, J.E., Ajani, U.A. and Buring, J.E. (1996) 'A prospective study of cigarette smoking and risk of age-related macular degeneration in men', *JAMA*, 276(14), pp. 1147-51.

Chu, C.T., Bayir, H. and Kagan, V.E. (2014) 'LC3 binds externalized cardiolipin on injured mitochondria to signal mitophagy in neurons: implications for Parkinson disease', *Autophagy*, 10(2), pp. 376-8.

Cimadamore, F., Curchoe, C.L., Alderson, N., Scott, F., Salvesen, G. and Terskikh, A.V. (2009) 'Nicotinamide rescues human embryonic stem cell-derived neuroectoderm from parthanatic cell death', *Stem Cells*, 27(8), pp. 1772-81.

Clay Montier, L.L., Deng, J.J. and Bai, Y. (2009) 'Number matters: control of mammalian mitochondrial DNA copy number', *J Genet Genomics*, 36(3), pp. 125-31.

Cohen, G.M. (1997) 'Caspases: the executioners of apoptosis', *Biochem J*, 326 (Pt 1), pp. 1-16.

Cohn, A.C., Toomes, C., Hewitt, A.W., Kearns, L.S., Inglehearn, C.F., Craig, J.E. and Mackey, D.A. (2008) 'The natural history of OPA1-related autosomal dominant optic atrophy', *Br J Ophthalmol*, 92(10), pp. 1333-6.

Cowan, C.A., Klimanskaya, I., McMahon, J., Atienza, J., Witmyer, J., Zucker, J.P., Wang, S., Morton, C.C., McMahon, A.P., Powers, D. and Melton, D.A. (2004) 'Derivation of embryonic stem-cell lines from human blastocysts', *N Engl J Med*, 350(13), pp. 1353-6.

Croze, R.H., Buchholz, D.E., Radeke, M.J., Thi, W.J., Hu, Q., Coffey, P.J. and Clegg, D.O. (2014) 'ROCK Inhibition Extends Passage of Pluripotent Stem Cell-Derived Retinal Pigmented Epithelium', *Stem Cells Transl Med*, 3(9), pp. 1066-78.

Daniele, T., Hurbain, I., Vago, R., Casari, G., Raposo, G., Tacchetti, C. and Schiaffino, M.V. (2014) 'Mitochondria and melanosomes establish physical contacts modulated by Mfn2 and involved in organelle biogenesis', *Curr Biol*, 24(4), pp. 393-403.

Darin, N., Oldfors, A., Moslemi, A.R., Holme, E. and Tulinius, M. (2001) 'The incidence of mitochondrial encephalomyopathies in childhood: clinical features and morphological, biochemical, and DNA anbormalities', *Ann Neurol*, 49(3), pp. 377-83.

Daruich, A., Matet, A. and Borruat, F.X. (2014) 'Macular dystrophy associated with the mitochondrial DNA A3243G mutation: pericentral pigment deposits or atrophy? Report of two cases and review of the literature', *BMC Ophthalmology*, 14, p. 77.

de Laat, P., Smeitink, J.A., Janssen, M.C., Keunen, J.E. and Boon, C.J. (2013) 'Mitochondrial retinal dystrophy associated with the m.3243A>G mutation', *Ophthalmology*, 120(12), pp. 2684-96.

Decanini, A., Nordgaard, C.L., Feng, X., Ferrington, D.A. and Olsen, T.W. (2007) 'Changes in select redox proteins of the retinal pigment epithelium in age-related macular degeneration', *Am J Ophthalmol*, 143(4), pp. 607-15.

Del Priore, L.V., Kuo, Y.H. and Tezel, T.H. (2002) 'Age-related changes in human RPE cell density and apoptosis proportion in situ', *Invest Ophthalmol Vis Sci*, 43(10), pp. 3312-8.

Ding, Y., Xia, B.H., Yu, J.F., Leng, J.H. and Huang, J.Y. (2013) 'Mitochondrial DNA mutations and essential hypertension', *International Journal of Molecular Medicine*, 32(4), pp. 768-774.

Dombi, E., Diot, A., Morten, K., Carver, J., Lodge, T., Fratter, C., Ng, Y.S., Liao, C., Muir, R., Blakely, E.L., Hargreaves, I., Al-Dosary, M., Sarkar, G., Hickman, S.J., Downes, S.M., Jayawant, S., Yu-Wai-Man, P., Taylor, R.W. and Poulton, J. (2016) 'The m.13051G>A mitochondrial DNA mutation results in variable neurology and activated mitophagy', *Neurology*, 86(20), pp. 1921-3.

Draper, J.S., Pigott, C., Thomson, J.A. and Andrews, P.W. (2002) 'Surface antigens of human embryonic stem cells: changes upon differentiation in culture', *J Anat*, 200(Pt 3), pp. 249-58.

Draper, J.S., Smith, K., Gokhale, P., Moore, H.D., Maltby, E., Johnson, J., Meisner, L., Zwaka, T.P., Thomson, J.A. and Andrews, P.W. (2004) 'Recurrent gain of chromosomes 17q and 12 in cultured human embryonic stem cells', *Nat Biotechnol*, 22(1), pp. 53-4.

Dunbar, D.R., Moonie, P.A., Jacobs, H.T. and Holt, I.J. (1995) 'Different cellular backgrounds confer a marked advantage to either mutant or wild-type mitochondrial genomes', *Proc Natl Acad Sci U S A*, 92(14), pp. 6562-6.

Dvorakova, V., Kolarova, H., Magner, M., Tesarova, M., Hansikova, H., Zeman, J. and Honzik, T. (2016) 'The phenotypic spectrum of fifty Czech m.3243A>G carriers', *Mol Genet Metab*, 118(4), pp. 288-95.

Eiraku, M., Takata, N., Ishibashi, H., Kawada, M., Sakakura, E., Okuda, S., Sekiguchi, K., Adachi, T. and Sasai, Y. (2011) 'Self-organizing optic-cup morphogenesis in three-dimensional culture', *Nature*, 472(7341), pp. 51-6.

El-Hattab, A.W., Adesina, A.M., Jones, J. and Scaglia, F. (2015) 'MELAS syndrome: Clinical manifestations, pathogenesis, and treatment options', *Mol Genet Metab*, 116(1-2), pp. 4-12.

Elliott, H.R., Samuels, D.C., Eden, J.A., Relton, C.L. and Chinnery, P.F. (2008) 'Pathogenic mitochondrial DNA mutations are common in the general population', *Am J Hum Genet*, 83(2), pp. 254-60.

Ellis, H.M. and Horvitz, H.R. (1986) 'Genetic control of programmed cell death in the nematode C. elegans', *Cell*, 44(6), pp. 817-29.

Enver, T., Soneji, S., Joshi, C., Brown, J., Iborra, F., Orntoft, T., Thykjaer, T., Maltby, E., Smith, K., Abu Dawud, R., Jones, M., Matin, M., Gokhale, P., Draper, J. and Andrews, P.W. (2005) 'Cellular differentiation hierarchies in normal and culture-adapted human embryonic stem cells', *Hum Mol Genet*, 14(21), pp. 3129-40.

Esteban, M.A., Wang, T., Qin, B., Yang, J., Qin, D., Cai, J., Li, W., Weng, Z., Chen, J., Ni, S., Chen, K., Li, Y., Liu, X., Xu, J., Zhang, S., Li, F., He, W., Labuda, K., Song, Y., Peterbauer, A., Wolbank, S., Redl, H., Zhong, M., Cai, D., Zeng, L. and Pei, D. (2010) 'Vitamin C enhances the generation of mouse and human induced pluripotent stem cells', *Cell Stem Cell*, 6(1), pp. 71-9.

Evans, M.J. and Kaufman, M.H. (1981) 'Establishment in culture of pluripotential cells from mouse embryos', *Nature*, 292(5819), pp. 154-6.

Feeney-Burns, L., Hilderbrand, E.S. and Eldridge, S. (1984) 'Aging human RPE: morphometric analysis of macular, equatorial, and peripheral cells', *Invest Ophthalmol Vis Sci*, 25(2), pp. 195-200.

Feher, J., Kovacs, I., Artico, M., Cavallotti, C., Papale, A. and Balacco Gabrieli, C. (2006a) 'Mitochondrial alterations of retinal pigment epithelium in age-related macular degeneration', *Neurobiology of Aging*, 27(7), pp. 983-93.

Feher, J., Kovacs, I., Artico, M., Cavallotti, C., Papale, A. and Balacco Gabrieli, C. (2006b) 'Mitochondrial alterations of retinal pigment epithelium in age-related macular degeneration', *Neurobiol Aging*, 27(7), pp. 983-93.

Filipczyk, A.A., Laslett, A.L., Mummery, C. and Pera, M.F. (2007) 'Differentiation is coupled to changes in the cell cycle regulatory apparatus of human embryonic stem cells', *Stem Cell Res*, 1(1), pp. 45-60.

Flynn, J.M. and Melov, S. (2013) 'SOD2 in mitochondrial dysfunction and neurodegeneration', *Free Radic Biol Med*, 62, pp. 4-12.

Folmes, C.D., Martinez-Fernandez, A., Perales-Clemente, E., Li, X., McDonald, A., Oglesbee, D., Hrstka, S.C., Perez-Terzic, C., Terzic, A. and Nelson, T.J. (2013) 'Disease-causing mitochondrial heteroplasmy segregated within induced pluripotent stem cell clones derived from a patient with MELAS', *Stem Cells*, 31(7), pp. 1298-308.

Folmes, C.D., Nelson, T.J., Martinez-Fernandez, A., Arrell, D.K., Lindor, J.Z., Dzeja, P.P., Ikeda, Y., Perez-Terzic, C. and Terzic, A. (2011) 'Somatic oxidative bioenergetics transitions into pluripotency-dependent glycolysis to facilitate nuclear reprogramming', *Cell Metab*, 14(2), pp. 264-71.

Forrester, J.V., Dick, A.D., McMenamin, P.G. and Roberts, F. (2008) *The Eye*. Third edn. Saunders Elsevier.

Frantz, G.D., Weimann, J.M., Levin, M.E. and McConnell, S.K. (1994) 'Otx1 and Otx2 define layers and regions in developing cerebral cortex and cerebellum', *J Neurosci*, 14(10), pp. 5725-40.

Fry, M. and Green, D.E. (1981) 'Cardiolipin requirement for electron transfer in complex I and III of the mitochondrial respiratory chain', *J Biol Chem*, 256(4), pp. 1874-80.

Fryer, R.H., Bain, J.M. and De Vivo, D.C. (2016) 'Mitochondrial Encephalomyopathy Lactic Acidosis and Stroke-Like Episodes (MELAS): A Case Report and Critical Reappraisal of Treatment Options', *Pediatr Neurol*, 56, pp. 59-61.

Fujikura, J., Nakao, K., Sone, M., Noguchi, M., Mori, E., Naito, M., Taura, D., Harada-Shiba, M., Kishimoto, I., Watanabe, A., Asaka, I. and Hosoda, K. (2012) 'Induced pluripotent stem cells generated from diabetic patients with mitochondrial DNA A3243G mutation', *Diabetologia*, 55(6), pp. 1689-98.

Fusaki, N., Ban, H., Nishiyama, A., Saeki, K. and Hasegawa, M. (2009) 'Efficient induction of transgene-free human pluripotent stem cells using a vector based on Sendai virus, an RNA virus that does not integrate into the host genome', *Proc Jpn Acad Ser B Phys Biol Sci*, 85(8), pp. 348-62.

Gal, A., Li, Y., Thompson, D.A., Weir, J., Orth, U., Jacobson, S.G., Apfelstedt-Sylla, E. and Vollrath, D. (2000) 'Mutations in MERTK, the human orthologue of the RCS rat retinal dystrophy gene, cause retinitis pigmentosa', *Nat Genet*, 26(3), pp. 270-1.

Garita-Hernandez, M., Diaz-Corrales, F., Lukovic, D., Gonzalez-Guede, I., Diez-Lloret, A., Valdes-Sanchez, M.L., Massalini, S., Erceg, S. and Bhattacharya, S.S. (2013) 'Hypoxia increases the yield of photoreceptors differentiating from mouse embryonic stem cells and improves the modeling of retinogenesis in vitro', *Stem Cells*, 31(5), pp. 966-78.

Gertow, K., Przyborski, S., Loring, J.F., Auerbach, J.M., Epifano, O., Otonkoski, T., Damjanov, I. and Ahrlund-Richter, L. (2007) 'Isolation of human embryonic stem cell-derived teratomas for the assessment of pluripotency', *Curr Protoc Stem Cell Biol*, Chapter 1, p. Unit1B 4.

Ghosh, Z., Wilson, K.D., Wu, Y., Hu, S., Quertermous, T. and Wu, J.C. (2010) 'Persistent donor cell gene expression among human induced pluripotent stem cells contributes to differences with human embryonic stem cells', *PLoS One*, 5(2), p. e8975.

Ghule, P.N., Medina, R., Lengner, C.J., Mandeville, M., Qiao, M., Dominski, Z., Lian, J.B., Stein, J.L., van Wijnen, A.J. and Stein, G.S. (2011) 'Reprogramming the pluripotent cell cycle: restoration of an abbreviated G1 phase in human induced pluripotent stem (iPS) cells', *J Cell Physiol*, 226(5), pp. 1149-56.

Gibbs, D., Kitamoto, J. and Williams, D.S. (2003) 'Abnormal phagocytosis by retinal pigmented epithelium that lacks myosin VIIa, the Usher syndrome 1B protein', *Proc Natl Acad Sci U S A*, 100(11), pp. 6481-6.

Giles, R.E., Blanc, H., Cann, H.M. and Wallace, D.C. (1980) 'Maternal inheritance of human mitochondrial DNA', *Proc Natl Acad Sci U S A*, 77(11), pp. 6715-9.

Giordano, C., Montopoli, M., Perli, E., Orlandi, M., Fantin, M., Ross-Cisneros, F.N., Caparrotta, L., Martinuzzi, A., Ragazzi, E., Ghelli, A., Sadun, A.A., d'Amati, G. and Carelli, V. (2011) 'Oestrogens ameliorate mitochondrial dysfunction in Leber's hereditary optic neuropathy', *Brain*, 134(Pt 1), pp. 220-34.

Gong, J., Fields, M.A., Moreira, E.F., Bowrey, H.E., Gooz, M., Ablonczy, Z. and Del Priore, L.V. (2015) 'Differentiation of Human Protein-Induced Pluripotent Stem Cells toward a Retinal Pigment Epithelial Cell Fate', *PLoS One*, 10(11), p. e0143272.

Gouras, P., Brown, K., Ivert, L. and Neuringer, M. (2011) 'A novel melano-lysosome in the retinal epithelium of rhesus monkeys', *Exp Eye Res*, 93(6), pp. 937-46.

Gouras, P., Ivert, L., Neuringer, M. and Nagasaki, T. (2016) 'Mitochondrial elongation in the macular RPE of aging monkeys, evidence of metabolic stress', *Graefes Arch Clin Exp Ophthalmol*, 254(6), pp. 1221-7.

Gratzner, H.G. (1982) 'Monoclonal antibody to 5-bromo- and 5-iododeoxyuridine: A new reagent for detection of DNA replication', *Science*, 218(4571), pp. 474-5.

Graziewicz, M.A., Day, B.J. and Copeland, W.C. (2002) 'The mitochondrial DNA polymerase as a target of oxidative damage', *Nucleic Acids Res*, 30(13), pp. 2817-24.

Greaves, L.C., Yu-Wai-Man, P., Blakely, E.L., Krishnan, K.J., Beadle, N.E., Kerin, J., Barron, M.J., Griffiths, P.G., Dickinson, A.J., Turnbull, D.M. and Taylor, R.W. (2010) 'Mitochondrial DNA defects and selective extraocular muscle involvement in CPEO', *Invest Ophthalmol Vis Sci*, 51(7), pp. 3340-6.

Griparic, L., van der Wel, N.N., Orozco, I.J., Peters, P.J. and van der Bliek, A.M. (2004) 'Loss of the intermembrane space protein Mgm1/OPA1 induces swelling and localized constrictions along the lengths of mitochondria', *J Biol Chem*, 279(18), pp. 18792-8.

Gronlund, M.A., Honarvar, A.K., Andersson, S., Moslemi, A.R., Oldfors, A., Holme, E., Tulinius, M. and Darin, N. (2010) 'Ophthalmological findings in children and young adults with genetically verified mitochondrial disease', *Br J Ophthalmol*, 94(1), pp. 121-7.

Guillausseau, P.J., Massin, P., Dubois-LaForgue, D., Timsit, J., Virally, M., Gin, H., Bertin, E., Blickle, J.F., Bouhanick, B., Cahen, J., Caillat-Zucman, S., Charpentier, G., Chedin, P., Derrien, C., Ducluzeau, P.H., Grimaldi, A., Guerci, B., Kaloustian, E., Murat, A., Olivier, F., Paques, M., Paquis-Flucklinger, V., Porokhov, B., Samuel-Lajeunesse, J. and Vialettes, B. (2001) 'Maternally inherited diabetes and deafness: a multicenter study', *Ann Intern Med*, 134(9 Pt 1), pp. 721-8.

Gurdon, J.B. (1962) 'The developmental capacity of nuclei taken from intestinal epithelium cells of feeding tadpoles', *J Embryol Exp Morphol*, 10, pp. 622-40.

Hamalainen, R.H., Ahlqvist, K.J., Ellonen, P., Lepisto, M., Logan, A., Otonkoski, T., Murphy, M.P. and Suomalainen, A. (2015) 'mtDNA mutagenesis disrupts pluripotent stem cell function by altering redox signaling', *Cell Rep*, 11(10), pp. 1614-24.

Hamalainen, R.H., Manninen, T., Koivumaki, H., Kislin, M., Otonkoski, T. and Suomalainen, A. (2013) 'Tissue- and cell-type-specific manifestations of heteroplasmic mtDNA 3243A>G mutation in human induced pluripotent stem cell-derived disease model', *Proc Natl Acad Sci U S A*, 110(38), pp. E3622-30.

Hancock, J.T., Desikan, R. and Neill, S.J. (2001) 'Role of reactive oxygen species in cell signalling pathways', *Biochem Soc Trans*, 29(Pt 2), pp. 345-50.

Hatakeyama, H., Katayama, A., Komaki, H., Nishino, I. and Goto, Y. (2015) 'Molecular pathomechanisms and cell-type-specific disease phenotypes of MELAS caused by mutant mitochondrial tRNA(Trp)', *Acta Neuropathol Commun*, 3, p. 52.

Hay, D.C., Sutherland, L., Clark, J. and Burdon, T. (2004) 'Oct-4 knockdown induces similar patterns of endoderm and trophoblast differentiation markers in human and mouse embryonic stem cells', *Stem Cells*, 22(2), pp. 225-35.

Hayasaka, S., Hara, S. and Mizuno, K. (1975) 'Distribution and some properties of cathepsin D in the retinal pigment epithelium', *Exp Eye Res*, 21(4), pp. 307-313.

He, Y., Ge, J., Burke, J.M., Myers, R.L., Dong, Z.Z. and Tombran-Tink, J. (2010) 'Mitochondria impairment correlates with increased sensitivity of aging RPE cells to oxidative stress', *J Ocul Biol Dis Infor*, 3(3), pp. 92-108.

He, Y., Leung, K.W., Ren, Y., Pei, J., Ge, J. and Tombran-Tink, J. (2014) 'PEDF improves mitochondrial function in RPE cells during oxidative stress', *Invest Ophthalmol Vis Sci*, 55(10), pp. 6742-55.

Heytler, P.G. and Prichard, W.W. (1962) 'A new class of uncoupling agents - carbonyl cyanide phenylhydrazones.', *Biochem Biophys Res Commun*, 7(4), pp. 272-275.

Hill, R.E., Favor, J., Hogan, B.L., Ton, C.C., Saunders, G.F., Hanson, I.M., Prosser, J., Jordan, T., Hastie, N.D. and van Heyningen, V. (1991) 'Mouse small eye results from mutations in a paired-like homeobox-containing gene', *Nature*, 354(6354), pp. 522-5.

Hirano, M., Ricci, E., Koenigsberger, M.R., Defendini, R., Pavlakis, S.G., DeVivo, D.C., DiMauro, S. and Rowland, L.P. (1992) 'Melas: an original case and clinical criteria for diagnosis', *Neuromuscul Disord*, 2(2), pp. 125-35.

Hochedlinger, K. and Jaenisch, R. (2002) 'Monoclonal mice generated by nuclear transfer from mature B and T donor cells', *Nature*, 415(6875), pp. 1035-8.

Hockemeyer, D., Soldner, F., Beard, C., Gao, Q., Mitalipova, M., DeKelver, R.C., Katibah, G.E., Amora, R., Boydston, E.A., Zeitler, B., Meng, X., Miller, J.C., Zhang, L., Rebar, E.J., Gregory, P.D., Urnov, F.D. and Jaenisch, R. (2009) 'Efficient targeting of expressed and silent genes in human ESCs and iPSCs using zinc-finger nucleases', *Nat Biotechnol*, 27(9), pp. 851-7.

Hockemeyer, D., Wang, H., Kiani, S., Lai, C.S., Gao, Q., Cassady, J.P., Cost, G.J., Zhang, L., Santiago, Y., Miller, J.C., Zeitler, B., Cherone, J.M., Meng, X., Hinkley, S.J., Rebar, E.J., Gregory, P.D., Urnov, F.D. and Jaenisch, R. (2011) 'Genetic engineering of human pluripotent cells using TALE nucleases', *Nat Biotechnol*, 29(8), pp. 731-4.

Hollenbeck, P.J. and Saxton, W.M. (2005) 'The axonal transport of mitochondria', *J Cell Sci*, 118(Pt 23), pp. 5411-9.

Holliday, E.G., Smith, A.V., Cornes, B.K., Buitendijk, G.H., Jensen, R.A., Sim, X., Aspelund, T., Aung, T., Baird, P.N., Boerwinkle, E., Cheng, C.Y., van Duijn, C.M., Eiriksdottir, G., Gudnason, V., Harris, T., Hewitt, A.W., Inouye, M., Jonasson, F., Klein, B.E., Launer, L., Li, X., Liew, G., Lumley, T., McElduff, P., McKnight, B., Mitchell, P., Psaty, B.M., Rochtchina, E., Rotter, J.I., Scott, R.J., Tay, W., Taylor, K., Teo, Y.Y., Uitterlinden, A.G., Viswanathan, A., Xie, S., Vingerling, J.R., Klaver, C.C., Tai, E.S., Siscovick, D., Klein, R., Cotch, M.F., Wong, T.Y., Attia, J. and Wang, J.J. (2013) 'Insights into the genetic architecture of early stage age-related macular degeneration: a genome-wide association study meta-analysis', *PLoS One*, 8(1), p. e53830.

Holt, I.J., Harding, A.E. and Morgan-Hughes, J.A. (1988) 'Deletions of muscle mitochondrial DNA in patients with mitochondrial myopathies', *Nature*, 331(6158), pp. 717-9.

Hong, S.H., Rampalli, S., Lee, J.B., McNicol, J., Collins, T., Draper, J.S. and Bhatia, M. (2011) 'Cell fate potential of human pluripotent stem cells is encoded by histone modifications', *Cell Stem Cell*, 9(1), pp. 24-36.

Hu, B.Y., Weick, J.P., Yu, J., Ma, L.X., Zhang, X.Q., Thomson, J.A. and Zhang, S.C. (2010) 'Neural differentiation of human induced pluripotent stem cells follows developmental principles but with variable potency', *Proc Natl Acad Sci U S A*, 107(9), pp. 4335-40.

Huangfu, D., Maehr, R., Guo, W., Eijkelenboom, A., Snitow, M., Chen, A.E. and Melton, D.A. (2008a) 'Induction of pluripotent stem cells by defined factors is greatly improved by small-molecule compounds', *Nat Biotechnol*, 26(7), pp. 795-7.

Huangfu, D., Osafune, K., Maehr, R., Guo, W., Eijkelenboom, A., Chen, S., Muhlestein, W. and Melton, D.A. (2008b) 'Induction of pluripotent stem cells from primary human fibroblasts with only Oct4 and Sox2', *Nat Biotechnol*, 26(11), pp. 1269-75.

Hung, S.S., Van Bergen, N.J., Jackson, S., Liang, H., Mackey, D.A., Hernandez, D., Lim, S.Y., Hewitt, A.W., Trounce, I., Pebay, A. and Wong, R.C. (2016) 'Study of mitochondrial respiratory defects on reprogramming to human induced pluripotent stem cells', *Aging (Albany NY).*

Huoponen, K., Vilkki, J., Aula, P., Nikoskelainen, E.K. and Savontaus, M.L. (1991) 'A new mtDNA mutation associated with Leber hereditary optic neuroretinopathy', *Am J Hum Genet*, 48(6), pp. 1147-53.

Hussein, S.M., Batada, N.N., Vuoristo, S., Ching, R.W., Autio, R., Narva, E., Ng, S., Sourour, M., Hamalainen, R., Olsson, C., Lundin, K., Mikkola, M., Trokovic, R., Peitz, M., Brustle, O., Bazett-Jones, D.P., Alitalo, K., Lahesmaa, R., Nagy, A. and Otonkoski, T. (2011) 'Copy number variation and selection during reprogramming to pluripotency', *Nature*, 471(7336), pp. 58-62.

Hyer, J., Mima, T. and Mikawa, T. (1998) 'FGF1 patterns the optic vesicle by directing the placement of the neural retina domain', *Development*, 125(5), pp. 869-77.

Idelson, M., Alper, R., Obolensky, A., Ben-Shushan, E., Hemo, I., Yachimovich-Cohen, N., Khaner, H., Smith, Y., Wiser, O., Gropp, M., Cohen, M.A., Even-Ram, S., Berman-Zaken, Y., Matzrafi, L., Rechavi, G., Banin, E. and Reubinoff, B. (2009) 'Directed differentiation of human embryonic stem cells into functional retinal pigment epithelium cells', *Cell Stem Cell*, 5(4), pp. 396-408.

Insausti, T.C. and Casas, J. (2009) 'Turnover of pigment granules: cyclic catabolism and anabolism of ommochromes within epidermal cells', *Tissue Cell*, 41(6), pp. 421-9.

Ito, S. and Wakamatsu, K. (2008) 'Chemistry of mixed melanogenesis--pivotal roles of dopaquinone', *Photochem Photobiol*, 84(3), pp. 582-92.

Itskovitz-Eldor, J., Schuldiner, M., Karsenti, D., Eden, A., Yanuka, O., Amit, M., Soreq, H. and Benvenisty, N. (2010) 'Differentiation of human embryonic stem cells into embryoid bodies comprising the three embryonic germ layers', *Molecular Medicine*, 6(2), pp. 88-95.

Jackson, E.B. and Brues, A.M. (1941) 'Studies on a transplantable embryoma of the mouse', *Cancer Res*, 1, pp. 494-498.

Jacobson, J., Duchen, M.R. and Heales, S.J. (2002) 'Intracellular distribution of the fluorescent dye nonyl acridine orange responds to the mitochondrial membrane

potential: implications for assays of cardiolipin and mitochondrial mass', *J Neurochem*, 82(2), pp. 224-33.

Jia, F., Wilson, K.D., Sun, N., Gupta, D.M., Huang, M., Li, Z., Panetta, N.J., Chen, Z.Y., Robbins, R.C., Kay, M.A., Longaker, M.T. and Wu, J.C. (2010) 'A nonviral minicircle vector for deriving human iPS cells', *Nat Methods*, 7(3), pp. 197-9.

Jiang, C., Qin, B., Liu, G., Sun, X., Shi, H., Ding, S., Liu, Y., Zhu, M., Chen, X. and Zhao, C. (2016) 'MicroRNA-184 promotes differentiation of the retinal pigment epithelium by targeting the AKT2/mTOR signaling pathway', *Oncotarget*.

Jin, S., Collin, J., Zhu, L., Montaner, D., Armstrong, L., Neganova, I. and Lako, M. (2016) 'A Novel Role for miR-1305 in Regulation of Pluripotency-Differentiation Balance, Cell Cycle, and Apoptosis in Human Pluripotent Stem Cells', *Stem Cells*.

Jo, A., Ham, S., Lee, G.H., Lee, Y.I., Kim, S., Lee, Y.S., Shin, J.H. and Lee, Y. (2015) 'Efficient Mitochondrial Genome Editing by CRISPR/Cas9', *Biomed Res Int*, 2015, p. 305716.

Johns, D.R., Neufeld, M.J. and Park, R.D. (1992) 'An ND-6 mitochondrial DNA mutation associated with Leber hereditary optic neuropathy', *Biochem Biophys Res Commun*, 187(3), pp. 1551-7.

Jones, M., Mitchell, P., Wang, J.J. and Sue, C. (2004) 'MELAS A3243G mitochondrial DNA mutation and age related maculopathy', *Am J Ophthalmol*, 138(6), pp. 1051-3.

Joshi, R., Mankowski, W., Winter, M., Saini, J.S., Blenkinsop, T.A., Stern, J.H., Temple, S. and Cohen, A.R. (2016) 'Automated Measurement of Cobblestone Morphology for Characterizing Stem Cell Derived Retinal Pigment Epithelial Cell Cultures', *J Ocul Pharmacol Ther*, 32(5), pp. 331-9.

Judson, R.L., Babiarz, J.E., Venere, M. and Blelloch, R. (2009) 'Embryonic stem cell-specific microRNAs promote induced pluripotency', *Nat Biotechnol*, 27(5), pp. 459-61.

Justilien, V., Pang, J.J., Renganathan, K., Zhan, X., Crabb, J.W., Kim, S.R., Sparrow, J.R., Hauswirth, W.W. and Lewin, A.S. (2007) 'SOD2 knockdown mouse model of early AMD', *Invest Ophthalmol Vis Sci*, 48(10), pp. 4407-20.

Juuti-Uusitalo, K., Delporte, C., Gregoire, F., Perret, J., Huhtala, H., Savolainen, V., Nymark, S., Hyttinen, J., Uusitalo, H., Willermain, F. and Skottman, H. (2013) 'Aquaporin expression and function in human pluripotent stem cell-derived retinal pigmented epithelial cells', *Invest Ophthalmol Vis Sci*, 54(5), pp. 3510-9.

Kaarniranta, K., Sinha, D., Blasiak, J., Kauppinen, A., Vereb, Z., Salminen, A., Boulton, M.E. and Petrovski, G. (2013) 'Autophagy and heterophagy dysregulation leads to retinal pigment epithelium dysfunction and development of age-related macular degeneration', *Autophagy*, 9(7), pp. 973-84.

Kadowaki, T., Kadowaki, H., Mori, Y., Tobe, K., Sakuta, R., Suzuki, Y., Tanabe, Y., Sakura, H., Awata, T., Goto, Y. and et al. (1994) 'A subtype of diabetes mellitus associated with a mutation of mitochondrial DNA', *N Engl J Med*, 330(14), pp. 962-8.

Kajiwara, M., Aoi, T., Okita, K., Takahashi, R., Inoue, H., Takayama, N., Endo, H., Eto, K., Toguchida, J., Uemoto, S. and Yamanaka, S. (2012) 'Donor-dependent variations in hepatic differentiation from human-induced pluripotent stem cells', *Proc Natl Acad Sci U S A*, 109(31), pp. 12538-43.

Kamao, H., Mandai, M., Wakamiya, S., Ishida, J., Goto, K., Ono, T., Suda, T., Takahashi, M. and Kiryu, J. (2014) 'Objective evaluation of the degree of pigmentation in human induced pluripotent stem cell-derived RPE', *Invest Ophthalmol Vis Sci*, 55(12), pp. 8309-18.

Kannagi, R., Cochran, N.A., Ishigami, F., Hakomori, S., Andrews, P.W., Knowles, B.B. and Solter, D. (1983) 'Stage-specific embryonic antigens (SSEA-3 and -4) are epitopes of a unique globo-series ganglioside isolated from human teratocarcinoma cells', *EMBO J*, 2(12), pp. 2355-61.

Kaufmann, P., Koga, Y., Shanske, S., Hirano, M., DiMauro, S., King, M.P. and Schon, E.A. (1996) 'Mitochondrial DNA and RNA processing in MELAS', *Ann Neurol*, 40(2), pp. 172-80.

Kelly, R.D., Sumer, H., McKenzie, M., Facucho-Oliveira, J., Trounce, I.A., Verma, P.J. and St John, J.C. (2013) 'The effects of nuclear reprogramming on mitochondrial DNA replication', *Stem Cell Rev*, 9(1), pp. 1-15.

Kevany, B.M. and Palczewski, K. (2010) 'Phagocytosis of retinal rod and cone photoreceptors', *Physiology (Bethesda)*, 25(1), pp. 8-15.

Khan, J.C., Thurlby, D.A., Shahid, H., Clayton, D.G., Yates, J.R., Bradley, M., Moore, A.T., Bird, A.C. and Genetic Factors in, A.M.D.S. (2006) 'Smoking and age related macular degeneration: the number of pack years of cigarette smoking is a major determinant of risk for both geographic atrophy and choroidal neovascularisation', *Br J Ophthalmol*, 90(1), pp. 75-80.

Khondrion (2014). Available at: http://www.khondrion.com (Accessed: 06.09.).

Kim, D., Kim, C.H., Moon, J.I., Chung, Y.G., Chang, M.Y., Han, B.S., Ko, S., Yang, E., Cha, K.Y., Lanza, R. and Kim, K.S. (2009) 'Generation of human induced pluripotent stem cells by direct delivery of reprogramming proteins', *Cell Stem Cell*, 4(6), pp. 472-6.

Kimbrel, E.A. and Lanza, R. (2015) 'Current status of pluripotent stem cells: moving the first therapies to the clinic', *Nat Rev Drug Discov*, 14(10), pp. 681-92.

Kirby, D.M., Rennie, K.J., Smulders-Srinivasan, T.K., Acin-Perez, R., Whittington, M., Enriquez, J.A., Trevelyan, A.J., Turnbull, D.M. and Lightowlers, R.N. (2009) 'Transmitochondrial embryonic stem cells containing pathogenic mtDNA mutations are compromised in neuronal differentiation', *Cell Prolif*, 42(4), pp. 413-24.

Kirino, Y. and Suzuki, T. (2005) 'Human mitochondrial diseases associated with tRNA wobble modification deficiency', *RNA Biol*, 2(2), pp. 41-4.

Kirino, Y., Yasukawa, T., Ohta, S., Akira, S., Ishihara, K., Watanabe, K. and Suzuki, T. (2004) 'Codon-specific translational defect caused by a wobble modification deficiency in mutant tRNA from a human mitochondrial disease', *Proc Natl Acad Sci U S A*, 101(42), pp. 15070-5.

Klimanskaya, I., Hipp, J., Rezai, K.A., West, M., Atala, A. and Lanza, R. (2004) 'Derivation and comparative assessment of retinal pigment epithelium from human embryonic stem cells using transcriptomics', *Cloning Stem Cells*, 6(3), pp. 217-45.

Kobayashi, T., Urabe, K., Orlow, S.J., Higashi, K., Imokawa, G., Kwon, B.S., Potterf, B. and Hearing, V.J. (1994) 'The Pmel 17/silver locus protein. Characterization and investigation of its melanogenic function', *J Biol Chem*, 269(46), pp. 29198-205.

Kodaira, M., Hatakeyama, H., Yuasa, S., Seki, T., Egashira, T., Tohyama, S., Kuroda, Y., Tanaka, A., Okata, S., Hashimoto, H., Kusumoto, D., Kunitomi, A., Takei,

M., Kashimura, S., Suzuki, T., Yozu, G., Shimojima, M., Motoda, C., Hayashiji, N., Saito, Y., Goto, Y. and Fukuda, K. (2015) 'Impaired respiratory function in MELAS-induced pluripotent stem cells with high heteroplasmy levels', *FEBS Open Bio*, 5, pp. 219-25.

Kokkinaki, M., Sahibzada, N. and Golestaneh, N. (2011) 'Human induced pluripotent stem-derived retinal pigment epithelium (RPE) cells exhibit ion transport, membrane potential, polarized vascular endothelial growth factor secretion, and gene expression pattern similar to native RPE', *Stem Cells*, 29(5), pp. 825-35.

Kolb, H. (2012) 'Gross anatomy of the eye', *Webvision*.

Kuroya, M. and Ishida, N. (1953) 'Newborn virus pneumonitis (type Sendai). II. The isolation of a new virus possessing hemagglutinin activity', *Yokohama Med Bull*, 4(4), pp. 217-33.

Lamba, D.A., Karl, M.O., Ware, C.B. and Reh, T.A. (2006) 'Efficient generation of retinal progenitor cells from human embryonic stem cells', *Proc Natl Acad Sci U S A*, 103(34), pp. 12769-74.

Lane, A., Philip, L.R., Ruban, L., Fynes, K., Smart, M., Carr, A., Mason, C. and Coffey, P. (2014) 'Engineering efficient retinal pigment epithelium differentiation from human pluripotent stem cells', *Stem Cells Translational Medicine*, 3(11), pp. 1295-304.

Lascaratos, G., Ji, D., Wood, J.P. and Osborne, N.N. (2007) 'Visible light affects mitochondrial function and induces neuronal death in retinal cell cultures', *Vision Res*, 47(9), pp. 1191-201.

Latkany, P., Ciulla, T.A., Cacchillo, P.F. and Malkoff, M.D. (1999) 'Mitochondrial maculopathy: geographic atrophy of the macula in the MELAS associated A to G 3243 mitochondrial DNA point mutation', *Am J Ophthalmol*, 128(1), pp. 112-4.

Latvala, T., Mustonen, E., Uusitalo, R. and Majamaa, K. (2002) 'Pigmentary retinopathy in patients with the MELAS mutation 3243A-->G in mitochondrial DNA', *Graefes Arch Clin Exp Ophthalmol*, 240(10), pp. 795-801.

Laurent, L.C., Ulitsky, I., Slavin, I., Tran, H., Schork, A., Morey, R., Lynch, C., Harness, J.V., Lee, S., Barrero, M.J., Ku, S., Martynova, M., Semechkin, R., Galat, V., Gottesfeld, J., Izpisua Belmonte, J.C., Murry, C., Keirstead, H.S., Park, H.S., Schmidt, U., Laslett, A.L., Muller, F.J., Nievergelt, C.M., Shamir, R. and Loring, J.F. (2011) 'Dynamic changes in the copy number of pluripotency and cell proliferation genes in human ESCs and iPSCs during reprogramming and time in culture', *Cell Stem Cell*, 8(1), pp. 106-18.

Lazebnik, Y.A., Kaufmann, S.H., Desnoyers, S., Poirier, G.G. and Earnshaw, W.C. (1994) 'Cleavage of poly(ADP-ribose) polymerase by a proteinase with properties like ICE', *Nature*, 371(6495), pp. 346-7.

Leach, L.L., Buchholz, D.E., Nadar, V.P., Lowenstein, S.E. and Clegg, D.O. (2015) 'Canonical/beta-catenin Wnt pathway activation improves retinal pigmented epithelium derivation from human embryonic stem cells', *Invest Ophthalmol Vis Sci*, 56(2), pp. 1002-13.

Lee, B., Song, H., Rizzoti, K., Son, Y., Yoon, J., Baek, K. and Jeong, Y. (2013) 'Genomic code for Sox2 binding uncovers its regulatory role in Six3 activation in the forebrain', *Dev Biol*, 381(2), pp. 491-501.

Lefort, N., Feyeux, M., Bas, C., Feraud, O., Bennaceur-Griscelli, A., Tachdjian, G., Peschanski, M. and Perrier, A.L. (2008) 'Human embryonic stem cells reveal recurrent genomic instability at 20q11.21', *Nat Biotechnol*, 26(12), pp. 1364-6.

Legros, F., Lombes, A., Frachon, P. and Rojo, M. (2002) 'Mitochondrial fusion in human cells is efficient, requires the inner membrane potential, and is mediated by mitofusins', *Mol Biol Cell*, 13(12), pp. 4343-54.

Li, H.O., Zhu, Y.F., Asakawa, M., Kuma, H., Hirata, T., Ueda, Y., Lee, Y.S., Fukumura, M., Iida, A., Kato, A., Nagai, Y. and Hasegawa, M. (2000) 'A cytoplasmic RNA vector derived from nontransmissible Sendai virus with efficient gene transfer and expression', *J Virol*, 74(14), pp. 6564-9.

Li, P., Sun, X., Ma, Z., Liu, Y., Jin, Y., Ge, R., Hao, L., Ma, Y., Han, S., Sun, H., Zhang, M., Li, R., Li, T. and Shen, L. (2016) 'Transcriptional Reactivation of OTX2, RX1 and SIX3 during Reprogramming Contributes to the Generation of RPE Cells from Human iPSCs', *Int J Biol Sci*, 12(5), pp. 505-17.

Li, R., Liang, J., Ni, S., Zhou, T., Qing, X., Li, H., He, W., Chen, J., Li, F., Zhuang, Q., Qin, B., Xu, J., Li, W., Yang, J., Gan, Y., Qin, D., Feng, S., Song, H., Yang, D., Zhang, B., Zeng, L., Lai, L., Esteban, M.A. and Pei, D. (2010) 'A mesenchymal-to-epithelial transition initiates and is required for the nuclear reprogramming of mouse fibroblasts', *Cell Stem Cell*, 7(1), pp. 51-63.

Li, Y., Shen, Z., Shelat, H. and Geng, Y.J. (2013) 'Reprogramming somatic cells to pluripotency: A fresh look at Yamanaka's model', *Cell Cycle*, 12(23), pp. 3594-8.

Liang, F.Q. and Godley, B.F. (2003) 'Oxidative stress-induced mitochondrial DNA damage in human retinal pigment epithelial cells: a possible mechanism for RPE aging and age-related macular degeneration', *Exp Eye Res*, 76(4), pp. 397-403.

Liang, G. and Zhang, Y. (2013) 'Genetic and epigenetic variations in iPSCs: potential causes and implications for application', *Cell Stem Cell*, 13(2), pp. 149-59.

Liao, J.L., Yu, J., Huang, K., Hu, J., Diemer, T., Ma, Z., Dvash, T., Yang, X.J., Travis, G.H., Williams, D.S., Bok, D. and Fan, G. (2010) 'Molecular signature of primary retinal pigment epithelium and stem-cell-derived RPE cells', *Hum Mol Genet*, 19(21), pp. 4229-38.

Lin, J., Zhao, C.B., Lu, J.H., Wang, H.J., Zhu, W.H., Xi, J.Y., Lu, J., Luo, S.S., Ma, D., Wang, Y., Xiao, B.G. and Lu, C.Z. (2014) 'Novel mutations m.3959G>A and m.3995A>G in mitochondrial gene MT-ND1 associated with MELAS', *Mitochondrial DNA*, 25(1), pp. 56-62.

Lopes, C. and Rego, A.C. (2016) 'Revisiting Mitochondrial Function and Metabolism in Pluripotent Stem Cells: Where Do We Stand in Neurological Diseases?', *Mol Neurobiol*.

Lu, B., Malcuit, C., Wang, S., Girman, S., Francis, P., Lemieux, L., Lanza, R. and Lund, R. (2009) 'Long-term safety and function of RPE from human embryonic stem cells in preclinical models of macular degeneration', *Stem Cells*, 27(9), pp. 2126-35.

Ma, H., Folmes, C.D., Wu, J., Morey, R., Mora-Castilla, S., Ocampo, A., Ma, L., Poulton, J., Wang, X., Ahmed, R., Kang, E., Lee, Y., Hayama, T., Li, Y., Van Dyken, C., Gutierrez, N.M., Tippner-Hedges, R., Koski, A., Mitalipov, N., Amato, P., Wolf, D.P., Huang, T., Terzic, A., Laurent, L.C., Izpisua Belmonte, J.C. and Mitalipov, S. (2015) 'Metabolic rescue in pluripotent cells from patients with mtDNA disease', *Nature*, 524(7564), pp. 234-8.

Mahmoudi, S. and Brunet, A. (2012) 'Aging and reprogramming: a two-way street', *Curr Opin Cell Biol*, 24(6), pp. 744-56.

Majamaa, K., Moilanen, J.S., Uimonen, S., Remes, A.M., Salmela, P.I., Karppa, M., Majamaa-Voltti, K.A., Rusanen, H., Sorri, M., Peuhkurinen, K.J. and Hassinen, I.E. (1998) 'Epidemiology of A3243G, the mutation for mitochondrial encephalomyopathy, lactic acidosis, and strokelike episodes: prevalence of the mutation in an adult population', *American Journal of Human Genetics*, 63(2), pp. 447-54.

Mancuso, M., Orsucci, D., Angelini, C., Bertini, E., Carelli, V., Comi, G.P., Donati, A., Minetti, C., Moggio, M., Mongini, T., Servidei, S., Tonin, P., Toscano, A., Uziel, G., Bruno, C., Ienco, E.C., Filosto, M., Lamperti, C., Catteruccia, M., Moroni, I., Musumeci, O., Pegoraro, E., Ronchi, D., Santorelli, F.M., Sauchelli, D., Scarpelli, M., Sciacco, M., Valentino, M.L., Vercelli, L., Zeviani, M. and Siciliano, G. (2014) 'The m.3243A>G mitochondrial DNA mutation and related phenotypes. A matter of gender?', *J Neurol*, 261(3), pp. 504-10.

Martin, G.R. (1981) 'Isolation of a pluripotent cell line from early mouse embryos cultured in medium conditioned by teratocarcinoma stem cells', *Proc Natl Acad Sci U S A*, 78(12), pp. 7634-8.

Martin, M.J., Muotri, A., Gage, F. and Varki, A. (2005) 'Human embryonic stem cells express an immunogenic nonhuman sialic acid', *Nat Med*, 11(2), pp. 228-32.

Maruotti, J., Sripathi, S.R., Bharti, K., Fuller, J., Wahlin, K.J., Ranganathan, V., Sluch, V.M., Berlinicke, C.A., Davis, J., Kim, C., Zhao, L., Wan, J., Qian, J., Corneo, B., Temple, S., Dubey, R., Olenyuk, B.Z., Bhutto, I., Lutty, G.A. and Zack, D.J. (2015) 'Small-molecule-directed, efficient generation of retinal pigment epithelium from human pluripotent stem cells', *Proc Natl Acad Sci U S A*, 112(35), pp. 10950-5.

Mathers, P.H., Grinberg, A., Mahon, K.A. and Jamrich, M. (1997) 'The Rx homeobox gene is essential for vertebrate eye development', *Nature*, 387(6633), pp. 603-7.

Matin, M.M., Walsh, J.R., Gokhale, P.J., Draper, J.S., Bahrami, A.R., Morton, I., Moore, H.D. and Andrews, P.W. (2004) 'Specific knockdown of Oct4 and beta2-microglobulin expression by RNA interference in human embryonic stem cells and embryonic carcinoma cells', *Stem Cells*, 22(5), pp. 659-68.

Mayshar, Y., Ben-David, U., Lavon, N., Biancotti, J.C., Yakir, B., Clark, A.T., Plath, K., Lowry, W.E. and Benvenisty, N. (2010) 'Identification and classification of chromosomal aberrations in human induced pluripotent stem cells', *Cell Stem Cell*, 7(4), pp. 521-31.

McBride, H.M., Neuspiel, M. and Wasiak, S. (2006) 'Mitochondria: more than just a powerhouse', *Curr Biol*, 16(14), pp. R551-60.

McFarland, R., Taylor, R.W. and Turnbull, D.M. (2002) 'The neurology of mitochondrial DNA disease', *Lancet Neurol*, 1(6), pp. 343-51.

Mellough, C.B., Collin, J., Khazim, M., White, K., Sernagor, E., Steel, D.H. and Lako, M. (2015) 'IGF-1 signaling plays an important role in the formation of three-dimensional laminated neural retina and other ocular structures from human embryonic stem cells', *Stem Cells*, 33(8), pp. 2416-30.

Mellough, C.B., Sernagor, E., Moreno-Gimeno, I., Steel, D.H. and Lako, M. (2012) 'Efficient stage-specific differentiation of human pluripotent stem cells toward retinal photoreceptor cells', *Stem Cells*, 30(4), pp. 673-86.

Meyer, J.S., Howden, S.E., Wallace, K.A., Verhoeven, A.D., Wright, L.S., Capowski, E.E., Pinilla, I., Martin, J.M., Tian, S., Stewart, R., Pattnaik, B., Thomson, J.A. and

Gamm, D.M. (2011) 'Optic vesicle-like structures derived from human pluripotent stem cells facilitate a customized approach to retinal disease treatment', *Stem Cells*, 29(8), pp. 1206-18.

Meyer, J.S., Shearer, R.L., Capowski, E.E., Wright, L.S., Wallace, K.A., McMillan, E.L., Zhang, S.C. and Gamm, D.M. (2009) 'Modeling early retinal development with human embryonic and induced pluripotent stem cells', *Proc Natl Acad Sci U S A*, 106(39), pp. 16698-703.

Mikkelsen, T.S., Hanna, J., Zhang, X., Ku, M., Wernig, M., Schorderet, P., Bernstein, B.E., Jaenisch, R., Lander, E.S. and Meissner, A. (2008) 'Dissecting direct reprogramming through integrative genomic analysis', *Nature*, 454(7200), pp. 49-55.

Mitalipova, M.M., Rao, R.R., Hoyer, D.M., Johnson, J.A., Meisner, L.F., Jones, K.L., Dalton, S. and Stice, S.L. (2005) 'Preserving the genetic integrity of human embryonic stem cells', *Nat Biotechnol*, 23(1), pp. 19-20.

Mitsui, K., Tokuzawa, Y., Itoh, H., Segawa, K., Murakami, M., Takahashi, K., Maruyama, M., Maeda, M. and Yamanaka, S. (2003) 'The homeoprotein Nanog is required for maintenance of pluripotency in mouse epiblast and ES cells', *Cell*, 113(5), pp. 631-42.

Miyagishima, K.J., Wan, Q., Corneo, B., Sharma, R., Lotfi, M.R., Boles, N.C., Hua, F., Maminishkis, A., Zhang, C., Blenkinsop, T., Khristov, V., Jha, B.S., Memon, O.S., D'Souza, S., Temple, S., Miller, S.S. and Bharti, K. (2016) 'In Pursuit of Authenticity: Induced Pluripotent Stem Cell-Derived Retinal Pigment Epithelium for Clinical Applications', *Stem Cells Transl Med*.

Momcilovic, O., Navara, C. and Schatten, G. (2011) 'Cell cycle adaptations and maintenance of genomic integrity in embryonic stem cells and induced pluripotent stem cells', *Results Probl Cell Differ*, 53, pp. 415-58.

Moraes, C.T., Ciacci, F., Silvestri, G., Shanske, S., Sciacco, M., Hirano, M., Schon, E.A., Bonilla, E. and DiMauro, S. (1993) 'Atypical clinical presentations associated with the MELAS mutation at position 3243 of human mitochondrial DNA', *Neuromuscul Disord*, 3(1), pp. 43-50.

Moustakas, A. and Heldin, C.H. (2009) 'The regulation of TGFbeta signal transduction', *Development*, 136(22), pp. 3699-714.

Mullen, R.J. and LaVail, M.M. (1976) 'Inherited retinal dystrophy: primary defect in pigment epithelium determined with experimental rat chimeras', *Science*, 192(4241), pp. 799-801.

Muller, F.J., Goldmann, J., Loser, P. and Loring, J.F. (2010) 'A call to standardize teratoma assays used to define human pluripotent cell lines', *Cell Stem Cell*, 6(5), pp. 412-4.

Munoz-Sanjuan, I. and Brivanlou, A.H. (2002) 'Neural induction, the default model and embryonic stem cells', *Nat Rev Neurosci*, 3(4), pp. 271-80.

Murphy, R., Turnbull, D.M., Walker, M. and Hattersley, A.T. (2008) 'Clinical features, diagnosis and management of maternally inherited diabetes and deafness (MIDD) associated with the 3243A>G mitochondrial point mutation', *Diabet Med*, 25(4), pp. 383-99.

Nakano, T., Ando, S., Takata, N., Kawada, M., Muguruma, K., Sekiguchi, K., Saito, K., Yonemura, S., Eiraku, M. and Sasai, Y. (2012) 'Self-formation of optic cups and storable stratified neural retina from human ESCs', *Cell Stem Cell*, 10(6), pp. 771-85.

Narsinh, K.H., Jia, F., Robbins, R.C., Kay, M.A., Longaker, M.T. and Wu, J.C. (2011) 'Generation of adult human induced pluripotent stem cells using nonviral minicircle DNA vectors', *Nat Protoc*, 6(1), pp. 78-88.

Neganova, I., Shmeleva, E., Munkley, J., Chichagova, V., Anyfantis, G., Anderson, R., Passos, J., Elliott, D.J., Armstrong, L. and Lako, M. (2016) 'JNK/SAPK signaling is essential for efficient reprogramming of human fibroblasts to induced pluripotent stem cells', *Stem Cells*, 34(5), pp. 1198-212.

Neganova, I., Zhang, X., Atkinson, S. and Lako, M. (2009) 'Expression and functional analysis of G1 to S regulatory components reveals an important role for CDK2 in cell cycle regulation in human embryonic stem cells', *Oncogene*, **28**(1), pp. 20-30.

Nguyen, M. and Arnheiter, H. (2000) 'Signaling and transcriptional regulation in early mammalian eye development: a link between FGF and MITF', *Development*, 127(16), pp. 3581-91.

Nichols, J. and Smith, A. (2009) 'Naive and primed pluripotent states', *Cell Stem Cell*, 4(6), pp. 487-92.

Nichols, J., Zevnik, B., Anastassiadis, K., Niwa, H., Klewe-Nebenius, D., Chambers, I., Scholer, H. and Smith, A. (1998) 'Formation of pluripotent stem cells in the mammalian embryo depends on the POU transcription factor Oct4', *Cell*, 95(3), pp. 379-91.

Nishishita, N., Shikamura, M., Takenaka, C., Takada, N., Fusaki, N. and Kawamata, S. (2012) 'Generation of virus-free induced pluripotent stem cell clones on a synthetic matrix via a single cell subcloning in the naive state', *PLoS One*, 7(6), p. e38389.

Nunnari, J., Marshall, W.F., Straight, A., Murray, A., Sedat, J.W. and Walter, P. (1997) 'Mitochondrial transmission during mating in Saccharomyces cerevisiae is determined by mitochondrial fusion and fission and the intramitochondrial segregation of mitochondrial DNA', *Mol Biol Cell*, 8(7), pp. 1233-42.

Okamoto, K., Okazawa, H., Okuda, A., Sakai, M., Muramatsu, M. and Hamada, H. (1990) 'A novel octamer binding transcription factor is differentially expressed in mouse embryonic cells', *Cell*, 60(3), pp. 461-72.

Okita, K., Matsumura, Y., Sato, Y., Okada, A., Morizane, A., Okamoto, S., Hong, H., Nakagawa, M., Tanabe, K., Tezuka, K., Shibata, T., Kunisada, T., Takahashi, M., Takahashi, J., Saji, H. and Yamanaka, S. (2011) 'A more efficient method to generate integration-free human iPS cells', *Nat Methods*, 8(5), pp. 409-12.

Okita, K., Yamakawa, T., Matsumura, Y., Sato, Y., Amano, N., Watanabe, A., Goshima, N. and Yamanaka, S. (2013) 'An efficient nonviral method to generate integration-free human-induced pluripotent stem cells from cord blood and peripheral blood cells', *Stem Cells*, 31(3), pp. 458-66.

Onder, T.T., Kara, N., Cherry, A., Sinha, A.U., Zhu, N., Bernt, K.M., Cahan, P., Marcarci, B.O., Unternaehrer, J., Gupta, P.B., Lander, E.S., Armstrong, S.A. and Daley, G.Q. (2012) 'Chromatin-modifying enzymes as modulators of reprogramming', *Nature*, 483(7391), pp. 598-602.

Osakada, F., Ikeda, H., Mandai, M., Wataya, T., Watanabe, K., Yoshimura, N., Akaike, A., Sasai, Y. and Takahashi, M. (2008) 'Toward the generation of rod and cone photoreceptors from mouse, monkey and human embryonic stem cells', *Nat Biotechnol*, 26(2), pp. 215-24.

Osakada, F., Jin, Z.B., Hirami, Y., Ikeda, H., Danjyo, T., Watanabe, K., Sasai, Y. and Takahashi, M. (2009) 'In vitro differentiation of retinal cells from human pluripotent stem cells by small-molecule induction', *J Cell Sci*, 122(Pt 17), pp. 3169-79.

Osborne, N.N., Kamalden, T.A., Majid, A.S., del Olmo-Aguado, S., Manso, A.G. and Ji, D. (2010) 'Light effects on mitochondrial photosensitizers in relation to retinal degeneration', *Neurochem Res*, 35(12), pp. 2027-34.

Owen, C.G., Fletcher, A.E., Donoghue, M. and Rudnicka, A.R. (2003) 'How big is the burden of visual loss caused by age related macular degeneration in the United Kingdom?', *Br J Ophthalmol*, 87(3), pp. 312-7.

Ozair, M.Z., Noggle, S., Warmflash, A., Krzyspiak, J.E. and Brivanlou, A.H. (2013) 'SMAD7 directly converts human embryonic stem cells to telencephalic fate by a default mechanism', *Stem Cells*, 31(1), pp. 35-47.

Pankratz, M.T., Li, X.J., Lavaute, T.M., Lyons, E.A., Chen, X. and Zhang, S.C. (2007) 'Directed neural differentiation of human embryonic stem cells via an obligated primitive anterior stage', *Stem Cells*, 25(6), pp. 1511-20.

Panopoulos, A.D., Yanes, O., Ruiz, S., Kida, Y.S., Diep, D., Tautenhahn, R., Herrerias, A., Batchelder, E.M., Plongthongkum, N., Lutz, M., Berggren, W.T., Zhang, K., Evans, R.M., Siuzdak, G. and Izpisua Belmonte, J.C. (2012) 'The metabolome of induced pluripotent stem cells reveals metabolic changes occurring in somatic cell reprogramming', *Cell Res*, 22(1), pp. 168-77.

Pardee, A.B. (1974) 'A restriction point for control of normal animal cell proliferation', *Proc Natl Acad Sci U S A*, 71(4), pp. 1286-90.

Park, H.J., Shin, J., Kim, J. and Cho, S.W. (2013) 'Nonviral delivery for reprogramming to pluripotency and differentiation', *Arch Pharm Res*, 37(1), pp. 107-19.

Pavlakis, S.G., Phillips, P.C., DiMauro, S., De Vivo, D.C. and Rowland, L.P. (1984) 'Mitochondrial myopathy, encephalopathy, lactic acidosis, and strokelike episodes: a distinctive clinical syndrome', *Ann Neurol*, 16(4), pp. 481-8.

Pennesi, M.E., Neuringer, M. and Courtney, R.J. (2012) 'Animal models of age related macular degeneration', *Mol Aspects Med*, 33(4), pp. 487-509.

Perry, S.W., Norman, J.P., Barbieri, J., Brown, E.B. and Gelbard, H.A. (2011) 'Mitochondrial membrane potential probes and the proton gradient: a practical usage guide', *Biotechniques*, 50(2), pp. 98-115.

Petit, J.M., Maftah, A., Ratinaud, M.H. and Julien, R. (1992) '10N-nonyl acridine orange interacts with cardiolipin and allows the quantification of this phospholipid in isolated mitochondria', *Eur J Biochem*, 209(1), pp. 267-73.

Petit, P.X., Lecoeur, H., Zorn, E., Dauguet, C., Mignotte, B. and Gougeon, M.L. (1995) 'Alterations in mitochondrial structure and function are early events of dexamethasone-induced thymocyte apoptosis', *J Cell Biol*, 130(1), pp. 157-67.

Phillips, P.H. and Newman, N.J. (1997) 'Mitochondrial diseases in pediatric ophthalmology', *Journal of AAPOS*, 1(2), pp. 115-22.

Picard, M., Zhang, J., Hancock, S., Derbeneva, O., Golhar, R., Golik, P., O'Hearn, S., Levy, S., Potluri, P., Lvova, M., Davila, A., Lin, C.S., Perin, J.C., Rappaport, E.F., Hakonarson, H., Trounce, I.A., Procaccio, V. and Wallace, D.C. (2014) 'Progressive increase in mtDNA 3243A>G heteroplasmy causes abrupt transcriptional reprogramming', *Proc Natl Acad Sci U S A*, 111(38), pp. E4033-42.

Pittack, C., Jones, M. and Reh, T.A. (1991) 'Basic fibroblast growth factor induces retinal pigment epithelium to generate neural retina in vitro', *Development*, 113(2), pp. 577-88.

Plaza Reyes, A., Petrus-Reurer, S., Antonsson, L., Stenfelt, S., Bartuma, H., Panula, S., Mader, T., Douagi, I., Andre, H., Hovatta, O., Lanner, F. and Kvanta, A. (2016) 'Xeno-Free and Defined Human Embryonic Stem Cell-Derived Retinal Pigment Epithelial Cells Functionally Integrate in a Large-Eyed Preclinical Model', *Stem Cell Reports*, 6(1), pp. 9-17.

Polo, J.M., Anderssen, E., Walsh, R.M., Schwarz, B.A., Nefzger, C.M., Lim, S.M., Borkent, M., Apostolou, E., Alaei, S., Cloutier, J., Bar-Nur, O., Cheloufi, S., Stadtfeld, M., Figueroa, M.E., Robinton, D., Natesan, S., Melnick, A., Zhu, J., Ramaswamy, S. and Hochedlinger, K. (2012) 'A molecular roadmap of reprogramming somatic cells into iPS cells', *Cell*, 151(7), pp. 1617-32.

Porter, F.D., Drago, J., Xu, Y., Cheema, S.S., Wassif, C., Huang, S.P., Lee, E., Grinberg, A., Massalas, J.S., Bodine, D., Alt, F. and Westphal, H. (1997) 'Lhx2, a LIM homeobox gene, is required for eye, forebrain, and definitive erythrocyte development', *Development*, 124(15), pp. 2935-44.

Pozarowski, P. and Darzynkiewicz, Z. (2004) 'Analysis of cell cycle by flow cytometry', *Methods Mol Biol*, 281, pp. 301-11.

Preynat-Seauve, O., de Rham, C., Tirefort, D., Ferrari-Lacraz, S., Krause, K.H. and Villard, J. (2009) 'Neural progenitors derived from human embryonic stem cells are targeted by allogeneic T and natural killer cells', *J Cell Mol Med*, 13(9B), pp. 3556-69.

Prigione, A., Lichtner, B., Kuhl, H., Struys, E.A., Wamelink, M., Lehrach, H., Ralser, M., Timmermann, B. and Adjaye, J. (2011) 'Human induced pluripotent stem cells harbor homoplasmic and heteroplasmic mitochondrial DNA mutations while maintaining human embryonic stem cell-like metabolic reprogramming', *Stem Cells*, 29(9), pp. 1338-48.

Pyle, A., Taylor, R.W., Durham, S.E., Deschauer, M., Schaefer, A.M., Samuels, D.C. and Chinnery, P.F. (2007) 'Depletion of mitochondrial DNA in leucocytes harbouring the 3243A->G mtDNA mutation', *J Med Genet*, 44(1), pp. 69-74.

Ramsden, C.M., Powner, M.B., Carr, A.J., Smart, M.J., da Cruz, L. and Coffey, P.J. (2013) 'Stem cells in retinal regeneration: past, present and future', *Development*, 140(12), pp. 2576-85.

Rath, P.P., Jenkins, S., Michaelides, M., Smith, A., Sweeney, M.G., Davis, M.B., Fitzke, F.W. and Bird, A.C. (2008) 'Characterisation of the macular dystrophy in patients with the A3243G mitochondrial DNA point mutation with fundus autofluorescence', *British Journal of Ophthalmology*, 92(5), pp. 623-629.

Ray, P.D., Huang, B.W. and Tsuji, Y. (2012) 'Reactive oxygen species (ROS) homeostasis and redox regulation in cellular signaling', *Cell Signal*, 24(5), pp. 981-90.

Reddy, P., Ocampo, A., Suzuki, K., Luo, J., Bacman, S.R., Williams, S.L., Sugawara, A., Okamura, D., Tsunekawa, Y., Wu, J., Lam, D., Xiong, X., Montserrat, N., Esteban, C.R., Liu, G.H., Sancho-Martinez, I., Manau, D., Civico, S., Cardellach, F., Del Mar O'Callaghan, M., Campistol, J., Zhao, H., Campistol, J.M., Moraes, C.T. and Izpisua Belmonte, J.C. (2015) 'Selective elimination of mitochondrial mutations in the germline by genome editing', *Cell*, 161(3), pp. 459-69.

Reers, M., Smith, T.W. and Chen, L.B. (1991) 'J-aggregate formation of a carbocyanine as a quantitative fluorescent indicator of membrane potential', *Biochemistry*, 30(18), pp. 4480-6.

Richardson, C., Smith, T., Schaefer, A., Turnbull, D. and Griffiths, P. (2005) 'Ocular motility findings in chronic progressive external ophthalmoplegia', *Eye (Lond)*, 19(3), pp. 258-63.

Rideout, W.M., 3rd, Hochedlinger, K., Kyba, M., Daley, G.Q. and Jaenisch, R. (2002) 'Correction of a genetic defect by nuclear transplantation and combined cell and gene therapy', *Cell*, 109(1), pp. 17-27.

Robl, J.M., Gilligan, B., Critser, E.S. and First, N.L. (1986) 'Nuclear transplantation in mouse embryos: assessment of recipient cell stage', *Biol Reprod*, 34(4), pp. 733-9.

Rogakou, E.P., Boon, C., Redon, C. and Bonner, W.M. (1999) 'Megabase chromatin domains involved in DNA double-strand breaks in vivo', *J Cell Biol*, 146(5), pp. 905-16.

Rogakou, E.P., Pilch, D.R., Orr, A.H., Ivanova, V.S. and Bonner, W.M. (1998) 'DNA double-stranded breaks induce histone H2AX phosphorylation on serine 139', *J Biol Chem*, 273(10), pp. 5858-68.

Ross, J.M., Stewart, J.B., Hagstrom, E., Brene, S., Mourier, A., Coppotelli, G., Freyer, C., Lagouge, M., Hoffer, B.J., Olson, L. and Larsson, N.G. (2013) 'Germline mitochondrial DNA mutations aggravate ageing and can impair brain development', *Nature*, 501(7467), pp. 412-5.

Rowland, T.J., Blaschke, A.J., Buchholz, D.E., Hikita, S.T., Johnson, L.V. and Clegg, D.O. (2013) 'Differentiation of human pluripotent stem cells to retinal pigmented epithelium in defined conditions using purified extracellular matrix proteins', *J Tissue Eng Regen Med*, 7(8), pp. 642-53.

Rowland, T.J., Buchholz, D.E. and Clegg, D.O. (2012) 'Pluripotent human stem cells for the treatment of retinal disease', *J Cell Physiol*, 227(2), pp. 457-66.

Rozanowski, B., Cuenco, J., Davies, S., Shamsi, F.A., Zadlo, A., Dayhaw-Barker, P., Rozanowska, M., Sarna, T. and Boulton, M.E. (2008) 'The phototoxicity of aged human retinal melanosomes', *Photochem Photobiol*, 84(3), pp. 650-7.

Ruiz, S., Panopoulos, A.D., Herrerias, A., Bissig, K.D., Lutz, M., Berggren, W.T., Verma, I.M. and Izpisua Belmonte, J.C. (2011) 'A high proliferation rate is required for cell reprogramming and maintenance of human embryonic stem cell identity', *Curr Biol*, **21**(1), pp. 45-52.

Rummelt, V., Folberg, R., Ionasescu, V., Yi, H. and Moore, K.C. (1993) 'Ocular pathology of MELAS syndrome with mitochondrial DNA nucleotide 3243 point mutation', *Ophthalmology*, 100(12), pp. 1757-66.

Samavarchi-Tehrani, P., Golipour, A., David, L., Sung, H.K., Beyer, T.A., Datti, A., Woltjen, K., Nagy, A. and Wrana, J.L. (2010) 'Functional genomics reveals a BMP-driven mesenchymal-to-epithelial transition in the initiation of somatic cell reprogramming', *Cell Stem Cell*, 7(1), pp. 64-77.

Sanchez, Y., Wong, C., Thoma, R.S., Richman, R., Wu, Z., Piwnica-Worms, H. and Elledge, S.J. (1997) 'Conservation of the Chk1 checkpoint pathway in mammals: linkage of DNA damage to Cdk regulation through Cdc25', *Science*, 277(5331), pp. 1497-501.

Sarna, T., Burke, J.M., Korytowski, W., Rozanowska, M., Skumatz, C.M., Zareba, A. and Zareba, M. (2003) 'Loss of melanin from human RPE with aging: possible role of melanin photooxidation', *Exp Eye Res*, 76(1), pp. 89-98.

Schaefer, A.M., McFarland, R., Blakely, E.L., He, L., Whittaker, R.G., Taylor, R.W., Chinnery, P.F. and Turnbull, D.M. (2008) 'Prevalence of mitochondrial DNA disease in adults', *Ann Neurol*, 63(1), pp. 35-9.

Schieke, S.M., Ma, M., Cao, L., McCoy, J.P., Jr., Liu, C., Hensel, N.F., Barrett, A.J., Boehm, M. and Finkel, T. (2008) 'Mitochondrial metabolism modulates differentiation and teratoma formation capacity in mouse embryonic stem cells', *J Biol Chem*, 283(42), pp. 28506-12.

Schmierer, B. and Hill, C.S. (2007) 'TGFbeta-SMAD signal transduction: molecular specificity and functional flexibility', *Nat Rev Mol Cell Biol*, 8(12), pp. 970-82.

Schraermeyer, U., Peters, S., Thumann, G., Kociok, N. and Heimann, K. (1999) 'Melanin granules of retinal pigment epithelium are connected with the lysosomal degradation pathway', *Exp Eye Res*, 68(2), pp. 237-45.

Schwartz, M. and Vissing, J. (2002) 'Paternal inheritance of mitochondrial DNA', *N Engl J Med*, 347(8), pp. 576-80.

Seddon, J.M., Silver, R.E. and Rosner, B. (2016) 'Response to AREDS supplements according to genetic factors: survival analysis approach using the eye as the unit of analysis', *Br J Ophthalmol*, 100(12), pp. 1731-1737.

Seki, T., Yuasa, S., Oda, M., Egashira, T., Yae, K., Kusumoto, D., Nakata, H., Tohyama, S., Hashimoto, H., Kodaira, M., Okada, Y., Seimiya, H., Fusaki, N., Hasegawa, M. and Fukuda, K. (2010) 'Generation of induced pluripotent stem cells from human terminally differentiated circulating T cells', *Cell Stem Cell*, 7(1), pp. 11-4.

Shoubridge, E.A. and Wai, T. (2007) 'Mitochondrial DNA and the mammalian oocyte', *Curr Top Dev Biol*, 77, pp. 87-111.

Singh, R., Phillips, M.J., Kuai, D., Meyer, J., Martin, J.M., Smith, M.A., Perez, E.T., Shen, W., Wallace, K.A., Capowski, E.E., Wright, L.S. and Gamm, D.M. (2013) 'Functional analysis of serially expanded human iPS cell-derived RPE cultures', *Invest Ophthalmol Vis Sci*, 54(10), pp. 6767-78.

Smith, P.R., Bain, S.C., Good, P.A., Hattersley, A.T., Barnett, A.H., Gibson, J.M. and Dodson, P.M. (1999) 'Pigmentary retinal dystrophy and the syndrome of maternally inherited diabetes and deafness caused by the mitochondrial DNA 3243 tRNA(Leu) A to G mutation', *Ophthalmology*, 106(6), pp. 1101-8.

Smith, Z.D., Nachman, I., Regev, A. and Meissner, A. (2010) 'Dynamic single-cell imaging of direct reprogramming reveals an early specifying event', *Nat Biotechnol*, 28(5), pp. 521-6.

Sonoda, S., Spee, C., Barron, E., Ryan, S.J., Kannan, R. and Hinton, D.R. (2009) 'A protocol for the culture and differentiation of highly polarized human retinal pigment epithelial cells', *Nat Protoc*, 4(5), pp. 662-73.

Sorkio, A., Hongisto, H., Kaarniranta, K., Uusitalo, H., Juuti-Uusitalo, K. and Skottman, H. (2014) 'Structure and barrier properties of human embryonic stem cell-derived retinal pigment epithelial cells are affected by extracellular matrix protein coating', *Tissue Eng Part A*, 20(3-4), pp. 622-34.

Sparrow, J.R., Hicks, D. and Hamel, C.P. (2010) 'The retinal pigment epithelium in health and disease', *Curr Mol Med*, 10(9), pp. 802-23.

Spits, C., Mateizel, I., Geens, M., Mertzanidou, A., Staessen, C., Vandeskelde, Y., Van der Elst, J., Liebaers, I. and Sermon, K. (2008) 'Recurrent chromosomal abnormalities in human embryonic stem cells', *Nat Biotechnol*, 26(12), pp. 1361-3.

Sproule, D.M. and Kaufmann, P. (2008) 'Mitochondrial encephalopathy, lactic acidosis, and strokelike episodes: basic concepts, clinical phenotype, and therapeutic management of MELAS syndrome', *Ann N Y Acad Sci*, 1142, pp. 133-58.

Stacpoole, S.R., Bilican, B., Webber, D.J., Luzhynskaya, A., He, X.L., Compston, A., Karadottir, R., Franklin, R.J. and Chandran, S. (2011) 'Derivation of neural precursor cells from human ES cells at 3% O(2) is efficient, enhances survival and presents no barrier to regional specification and functional differentiation', *Cell Death Differ*, 18(6), pp. 1016-23.

Stern, C.D., Charite, J., Deschamps, J., Duboule, D., Durston, A.J., Kmita, M., Nicolas, J.F., Palmeirim, I., Smith, J.C. and Wolpert, L. (2006) 'Head-tail patterning of the vertebrate embryo: one, two or many unresolved problems?', *Int J Dev Biol*, 50(1), pp. 3-15.

Stevens, L.C. and Little, C.C. (1954) 'Spontaneous Testicular Teratomas in an Inbred Strain of Mice', *Proc Natl Acad Sci U S A*, 40(11), pp. 1080-7.

Stevenson, B.R., Siliciano, J.D., Mooseker, M.S. and Goodenough, D.A. (1986) 'Identification of ZO-1: a high molecular weight polypeptide associated with the tight junction (zonula occludens) in a variety of epithelia', *J Cell Biol*, 103(3), pp. 755-66.

Stewart, M.H., Bendall, S.C., Levadoux-Martin, M. and Bhatia, M. (2010) 'Clonal tracking of hESCs reveals differential contribution to functional assays', *Nat Methods*, 7(11), pp. 917-22.

Stewart, M.H., Bosse, M., Chadwick, K., Menendez, P., Bendall, S.C. and Bhatia, M. (2006) 'Clonal isolation of hESCs reveals heterogeneity within the pluripotent stem cell compartment', *Nat Methods*, 3(10), pp. 807-15.

Strauss, O. (2005) 'The retinal pigment epithelium in visual function', *Physiol Rev*, 85(3), pp. 845-81.

Sue, C.M., Mitchell, P., Crimmins, D.S., Moshegov, C., Byrne, E. and Morris, J.G. (1997) 'Pigmentary retinopathy associated with the mitochondrial DNA 3243 point mutation', *Neurology*, 49(4), pp. 1013-7.

Sundelin, S., Wihlmark, U., Nilsson, S.E. and Brunk, U.T. (1998) 'Lipofuscin accumulation in cultured retinal pigment epithelial cells reduces their phagocytic capacity', *Curr Eye Res*, 17(8), pp. 851-7.

Sutovsky, P., Moreno, R.D., Ramalho-Santos, J., Dominko, T., Simerly, C. and Schatten, G. (1999) 'Ubiquitin tag for sperm mitochondria', *Nature*, 402(6760), pp. 371-2.

Suzuki, T. (2014) 'A complete landscape of post-transcriptional modifications in mammalian mitochondrial tRNAs', *Nucleic Acids Res*, 42(11), pp. 7346-57.

Suzuki, T. and Nagao, A. (2011) 'Human mitochondrial tRNAs: biogenesis, function, structural aspects, and diseases', *Annu Rev Genet*, 45, pp. 299-329.

Taapken, S.M., Nisler, B.S., Newton, M.A., Sampsell-Barron, T.L., Leonhard, K.A., McIntire, E.M. and Montgomery, K.D. (2011) 'Karotypic abnormalities in human

induced pluripotent stem cells and embryonic stem cells', *Nat Biotechnol*, 29(4), pp. 313-4.

Tachibana, M., Amato, P., Sparman, M., Gutierrez, N.M., Tippner-Hedges, R., Ma, H., Kang, E., Fulati, A., Lee, H.S., Sritanaudomchai, H., Masterson, K., Larson, J., Eaton, D., Sadler-Fredd, K., Battaglia, D., Lee, D., Wu, D., Jensen, J., Patton, P., Gokhale, S., Stouffer, R.L., Wolf, D. and Mitalipov, S. (2013) 'Human embryonic stem cells derived by somatic cell nuclear transfer', *Cell*, 153(6), pp. 1228-38.

Takahashi, K., Tanabe, K., Ohnuki, M., Narita, M., Ichisaka, T., Tomoda, K. and Yamanaka, S. (2007) 'Induction of pluripotent stem cells from adult human fibroblasts by defined factors', *Cell*, **131**(5), pp. 861-72.

Temperley, R., Richter, R., Dennerlein, S., Lightowlers, R.N. and Chrzanowska-Lightowlers, Z.M. (2010) 'Hungry codons promote frameshifting in human mitochondrial ribosomes', *Science*, 327(5963), p. 301.

Terluk, M.R., Kapphahn, R.J., Soukup, L.M., Gong, H., Gallardo, C., Montezuma, S.R. and Ferrington, D.A. (2015) 'Investigating mitochondria as a target for treating age-related macular degeneration', *J Neurosci*, 35(18), pp. 7304-11.

Terman, A., Kurz, T., Navratil, M., Arriaga, E.A. and Brunk, U.T. (2010) 'Mitochondrial turnover and aging of long-lived postmitotic cells: the mitochondrial-lysosomal axis theory of aging', *Antioxid Redox Signal*, 12(4), pp. 503-35.

TeSlaa, T. and Teitell, M.A. (2014) 'Techniques to monitor glycolysis', *Methods Enzymol*, 542, pp. 91-114.

Thiery, J.P., Acloque, H., Huang, R.Y. and Nieto, M.A. (2009) 'Epithelial-mesenchymal transitions in development and disease', *Cell*, 139(5), pp. 871-90.

Thomson, J.A., Itskovitz-Eldor, J., Shapiro, S.S., Waknitz, M.A., Swiergiel, J.J., Marshall, V.S. and Jones, J.M. (1998) 'Embryonic stem cell lines derived from human blastocysts', *Science*, 282(5391), pp. 1145-7.

Thomson, J.A. and Marshall, V.S. (1998) 'Primate embryonic stem cells', *Curr Top Dev Biol*, 38, pp. 133-65.

Tondera, D., Grandemange, S., Jourdain, A., Karbowski, M., Mattenberger, Y., Herzig, S., Da Cruz, S., Clerc, P., Raschke, I., Merkwirth, C., Ehses, S., Krause, F., Chan, D.C., Alexander, C., Bauer, C., Youle, R., Langer, T. and Martinou, J.C. (2009) 'SLP-2 is required for stress-induced mitochondrial hyperfusion', *EMBO J*, 28(11), pp. 1589-600.

Toops, K.A., Tan, L.X. and Lakkaraju, A. (2014) 'A detailed three-step protocol for live imaging of intracellular traffic in polarized primary porcine RPE monolayers', *Exp Eye Res*, 124, pp. 74-85.

Trifunovic, A., Wredenberg, A., Falkenberg, M., Spelbrink, J.N., Rovio, A.T., Bruder, C.E., Bohlooly, Y.M., Gidlof, S., Oldfors, A., Wibom, R., Tornell, J., Jacobs, H.T. and Larsson, N.G. (2004) 'Premature ageing in mice expressing defective mitochondrial DNA polymerase', *Nature*, 429(6990), pp. 417-23.

Trokovic, R., Weltner, J., Noisa, P., Raivio, T. and Otonkoski, T. (2015) 'Combined negative effect of donor age and time in culture on the reprogramming efficiency into induced pluripotent stem cells', *Stem Cell Res*, 15(1), pp. 254-62.

Tropepe, V., Hitoshi, S., Sirard, C., Mak, T.W., Rossant, J. and van der Kooy, D. (2001) 'Direct neural fate specification from embryonic stem cells: a primitive

mammalian neural stem cell stage acquired through a default mechanism', *Neuron*, 30(1), pp. 65-78.

Tsunoda, Y., Yasui, T., Shioda, Y., Nakamura, K., Uchida, T. and Sugie, T. (1987) 'Full-term development of mouse blastomere nuclei transplanted into enucleated two-cell embryos', *J Exp Zool*, 242(2), pp. 147-51.

Vaajasaari, H., Ilmarinen, T., Juuti-Uusitalo, K., Rajala, K., Onnela, N., Narkilahti, S., Suuronen, R., Hyttinen, J., Uusitalo, H. and Skottman, H. (2011) 'Toward the defined and xeno-free differentiation of functional human pluripotent stem cell-derived retinal pigment epithelial cells', *Mol Vis*, 17, pp. 558-75.

Vafai, S.B. and Mootha, V.K. (2012) 'Mitochondrial disorders as windows into an ancient organelle', *Nature*, 491(7424), pp. 374-83.

van den Ouweland, J.M., Lemkes, H.H., Ruitenbeek, W., Sandkuijl, L.A., de Vijlder, M.F., Struyvenberg, P.A., van de Kamp, J.J. and Maassen, J.A. (1992) 'Mutation in mitochondrial tRNA(Leu)(UUR) gene in a large pedigree with maternally transmitted type II diabetes mellitus and deafness', *Nat Genet*, 1(5), pp. 368-71.

van den Ouweland, J.M., Lemkes, H.H., Trembath, R.C., Ross, R., Velho, G., Cohen, D., Froguel, P. and Maassen, J.A. (1994) 'Maternally inherited diabetes and deafness is a distinct subtype of diabetes and associates with a single point mutation in the mitochondrial tRNA(Leu(UUR)) gene', *Diabetes*, 43(6), pp. 746-51.

Vera-Díaz, F.A. and Doble, N. (2012) *The Human Eye and Adaptive Optics*. InTech.

Vives-Bauza, C., Anand, M., Shiraz, A.K., Magrane, J., Gao, J., Vollmer-Snarr, H.R., Manfredi, G. and Finnemann, S.C. (2008) 'The age lipid A2E and mitochondrial dysfunction synergistically impair phagocytosis by retinal pigment epithelial cells', *J Biol Chem*, 283(36), pp. 24770-80.

Vugler, A., Carr, A.J., Lawrence, J., Chen, L.L., Burrell, K., Wright, A., Lundh, P., Semo, M., Ahmado, A., Gias, C., da Cruz, L., Moore, H., Andrews, P., Walsh, J. and Coffey, P. (2008) 'Elucidating the phenomenon of HESC-derived RPE: anatomy of cell genesis, expansion and retinal transplantation', *Exp Neurol*, 214(2), pp. 347-61.

Wahlestedt, M., Ameur, A., Moraghebi, R., Norddahl, G.L., Sten, G., Woods, N.B. and Bryder, D. (2014) 'Somatic cells with a heavy mitochondrial DNA mutational load render induced pluripotent stem cells with distinct differentiation defects', *Stem Cells*, 32(5), pp. 1173-82.

Wallace, D.C., Singh, G., Lott, M.T., Hodge, J.A., Schurr, T.G., Lezza, A.M., Elsas, L.J., 2nd and Nikoskelainen, E.K. (1988) 'Mitochondrial DNA mutation associated with Leber's hereditary optic neuropathy', *Science*, 242(4884), pp. 1427-30.

Wallin, I.E. (1926) 'Bacteria and the Origin of Species', *Science*, 64(1651), pp. 173-5.

Wang, A.L., Lukas, T.J., Yuan, M. and Neufeld, A.H. (2008a) 'Increased mitochondrial DNA damage and down-regulation of DNA repair enzymes in aged rodent retinal pigment epithelium and choroid', *Mol Vis*, 14, pp. 644-51.

Wang, T., Chen, K., Zeng, X., Yang, J., Wu, Y., Shi, X., Qin, B., Zeng, L., Esteban, M.A., Pan, G. and Pei, D. (2011) 'The histone demethylases Jhdm1a/1b enhance somatic cell reprogramming in a vitamin-C-dependent manner', *Cell Stem Cell*, 9(6), pp. 575-87.

Wang, X., Fang, H., Huang, Z., Shang, W., Hou, T., Cheng, A. and Cheng, H. (2013) 'Imaging ROS signaling in cells and animals', *J Mol Med (Berl)*, 91(8), pp. 917-27.

Wang, X., Xiong, K., Lin, C., Lv, L., Chen, J., Xu, C., Wang, S., Gu, D., Zheng, H., Yu, H., Li, Y., Xiao, H. and Zhou, G. (2015) 'New medium used in the differentiation of human pluripotent stem cells to retinal cells is comparable to fetal human eye tissue', *Biomaterials*, 53, pp. 40-9.

Wang, Y., Baskerville, S., Shenoy, A., Babiarz, J.E., Baehner, L. and Blelloch, R. (2008b) 'Embryonic stem cell-specific microRNAs regulate the G1-S transition and promote rapid proliferation', *Nat Genet*, 40(12), pp. 1478-83.

Wang, Y., Medvid, R., Melton, C., Jaenisch, R. and Blelloch, R. (2007) 'DGCR8 is essential for microRNA biogenesis and silencing of embryonic stem cell self-renewal', *Nat Genet*, 39(3), pp. 380-5.

Warren, L., Manos, P.D., Ahfeldt, T., Loh, Y.H., Li, H., Lau, F., Ebina, W., Mandal, P.K., Smith, Z.D., Meissner, A., Daley, G.Q., Brack, A.S., Collins, J.J., Cowan, C., Schlaeger, T.M. and Rossi, D.J. (2010) 'Highly efficient reprogramming to pluripotency and directed differentiation of human cells with synthetic modified mRNA', *Cell Stem Cell*, 7(5), pp. 618-30.

Westenskow, P.D., Moreno, S.K., Krohne, T.U., Kurihara, T., Zhu, S., Zhang, Z.N., Zhao, T., Xu, Y., Ding, S. and Friedlander, M. (2012) 'Using flow cytometry to compare the dynamics of photoreceptor outer segment phagocytosis in iPS-derived RPE cells', *Invest Ophthalmol Vis Sci*, 53(10), pp. 6282-90.

Wilmut, I., Schnieke, A.E., McWhir, J., Kind, A.J. and Campbell, K.H. (1997) 'Viable offspring derived from fetal and adult mammalian cells', *Nature*, 385(6619), pp. 810-3.

Wilson, S.W. and Houart, C. (2004) 'Early steps in the development of the forebrain', *Dev Cell*, 6(2), pp. 167-81.

Wong, L.J., Perng, C.L., Hsu, C.H., Bai, R.K., Schelley, S., Vladutiu, G.D., Vogel, H. and Enns, G.M. (2003) 'Compensatory amplification of mtDNA in a patient with a novel deletion/duplication and high mutant load', *J Med Genet*, 40(11), p. e125.

Wright, L.S., Phillips, M.J., Pinilla, I., Hei, D. and Gamm, D.M. (2014) 'Induced pluripotent stem cells as custom therapeutics for retinal repair: Progress and rationale', *Exp Eye Res*.

Xiao, J., Mai, D.H. and Xie, L. (2016) 'Resetting Human Naive Pluripotency', *Genet Epigenet*, 8, pp. 37-41.

Yakubov, E., Rechavi, G., Rozenblatt, S. and Givol, D. (2010) 'Reprogramming of human fibroblasts to pluripotent stem cells using mRNA of four transcription factors', *Biochem Biophys Res Commun*, 394(1), pp. 189-93.

Yamanaka, S. (2009) 'Elite and stochastic models for induced pluripotent stem cell generation', *Nature*, 460(7251), pp. 49-52.

Yamashita, S., Nishino, I., Nonaka, I. and Goto, Y. (2008) 'Genotype and phenotype analyses in 136 patients with single large-scale mitochondrial DNA deletions', *J Hum Genet*, 53(7), pp. 598-606.

Yan, F., Cooper, N.G. and McLaughlin, B.J. (1998) 'Temperature-sensitive interactions between RPE and rod outer segment surface proteins', *Exp Eye Res*, 66(6), pp. 783-90.

Ylikallio, E. and Suomalainen, A. (2012) 'Mechanisms of mitochondrial diseases', *Ann Med*, 44(1), pp. 41-59.

Yokota, M., Hatakeyama, H., Okabe, S., Ono, Y. and Goto, Y. (2015) 'Mitochondrial respiratory dysfunction caused by a heteroplasmic mitochondrial DNA mutation blocks cellular reprogramming', *Hum Mol Genet*, 24(16), pp. 4698-709.

Yoneda, M., Chomyn, A., Martinuzzi, A., Hurko, O. and Attardi, G. (1992) 'Marked replicative advantage of human mtDNA carrying a point mutation that causes the MELAS encephalomyopathy', *Proc Natl Acad Sci U S A*, 89(23), pp. 11164-8.

Yu-Wai-Man, P., Griffiths, P.G., Brown, D.T., Howell, N., Turnbull, D.M. and Chinnery, P.F. (2003) 'The epidemiology of Leber hereditary optic neuropathy in the North East of England', *Am J Hum Genet*, 72(2), pp. 333-9.

Yu-Wai-Man, P., Griffiths, P.G., Burke, A., Sellar, P.W., Clarke, M.P., Gnanaraj, L., Ah-Kine, D., Hudson, G., Czermin, B., Taylor, R.W., Horvath, R. and Chinnery, P.F. (2010) 'The prevalence and natural history of dominant optic atrophy due to OPA1 mutations', *Ophthalmology*, 117(8), pp. 1538-46, 1546 e1.

Yu-Wai-Man, P., Griffiths, P.G. and Chinnery, P.F. (2011a) 'Mitochondrial optic neuropathies - disease mechanisms and therapeutic strategies', *Prog Retin Eye Res*, 30(2), pp. 81-114.

Yu-Wai-Man, P., Shankar, S.P., Biousse, V., Miller, N.R., Bean, L.J., Coffee, B., Hegde, M. and Newman, N.J. (2011b) 'Genetic screening for OPA1 and OPA3 mutations in patients with suspected inherited optic neuropathies', *Ophthalmology*, 118(3), pp. 558-63.

Yu, J., Hu, K., Smuga-Otto, K., Tian, S., Stewart, R., Slukvin, II and Thomson, J.A. (2009) 'Human induced pluripotent stem cells free of vector and transgene sequences', *Science*, 324(5928), pp. 797-801.

Yu, J. and Thomson, A.J. (2006) *Embryonic Stem Cells*. Available at: https://stemcells.nih.gov/info/Regenerative_Medicine/2006Chapter1.htm (Accessed: February 2017).

Yu, J., Vodyanik, M.A., Smuga-Otto, K., Antosiewicz-Bourget, J., Frane, J.L., Tian, S., Nie, J., Jonsdottir, G.A., Ruotti, V., Stewart, R., Slukvin, II and Thomson, J.A. (2007) 'Induced pluripotent stem cell lines derived from human somatic cells', *Science*, 318(5858), pp. 1917-20.

Yuan, J., Shaham, S., Ledoux, S., Ellis, H.M. and Horvitz, H.R. (1993) 'The C. elegans cell death gene ced-3 encodes a protein similar to mammalian interleukin-1 beta-converting enzyme', *Cell*, 75(4), pp. 641-52.

Zahabi, A., Shahbazi, E., Ahmadieh, H., Hassani, S.N., Totonchi, M., Taei, A., Masoudi, N., Ebrahimi, M., Aghdami, N., Seifinejad, A., Mehrnejad, F., Daftarian, N., Salekdeh, G.H. and Baharvand, H. (2012) 'A new efficient protocol for directed differentiation of retinal pigmented epithelial cells from normal and retinal disease induced pluripotent stem cells', *Stem Cells Dev*, 21(12), pp. 2262-72.

Zanna, C., Ghelli, A., Porcelli, A.M., Karbowski, M., Youle, R.J., Schimpf, S., Wissinger, B., Pinti, M., Cossarizza, A., Vidoni, S., Valentino, M.L., Rugolo, M. and Carelli, V. (2008) 'OPA1 mutations associated with dominant optic atrophy impair oxidative phosphorylation and mitochondrial fusion', *Brain*, 131(Pt 2), pp. 352-67.

Zeviani, M., Moraes, C.T., DiMauro, S., Nakase, H., Bonilla, E., Schon, E.A. and Rowland, L.P. (1988) 'Deletions of mitochondrial DNA in Kearns-Sayre syndrome', *Neurology*, 38(9), pp. 1339-46.

Zhang, K., Liu, G.H., Yi, F., Montserrat, N., Hishida, T., Rodriguez Esteban, C. and Izpisua Belmonte, J.C. (2013) 'Direct conversion of human fibroblasts into retinal pigment epithelium-like cells by defined factors', *Protein Cell*.

Zhang, Y.S., Lu, Z.Y., Yu, Y., Li, X.R., Li, W.B., Wang, Y.N. and Geng, Y. (2012) 'Derivation, culture and retinal pigment epithelial differentiation of human embryonic stem cells using human fibroblast feeder cells', *J Assist Reprod Genet*, 29(8), pp. 735-44.

Zhao, H., Joseph, J., Fales, H.M., Sokoloski, E.A., Levine, R.L., Vasquez-Vivar, J. and Kalyanaraman, B. (2005) 'Detection and characterization of the product of hydroethidine and intracellular superoxide by HPLC and limitations of fluorescence', *Proc Natl Acad Sci U S A*, 102(16), pp. 5727-32.

Zhao, S., Thornquist, S.C. and Barnstable, C.J. (1995) 'In vitro transdifferentiation of embryonic rat retinal pigment epithelium to neural retina', *Brain Res*, 677(2), pp. 300-10.

Zhou, H., Wu, S., Joo, J.Y., Zhu, S., Han, D.W., Lin, T., Trauger, S., Bien, G., Yao, S., Zhu, Y., Siuzdak, G., Scholer, H.R., Duan, L. and Ding, S. (2009) 'Generation of induced pluripotent stem cells using recombinant proteins', *Cell Stem Cell*, 4(5), pp. 381-4.

Zhou, W. and Freed, C.R. (2009) 'Adenoviral gene delivery can reprogram human fibroblasts to induced pluripotent stem cells', *Stem Cells*, 27(11), pp. 2667-74.

Zhu, C.C., Traboulsi, E.I. and Parikh, S. (2016) 'Ophthalmological findings in 74 patients with mitochondrial disease', *Ophthalmic genetics*, pp. 1-3.

Zhu, Y., Carido, M., Meinhardt, A., Kurth, T., Karl, M.O., Ader, M. and Tanaka, E.M. (2013) 'Three-dimensional neuroepithelial culture from human embryonic stem cells and its use for quantitative conversion to retinal pigment epithelium', *PLoS One*, 8(1), p. e54552.

Chapter 8. Appendix: List of publications

1. **<u>Chichagova, V.,</u>** Hallam, D., Collin, J., Buskin, A., Saretzki, G., Armstrong, L., Yu-Wai-Man, P., Lako, M., Steel, D. 'Human iPSC disease modelling reveals functional and structural defects in retinal pigment epithelial cells harbouring the m.3243A>G mitochondrial DNA mutation, *Hum Mol Genet* (submitted)

2. Neganova, I., **<u>Chichagova, V.</u>**, Armstrong, L., Lako, M. (2017) 'Critical role of p38MAPK pathway during reprogramming of human fibroblasts to iPSCs', *Sci Rep,* 7, 41673.

3. Hunt, N., Hallam, D., **<u>Chichagova, V.</u>**, Steel, D., Lako, M. 'The application of biomaterials to tissue engineering neural retina and retinal pigmented epithelium', *Biomaterials* (in preparation)

4. Wadkin, L., Elliot, L., Neganova, I., Parker, N., **<u>Chichagova, V.</u>**, Swan, G., Laude, A., Lako, M., Shukurov, A. (2016) 'Dynamics of single human embryonic stem cells and their pairs: a quantitative analysis', *Sci Rep* (submitted)

5. Neganova, I., Shmeleva, E., Munkley, J., **<u>Chichagova, V.</u>**, Anyfantis, G., Anderson, R., Passos, J., Elliott, D.J., Armstrong, L. and Lako, M. (2016) 'JNK/SAPK signaling is essential for efficient reprogramming of human fibroblasts to induced pluripotent stem cells', *Stem Cells*, 34(5), pp. 1198-212.

6. **<u>Chichagova, V.</u>**, Sanchez-Vera, I., Armstrong, L., Steel, D. and Lako, M. (2015) 'Generation of human induced pluripotent stem cells using RNA-based Sendai virus system and pluripotency validation of the resulting cell population', *Methods Mol Biol*, 1353, pp. 285-307.